Exploring the mechanisms that regulate $Ca_V2.2$ trafficking and function

James Frederick Otto Meyer

Doctor of Philosophy

UCL

2019

Department of Neuroscience, Physiology and Pharmacology
Division of Biosciences
Andrew Huxley Building
University College London
Gower Street
London WC1E 6BT

I, James Frederick Otto Meyer confirm that the work presented in this thesis is my own. Where information has been derived from other sources, I confirm that this has been indicated in this thesis.

James Frederick Otto Meyer

Acknowledgement

I, James Frederick Otto Meyer, of sound(ish) mind and body would like first to thank my supervisor Professor Annette Dolphin for her continued support and for giving me the opportunity to study in such a privileged environment. Throughout my time here, Annette has always provided me with her wealth of scientific knowledge and experience whenever sought. I am and will always remain grateful. I would also like to extend my gratitude to all members, past and present, of the Dolphin lab, without whom I would not have reached this point. Each and every member, I consider a friend and trusted advisor, each and every member I'll miss. A special mention goes to Dr Laurent Ferron (and previously Dr Simon Rothwell), I shall miss those Friday lunches. Another to Dr Ivan Kadurin, whom reluctantly I'll admit probably has the better music taste. Dr Shehrazade Dahimene and (soon to be Dr) Krishma Ramgoolam also get brownie points as an unending source of both emotional support and entertainment. Lastly, I'd like to thank Amelia (Finn) Mannerings, my partner in crime over all these years, for her constant loving support, I only wish I had her intellect and writing ability.

Dolphin lab members (past and present) in no particular order

Annette Dolphin, Laurent Ferron, Ivan Kadurin, Shehrazade Dahimene, Manuela Nieto-Rostro, Karen Page, Krishma Ramgoolam, Kanchan Chaggar, Simon Rothwell, Wojciech Margas, Marianna D'Arco, Natsuko Macabuag, John Cassidy, Kjara Pilch, Stuart Martin

James Frederick Otto Meyer

Publications

Kadurin I, Ferron L, Rothwell S, Meyer J, Douglas L, Bauer C, Lana B, Margas W, Alexopoulos O, Nieto-Rostro M, Pratt W, Dolphin A. (2016) 'Proteolytic maturation of $\alpha_2\delta$ represents a checkpoint for activation and neuronal trafficking of latent calcium channels', *Elife*

Yu H, Kistler A, Faridi M, Meyer J, Tryniszewska B, Mehta D, Yue L, Dryer S, Reiser J. (2016) 'Synaptopodin Limits TRPC6 Podocyte Surface Expression and Attenuates Proteinuria', *Journal of American Society of Nephrology*

Tauseef M, Farazuddin M, Sukriti S, Rajput C, Meyer J, Ramasamy S, Mehta D. (2016) 'Transient receptor potential channel 1 maintains adherens junction plasticity by suppressing sphingosine kinase 1 expression to induce endothelial hyperpermeability', *Federation of American Societies for Experimental Biology*

Chavan T, Meyer J, Chisholm L, Dobosz-Bartoszek M, Gaponenko V. (2014) 'A novel method for the production of fully modified K-Ras 4B', *Methods in Molecular Biology*

Moroni M, Meyer J, Lahmann C, Sivilotti L. (2011) 'In glycine and GABA(A) channels, different subunits contribute asymmetrically to channel conductance via residues in the extracellular domain', *Journal of Biological Chemistry*

Abstract

N-type calcium channels ($Ca_V2.2$) are pseudotetrameric voltage-gated calcium channels (VGCCs) predominantly expressed at the presynaptic terminals in the peripheral and central nervous system. $Ca_V2.2$ channels are highly calcium selective and play a crucial role in neurotransmitter release, coupling extracellular calcium entry to neurotransmitter exocytosis. The activity of $Ca_V2.2$ has multiple forms of regulation including: post-translational modifications (PMTs), proteolytic degradation and subcellular localisation. In addition, the behaviour of VGCCs is modulated by their auxiliary $\alpha_2\delta$ and β subunits. In this study, I first examine the role of proteolytic $\alpha_2\delta$ processing on $Ca_V2.2$. I find that unprocessed $\alpha_2\delta$ subunits, while unable to enhance whole-cell $Ca_V2.2$ currents, retain the ability to promote cell-surface expression of $Ca_V2.2$ in cell lines. Subsequent restoration of $\alpha_2\delta$ processing did not influence the protein expression of $\alpha_2\delta$ or of coexpressed $Ca_V2.2$. Thereafter, I examined the properties of $Ca_V2.2$ mutants featuring substitutions of crucial P-loop glutamate residues within the selectivity filter. I find that mutation of these glutamate residues renders these channels deficient in trafficking both in non-neuronal cell lines and primary neuronal cultures. These data are pertinent given the use of P-loop Ca_V mutants as dominant negative channels in previous studies. Finally, I compare the influence of $\alpha_2\delta$-1, $\alpha_2\delta$-2 and $\alpha_2\delta$-3 subtypes on the cell-surface and total expression of $Ca_V2.2$. Both cell-surface and total expression of $Ca_V2.2$ was found to be enhanced by all three subtypes albeit to differing degrees. Further investigation reveals that $\alpha_2\delta$-1 and $\alpha_2\delta$-2 promote the net forward trafficking of $Ca_V2.2$ through Rab11a-dependent recycling. $Ca_V2.2$ does not appear to participate in Rab11a-dependent recycling when expressed in the absence of $\alpha_2\delta$ or with $\alpha_2\delta$-3. This study reveals differential regulation of $Ca_V2.2$ channels among $\alpha_2\delta$ subtypes through targeted endosomal trafficking.

Impact Statement

Voltage-gated calcium channels are essential components in a range of biological processes such neurotransmission, gene transcription muscle contraction to name a few. Given the importance of these channels, it is unsurprising that dysregulation of their function is associated with numerous pathologies such as neuropathic pain associated with nerve injury. Currently, there are relatively few viable therapeutics that treat neuropathic pain, with Gabapentinoid drugs being the most commonly used. However, existing therapeutics are noted to have variable efficacy or - in the case of Ziconotide - require intrathecal administration and have a narrow therapeutic window, necessitating hospital-bound treatment. Of note, Ziconotide is a direct inhibitor of N-type calcium channels, while gabapentinoids appear to influence N-type channels indirectly by targeting their auxiliary $\alpha_2\delta$ subunits. In order to develop therapeutic options for neuropathic pain with more desirable traits, it important to improve our understanding of N-type channels and the mechanisms that regulate them. I believe the work presented in this thesis will contribute to the field of voltage-gated calcium channel research by examining the interplay between N-type voltage-gated calcium channels and their auxiliary subunits. Furthermore, it is likely that many of the processes that govern N-type channel function are conserved among other voltage-gated calcium channel members, giving this work potentially broader application to the field of calcium channel research.

Table of Contents

List of Figures

List of Tables

Abbreviations

$Ca_V2.2$	N-type calcium channels
ATP	adenosine triphosphate
AP	action potential
Na_V	voltage-gated Na^+ channel
K_V	voltage-gated K^+ channel
AMPA	α-amino-3-hydroxy-5-methyl-4-isoxazolepropionic acid
NMDA	*N*-methyl-D-aspartate
GPCR	G protein-coupled receptor
nACh	nicotinic acetylcholine
GABA	γ-aminobutyric acid
NSF	N-ethylmaleimide sensitive fusion protein
SNARE	Soluble NSF attachment receptor
VAMP	synaptobrevin
SNAP-25	Synaptosomal Associated Protein 25
SM	Sec1/Munc- like
RIM	Rab3-interacting molecule
RIM-BP	RIM-binding protein
Rab	Ras-related protein
HVA	high-voltage activated
LVA	low-voltage activated
cryoEM	cryo-electron microscopy
CTC	Charge Transfer Centre
DHP	Dihydropyridine
GTP	Guanosine-5'-triphosphate
VDI	voltage-dependent inactivation
mGluR	metabotropic glutamate receptor
D	dopamine
CaM	Calmodulin
CDI	Ca^{2+}-dependent inactivation
PTM	Post-translational modification
PKA	Protein Kinase A
PKC	Protein Kinase C
CamK	CaM Kinase

AKAP15	15 kDa cAMP-dependent protein kinase anchoring protein
SDS-PAGE	sodium dodecyl sulfate–polyacrylamide gel electrophoresis
RFP2	RING finger protein 2
USP5	Ubiquitin carboxyl-terminal hydrolase 5
DRG	Dorsal root ganglion
PDZ	PSD95, Drosophila disc large tumour suppressor, zonula occludens-1
AP-1	Adaptor protein complex-1
VWA	Von Willebrand Factor A
MIDAS	metal ion adhesion site
Cache	bacterial chemosensory-like
RNA	ribonucleic acid
mRNA	Messenger ribonucleic acid
GPI	glycosylphosphatidylinositol
DRMs/lipid raft	detergent-resistant membrane
du	Ducky
SH3	Src Homology domain 3
GK	Guanylate kinase domain
MAGUK	Membrane-Associated GK protein
AID	α-interacting-domain
ABP	α-binding pocket
SNP	single nucleotide polymorphism
TARP	Transmembrane AMPA Receptor Protein
RabGEF	Rab Guanine Nucleotide exchange factor
RabGAP	Rab GTPase activating protein
GDI	GDP-dissociation inhibitor
TBC	Trc-2/Bud2/Cdc16
GTD	globular tail domain
LIC	light intermediate chain
FIP	FH protein interacting protein
APPL	Adaptor protein, phosphotyrosine interacting with PH domain and leucine zipper
GSK	Glycogen synthase kinase

TSC	Tuberosclerosis complex
CMT2B	Charcot-Marie-Tooth type 2
HEK293	Human Embryonic Kidney cells
DMEM	Dulbecco's Modified Eagle Medium
N2a	Neuro2a
DAPI	4',6'-diamidino-2-phenylindole
KRH	Krebs-Ringer-HEPES
α-BTX	α-bungarotoxin
HA	Haemeglutinin
HRV	Human Rhinovirus
ER	Endoplasmic reticulum
TRIC	Trimeric Intracellular Cation
Na_VAb	bacterial voltage-gated Na^+ channel,
WT	Wild-type
G_{max}	conductance
V_{rev}	reversal potential
V_{50}, act	Half maximal activation voltage
TSP	Thrombospondin
EGF	Epidermal growth factor
vGlut	vesicular glutamate transporter
IS6	S6 of domain I
LRP	Low-density Lipoprotein Receptor-related Protein
RAP	Receptor-Associated Protein
TGN	trans-Golgi network
SNX	Sorting Nexin
NRX	Neurexin
HCN	Hyperpolarization-activated cyclic nucleotide–gated
KCNQ	Potassium voltage-gated channel subfamily KQT
TKO	Triple knockout
AnkG	Ankyrin G

Chapter 1 Introduction

1.1 Background

1.1.1 Resting membrane potential

The resting membrane potential is determined by the ionic balance between the intra and extracellular composition of a cell. The principal ions involved are K^+, Na^+, Ca^{2+}, HCO^{3-} and Cl^- with the general intra to extracellular concentrations shown in Table 1 below. Each ion has an equilibrium potential at which there is no net movement across the plasma membrane. Taken together, these equilibrium potentials determine the resting membrane potential which can be calculated using the Nernst equation shown below (equation 1). Ions are able to cross the plasma membrane through channels, pumps and transporters with the resting potential most heavily influenced by K^+ which moves passively through leak K^+ channels which have a reversal potential of around -70mV. The resting potential of a cell tends to be negative with regards to the extracellular solution so active transport of positively charged ions is required for the gradient to be maintained. Na^+/K^+ pumps are particularly important as they transport two K^+ into the cell and three Na^+ ions out of the cell; this is an active process and requires adenosine triphosphate (ATP).

$$E = E° - \frac{RT}{nF} LnQ_C$$

Equation 1. Nernst equation for calculating the electrical potential of a cell

E = Cell potential under specific conditions (V), *E*˚= Cell potential under standard state conditions, *R* = ideal gas constant, *T* = temperature (Kelvin), *n* = number of moles of electrons transferred in balanced equation, *F* = Faraday constant, *Qc* = reaction quotient, the product of the concentrations of reaction products divided by the product of the concentrations of reactants, *Ln* = natural log.

Table 1. Typical ion concentrations for mammalian cells under physiological conditions.

Ion	Intracellular (mM)	Extracellular (mM)
K^+	140	5
Na^+	12	145
Cl^-	4	116
Ca^{2+}	0.0001	1.8
Mg^{2+}	0.8	1.5

1.1.2 Ion channels

Ion channels are intrinsic membrane proteins that allow the movement of ions across phospholipid bilayers. Ions can pass through ion channels via a permeation pathway through a water-filled pore within the channel. The conductance of ions through the channel pore is generally close to the limit of diffusion allowing

extremely fast movement of ions through the permeation pathway. Ion channels are often highly selective with rigid constraints on the charge and size of permeant ions. Ion channels can exist in both open and closed states and are broadly divided into two major classes based on their mechanism of gating between these states. These classes are voltage-gated and ligand-gated ion channels. Voltage-gated channels respond to changes in local membrane potentials through the movement of a voltage-sensing motif, whereas ligand-gated channels possess binding sites for specific ligands that induce a conformational rearrangement of the channel.

1.1.3 Action potential

First measured by Hodgkin and Huxley in the squid giant axon, an action potential (AP) is a large plasma membrane depolarisation and repolarisation in excitable cells. Work by Hodgkin & Huxley determined the time and voltage-dependence of inward Na^+ and outward K^+ currents in AP generation, while later studies have detailed in-depth the coordinated activity of ion channels during each step (Hodgkin & Huxley, 1952; Narahashi, 1964). When the membrane potential of an excitable cell is sufficiently depolarised, voltage-gated Na^+ channels (Na_Vs) in the plasma membrane open allowing an influx of Na^+ into the cell along an electrochemical gradient. The influx of Na^+ further depolarises the membrane potential which is capped by the inactivation of Na_Vs at around +40mV. At this depolarised potential voltage-gated K^+ channels (K_Vs) open, allowing efflux of K^+ down its electrochemical gradient which repolarises the cells. This process initially reduces the membrane potential below resting potential, known as hyperpolarisation. As the membrane is repolarised, voltage-gated Na^+ and K^+ channels inactivate and remain desensitised. This phase is known as the refractory period, during which no new action potentials can be generated. In neurons, the

initial depolarisation that elicits an action potential is often caused by the activation of post-synaptic ligand-gated ion channels, such as α-amino-3-hydroxy-5-methyl-4-isoxazolepropionic acid (AMPA) and *N*-methyl-D-aspartate (NMDA) receptors. Plasma membrane depolarisation must reach a threshold potential (approx. -55mV) to activate Na_Vs and generate an action potential. The action potential is propagated along the axon as the depolarisation activates adjacent Na_Vs along its length to the presynaptic terminal. A general schematic of AP generation is shown below (Figure 1.1)

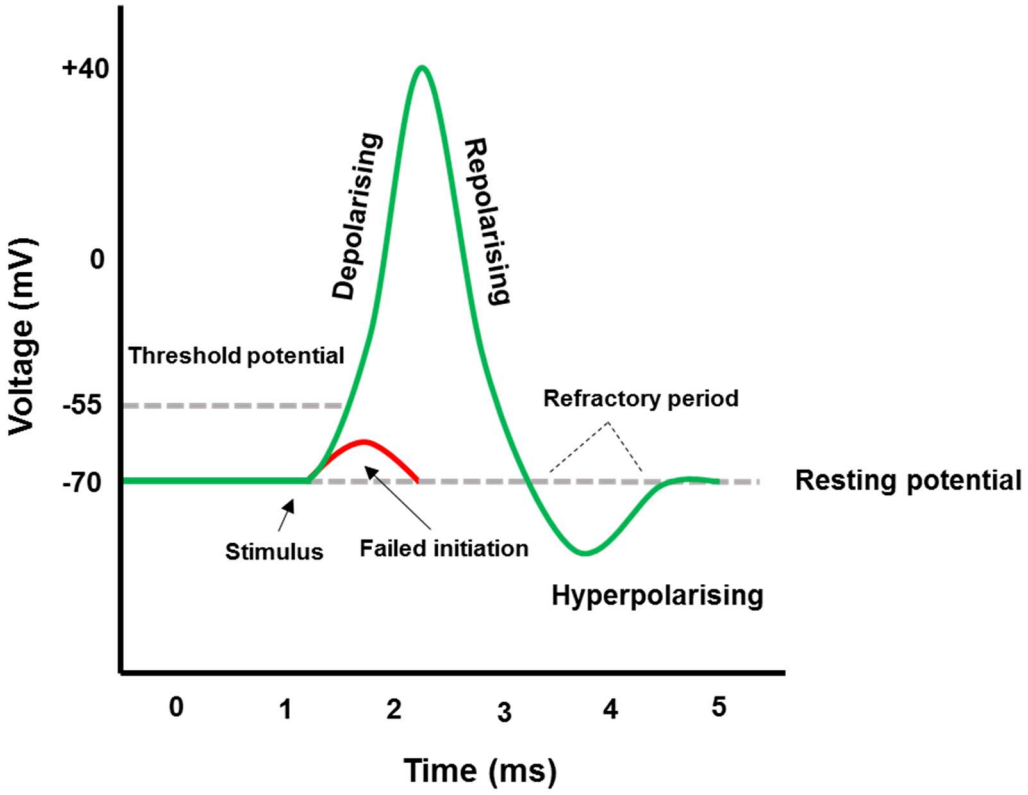

Figure 1.1 The action potential

At rest, a typical neuron has a membrane potential of ~-70 mV. Electrical stimulation of the neurons depolarises the membrane potential. If the membrane potential reaches a threshold of ~-55 mV, Na_V channels open allowing an influx of Na^+ which further depolarises the cell to a maximal potential of ~+40mV. After reaching the maximal potential, the neuron is rapidly depolarised by the inactivation of Na_Vs and opening of K_Vs. Repolarisation of the neuron overshoots the resting potential (hyperpolarisation). Following this is a brief refractory period during which further action potentials cannot be generated.

1.1.4 Neurons

In humans, a network of approx. 86 billion neurons comprise the central and peripheral nervous systems (Herculano-Houzel, 2009). Neurons are excitable cells with a typical resting potential of around -70 mV maintained by a plethora of plasma membrane ion channels and transporters (Bean, 2007). Functionally, neurons transmit information between one another through coordinated changes in membrane potential and chemical signals at the synaptic junctions between connected neurons. Neurons are highly specialised cells with a variety of adaptations to suit their role as conduits and integrators of information. Neurons differentiate to form structurally and functionally distinct compartments: axons, dendrites and cell body (soma). Axons are generally long, thin projections and their synaptic terminals contain neurotransmitter-laden synaptic vesicles which are released in response to changing membrane potential. Dendrites are relatively short projections from the soma, becoming thinner with increasing distance from the cell body. Dendrites possess neurotransmitter receptors allowing them to respond to incoming signals from connected neurons (reviewed in Arimura & Kaibuchi, 2007).

1.1.5 Neurotransmission

By altering the ionic balance of their intra and extracellular environments, cells can transmit information between one another. A neuron utilises many neurotransmitters and ion channels to transmit information between connected neurons, endocrine cells and other targets. In addition, neurons convert this information from an electric signal (changing membrane potential) into a chemical one. This process occurs at the junctions between connected neurons and

synapses. Here, arriving action potentials depolarise the presynaptic terminal which allows the entry of extracellular Ca^{2+} through presynaptic VGCCs. Entrant Ca^{2+} triggers vesicular fusion and exocytosis of neurotransmitters across the synaptic cleft to connected post-synaptic membranes (Katz & Miledi.,1965). Typically, neurotransmitters are ligands that bind to and activate ion channels or G protein-coupled receptors (GPCRs) at the post-synaptic membrane. This can either be excitatory or inhibitory depending on the channels involved. Activation of post-synaptic cation channels - for example nicotinic acetylcholine (nACh) receptors or AMPA receptors - facilitates an influx of positive ions that reduces the membrane potential of the post-synaptic neuron. If this depolarisation is sufficient to reach a threshold potential, then a new action potential will be generated and propagated along the neuron. Conversely, inhibitory ion channels, such as γ-aminobutyric acid $(GABA)_A$ receptors, allow the entry of negatively charged ions that hyperpolarise the post-synaptic neuron, moving it further from the activating threshold thereby suppressing action potential generation.

1.1.6 Neurotransmitter release

Fundamental to neurotransmission is the process of neurotransmitter release from a presynaptic terminal to a postsynaptic interface. This process occurs at the junctions between integrated neurons and converts an electrical signal (changing membrane potential) to a chemical one (neurotransmitter release). The events that underlie neurotransmitter release are orchestrated to allow extremely fast coupling between arriving depolarisation, presynaptic Ca^{2+} entry and exocytosis of synaptic vesicles, which can be achieved within a 1 ms period (see Südhof, 2012 for more details). Presynaptic terminals contain an abundance of neurotransmitter-filled synaptic vesicles which can be triggered by intracellular Ca^{2+} to fuse with the presynaptic plasma membrane, thereby releasing their contents into the synaptic

cleft. The cycle of vesicle fusion events is illustrated below (Figure 1.2) and will be described here. Initially a synaptic vesicle is docked to an active zone at the presynaptic membrane by the assembly of a “trans-SNARE” complex. The trans-SNARE complex is formed between the vesicular Soluble NSF Attachment REceptor (SNARE) proteins: synaptobrevin (VAMP) and synaptotagmin, with the presynaptic membrane SNAREs: syntaxin-1 and Synaptosomal Associated Protein 25 (SNAP-25) (Söllner *et* al,.1993). The Sec1/Munc-like (SM) protein, Munc-18-1, binds to the trans-SNARE assembly via an interaction with the N-peptide of Syntaxin-1 (Dulubova *et al*., 2007; Hata *et al*,. 1993). Next, the pre-fusion complex is joined by complexin, which appears to be essential for Ca^{2+} mediated vesicle fusion. With this assembly, the pre-fusion complex is “super-primed” and awaits Ca^{2+} binding to synaptotagmin to trigger fusion-pore opening (McMahon *et al*., 1995). Initial fusion-pore opening involves a progressive zipping of the four-helical SNARE complex in an N-C direction (Hanson *et al*,. 1997). The progressive zipping of the trans-SNARE complex forces the vesicular and presynaptic membranes in close proximity thereby destabilising these hydrophobic surfaces. After fusion-pore opening additional N-ethylmaleimide sensitive fusion (NSF) and SNAP proteins join the complex mediating fusion-pore expansion. The resulting “cis-SNARE” complex is subsequently disassembled by NSF/SNAP ATPases to be recycled for future fusion events (Söllner *et al*., 1993).

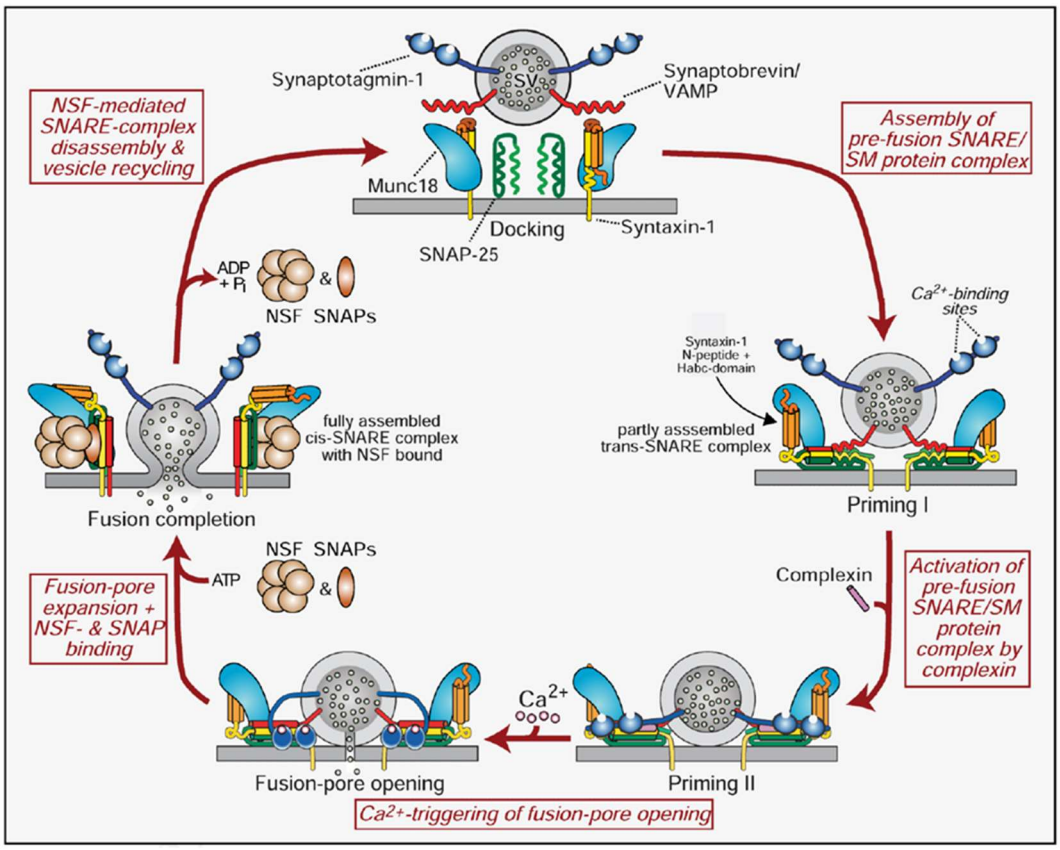

Figure 1.2 Schematic of the SNARE/SM protein cycle mediating vesicle fusion (modified from Südhof, 2013)

Assembly of the pre-fusion “trans” SNARE complex sees vesicular SNARE proteins, synaptobrevin and synaptotagmin bind the presynaptic SNARES, syntaxin-1 and SNAP-25. Following this, the SM protein munc-18-1 and complexin join the trans-SNARE complex which is now “super-primed”. The super-primed SNARE complex awaits Ca^{2+} entry through associated VGCCs which binds to sites on synaptotagmin to trigger fusion-pore opening. Fusion-pore expansion is then mediated by arriving NSF and SNAP proteins which join the complex. Following complete membrane-fusion, the “cis” SNARE complex is disassembled by NSF/SNAP ATPases with the component proteins recycled for future fusion events.

1.1.8 Organisation of neurotransmitter release machinery

Fast and coordinated neurotransmitter release in response to presynaptic depolarisation requires close association between primed synaptic vesicles and Ca_V channels at the active zone. Tethering of Ca_Vs to docked synaptic vesicles is mediated by a multi-protein complex comprised of Rab3-interacting molecule (RIM), RIM-binding protein (RIM-BP) and munc13 (Kaeser *et al.*, 2011). RIM is able to bind to the Ras-related proteins (Rabs) Rab3 and Rab27 which are localised to synaptic vesicles as well as binding to and activating Munc13 (Kaeser *et al.*, 2011). In turn, munc13 acts as a priming factor that catalyses the conformational switch of syntaxin-1 from a close to open state which promotes SNARE complex assembly (Dulubova *et al.*, 2005; Lu *et al.*, 2006). Both RIM and RIM-BP bind to Ca_Vs as well as to one another positioning these channels generally within 100 nm of docked synaptic vesicles. The importance of RIM and RIM-BP to Ca_V tethering can be seen by deletion of RIM in mice and deletion of RIM-BP in Drosophila which both lead to a loss of Ca_V abundance at the active zone and a loss of Ca^{2+} influx (Kaeser *et al.*, 2011; Liu *et al.*, 2011).

1.2 Voltage-gated calcium channels

VGCCs are comprised of an α_1 subunit – encoded by the CACNA1*x* genes – which contains all the functional machinery of the channel, including the channel pore, voltage-sensor and selectivity filter. To date, 10 mammalian isoforms have been identified (Fig 1.3) which were initially divided into two major classes: high-voltage activated (HVA) Ca_V1 and Ca_V2 channels, and low-voltage activated (LVA) Ca_V3 channels. Later, these Ca_V subtypes were categorised based on their susceptibility to a range of pharmacological blockers (detailed in table 1.2).

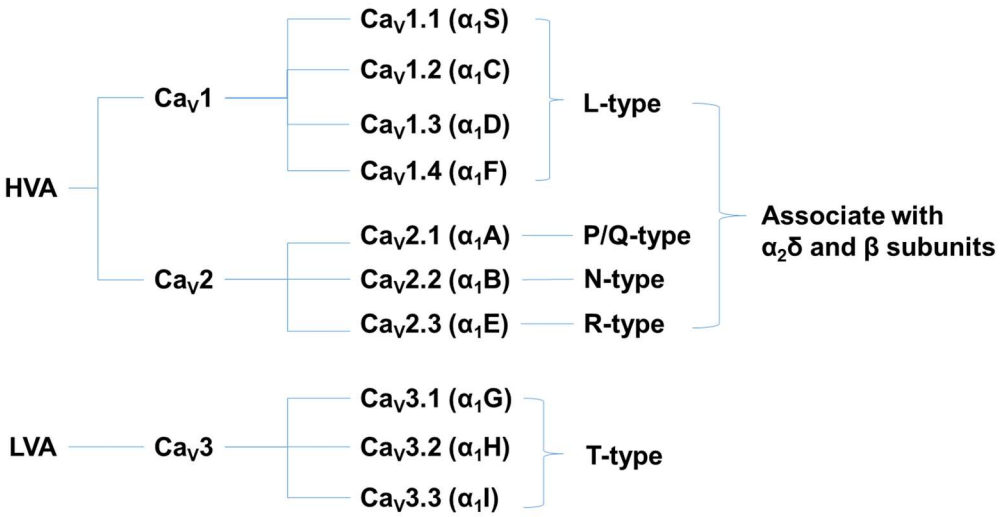

Figure 1.3 VGCC subtypes

The VGCC family contains 10 distinct members which can be broadly divided into two major classes, HVA (Ca_V1s and Ca_V2s) and LVA (Ca_V3s). Members of the HVA class associate with auxiliary $\alpha_2\delta$ and β subunits whereas LVA are not dependent on auxiliary subunits. Previously used nomenclature is shown in brackets.

Table 1.2 General characteristics of VGCCs in terms of tissue distribution, known pharmacological blockers and principal functions (adapted from Catterall 2000)

Type	Subtype	Tissue distribution	Pharmacological blockers	Known functions
L	$Ca_V1.1$	Skeletal muscle	DHPs	Excitation-contraction coupling Ca^{2+} homeostasis Gene regulation
	$Ca_V1.2$	Cardiac muscle Endocrine cells Neurons		Excitation-contraction coupling Ca^{2+} homeostasis Gene regulation
	$Ca_V1.3$	Neurons		Hormone secretion Gene regulation
	$Ca_V1.4$	Retina		Tonic transmitter release
P/Q	$Ca_V2.1$	Nerve terminals Dendrites	ω-Agatoxin IVA	Neurotransmitter release Dendritic Ca^{2+} transients
N	$Ca_V2.2$	Nerve terminals Dendrites	ω-Conotoxin GIVA	Neurotransmitter release Dendritic Ca^{2+} transients
R	$Ca_V2.3$	Nerve cell bodies Nerve terminals Dendrites	SNX-482	Neurotransmitter release
T	$Ca_V3.1$	Cardiac muscle Skeletal muscle Neurons	TTA-A2 TTA-P2	Pacemaking and repetitive AP firing
	$Ca_V3.2$	Cardiac muscle Neurons	None	
	$Ca_V3.3$	Neurons	None	

1.2.1 Domain structure of VGCCs

The structure of the α_1 subunit is a pseudotetramer having four homologous repeating domains, each containing six transmembrane segments (S1-S6) arranged in a clockwise orientation from an extracellular view (Catterall, 2011). VGCCs are closely related to Na_Vs and are believed to share a common ancestor with bacterial Na_Vs like Na_VAb and NaChBac, sharing many key structural features. Much of our understanding of VGCC mechanics has been gleaned from structure-function studies of bacterial Na_Vs, with more recent structural information coming from direct cryo-electron mycroscopy (cryoEM) studies of Ca_V1.1 (Ren, 2001; Koishi *et al.*, 2004; Wu *et al.*, 2016). A general schematic of a VGCC in complex with auxiliary subunits is shown on page 31 (Figure 1.4).

1.2.2 Entering the permeation pathway

Extended extracellular L5 loops of Domain I, II and III of α_1 appear to be stabilised by multiple intraloop disulphide bonds, forming a “windowed dome” above the selectivity filter (Wu *et al.*, 2016). The L5 loops are enriched with negatively charge residues and may constitute the main entrance for Ca^{2+} ions to the selectivity filter (Wu *et al.*, 2016).

1.2.3 Selectivity filter

VGCCs possess exquisite ion selectivity, allowing the movement of Ca^{2+} through the channel pore while excluding monovalent cations, despite their far higher extracellular concentration (Ellinor *et al.*, 1995; Yang & Tsien, 1993). Ca^{2+} ion selectivity is largely determined by conserved glutamate residues in the pore-forming S5-S6 loop. Excellent work by Tang et al (2014) and supported by recent cryoEM data, suggest there are three consecutive Ca^{2+} binding sites (site 1-3 from

an extracellular view). The conserved glutamates residues form a high affinity Ca^{2+} binding site (site 2) (Tang *et al.*, 2014; Wu *et al.*, 2016). Site 1 and 2 are predicted to have high Ca^{2+} affinity with site 2 thought to mediate divalent cation block. Site 3 is predicted to be a lower affinity binding site, consistent with a role facilitating entry of Ca^{2+} into the central vestibule. The proximity of these Ca^{2+} binding sites to one another and the electrostatic repulsion of bound Ca^{2+} ions make it energetically unfavourable for Ca^{2+} to bind adjacent sites simultaneously. Instead, Tang et al (2014) propose a mechanism whereby either Sites 1 and 3 (State 1), or Site 2 alone (State 2) are occupied. In this model, Ca^{2+} from either side would prompt a transition between these two states, with a transition from State 1 to State 2 expelling a distal Ca^{2+} ion. This process results in a “knock-on” movement of Ca^{2+} through the selectivity filter and into the central vestibule.

1.2.4 Voltage sensor

As the name implies, VGCCs respond to changes in local membrane potentials through structural rearrangements within the channel that permit or deny Ca^{2+} access to the permeation pathway. In the resting (closed) state, the S6 transmembrane domains converge at the intracellular side of the channel obstructing the permeation pathway, serving as an activation gate. The voltage sensor itself is comprised of the S4 units of each domain, which lie parallel to the pore domains of the channel. In the resting state, these S4 units sit in a “down state”, below the Charge Transfer Centre (CTC). The CTC is formed by negative or polar residues as well as a highly conserved hydrophobic residue on S2 (Wu *et al.*, 2016). Upon membrane depolarisation, the S4 domains move upwards (towards the extracellular side); once each S4 unit is in the “up state” the S6 units are able to disengage from the permeation pathway, allowing ion flux through the

channel pore. The S4 units contain numerous positively charged residues, whose interactions with negative residues of the CTC facilitate the sequential upward movement of the S4 units (Domene *et al*., 2005; Hering et al., 2018). Upon membrane repolarisation, the S4 units return to the down state allowing the S6 units to re-engage, obstruct the pore and close the channel (Domene *et al*., 2005; Hering *et al*., 2018).

1.2.5 Channel pore

The pore-forming region of α_1 is comprised of segments of the S5 and S6 transmembrane units from each domain and the re-entrant P-loop between them (Wu *et al*., 2016). Each of the P-loop regions contains highly conserved negative residues that cooperate to form a highly selective permeation pathway, permitting permeant cations such as Ca^{2+} and Ba^{2+}. The inner pore is lined by S6 segments which form the dihydropyridine (DHP) binding site for DHP-sensitive VGCCs (Wu *et al*., 2016). Interestingly, the N-type specific peptide inhibitor ω-conotoxin GVIA, binds with high affinity to a site between the S5 and S6 segments of domain III and was initially thought to obstruct the channel pore (Ellinor *et al*.,1994), however more recent work suggests that ω-conotoxin GVIA may in fact modulate channel gating properties, acting to destabilise the open state of the channel (Yarotskyy & Elmslie, 2010; Yarotskyy *et al*., 2012).

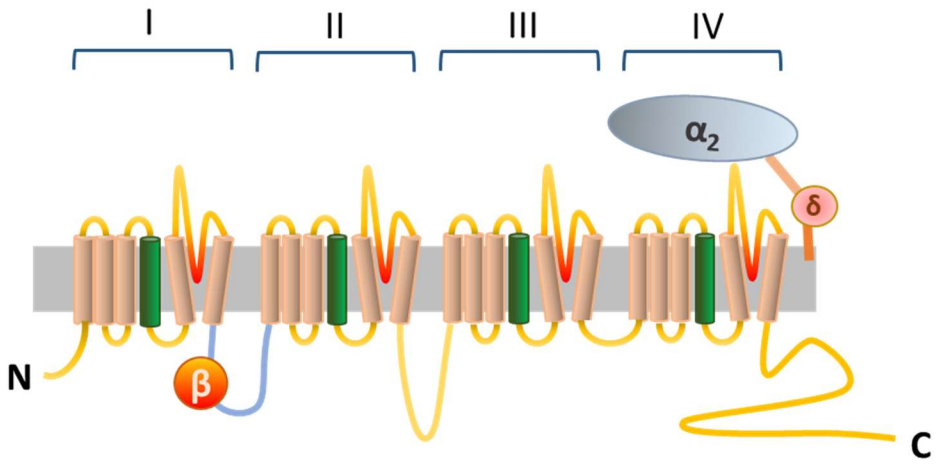

Figure 1.4 Schematic of a VGCC in complex with auxiliary $\alpha_2\delta$ and β subunits

The principal α_1 subunit is a pseudotetramer with each domain repeat comprised of six transmembrane units (S1-S6) connected by intracellular loop regions between these domains. The pore of the channels is formed by re-entrant P-loops between S5 and S6 of each domain (shown in red). The voltage-sensor is comprised of the S4 segments of each domain (shown in green). The β subunit binds to the AID sequence of the domain I-II linker (shown in blue) to promote refolding of the loop and channel trafficking. $\alpha_2\delta$ is extracellular and remains anchored to the plasma membrane through a GPI-anchor, interacting with extracellular loops of α_1 via its VWA domain.

1.3 Regulation of VGCCs

VGCCs are key mediators for a variety of cellular functions, permitting entry of extracellular Ca^{2+}, an extremely potent second messenger. As such, VGCC activity is tightly regulated at both translational and post-translational levels, as well as through protein-protein interactions with regulatory partners. In this section, I discuss a number of processes though which VGCC function is modulated.

1.3.1 GPCR modulation of VGCCs

The activity of VGCCs is modulated by a range of GPCRs including those activated by dopamine, glutamate and opioids. Upon GPCR activation, Guanosine-5'-triphosphate (GTP)-loading of the Gα subunit induces a conformational shift in the heterotrimeric complex resulting in dissociation of Gαβγ into two active signalling molecules, Gα-GTP and Gβγ. Gαs-GTP activates adenylate cyclase which generates cyclic-adenosine monophosphate (cAMP), a potent second messenger. cAMP activates Protein kinase A (PKA) which can in turn phosphorylate VGCCs (Arnot *et al*., 2000; Herlitze *et al*., 1996). Gβγ has been shown to interact directly with both $Ca_V2.1$ and $Ca_V2.2$ channels, with in-depth structural analysis of $Ca_V2.2$ revealing the presence of a Gβγ-binding pocket comprised of the I-II linker and N-terminal regions of the α_1 subunit (Cantí *et al.*, 1999). The binding of Gβγ to $Ca_V2.2$ appears to stabilise the closed conformation of the channel reflected by a depolarising shift in voltage-activation. This form of inhibition can be overcome by repeated application of short depolarising pulses and is thereby referred to as voltage-dependent inactivation (VDI) (Boland & Bean, 1993). In this instance, depolarisation causes a temporary dissociation of Gβγ from the channel, which is now unmodulated, prior to re-association of Gβγ and subsequent re-inhibition of the channel.

In addition to regulation by heterotrimeric G proteins, there are numerous examples of physical coupling of Ca_V channels and GPCRs. The first description of such a complex was between $Ca_V1.2$ and β-adrenergic receptors, followed by reports of an interaction between $Ca_V2.1$ and metabotropic glutamate receptor 1 (mGluR1) (Davare *et al.*, 2001; Kitano *et al.*, 2003). Interactions have also been reported between $Ca_V2.2$ and all four members of the opioid receptor family

(Beedle *et al.*, 2004; Altier *et al.*, 2006). Further to this $Ca_V2.2$ interacts directly with both dopamine (D)1 and D2 receptors, $GABA_B$ receptors and melatonin 1 receptors (MT1) (Kisilevsky *et al.*, 2008; Laviv *et al.*, 2011; Benleulmi-Chaachoua *et al.*, 2016). The interaction of $Ca_V2.2$ and D1 receptors appears to occur through intracellular regions of the D1 receptor and the C-terminus of $Ca_V2.2$ (Kisilevsky *et al.*, 2008). However, it remains unclear if other reported GPCR-$Ca_V2.2$ interactions are direct or occur through an intermediate scaffolding protein.

1.3.2 Ca^{2+}-dependent regulation of VGCCs

Ca^{2+}-dependent regulation offers a means to fine tune VGCC activity, often in the form of negative-feedback inhibition that prevents excessive Ca^{2+} influx following channel activation. Ca^{2+}-dependent regulation of VGCCs is mediated by the Ca^{2+}-sensor, Calmodulin (CaM) (Tadross *et al*., 2008). CaM interacts with the C-terminal IQ-like domain and EF-hand region of α_1 subunits, acting as a resident Ca^{2+}-sensor for the channel (Kim *et al.*, 2008; Ben-Johny & Yue, 2014). CaM possesses Ca^{2+} binding sites on both its N- and C-lobes, which induce conformational change in the C-terminus/CaM complex upon Ca^{2+} binding. The N- and C-lobe Ca^{2+}-binding sites have distinct Ca^{2+} affinities and impart different forms of channel regulation depending on which site is occupied (Ben-Johny & Yue, 2014). The most well documented form of Ca_V-CaM regulation is Ca^{2+}-dependent inactivation (CDI). CDI can be observed when comparing current-decay kinetics in the presence of Ca^{2+} or Ba^{2+}, with the speed of current decay drastically increased with Ca^{2+} present. Mechanistically, local increases of Ca^{2+} at the inner mouth of the channel pore lead to Ca^{2+}-CaM binding and conformational changes in the C-terminal/CaM complex that inactivate the channel (Ben-Johny and Yue, 2014). Early experiments, demonstrated CDI for all Ca_V1 subtypes, however it was not initially apparent in

Ca_V2 channels (Zamponi, 2003). It has since emerged that CDI of Ca_V2 channels requires a global rise in intracellular Ca^{2+} as opposed to a local increase for Ca_V1s. Site-directed mutagenesis of the N- and C-lobe Ca^{2+}-binding sites of CaM have revealed that differing sensitivity of Ca_V1s and Ca_V2s to CDI, is due to the differential involvement of the high and low affinity CaM binding sites (Kim *et al*., 2008; Mori *et al*., 2008).

1.3.3 Post-translational modifications of VGCCs

PTMs are covalent modifications of proteins that occur following biosynthesis. PTMs may involve the addition of functional groups such as phosphates, glycans or lipid moieties or the removal of existing features i.e. through proteolytic processing or phosphatase activity. PTMs play an essential role in regulating signalling pathways and may influence the activity of their protein targets or subcellular localisation, as well as facilitating or inhibiting protein-protein interactions.

1.3.3.1 Phosphorylation of VGCCs

The addition of phosphate groups to the side chains of residues – most commonly serine and threonine – by protein kinases, modulates the function of an abundance of proteins including VGCCs. Indeed, all VGCC subtypes are phosphorylation targets for prominent kinases such as PKA, Protein Kinase C (PKC) and CaM Kinase (CamK) among others. The earliest reported example of VGCC-kinase interplay was the PKA-dependent phosphorylation of cardiac $Ca_V1.2$ channels which produced a sizeable increase in whole-cell current amplitude (Yue *et al*., 1990). This form of regulation is believed to be part of the fight-or-flight response,

whereby the activity of cardiac and skeletal $Ca_V1.2$ and $Ca_V1.1$ is enhanced in response to noradrenaline release (Catterall, 2013). However, it was a number of years before examples of VGCC-kinase regulation could be reproduced in heterologous expression systems. The first demonstrated case of VGCC phosphorylation in a heterologous expression system required coexpression of the 15 kDa cAMP-dependent protein kinase anchoring protein (AKAP15) to observe $Ca_V1.2$ current enhancement (Gao *et al.*, 1997). The involvement of AKAP15 as necessary for $Ca_V1.2$ phosphorylation revealed greater complexity to VGCC-kinase regulation than had previously been thought. Ultimately, it has emerged that the C-terminus of $Ca_V1.2$ contains a cleavage site allowing for proteolytic processing of the channel (Fu *et al.*, 2011). The C-terminal processing of Ca_V1 was not initially reproduced in heterologous expression systems leaving an intact C-terminus which was found to act as an auto-inhibitory domain preventing the binding of AKAP15 to a site present in the C-terminal region (Fu *et al.*, 2011). Proof of this principle was demonstrated through heterologous expression of truncated $Ca_V1.2$ lacking the auto-inhibitory C-terminal domain, which was found to have increased whole-cell currents and a loss of β-adrenergic sensitivity (Fu *et al.*, 2011). More recently, a study was carried out using mass spectrometry to identify phosphorylated Ca_V3 residues immunoprecipitated from rat brain tissue as well as transfected tsA-201 cells (Blesneac *et al.*, 2015). Such analysis revealed over 30 basally phosphorylated sites for $Ca_V3.2$, many of which were clustered in functionally important intracellular residues (Blesneac *et al.*, 2015). It therefore seems likely that VGCC phosphorylation constitutes a major component of channel regulation.

1.3.3.2 Glycosylation of VGCCs

Glycosylation is a post- or co-translational addition of glycans to a protein and is a common feature among extracellular and intrinsic membrane proteins. Glycosylation typically occurs in the endoplasmic reticulum (ER) and Golgi network with the most common form being N-linked glycosylation. N-linked glycosylation targets asparagine residues within an NxS or NST consensus sequence often playing a role in protein folding and cell sorting. Based on amino acid sequence analysis, canonical N-linked glycosylation sites are present in all ten VGCC subtypes (Lazniewska & Weiss, 2017). In $Ca_V3.2$, four potential N-glycosylation sites have been identified. Mutating two of the four N-linked sites was found to reduce cell-surface expression of the channel as well as alter gating properties (Orestes *et al.*, 2013). In line with this observation, Ca_V3 activity is upregulated *in vivo* in hyperglycaemic rodents, but downregulated by the introduction of the deglycosylating enzyme neuraminidase (Orestes *et al.*, 2013). Four potential sites of N-linked glycosylation are also present in rabbit $Ca_V1.2$, two in domain I (N124, N299) and two in domain IV (N1359 and N1410). Site-directed mutagenesis of these positions individually was not found to influence biophysical properties of the channel (Park *et al.*, 2015). However, concurrent N to Q mutations at sites N124 and N299 did produce a depolarising shift in voltage-dependent activation when expressed in Xenopus oocytes (Park *et al.*, 2015). In addition, simultaneous mutation of all four N-linked sites in $Ca_V1.2$ expressed in Xenopus oocytes leads to a substantial decrease in current density correlating with a reduction in cell-surface expression of the channel (Park *et al.*, 2015).

1.3.3.3 Proteolytic processing of VGCCs

Recent, and somewhat controversial, analysis of $Ca_V1.2$ in mice have reported that the channel undergoes extensive mid-channel proteolysis in the domain II-III linker regions, mediated by the Ca^{2+}-dependent Calpain proteases. The authors suggest the presence of activity-dependent feedback inhibition whereby Ca^{2+} entry through $Ca_V1.2$ leads to calpain-mediated downregulation of channel activity (Michailidis *et al.*, 2014). However, more recent work by Buonarati et al (2017) provides compelling evidence that previously reported "mid-channel" proteolysis of $Ca_V1.2$ was due to misidentification of cross-reactive proteins for cleaved $\alpha_1$1.2 fragments (Buonarati *et al.*, 2017). Systematic analysis of $Ca_V1.2$ size forms was carried out using region specific antibodies and increasing acrylamide concentrations for sodium dodecyl sulfate–polyacrylamide gel electrophoresis (SDS-PAGE) in conjunction with analysis of $\alpha_1$1.2 KO samples. This analysis supports previous observations of distal C-terminal proteolysis, while suggesting that 150 and 90 kDa fragments, identified by Michailidis et al (2014) as proteolytically processed $\alpha_1$1.2 fragments, are due to antibody cross-reactivity (Buonarati *et al.*, 2017).

1.3.3.4 Ubiquitination of VGCCs

Ubiquitination is a process whereby ubiquitin ligases attach single or multiple ubiquitin groups to lysine residues of target proteins. The outcome for an ubiquitinated protein is variable depending on the type of ubiquitination involved (poly versus mono-ubiquitination). $Ca_V1.2$ is a known target of the ubiquitin ligase, RING finger protein 2 (RFP2), which takes place in the ER and leads to association of $Ca_V1.2$ with the chaperone proteins P97 and Derlin-1, which results in retrotranslocation and proteasomal degradation (Altier *et al.*, 2011). Notably, this process is strongly antagonised by coexpression of auxiliary $Ca_V\beta$ subunits.

Another example of VGCC-ubiquitin regulation is reported for $Ca_V3.2$, which is targeted by the cell-surface ubiquitin ligases WWP1 and WWP2 (García-Caballero *et al.*, 2014). The $Ca_V3.2$ residues targeted for ubiquitination sit upstream of an interaction site for the deubiquitinating enzyme Ubiquitin carboxyl-terminal hydrolase 5 (USP5). USP5 is known to be upregulated in various chronic pain conditions (Garcia-Caballero *et al*., 2016).

1.4 $Ca_V2.2$/N-types

$Ca_V2.2$ channels are encoded by the *CACNA2B* gene which is widely expressed in both the central and peripheral nervous systems. Initial identification of $Ca_V2.2$ currents was based on observed differences in voltage dependence from isolated chick Dorsal Root Ganglion neurons (DRGs) (Nowycky *et al*., 1985). $Ca_V2.2$s can be further distinguished pharmacologically through their insensitivity to dihydropyridines (DHPs) and selective block by ω-conotoxin GVIA.

1.4.1 Role of $Ca_V2.2$

As a VGCC, $Ca_V2.2$ mediates extracellular Ca^{2+} entry in response to membrane depolarisation. While entrant Ca^{2+} can influence a multitude of cellular functions, $Ca_V2.2$ activity is most commonly associated with fast Ca^{2+}-neurotransmitter release coupling at presynaptic terminals. $Ca_V2.2$ is localised to presynaptic active zones through interactions between the C-terminus of $Ca_V2.2$ and PSD95, Drosophila disc large tumour suppressor, zonula occludens-1 (PDZ) domain of the active zone scaffold, RIM (Kaeser *et al.*, 2011). Upon membrane depolarisation by an arriving action potential, presynaptic $Ca_V2.2$ channels open prompting an influx of extracellular Ca^{2+} which binds to and activates Synaptotagmin, initiating fusion

of primed vesicles and exocytosis of neurotransmitter into the synaptic cleft (Südhof, 2012). In the somatodendritic compartments of neurons, $Ca_V2.2$ also plays a role in excitation-transcription coupling, although this function is predominantly mediated by Ca_V1 channels. In addition, a study by Wheeler et al (2012) reported that Ca^{2+} entry through Ca_V2 channels is preferentially buffered by the ER and Mitochondria relative to Ca_V1 (Wheeler *et al.*, 2012). Preferential Ca^{2+} buffering in this fashion was suggested to indicate a form of excitation-metabolism coupling (Wheeler *et al.*, 2012). Both $Ca_V2.1$ and $Ca_V2.2$ participate in excitation-release coupling at presynaptic nerve terminals (Iwasaki *et al.*, 2000). However, the relative contribution of these channels is variable between synapses. For example, $Ca_V2.2$ is the predominant mediator of neurotransmitter release at presynaptic DRG terminals (Kerr *et al.*, 1988).

1.4.2 Alternative splicing of $Ca_V2.2$

$Ca_V2.2$ is encoded by 46 exons and several alternatively spliced variants have been identified which exhibit differential biophysical properties, such as voltage-dependence of activation, as well as augmented trafficking and tissue distribution. For example, the peripheral isoform of $Ca_V2.2$ contains an alternative exon 31a which inserts a two residue ET sequence into the S3-S4 loop of domain IV, resulting in a hyperpolarising shift of voltage activation, thereby reducing channel activity (Lin *et al.*,1997; Lin *et al.*, 1999). Alternative splicing of exon 37 – located at the C-terminus of $Ca_V2.2$ – has been shown to produce two mutually exclusive variants, e37a and e37b. Notably, $Ca_V2.2a$ has an extremely restricted distribution being mainly expressed at nociceptive DRG neurons (Bell *et al.*, 2004; Castiglioni *et al.*, 2006). Functionally, $Ca_V2.2$ e37a expression is associated with larger whole-cell currents than e37b. Recently, a study by Macabuag & Dolphin (2015) revealed

that canonical binding motifs for the clathrin-associated adaptor protein complex-1 (AP-1) (Yxxϕ and [DE]xxx[LI]) are present in e37a but absent in e37b (Macabuag and Dolphin, 2015). AP-1 is primarily functional at the trans-Golgi network (TGN) generating vesicles destined for endosomes although it is also found on sorting endosomes suggesting a role in recycling to the plasma membrane. Abolition of these AP-1 binding motifs in $Ca_V2.2$ e37a severely disrupts channel trafficking to the plasma membrane and neurites of DRG neurons (Macabuag and Dolphin, 2015).

1.5 Auxiliary VGCC subunits

1.5.1 The $\alpha_2\delta$ subunit

There are four mammalian $\alpha_2\delta$ subtypes, $\alpha_2\delta$-1-4, encoded by the genes *CACNA2D1-4* respectively. Each $\alpha_2\delta$ subtype is expressed from a single gene with the protein product post-translationally cleaved between the α_2 and δ domains. Heterologous expression of $\alpha_2\delta$ in *Xenopus laevis* oocytes or tsA-201 cells produces an increase in whole-cell Ca_V currents between 3-9 fold depending on the specific subunit pairing (Felix *et al*., 1997; Gurnett *et al*., 1996). There is limited evidence that $\alpha_2\delta$s influence single-channel Ca_V properties and they are not reported to affect these properties for natively or heterologously expressed $Ca_V2.1$ or $Ca_V2.2$ (Wakamori *et al*., 1999). However, $\alpha_2\delta$-1 coexpressed with $Ca_V2.2$ and β1b was reported to reduce single-channel opening times, while also reducing the % of null sweeps recorded (Wakamori *et al*., 1999). It should be noted that low levels of endogenous $\alpha_2\delta$ and β are present in a number of expression systems complicating the task of assessing the roles of individual channel subunits. There are however several, sometimes contradictory, reports that $\alpha_2\delta$ subunits can influence the voltage-dependence of Ca_V activation/inactivation. A study by Felix

et al (1997) found $\alpha_2\delta$-1 produced a 10 mV hyperpolarising shift in voltage-dependent activation of $Ca_V1.2/\beta1b$, while another report found $\alpha_2\delta$-1 to cause a depolarising shift in voltage-dependent activation of $Ca_V2.3$ (Felix *et al*., 1997; Qin *et al*., 1998). Since $\alpha_2\delta$s appear to have a modest effect on single-channel Ca_V properties, whole-cell Ca_V current enhancement has generally been attributed to increased plasma membrane Ca_V expression under these conditions. Indeed, $\alpha_2\delta$s have established roles in enhancing plasma membrane Ca_V expression in heterologous systems, as well as increasing the presynaptic and active zone Ca_V population in neurons (Cassidy *et al.,* 2014; Hoppa *et al*., 2012).

1.5.1.1 $\alpha_2\delta$ topology and domain structure

Despite considerable variance in sequence homology, the general topology of all $\alpha_2\delta$ subtypes is believed to be quite similar. All $\alpha_2\delta$s possess an N-terminal signal sequence, notably longer for $\alpha_2\delta$-2, which is absent in the cell-surface expressed protein (Brodbeck *et al*., 2002; Douglas *et al*., 2006). The N-terminal signal sequence is co-translationally cleaved with the α_2 domain inserted into the lumen of the ER, ultimately becoming extracellular. Detailed bioinformatics analysis has revealed that all $\alpha_2\delta$s possess a Von Willebrand Factor A (VWA) domain (Whittaker & Hynes, 2004). VWA domains are approximately 200 residues in length and present in a number of extracellular proteins such as laminins, collagens and some integrins (Humphries, 2000). VWA domains possess a metal ion adhesion site (MIDAS) motif that serves to coordinate a divalent cation, usually Ca^{2+} or Mg^{2+} (Whittaker & Hynes, 2004). VWA domains are generally thought to be involved in protein-protein interactions via shared coordination of a divalent cation. A functional MIDAS motif contains a 5-residue sequence near the N-terminus of the VWA domain which must include DxSxS residues in order to coordinate the divalent cation. $\alpha_2\delta$-1 and $\alpha_2\delta$-2 possess a perfect MIDAS sequence, in which all

coordinating residues are present. $\alpha_2\delta$-3 and $\alpha_2\delta$-4 are not predicted to have a perfect MIDAS sequence although the DxSxS sequence is present in both. $\alpha_2\delta$s have four bacterial chemosensory-like (Cache) domains positioned downstream of the VWA domain. In bacteria, Cache domains are associated with nutrient sensing as well as avoiding harmful substances; however, the role of Cache domains in $\alpha_2\delta$ function remains unclear (Anantharaman & Aravind, 2000; Cheung & Hendrickson, 2010).

1.5.1.2 Post-translational modifications of $\alpha_2\delta$s

All $\alpha_2\delta$ subtypes are expressed as a single pre-protein that is post-translationally cleaved between its α_2 and δ domains. This initially led to the misidentification of α_2 and δ as distinct proteins, however, western blotting of purified $\alpha_2\delta$ under non-reducing conditions revealed that these domains remain associated throughout via pre-existing disulphide bonds (Jay *et al.*, 1991). While post-translational cleavage has long been established for all $\alpha_2\delta$ subtypes, the functional role of this processing step has remained elusive until recently. One of the first insights into the role of $\alpha_2\delta$ processing was a study by Andrade et al (2007) in which point mutations were introduced around the endogenous cleavage site of heterologously expressed $\alpha_2\delta$-1, resulting in a reduction of associated Ca_V currents (Andrade *et al.*, 2007). More recently two studies by the Dolphin lab have shed light on $\alpha_2\delta$ processing. In these studies, the group generated $\alpha_2\delta$-1 and $\alpha_2\delta$-3 mutants in which the endogenous cleavage sequence was substituted for an artificial inducible cleavage sequence (Ferron *et al.*, 2018; Kadurin *et al.*, 2016). Heterologous expression of these $\alpha_2\delta$ cleavage mutants in non-neuronal cell lines showed they were unable to enhance whole-cell Ca_V2 currents but retain the ability to enhance Ca_V plasma membrane expression. However, when expressed in primary hippocampal cultures, it was

found that unprocessed $\alpha_2\delta$ lacked the ability to traffic Ca_V channels to the neurites despite being able to do so itself, when expressed independently of other Ca_V subunits (Kadurin *et al.*, 2016). These somewhat surprising results reveal that $\alpha_2\delta$s play a role in both enhancing Ca_V trafficking and in activation of Ca_V channels, although these roles appear to be only partially related. Furthermore, the inability of unprocessed $\alpha_2\delta$ to facilitate neurite trafficking of Ca_V2s strongly suggests the presence of a neuron specific regulatory step, in which the immature $Ca_V\alpha1{:}\beta{:}\alpha_2\delta$ complex is unable to exit the soma prior to proteolytic $\alpha_2\delta$ processing (Kadurin *et al.*, 2016). As proof of principle, induced cleavage of these $\alpha_2\delta$ mutants rescued their ability to enhance Ca_V currents in cell lines and facilitate Ca_V trafficking in neurons. Following their initial study, the Dolphin lab went on to demonstrate that stimulus-dependent vesicular release probability and asynchronous release in rat hippocampal neurons is inhibited by expression of unprocessed $\alpha_2\delta$ and rescued by induction of $\alpha_2\delta$ cleavage (Ferron *et al.*, 2018). In addition, $Ca_V2.2$ was found to co-immunoprecipitate preferentially with cleaved wild-type (WT) $\alpha_2\delta$ suggesting a stronger association between these subunits following $\alpha_2\delta$ cleavage (Ferron *et al.*, 2018).

1.5.1.3 Recent tools to study proteolytic $\alpha_2\delta$ processing

As mentioned in section 1.5.1.2, the Dolphin lab developed several non-cleavable or cleavage-inducible $\alpha_2\delta$ mutants in order to study this processing step. Three such $\alpha_2\delta$ mutants, termed (V6), (Th) and (3C) were developed with their properties relative to WT $\alpha_2\delta$ described below.

When expressed in tsA-201 cell lines, the (V6), (Th) and (3C) $\alpha_2\delta$ mutants are not cleaved into α_2 and δ polypeptides. Western blotting of (V6), (Th) and (3C) $\alpha_2\delta$s shows the presence of a single 150 kDa band corresponding to the combined molecular weight of these polypeptides; this is shown below in data from (Kadurin *et al.*, 2016) (Fig 1.5A, B). For α_2(Th)δ and α_2(3C)δ, cleavage between α_2 and δ

can be induced by coexpression of Thrombin or 3C-protease respectively, producing the expected lower weight band around 125 kDa correlating to the cleaved α_2 domain (Fig 1.5B). Cell surface biotinylation – shown below for α_2(3C)δ-3 – also confirms that the $\alpha_2\delta$ mutants can reach the plasma membrane in tsA-201 cells (Fig 1.5B). Crucially, unprocessed $\alpha_2\delta$ mutants were shown to be unable to enhance whole-cell currents through $Ca_V2.2$, unlike their WT counterparts, although this effect could be rescued by expression of the relevant protease (Fig 1.5C).

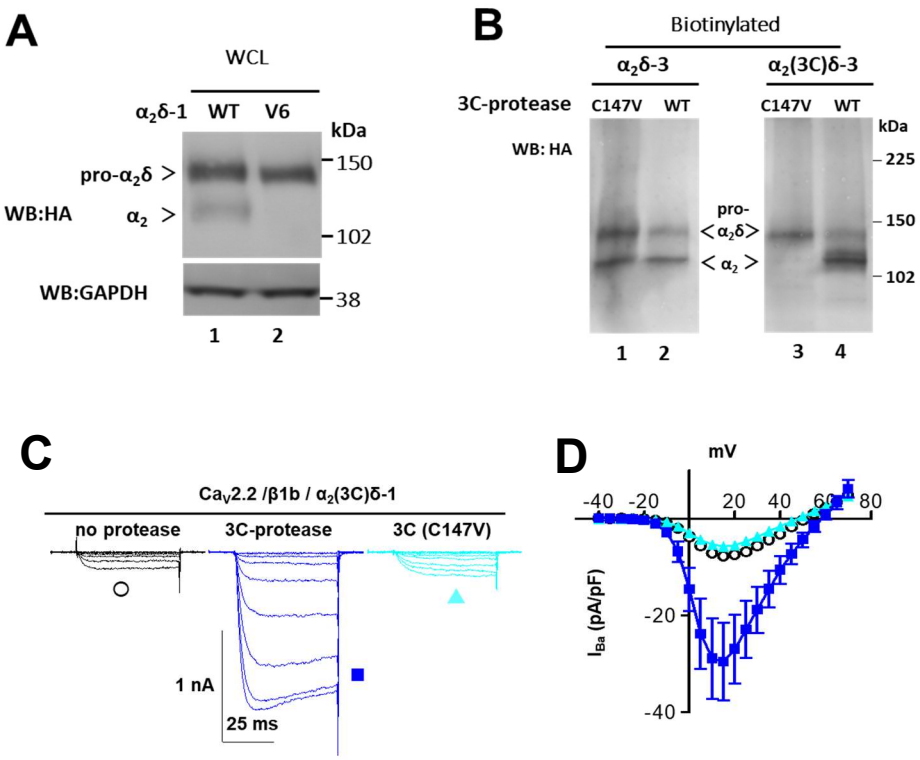

Figure 1.5 Data from Kadurin et al., 2016, western blotting and whole-cell Ca_V currents with α2δ cleavage mutants

(A) Western blot from WCL of WT $\alpha_2\delta$-1-HA (lane 1) and α_2(V6)δ-1-HA (lane 2). **(B)** Western blot of cell-surface biotinylated WT $\alpha_2\delta$-3 (lane 1, lane 2) and α_2(3C)δ-3-HA (lane 3, lane 4) coexpressed with either inactive 3C-protease C147V or WT 3C-protease. **(C, D)** Example traces and mean whole-cell Ba^{2+} currents through Ca_V2.2 coexpressed with β1b, α_2(3C)δ-1 and either WT 3C-protease (blue), inactive C137V 3C-protease (cyan) or no protease (black). All experiments carried out in tsA-201 cells. This work was carried out by Ivan Kadurin and Simon Rothwell.

1.5.1.4 Glycosylation of $\alpha_2\delta$

For all $\alpha_2\delta$ subtypes, there are numerous potential glycosylation sites in both the α_2 and δ domains. $\alpha_2\delta$s are likely to be heavily glycosylated based on the observed

reduction in molecular weight when treated with deglycosylating enzymes (Kadurin *et al.*, 2012). Experimental evidence for the importance of $\alpha_2\delta$ glycosylation was provided in a study by Sandoval et al (2007) in which two sites of N-linked glycosylation, N-136 and N-184, in the α_2 domain of $\alpha_2\delta$-1 were substituted for glutamine and heterologously expressed with $Ca_V2.2$ and β_4 (Sandoval *et al.*, 2007). The study found that whole-cell Ba^{2+} currents through $Ca_V2.2$ were reduced by approx. 45% with mutation of either residue and by approx. 70% with mutation of both residues concurrently (Sandoval *et al.*, 2007). The authors note that there was little difference in currents between conditions lacking $\alpha_2\delta$ entirely and those expressing N136Q/N184Q $\alpha_2\delta$ (Sandoval *et al.*, 2007). In addition, Sandoval et al (2007) observed significant changes in $Ca_V2.2$ current amplitude but minimal changes in other channel properties when expressed with N136Q/N184Q $\alpha_2\delta$. These results are indicative of a reduction in the plasma membrane population of $Ca_V2.2$, and likely reflect a loss of the trafficking functionality of $\alpha_2\delta$-1 (Sandoval *et al.*, 2007). One possible interpretation for these results would be that glycosylation of $\alpha_2\delta$ promotes correct folding of the protein and exit from ER, as the study notes that WT $\alpha_2\delta$-1 appeared to have a faster rate of ER exit than mutant $\alpha_2\delta$-1 (Sandoval *et al.*, 2007).

1.5.1.5 $\alpha_2\delta$ membrane anchoring

All $\alpha_2\delta$ subtypes are predicted to have a short intracellular sequence following a C-terminal hydrophobic stretch that forms a potential transmembrane region (Davies *et al.*, 2007). However, the putative intracellular domain for each subtype is likely too short to form a transmembrane α-helix and it has since been shown through numerous biochemical, immunological and electrophysiological assays that $\alpha_2\delta$s

are highly likely to be membrane-associated through Glycosylphosphatidylinositol (GPI) anchoring (Davies *et al.*, 2010). The predicted GPI anchoring motifs, GCC and GAS are present in all $\alpha_2\delta$ subtypes (Fankhauser & Maser, 2005; Davies *et al.*, 2010). A previous study into the behaviour of a truncated $\alpha_2\delta$-1 construct lacking the putative GPI-site found the construct to be predominantly secreted in the extracellular medium, strongly suggesting GPI-anchoring to be a principal means of membrane association (Kadurin *et al*., 2012). The study by Kadurin et al (2012) also found that some GPI-truncated $\alpha_2\delta$-1 remained associated to detergent-resistant membrane fractions (DRMs/lipid rafts) presumably bound to as yet unidentified binding partners (Kadurin *et al*., 2012)

1.5.1.6 Tissue and subcellular distribution of $\alpha_2\delta$s

$\alpha_2\delta$-1 is strongly expressed in skeletal muscle and is a principal associate of $Ca_V1.2$ in cardiac muscle (Gong *et al*., 2001; Marais *et al*., 2001). However expression of $\alpha_2\delta$-1 is fairly ubiquitous with both messenger ribonucleic acid (mRNA) and protein detectable in central and peripheral neurons (Bauer *et al*., 2009; Newton *et al*., 2001). In addition, $\alpha_2\delta$-1 mRNA expression is partially correlated with excitatory neurons (Cole *et al.*, 2005). $\alpha_2\delta$-2 is less widely expressed than $\alpha_2\delta$-1 but is present in both the human and rodent brain and is particularly high in Purkinje cells of the cerebellum as well as in the striatum and hippocampus (Hobom *et al.*, 2000). In addition, $\alpha_2\delta$-2 mRNA expression in the central nervous system was found to partially correlate with GABAergic neurons (Cole *et al.*, 2005). $\alpha_2\delta$-3 expression in mice is restricted to the brain with particularly high expression in the caudate putamen, cerebral cortex and hippocampus (Gong *et al.*, 2001; Cole *et al.*, 2005). However, there is wider distribution in humans with $\alpha_2\delta$-3 detectable throughout the brain as well as in skeletal and cardiac muscle. $\alpha_2\delta$-4 differs significantly from other $\alpha_2\delta$ subtypes,

having very low expression in the brain. $\alpha_2\delta$-4 expression is largely restricted to endocrine tissues and the retina (Wycisk *et al.*, 2006).

Concentration of $\alpha_2\delta$ in cholesterol-rich DRMs has been reported for both heterologous and natively expressed $\alpha_2\delta$ *(*Kadurin *et al*., 2012). The existence of DRMs remains controversial but was first proposed by Simons & Ikonen (1997) after observing that glycosphingolipid clusters were formed within the exoplasmic leaflet of the Golgi membrane, these microdomains appeared to act as sorting centres for proteins destined for delivery to the apical plasma membrane in epithelial cells (Simons & Ikonen, 1997)

An interesting possibility is that DRMs serve as a platform to coordinate and colocalise functionally related membrane proteins. In line with this concept, $\alpha_2\delta$-4 in the retina has been shown to localise to DRMs (Mercer *et al*., 2011). Disruption of DRMs using cholesterol-depleting agents such as MβCD and COase results in increased $\alpha_2\delta$-4 plasma membrane movement (Mercer *et al*., 2011).

1.5.1.7 $\alpha_2\delta$s in health and disease

$\alpha_2\delta$-1 has a well-established role in the development of neuropathic pain. Experimental peripheral nerve injury models have shown increased $\alpha_2\delta$-1 mRNA in trigeminal and DRG neurons using *in situ* hybridisation, quantitative-polymerase chain reaction (Q-PCR) and microarrays (Newton *et al.*, 2001; Wang *et al.*, 2002). Increased $\alpha_2\delta$-1 mRNA levels have corresponded to elevated $\alpha_2\delta$-1 expression using western blotting and immunohistochemical approaches in DRGs and the spinal cord (Luo *et al.*, 2001; Bauer *et al.*, 2010). Interestingly, these models do not show a change in $Ca_V2.2$ expression. However, increased $\alpha_2\delta$ expression correlates well with enhanced neurotransmitter release in hippocampal cultures, despite an apparently paradoxical reduction in Ca^{2+} entry upon presynaptic

depolarisation. It has been proposed that $\alpha_2\delta$-1 tightens the coupling of Ca^{2+}-dependent neurotransmitter release, thereby reducing the amount of intracellular Ca^{2+} required to elicit vesicle-fusion events (Hoppa *et al.*, 2012).

$\alpha_2\delta$-1 is the likely therapeutic target of the antiepileptic drugs Gabapentin and Pregabalin which are used in the treatment of chronic pain associated with nerve injury. While Gabapentinoids bind to both $\alpha_2\delta$-1 (K_d = 59nM/L) and $\alpha_2\delta$-2 (K_d = 153nM/L), mutational studies in mice strongly suggest that $\alpha_2\delta$-1 is the principal therapeutic target (Gee *et al.*, 1996; Field *et al.*, 2006). In these studies, Gabapentinoid binding was abolished by mutation of the putative Gabapentin binding sites of $\alpha_2\delta$-1/2 (R217A in $\alpha_2\delta$-1 and R279A in $\alpha_2\delta$-2). Pregabalin's therapeutic effect was abolished by mutation of $\alpha_2\delta$-1 but unaffected by mutation of $\alpha_2\delta$-2 (Davies *et al.*, 2006; Hendrich *et al.*, 2008). Mechanistically, gabapentinoids reduce the cell-surface expression of $\alpha_2\delta$-1 by inhibiting $\alpha_2\delta$-1 recycling from Rab11-positive recycling endosomes (Tran-Van-Minh & Dolphin, 2010). As $\alpha_2\delta$-1 has the well-defined function of enhancing presynaptic expression of – and whole-cell currents through – Ca_Vs, the Gabapentin-mediated reduction in plasma membrane $\alpha_2\delta$-1 expression reduces $Ca_V2.2$ activity.

Studies of $\alpha_2\delta$-1 knockout mice, reveal deficits in the behavioural response to mechanical and cold stimulus, which corresponds to the action of wide-dynamic range neurons. This is believed to be a result of reduced $Ca_V2.2$ activity at primary sensory afferents in the dorsal horn (Li *et al*., 2006; Patel *et al*., 2013). A corollary of this data, is the observation that $\alpha_2\delta$-1 overexpressing mice show mechanical withdrawal thresholds comparable to that of WT nerve-ligated control mice. In addition, $\alpha_2\delta$-1 null mice have delayed onset of mechanical hypersensitivity following nerve injury, suggesting that $\alpha_2\delta$-1 activity is highly involved in, but non-essential to, the onset of chronic hypersensitivity.

Mutation of the *CACNA2D2* gene, which encodes $\alpha_2\delta$-2, is found to occur in mice producing a phenotype of spike-wave epilepsy and cerebellar ataxia (Barclay *et al.*, 2001). The *CACNA2D2* mutation of these "Ducky" (*du*) mice results in a loss of full-length $\alpha_2\delta$-2 expression with *du/du* mice exhibiting reduced Ca^{2+} currents from Purkinje cells (Donato *et al.*, 2006).

Deletion of the $\alpha_2\delta$-3 gene in mice or the fly homolog "Straightjacket" in Drosophila has been shown to produce impairments of noxious heat-avoidance which is attributed to altered central processing (Neely *et al.*, 2010). In addition, Neely et al (2010) reported two intronic $\alpha_2\delta$-3 SNPs associated with altered pain perception in humans (Neely *et al.*, 2010).

There are relatively few examples of diseases associated with $\alpha_2\delta$ mutations in humans. However, several missense *CACNA2D1* mutations have been identified that correlate with congenital arrhythmias (Burashnikov *et al.*, 2010). Two $\alpha_2\delta$-1 mutants identified by Burashnikov et al (2010), D550Y and S709N, were found to have decreased cell-surface expression in HEK293T cells, with reduced peak currents through associated $Ca_V1.2$ channels (Bourdin *et al.*, 2010). A missense $\alpha_2\delta$-2 mutant, L1040P, was also identified in three siblings, offspring to cosanguinous parents, presenting early-onset encephalopathy and global developmental delay (Edvardson *et al.*, 2013). $\alpha_2\delta$-2 L1040P expression in *Xenopus laevis* oocytes was found to reduce Ba^{2+} currents through $Ca_V2.2$ and $Ca_V1.2$ currents by 65% and 85% respectively (Edvardson et al 2013). Truncating mutations of the $\alpha_2\delta$-4 gene have been found to underlie a disease phenotype featuring dysfunctional photoreceptors, night blindness and slowly progressing cone cell dystrophy (Dolphin, 2012). In addition, spontaneous mutations have been identified in mouse $\alpha_2\delta$-4, which produce a similar phenotype to that observed in humans. Reported $\alpha_2\delta$-4 disease mutations all produce a truncated protein product and reduced $Ca_V1.4$ activity (Wycisk *et al.*, 2006).

1.5.2 The β subunit

The first β subunit to be cloned was a skeletal muscle isoform termed β1a (Curtis & Catterall, 1984). Following this, three further subtypes were identified: β2, β3, β4 and a neuronal splice variant β1b. Unlike $\alpha_2\delta$, the functional role of β is reasonably well understood and is predominantly a mediator of correct α_1 folding and trafficking through intracellular interactions with the main subunit.

1.5.2.1 Domain structure

β subunits are 50-75 kDa cytosolic proteins with a conserved motif of three core domains: Src Homology domain 3 (SH3). Guanylate kinase domain (GK) and a HOOK domain flanked by highly variable N- and C-terminal regions (Elias & Nicoll, 2007; Funke *et al*., 2005). SH3 is highly conserved between β subtypes and mediates hydrophobic protein-protein interactions via a PxxP site in SH3 and target proteins. The GK domain is also highly conserved but does not retain the enzymatic function of a nucleotide monophosphate kinase, which can convert ATP to guanosine monophosphate (GMP) in order to generate adenosine diphosphate (ADP) and GDP; this domain identifies β as a member of the Membrane-Associated GK protein (MAGUK) family. The GK domain of β subunits are involved in a number of protein-protein interactions with RGKs, GTPases and BK channels among those shown to interact (For details see Buraei & Yang, 2010).

1.5.2.2 Role as an auxiliary subunit of Cavs

β subunits have a well-defined role as chaperones of Ca_V1 and Ca_V2 channels with very little cell-surface expression of these channels in the absence of β. β subunits interact directly with the proximal part of the domain I-II linker of Ca_V1 and Ca_V2 channels. Specifically, β subunits bind to an 18-residue sequence within the I-II linker termed the α-interacting-domain (AID) (Chen *et al.*, 2004). The AID sequence has the conserved residues "QQxExxLxGYxxWIxxxE" in Ca_V1 and Ca_V2 channels and these channels interact with all known β subtypes with an affinity between 2-52 nM depending on the specific Ca_V-β pairing (De Waard *et al*., 1995). Mutation of the conserved AID residues dramatically reduces binding which has been demonstrated with *in vitro* binding assays as well as through reductions in β-mediated Ca_V current enhancement in heterologous expression systems (Campiglio *et al*., 2013). Mechanistically, the AID sequence of α_1 binds to a groove in the GK domain of β formed by three hydrophobic regions termed the α-binding pocket (ABP), this interaction induces a dramatic change in the secondary structure of the I-II linker from a random coil in solution to an α-helix, seen in crystal structures (Chen *et al*., 2004; Opatowsky *et al*., 2004; Van Petegem *et al*., 2004). Restructuring of the I-II linker is extremely important in allowing Ca_Vs to exit the ER although the nature of this regulation appears to differ among Ca_V subtypes. In the case of $Ca_V1.2$ for example, the absence of β leads to ubiquitination and degradation of the channel (Altier *et al.*, 2011). Similarly, β binding, originally thought to hide an ER retention sequence (Bichet *et al.*, 2000), protects $Ca_V2.2$ from polyubiquitination and allows Ca_V2s to exit the ER (Waithe et al., 2011).

1.5.2.3 Role of β subunits in disease

As β subunits are associated with a number of physiological roles, it is unsurprising that mutations and deletions of these genes have deleterious effects in both humans and mouse models. Homozygous deletion of β1 and β2 genes in mice are lethal (Arikkath & Campbell, 2003; Karunasekara *et al*., 2009). Homozygous β1-null mice die shortly after birth due to asphyxiation and exhibit reduced L-type currents as well as diminished muscle mass and other structural abnormalities (Arikkath & Campbell, 2003; Karunasekara *et al*., 2009). Interestingly, heterozygous β1 deletion appears to be asymptomatic, suggesting that 50% β1 expression is sufficient for normal function. The lethality of homozygous β1 deletion is likely due to the lack of alternative neuronal β subtypes.

Analysis of genome-wide single nucleotide polymorphisms (SNP) associated with psychiatric disorders revealed four loci in the β2 gene *CACNB2*. In addition, a separate genome-wide association study (GWAS) for schizophrenic patients revealed 3 loci in *CACNB2* (Breitenkamp *et al.*, 2014). These findings are consistent with a study by Breitenkamp et al (2014) which found three mutations of *CACNB2* in patients with Autism spectrum disorder. Further to this, human juvenile myoclonic epilepsy is associated with mutations in both coding and non-coding regions of *CACNB4*. One such mutation, R482X leads to truncation of the final 38 residues of β4. Expression of this truncated β4 with $Ca_V2.1$ was found to produce alterations in channel gating kinetics which are believed to underlie the pathology. Together these data show that β mutations are associated with a number of neurological disorders which likely result from a loss of associated VGCC activity.

1.5.3 γ subunits

The γ_1 subunit was originally identified as a subunit of skeletal Ca_V1 (Jay *et al.*, 1990). In skeletal muscle γ_1 appears to have a suppressive effect on Ca_V1 currents with γ_1 knockout studies showing increased skeletal Ca_V currents. A further 6 neuronal γ subtypes have since been identified (γ_2- γ_7), although there is little evidence that these proteins can act as Ca_V subunits (Klugbauer *et al.*, 2000). γ_2-γ_8 have however been shown to interact, through a PDZ domain, with AMPA receptors, hence the term Transmembrane AMPA Receptor Proteins (TARPs) (Kato *et al.*, 2007). Previous studies by Moss et al (2002) in which γ_7 was cloned, and Ferron et al (2008) examined whether γ_7 might act as an auxiliary subunit of Ca_Vs. γ_7 expression was found to abolish expression of $Ca_V2.2$ with the study suggesting that γ_7 does not act as a Ca_V subunit but instead binds and sequesters the RNA binding protein, hnRPR A2, doing so prevents interactions between hnRPR A2 and specific mRNA targets (Ferron *et al.*, 2008).

1.6 Rab GTPases guardians of endocytic trafficking

The Rabs constitute the largest family of small GTPases with 66 distinct members of the Rab family expressed in humans (Hutagalung & Novick, 2011). Rabs are known as key regulators of intracellular traffic with different Rabs localising to, and regulating traffic of, distinct membrane compartments. Typically, Rabs control the specificity and directionality of membrane trafficking pathways and are commonly associated with vesicle transport. As individual Rabs tend to localise to distinct membrane compartments, they confer a membrane “identity” that ensures cargoes are transported to the correct destinations (Chavrier *et al.*, 1990; Pfeffer, 2013).

1.6.1 How Rabs work

Similar to other small GTPases, Rabs principally function as molecular switches which cycle between a GTP-bound “on state” and GDP-bound “off state”. Conformational differences between these GDP and GTP bound states generally involves restructuring of 2 regions, Switch I and Switch II, which appear unfolded in a GDP-bound state, but adopt well defined helices when GTP-bound that interact with effector proteins (Sato *et al.*, 2007; Dong *et al.*, 2007) .

1.6.2 Membrane targeting by Rabs

Membrane targeting requires C-terminal prenylation (geranylgeranylation) of two cysteine residues of each Rab as well as the cognate Rab Guanine Nucleotide exchange factor (RabGEF) on the target membrane (Blümer *et al.*, 2013; Pfeffer, 2013). Upon membrane association RabGEFs catalyse a GDP-GTP exchange, activating Rab and allowing it to interact with effectors. Active Rab is subsequently packaged into transport vesicles to mediate formation, movement and fusion of a vesicle with the target membrane. Having reached the target membrane, Rab GTPase activating proteins (RabGAPs) catalyse GTP hydrolysis, inactivating the Rab which is subsequently transported back to the donor compartment with the assistance of GDP-dissociation inhibitor (GDI) (Soldati *et al*., 1993; Ullrich *et al*.,1994).

1.6.3 RabGEFs

The general mechanism of RabGEF activity involves displacing the Switch I region of Rabs, disrupting Mg^{2+} coordination and stabilising of the nucleotide-free form of Rab (Li & Marlin, 2015). This process facilitates GDP-GTP exchange in cells in

which GTP concentrations are 2 orders higher than GDP (Li & Marlin, 2015). There are 5 identified RabGEF families in humans. The principles of RabGEF activity are similar between different RabGEF families, however, they share no sequence or structural homology to one another in the catalytic domain (Barr & Lambright, 2010; Blümer *et al.*, 2013).

1.6.4 RabGAPs

By contrast to RabGEFs, RabGAPs possess a common Trc-2/Bud2/Cdc16 (TBC) domain for catalysis. The TCB domains contain conserved “IxxDxxR” and “YxQ” motifs from which Arg and Gln side chains insert into the GTP-binding site of Rab and stabilise the transition state for GTP hydrolysis, known as the “dual finger” mechanism (Barr & Lambright, 2010). While Rabs do possess innate GTPase activity, this process is typically very slow with RabGAPs being required for efficient GTP hydrolysis.

1.6.5 Rab mediation of vesicular transport

GTP-bound “active” Rabs can interact with multiple effectors to facilitate cargo selection, vesicle movement along actin/microtubulin filaments and vesicle tethering for subsequent fusion events (Hutagalung & Novick, 2011). Rabs may interact directly with cargo, for example Rab5 – in the early endocytic pathway – binds directly to the α subunit of β1 integrins to promote endocytosis (Pellinen *et al.*, 2006). Cargo selection may also be achieved indirectly through Rab effectors such as Rab9 which recruits Mannose-6-phosphate receptors into late endocytic transport vesicles via the effector tail-interacting protein 47 (TIP47) (Carroll *et al.*, 2001). Exocytotic and recycling Rabs such as: Rab3, Rab 8, Rab11 and Rab25,

interact with microtubule motor proteins: Myosins, Kinesins and Dyneins to promote vesicle transport (Lindsay *et al.*, 2013). Class V myosins for example; possess an N-terminal actin-binding motor domain and C-terminal cargo-binding globular tail domain (GTD) which can bind to a number of Rabs on post-Golgi secretory vesicles and recycling endosomes. Recruitment of motor proteins by Rabs can also be indirect, for example Rab11 which can recruit Kinesin I, Kinesin II, Dynein light intermediate chain (LIC)1 and Dynein LIC2 via the Rab11 effectors FH protein interacting protein (FIP)3 and FIP5 (Horgan *et al*.,2010).

1.6.6 Additional Rab functions

While Rab function is typically associated with cargo selection and vesicle transport, a number of Rab effectors have defined signalling properties suggesting a role for Rabs in these signalling pathways. This can be seen through with the Rab5 effectors Adaptor protein, phosphotyrosine interacting with PH domain and leucine zipper **(**APPL)1 and APPL2 which are localised to early endosomes by Rab5 and in turn recruit protein kinase B (AKT) and modulate its target specificity for Glycogen synthase kinase (GSK)-β, rather than Tuberosclerosis complex (TSC)2 (Miaczynska *et al.*, 2004).

1.6.7 Rabs in disease

Despite the primacy of Rabs in numerous trafficking pathways, there are relatively few pathologies associated with mutations to, or altered expression of, Rab genes. This is likely due to a significant degree of redundancy between Rab isoforms. Nonetheless, 5 of the 66 human Rab genes (Rab7, Rab23, Rab27, Rab38 and Rab39b) are linked with genetic disorders (Li & Marlin, 2015). Among the Rab

family, only Rab7 has ubiquitous expression with other Rab members exhibiting cell and tissue type specificity. For Rab7, 4 gain-of-function mutations are associated with Charcot-Marie-Tooth type 2 (CMT2B) disease, a hereditary motor and sensory neuropathy (Verhoeven *et al.*, 2003). All 4 Rab7 mutations increase the rate of nucleotide exchange with Rab7 GEFs, thereby promoting the GTP-bound active form of Rab7 (Spinosa *et al.*, 2008). Interestingly, increased Rab7 activity is most strongly felt in peripheral neurons, with CMT2B also being a neurological disorder, despite the ubiquitous expression of Rab7 (Li & Marlin, 2015). This could reflect a lack of redundancy in peripheral neurons for Rab7 functionality.

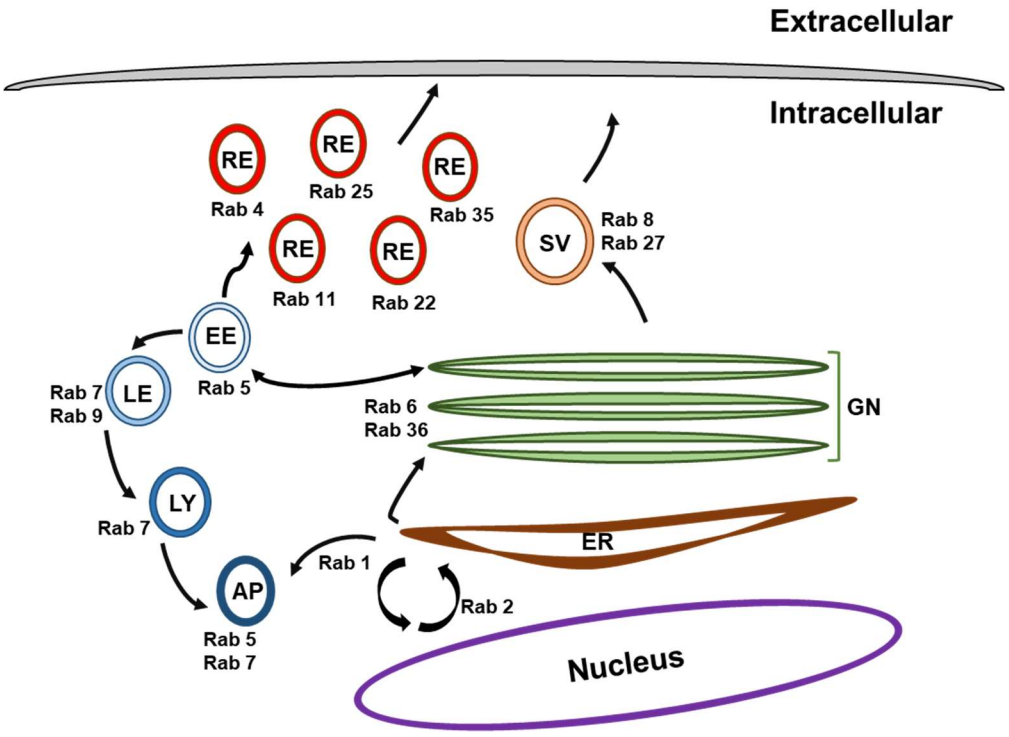

Figure 1.6 Schematic overview of the endocytic pathway

Endoplasmic Reticulum (ER), Golgi Network (GN), Synaptic Vesicle (SV), Recycling Endosome (RE), Early/Sorting Endosome (EE), Late Endosome (LE), Lysosome (LY), Autophagosome (AP).

1.7 Aim of thesis

The principal aim of this thesis is to determine the mechanisms through which $Ca_V2.2$ trafficking is regulated in terms of the relationship between the principal α_1B ($Ca_V2.2$) subunit and associated $\alpha_2\delta$ and β subunits. In particular, this study will examine the trafficking influence of post-translational $\alpha_2\delta$ processing and the role of P-loop glutamate residues in α_1B. In addition, this study seeks to evaluate whether the previously described ability of $\alpha_2\delta$ to influence $Ca_V2.2$ expression is consistent between $\alpha_2\delta$ subtypes, and the basis for the differences observed.

The functional importance of proteolytic $\alpha_2\delta$ processing has been alluded to in previous mutational studies (Andrade *et al.*, 2007; Kadurin *et al.*, 2016). Whole-cell Ca_V currents have been shown to be diminished in the presence of unprocessed $\alpha_2\delta$ mutants. However, the mechanistic explanation for this current decrease has yet to be established. The present study attempts to address this question by examining the behaviour of inducible-cleavage $\alpha_2\delta$ mutants in cell lines and primary neuronal cultures.

Previous work by Kadurin et al (2016) has strongly suggested the presence of a neuron specific mechanism that regulates the trafficking of immature $Ca_V2.2$. Kadurin et al (2016) considered the possibility that such a mechanism may be dependent on the functionality of $Ca_V2.2$. The present study will attempt to address this question by comparing the trafficking and localisation of wild-type and pore-mutated $Ca_V2.2$ channels in primary neurons and non-neuronal cultures.

Lastly, the work presented here utilises the exofacially-tagged $Ca_V2.2$ developed by Cassidy et al (2014) to study the differential effect of $\alpha_2\delta$ subtypes on $Ca_V2.2$ trafficking and localisation. While $\alpha_2\delta$-1 has been demonstrated to reliably increase cell-surface $Ca_V2.2$ expression, this has yet to be demonstrated for other $\alpha_2\delta$ subtypes. $\alpha_2\delta$-1 is an established therapeutic target in the treatment of neuropathic

pain. As such, establishing the distinct properties of $\alpha_2\delta$ subtypes may be important in the development of novel $\alpha_2\delta$-targeting therapeutics as well as understanding the off-target effects of currently used drugs such as gabapentin and pregabalin.

Chapter 2 Materials and Methods

2.1 cDNA constructs

Table 2.1 Description of all cDNA constructs used in this study

Construct	Vector	Tag	Species	Genbank Accession number	Source
HA - $Ca_V2.2$	PCDNA3	2xHA (A566 - V567)	Rabbit	D14157	(Cassidy et al., 2014)
bbs - $Ca_V2.2$	PCDNA3	2xBBS (A566 - V567)	Rabbit	D14157	(Cassidy et al., 2014)
HA - $Ca_V2.2$-GFP	PCAGGS	GFP- (N terminus), 2xHA (A566 - V567)	Rabbit	D14157	Subcloned by J. Meyer
HA - $Ca_V2.2$-$E_{IV}A$	PCDNA3 PCAGGS	2xHA (A566 - V567)	Rabbit	D14157	Developed by W. Pratt
HA - $Ca_V2.2$-$E_{IV}K$	PCDNA3	2xHA (A566 - V567)	Rabbit	D14157	Developed by W. Pratt
HA - $Ca_V2.2$-$E_{I\text{-}IV}A$	PCDNA3 PCAGGS	2xHA (A566 - V567)	Rabbit	D14157	Developed by W. Pratt
$Ca_V2.2$	PMT2		Rabbit	D14157	
$\alpha_2\delta1$- HA	PCDNA3	HA (N549 - D550)	Rat	M86621	(Davis et al 2006)
$\alpha_2\delta1$ - bbs	PCDNA3	BBS (N549 - D550)	Rat	M86621	
$\alpha_2\delta1$	PCDNA3 PCAGGS PMT2		Rat	M86621	
α_2(3C)$\delta1$ - HA	PCDNA3 PCAGGS	HA (N549 - D550)	Rat	M86621	Developed by I. Kadurin
$\alpha_2\delta2$ - HA	PCDNA3	HA (L652 - Q653)	Mouse	AF247139	
$\alpha_2\delta3$ - HA	PCDNA3	HA (K595 - R596)	Mouse	AJ010949	
$\alpha_2\delta3$ - bbs	PCDNA3	BBS (K595 - R596)	Mouse	AJ010949	Subcloned by J. Meyer
$\alpha_2\delta3$	PCDNA3 PCAGGS PMT2		Mouse	AJ010949	Developed by Dolphin lab
β1b	PCDNA3 PMT2			X61394	From Dr T.P. Snutch
Rab11 S25N	pCMV		Human	AF000231	From Prof. T. Hebert, McGill University
CD8					
mCherry	PCAGGS				

2.2 Primary antibodies used in experiments

Name	Epitope	Species	Dilution	Source
HA	(3F10), YPYDVPDYA	Rat	1:500	Roche
II-III loop	II-III loop Ca_V	Rabbit	1:500	In-house (Raghib et al., 2001)
GAPDH		Mouse	1:25000	Ambion

2.2.1 Secondary antibodies used in experiments

Name	Species	Dilution	Conjugate
Anti rabbit IgG	Goat	1:500	AF488, AF594
Anti rat IgG	Goat	1:500 1:1000	AF488, AF594, Biotin, Horseradish peroxidase
Anti Mouse IgG	Goat	1:1000	Horseradish peroxidase
α-Biotin		1:100	AF488, unlabelled
Streptavidin		1:500	AF594, AF633

2.3 Cell lines: culture and transfection

2.3.1 tsA-201 Cells

tsA-201 cells are a variant of Human Embryonic Kidney cells (HEK293), that have been stably transfected with the SV40 large T-antigen, a protein from the Simian Vacuolating Virus 40. This antigen promotes the replication of transfected plasmids containing a SV40 origin of replication. tsA-201 cells were grown in Dulbecco's Modified Eagle Medium (DMEM) (Invitrogen) supplemented with 10% Foetal Bovine Serum, 50 U/ml penicillin/streptomycin and 1% GlutaMAX (Invitrogen). Cells were maintained in tissue culture flasks at 37°C in a humidified atmosphere of 5% CO2 and grown up to 70-90% confluence prior to transfection or further passage.

2.3.2 N2a cell culture

Neuro2a (N2a) cells are a fast-growing cell line derived from a mouse neuroblastoma. N2as may be differentiated by a number of environmental factors to expresses classical neuronal features such a neurofilaments or be used in an undifferentiated “non-neuronal” state. In this study, N2as were cultured in 50% DMEM (with high glucose and L-glutamine) and 50% OPTI-MEM (with L-glutamine), supplemented with 50 U/ml penicillin/streptomycin, 5% FBS, and 1% GlutaMAX (Life Technologies). The N2a cells were cultured to 80% confluence in a 5% CO2 incubator at 37 °C and passaged every 3 to 4 days.

2.3.3 tsA-201 and N2a cell transfection

To transiently express recombinant proteins, N2a or tsA-201 cells were transfected using either PolyJet™ (SignaGen Laboratories) or Fugene® 6 (Promega) in a 3:1 ratio with cDNA mix. tsA-201 cells were plated to 30-60% confluence >3 h prior to transfection. Typically for a 35mm cell culture dish, 2µg cDNA was mixed in a 100µl total with serum-free DMEM, and 6µl PolyJet™ was mixed in a 100µl total volume with serum-free DMEM in separate tubes by pipetting; mixing was done by additional gentle pipetting. DNA and transfection reagent mixes were then combined and incubated for 15 min at room temperature before being added dropwise to the cells. Fugene-transfections were used for electrophysiological experiments with tsA-201 cells, these followed a similar protocol to Polyjet™, with the following changes: DNA and Fugene reagent mixes were incubated for 5 min at room temperature before being combined, once combined the mixture was incubated for a further 30 min at room temperature before being added dropwise to cells.

A typical cDNA mix was 2µg total DNA per 35mm culture dish at a ratio of 3:2:2 = $Ca_V2.2$: β1b: $\alpha_2\delta$. In experiments using Rab11aS25N the cDNA mix was 3:2:2:1 = $Ca_V2.2$: β1b: $\alpha_2\delta$: Rab11aS25N. In conditions lacking a given construct, the DNA mix was supplemented with the appropriate empty vector to have the same total DNA.

For fluorescence imaging experiments in either tsA-201 or N2a cells, all constructs were expressed in a PCDNA3, PRK5 or CMV vector. In electrophysiological experiments using tsA-201 cells, all constructs were expressed in a PMT2 vector, with the exception of Rab11aS25N (CMV).

2.3.4 Hippocampal culture and transfection

Hippocampal neurons were isolated from the hippocampus of P0 rats, which were killed under the Schedule 1 procedure. The cerebrum was cut into two, and the hippocampi were extracted from each hemisphere in ice cold HBSS with 10 mM HEPES. The hippocampi were then cut into small segments and digested gently in Papain solution (7 U/ml Papain, 0.2 mg/ml L-Cysteine, 0.2 mg/ml Bovine Serum Albumin (BSA), 5 mg/ml glucose, 10 mM HEPES in HBSS with 200 µl DNase) in a shaking water both for 40 min at 37 °C. The cells were washed twice with the growth medium (NeuroBasal, 2% B27supplement, 1 unit/ml penicillin, 1 µg/ml streptomycin, 1% Glutamax, 0.1% β-mercaptoethanol), and triturated gently. The cells were plated onto the coverslips that are coated with poly-L-lysine and laminin at 750 cell/µl, 100 µl per coverslip. The entire growth medium was changed after 2 h of plating, and half of the medium was then changed every 3-4 days.

Hippocampal neurons were transfected after 7 days in culture. 2 hours prior to transfection, the growth medium was replaced with a mixture of 50% conditioned, and 50% fresh growth medium. The transfection process was as follows: 4 µg

cDNA was mixed in a 50 µl total with OPTI-MEM™ (Thermo Fischer), 2 µl Lipofectamine®2000 (Thermo Fischer) was mixed in a 50µl total volume of OPTI-MEM™ in separate tubes by pipetting; mixing was done by gentle pipetting. DNA and transfection reagent mixes were then combined and incubated for 5 min at room temperature before being added dropwise to cultures. Hippocampal neurons were cultured for a further 7 days after transfection before fixation and immunostaining.

2.4 Visualisation of calcium ion channels

2.4.1 Immunocytochemistry

Cells were plated onto either coverslips or glass-bottomed dishes (MatTek Corporation) which were coated with poly-L-lysine prior to transfection, and cultured in a 5% CO2 incubator at 37°C. After 36-48 h expression, cells were fixed with ice cold 4% paraformaldehyde (PFA), 4% sucrose in phosphate-buffered saline (PBS), pH 7.4 at room temperature for 5 min. For labelling the HA epitope on the cell surface in non-permeabilised conditions, cells were incubated with primary antibody with 2% BSA and 10% goat serum in PBS at room temperature for 1 h for cell lines or overnight at 4°C for neurons. The secondary antibody was added with 2.5% BSA and 10% goat serum in PBS and incubated for 1 h at room temperature. Cell nuclei were stained with 0.5 µM 4',6'-diamidino-2-phenylindole (DAPI) in PBS for 10 min. The coverslips were mounted onto glass slides using VECTASHIELD® mounting medium (Vector Laboratories). In experiments probing for both cell-surface and intracellular HA epitopes, cells were fixed and blocked as described above, then immunostained for 1 h incubation anti-HA rat antibody, 1 h incubation with anti-rat biotin to mask extracellular HA epitopes. Following this,

cells were permeabilised with 0.2% triton-x-100 for 5 min and re-probed with anti-rat HA antibody 1 h.

2.4.2 Antigen retrieval

This process serves to improve immunocytochemical (ICC) staining by partially denaturing fixed samples as well as breaking some of the covalent bonds created by PFA fixation. By doing so, epitopes that may have been masked - by protein-protein interactions for example - can be exposed for antibody binding.

In this study, the method used for antigen retrieval was achieved by incubating fixed samples in pH 6 citrate buffer at 98˚C for 10 minutes prior to carrying out ICC steps.

2.4.3 Forward trafficking assay

Transfected cells were plated onto 22x22 mm glass coverslips coated with poly-L-lysine, and cultured in a 5% CO2 incubator at 37°C. After 40 h expression, N2a or tsA-201 cells were washed twice with Krebs-Ringer-HEPES (KRH) buffer and incubated with 10 µg/ml unlabelled α-bungarotoxin (α-BTX) (Life technologies) for 30 min at 17°C. The unbound BTX was washed off with KRH, and the cells were then incubated with 10 µg/ml BTX-488 in KRH at 37°C. To terminate the reaction, cells were washed twice with cold KRH and then fixed with 4% PFA, 4% sucrose in PBS at specified times for the kinetic assay. After fixation cells were permeabilised and intracellular expression markers and/or nuclei were labelled as described above. The 22x22 mm coverslips were mounted onto glass slides using VECTASHIELD® mounting medium.

2.4.4 Confocal microscopy

All images were acquired using a LSM 780 Meta scanning confocal microscope (Zeiss), equipped with a Plan-Apochromat 63x/1.4 or a Plan-Apochromat 20x/0.8 M27 objective lens, 16-bit mode. For each experiment, the laser power, gain and acquisition settings were kept constant between images that were used for quantification, although laser power and gain settings may have been adjusted between experiments depending on expression and staining quality of the samples. Where possible, the region of interest was determined by identifying cells with expression of a transfection marker or intracellular staining of the protein of interest (e.g. GFP, $Ca_V2.2$ II-III loop staining), without selecting for the cell surface immunostaining to avoid bias. In experiments where an appropriate intracellular expression marker was absent, nuclei staining with DAPI was used to identify viable cells (having an intact nucleus); cell surface measurements were made for all viable cells per field of view. In addition, on the LSM 780 confocal microscope, the region of interest was selected as described here, and a tile scan of 2x2 or 3x3 was performed to further remove the bias in selecting cells with high expression. For cell surface expression analysis, images were taken with 1 µm optical section when using 63x magnification and a 4.5 µm optical section when using 20x magnification. Confocal images were imported and analysed in ImageJ (National Institutes of Health). The plasma membrane fluorescence was quantified using the freehand brush tool with a selection width of 0.66 µm and tracing the membrane region manually. Intracellular fluorescence was quantified using the freehand selection tool, omitting the signal intensity from the nuclei. The background fluorescence in each channel was measured and subtracted from mean cell surface or intracellular fluorescence measurements in image analysis.

For analysis of neurite expression in hippocampal neurons, an average of 10-15 cells were selected per condition for an individual experiment. Neurons were

selected based on expression of free mCherry as a transfection marker. The freehand brush tool was used to manually trace neurite lengths 25-60 μm in length and 2 μm in width, beginning from a 100 μm distance of the cell soma. Neurites were selected and traced using mCherry to avoid bias, measurements then taken in channels for expression of HA and/or green fluorescent protein (GFP) tags on expressed $Ca_V2.2$ constructs. Background fluorescence measurements were taken for each condition and subtracted from mean fluorescence values during image analysis. Mean neurite signal intensity for each channel was calculated per cell in a given condition and normalised to internal controls. Normalised data was then pooled between experiments with a minimum of three separate experiments. Fluorescence measurements at the neuronal soma were done using the freehand brush tool to manually draw and measure around the cell surface with the freehand selection tool used to measure intracellular fluorescence excluding the nuclei.

In cell surface expression and forward trafficking experiments, all cells chosen for analysis contained $Ca_V2.2$ II-III loop immunostaining, confirming the $Ca_V2.2$ α_1 subunit expression.

For the forward trafficking assay, the membrane fluorescent intensities were fitted to the single exponential association equation (Equation 2), where x is time, y is intensity, y0 is the initial intensity, A is amplitude, and τ is the time constant.

(Equation 2)

$$y = y0 + A(1 - e\frac{^{-x}}{\tau})$$

All experiments were repeated n=3 to n=5, and approximately 30 to 50 cells (N2a) were analysed for each experiment. All data were presented as pooled in the

resulting graphs, except for the trafficking rates and time constants, which are averages of separate experiments.

2.5 Electrophysiology

tsA-201 cells were transfected with cDNA mix containing $Ca_V2.2$, α2δ-1, β1b, and CD8 at a ratio of 3:2:2:0.8 using a Fugene transfection protocol. After 40 h expression, cells were replated in cell culture medium at 1 in 3 or 5 dilution depending on their confluency. Transfected cells were identified by co-expression of CD8. CD8 expression was detected with CD8 Dynabeads (Life Technologies). Whole-cell currents were recorded in voltage-clamp mode in following solutions; intracellular (electrode) solution (mM): 140 Cs-aspartate*, 5 EGTA, 2 $MgCl_2$, 0.1 $CaCl_2$, 2 K_2ATP, 20 HEPES, pH 7.2, 310 mOsm (* 0.5 M stock is made with 6.65 g L-aspartic acid in 50 ml H_2O and 3 M CsOH was added to adjust the pH to 7.2, then H2O was added to make up to 100 ml). Extracellular solution (mM): 1 $BaCl_2$, 3 KCl, 1 $NaHCO_3$, 1 $MgCl_2$, 10 HEPES, 4 D-glucose, 160 tetraethylammonium bromide, pH 7.4, 320 mOsm. The borosilicate glass electrode resistance was between 1.5 and 4 MΩ. Cell capacitance and series resistance were compensated to 60-70 %. Whole-cell currents were recorded on Axopatch-200B amplifier using pClamp 9 or 10 (Molecular Devices). The cells were held at -90 mV, and 50 ms pulses were applied in +10 mV steps between -50 mV and +50 mV. To correct for the leak current, P/8 leak subtraction protocol was applied. Recordings were made at 20 kHz sampling frequency and filtered at 5 kHz (lowpass 4-pole Bessel filter) in the amplifier. The digital low-pass 8-pole Bessel filter with 1 kHz 3dB cut-off was applied in Clampfit 10.7 (Molecular Devices) before the current amplitudes were determined. Average peak currents were taken between 8–13 ms after the test potentials were applied and normalized to the cell capacitance to obtain current

density. Current-voltage (IV) relationships were fitted to a modified Boltzmann equation (Equation 3) to give V_{50} activation (V_{50}, act), conductance (G_{max}), and reversal potential (V_{rev}) using OriginPro 2018.

(equation 3)

$$I = \frac{Gmax(V - Vre\ )}{1 + e^{\frac{-(V - V50\ act)}{K}}}$$

2.6 Sample numbers

The number of samples (n) in most of the experiments in this study is the total number of individual cells analysed, which are pooled from a minimum of three separate experiments unless stated otherwise. Data from individual experiments were normalised to their control conditions prior to being pooled to account for inter-experimental variance. Mean values and standard error of mean (SEM) were calculated for normalised, pooled data. The only exception is for the experiments determining the rates of $Ca_V2.2$ trafficking, in which the rate of $Ca_V2.2$ trafficking was determined from each experiment by analysing 20 to 50 cells per data point, with the mean and SEM values determined from the repeated experiments.

2.7 Statistical analysis

Statistical analysis was performed using Student's t test or one-way ANOVA with Bonferroni post-hoc test as appropriate in GraphPad Prism. All the data were expressed as mean ± SEM.

Chapter 3

Establishing the role of proteolytic α2δ processing

3.1. Introduction

$\alpha_2\delta$ was first purified from skeletal muscle tissue along with the L-type calcium channel (Curtis & Catteral., 1984). This work identified 5 components: α_1 (170 kDa), α_2 (150 kDa), δ (17-25 kDa), β (52 kDa) and γ (30 kDa) (Takahashi *et al.*, 1987). Initially α_2 and δ were thought to exist as distinct proteins. However, subsequent purification of these subunits under non-reducing conditions suggested that α_2 and δ remain associated through disulphide bonding. It has since been established that all $\alpha_2\delta$ subtypes are expressed as a single protein that is proteolytically cleaved between the α_2 and δ domains, which remain associated by pre-existing disulphide bonds (Jay *et al.*, 1991; Patel *et al.,* 2003). When purified from plasma membrane fractions, endogenously expressed $\alpha_2\delta$ is found to be almost universally cleaved (Kadurin *et al.*, 2012). However, unprocessed "pro-$\alpha_2\delta$" is observed at the plasma membrane in heterologous overexpression systems such as tsA-201 cells (Kadurin *et al.*, 2012, 2016). This result indicates that pro-$\alpha_2\delta$ is able localise to the plasma membrane, at least in cell lines. In addition, pro-$\alpha_2\delta$ has been shown to accumulate within the cell bodies of DRG neurons from spinal nerve ligated rats (Bauer *et al.*, 2009). In both native and heterologous systems, significant fractions of pro-$\alpha_2\delta$ seem only to be found under conditions of elevated $\alpha_2\delta$ expression. This could suggest that sizeable pro-$\alpha_2\delta$ populations are present only when $\alpha_2\delta$ expression exceeds the capacity of an as-yet-unknown protease(s). Consistent with this interpretation, an upregulation of $\alpha_2\delta$-1 mRNA and protein levels in sensory neurons is observed in a number of peripheral nerve injury (Luo *et al.*, 2001; Newton *et al.*, 2001; Bauer, Tran-Van-Minh, *et al.*, 2010). It is

also possible that proteolytic $\alpha_2\delta$ processing activity is reduced in peripheral nerve injury models; however, the responsible protease(s) would need to be identified before this could be investigated.

While $\alpha_2\delta$ processing has long been established, the functional purpose, subcellular location of proteolysis and responsible proteases have been poorly understood. Seminal work by the Catterall and Campbell groups identified the cleavage site of $\alpha_2\delta$-1 through peptide sequencing (De Jongh *et al*., 1990; Jay *et al.*, 1991). To study the function of $\alpha_2\delta$ processing, a number of $\alpha_2\delta$ mutants were developed in our lab in which the residues of the predicted $\alpha_2\delta$ cleavage site had been mutated to prevent endogenous cleavage. The first of these α_2(V6)δ-1, features a hexavaline substitution in place of the endogenous $\alpha_2\delta$-1 cleavage site, following unsuccessful attempts to prevent cleavage with more conservative mutations.

In the present study, three $\alpha_2\delta$ cleavage mutations were used: α_2(3C)δ, α_2(Th)δ and α_2(V6)δ, with variants for both $\alpha_2\delta$-1 and $\alpha_2\delta$-3; these constructs were also Haemeglutinin (HA) tagged as described in (Davies *et al.*, 2007). The endogenous cleavage sequence of $\alpha_2\delta$-1 and $\alpha_2\delta$-3 as well the mutations used and key structural features of $\alpha_2\delta$s are shown in (figure 3.1) below:

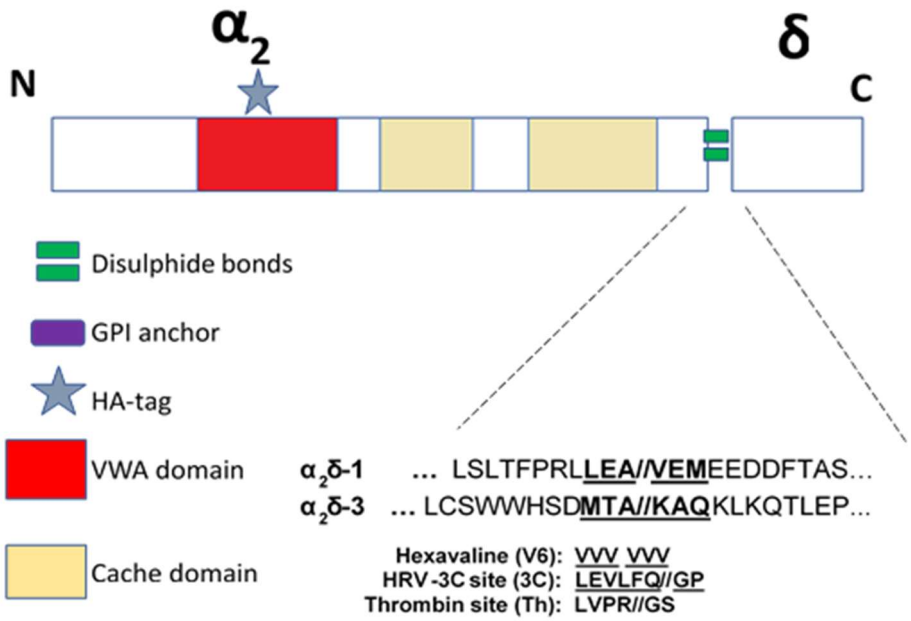

Figure 3.1. Schematic of $\alpha_2\delta$ structure

Shows key conserved $\alpha_2\delta$ structural domains, position of inserted HA-tag, site of proteolytic processing for $\alpha_2\delta$-1 and $\alpha_2\delta$-3 and sequences for (V6), (Th) and (3C) cleavage mutations, N and C termini are indicated.

The purpose of this study was to identify the role of proteolytic $\alpha_2\delta$ processing. Since $\alpha_2\delta$ cleavage mutants do not enhance whole-cell Ca_V2 currents, I examined whether incomplete processing might prevent efficient trafficking of $\alpha_2\delta$ to the plasma membrane or the ability of $\alpha_2\delta$ to enhance cell-surface $Ca_V2.2$ expression. To achieve this, I used confocal microscopy to compare the expression level and localisation HA-tagged WT and unprocessed $\alpha_2\delta$ mutants in N2a cells. After this, I assessed the ability of processed and unprocessed $\alpha_2\delta$ variants to enhance cell-surface and total expression of exofacially-tagged $Ca_V2.2$ in both N2a and tsA-201 cells.

3.2 Expression and localisation of non-cleavable $\alpha_2\delta$ mutants

3.2.1 α_2(V6)δ-1 shows limited cell-surface expression but high intracellular expression relative to WT $\alpha_2\delta$-1

Western blotting analysis has shown that α_2(V6)δ-1 can be expressed in tsA-201 cells and resists proteolytic processing (Chapter 1, Fig 1.5A). Here, I express HA-tagged α_2(V6)δ-1 or $\alpha_2\delta$-1 WT in N2a cells with and without additional channel subunits. After 48 h expression, cells were fixed and immunostained for cell-surface and intracellular HA expression prior to confocal imaging and analysis (Fig 3.2A). When expressed without additional Ca_V subunits, cell-surface α_2(V6)δ-1 was 62% lower than WT (Fig 3.2B), while intracellular α_2(V6)δ-1 expression was 60% higher than WT (Fig 3.2C). When either HA-tagged WT or (V6) $\alpha_2\delta$-1 are coexpressed with $Ca_V2.2$ and β1b subunits, I observe a reduction in cell-surface and intracellular HA signal intensity; cell-surface signal intensity was 65% lower for WT and 70% lower for (V6) $\alpha_2\delta$-1 (Fig 3.2B), while intracellular signal was reduced by 42 and 70% for WT and (V6) respectively (Fig 3.2C).

When directly compared, α_2(V6)δ-1 appears to be far less efficient at either trafficking to – or occupying – the plasma membrane than WT $\alpha_2\delta$-1 (Fig 3.2A,B). Reduced cell membrane α_2(V6)δ-1 is unlikely to be a consequence of diminished protein expression as α_2(V6)δ-1 displayed notably higher intracellular signal than WT (Fig 3.2C). These results could suggest that α_2(V6)δ-1 is retained intracellularly although not subject to extensive proteolytic degradation, which might be expected if α_2(V6)δ-1 were misfolded. A loss of HA signal intensity was observed for WT and (V6) $\alpha_2\delta$-1 when expressed with $Ca_V2.2$/β1b subunits; this effect has previously been reported by Cassidy et al (2014) who provided evidence that protein-protein interactions between $Ca_V\alpha_1$ and $\alpha_2\delta$-1 occlude the HA epitope which is positioned

in the α_2 domain. It therefore seems likely that the α_2 domain of α_2(V6)δ-1 retains an interaction with the principal α_1 subunit.

It is tempting to consider that α_2δ-1 requires proteolytic processing for normal cell-surface expression. However, this is difficult to verify with α_2(V6)δ-1 as it is not possible to induce cleavage unlike with α_2(Th)δ-1 and α_2(3C)δ-1. It should also be considered that the introduction of the 6-valine sequence to α_2δ-1 could promote hydrophobic interactions, potentially making the protein susceptible to aggregation.

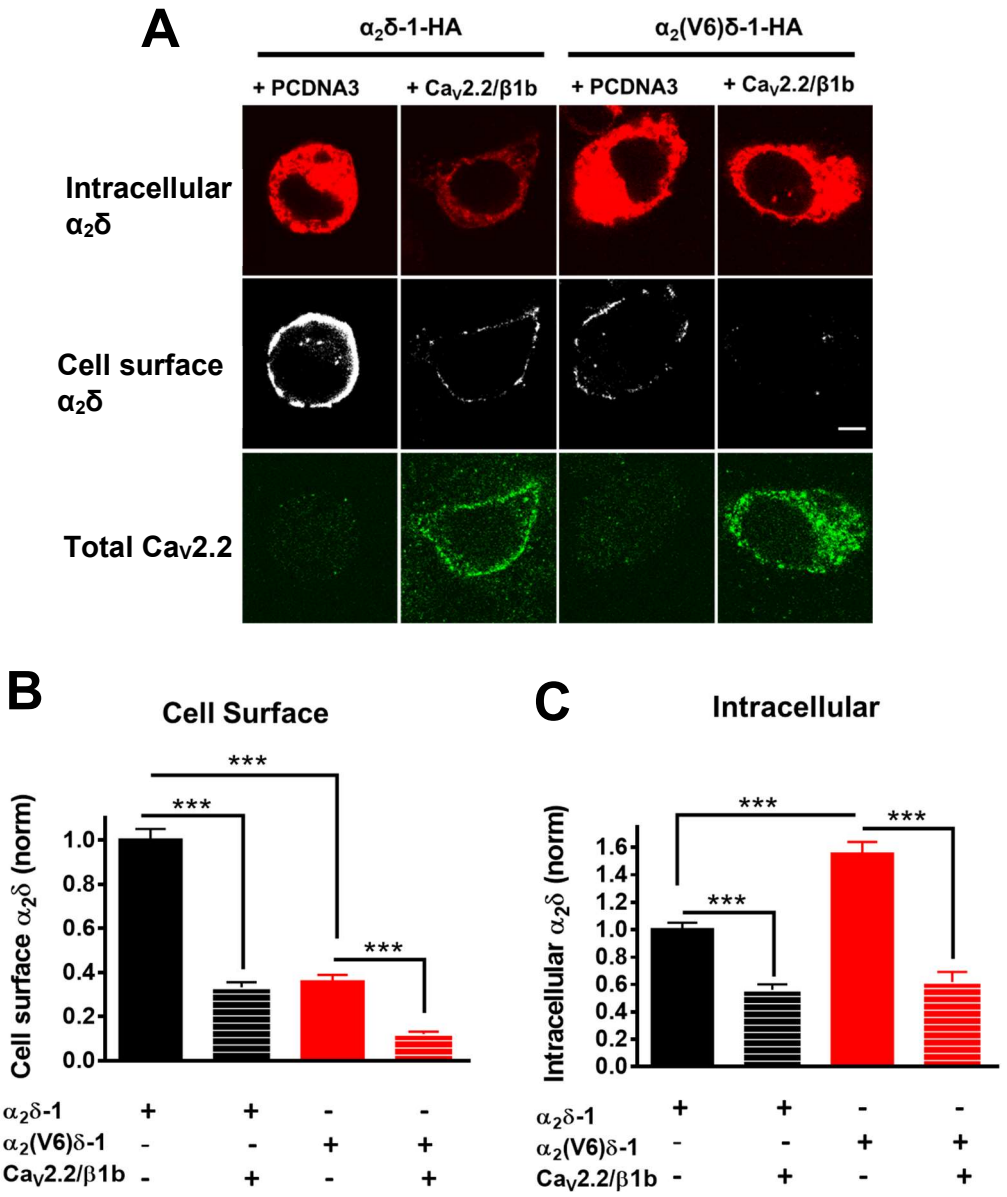

Figure 3.2 Cell-surface and intracellular expression of WT and (V6) $\alpha_2\delta$-1 in the presence or absence of $Ca_V2.2$ and β1b

(A) Example confocal images of intracellular (top row) and cell-surface (middle row) HA-tagged $\alpha_2\delta$-1 WT or α_2(V6)δ-1 expressed in N2a cells with either $Ca_V2.2$/β1b or empty vector PCDNA3 (bottom row). (Scale bar 5μm). **(B)** Normalised mean cell surface fluorescence (bar chart) of $\alpha_2\delta$-1 (black, n = 193), $\alpha_2\delta$-1 + $Ca_V2.2$/β1b (black striped, n = 183), α_2(V6)δ-1 (red, n = 137), α_2 (V6)δ-1 + $Ca_V2.2$/β1b (red striped, n = 121). **(C)** Normalised mean intracellular fluorescence (bar chart) of $\alpha_2\delta$-1 (black), $\alpha_2\delta$-1 + $Ca_V2.2$/β1b (black striped), α_2(V6)δ-1 (red), α_2 (V6)δ-1 + $Ca_V2.2$/β1b (red striped). Data collected from 3 separate transfections. Data are plotted ± SEM values. Data analysis was blinded. Statistical significance was determined using 1-way ANOVA and Bonferroni post hoc tests ****p<0.001*.

3.2.2 α_2(Th)δ-1 shows reduction in cell-surface expression relative to WT α_2δ-1

Here I compare the cell-surface and intracellular expression of α_2(Th)δ-1 to WT α_2δ-1 in N2a cells using the same immunocytochemical approach as carried out for α_2(V6)δ-1. WT α_2δ-1-HA or α_2(Th)δ-1-HA were transiently expressed in N2a cells for 48 h with either empty vector PCDNA3 or $Ca_V2.2$ and β1b subunits. After this, cells were immunostained for cell-surface HA, intracellular HA and II-III loop expression (Fig 3.3A) as described in section 2.4.1 In the absence of $Ca_V2.2$ and β1b subunits, cell-surface α_2(Th)δ-1 expression is 33% lower than α_2δ-1 WT (Fig 3.3B), however there was no statistically significant difference in intracellular HA expression between WT and (Th) α_2δ-1 (Fig 3.3C). I observe a large reduction in cell-surface α_2δ-1 signal intensity for both α_2δ-1 WT and α_2(Th)δ-1 when expressed with $Ca_V2.2$ and β1b subunits; cell-surface α_2δ-1 WT with $Ca_V2.2$ and β1b was 91% lower than when α_2δ-1 was expressed alone (Fig 3.3B). Cell-surface α_2(Th)δ-1 with $Ca_V2.2$ and β1b was similarly reduced by 89% relative to α_2(Th)δ-1 expressed with empty vector (Fig 3.3B). Interestingly, intracellular α_2(Th)δ-1 signal intensity was not significantly different whether expressed with empty vector or Ca_V subunits (Fig 3.3C). I do however observe a statistically significant 44% reduction in intracellular signal intensity for WT α_2δ-1 with $Ca_V2.2$ and β1b coexpressed, relative to WT α_2δ-1 with empty vector (Fig 3.3C).

As with seen with α_2(V6)δ-1, cell-surface α_2(Th)δ-1 signal intensity was found to be consistently lower than that of WT α_2δ-1 (Fig 3.3A), although the 33% difference in cell-surface intensity between WT and (Th) α_2δ-1 was considerably smaller than the 62% disparity between WT and (V6) α_2δ-1 (Fig 3.3B). This would suggest that that α_2(Th)δ-1 is more efficiently trafficked to, or maintained at, the cell-surface than α_2(V6)δ-1. The reduced cell-surface intensity of α_2(Th)δ-1 is unlikely to be a

result of diminished total expression as I do not observe a difference between WT and (Th) $\alpha_2\delta$-1 in this regard.

As with WT and (V6) $\alpha_2\delta$-1, cell-surface α_2(Th)δ-1 signal intensity is reduced by coexpression of $Ca_V2.2$ and β1b subunits (Fig 3.3A), possibly indicating a conserved $Ca_V2.2$-α_2(Th)δ-1 interaction masking the antibody binding epitope. However, unlike for WT $\alpha_2\delta$-1, I do not observe a decrease in intracellular α_2(Th)δ-1 signal intensity with $Ca_V2.2$/β1b coexpression. A possible explanation is that the interaction between α_2(Th)δ-1 and $Ca_V2.2$ is diminished or that there is a change in the spatial orientation of the complex in which the HA-tag of α_2(Th)δ-1 is not occluded by $Ca_V2.2$. As previously mentioned (section 3.1), α_2(Th)δ-1 does not undergo proteolytic cleavage in the absence of thrombin. During this study it was discovered that α_2(Th)δ-1, possesses an additional ectopic thrombin cleavage site. As such, it was not possible to test the effect of specific α_2 and δ-1 cleavage through thrombin coexpression or extracellular application. However, subsequent work using an α_2(Th)δ-3 construct, which does not possess ectopic thrombin sites, reveals that α_2(Th)δ-3 cleavage can be induced by application of extracellular thrombin. Furthermore, thrombin-cleaved α_2(Th)δ-3 is able to enhance whole-cell $Ca_V2.2$ currents (Kadurin et al, 2016).

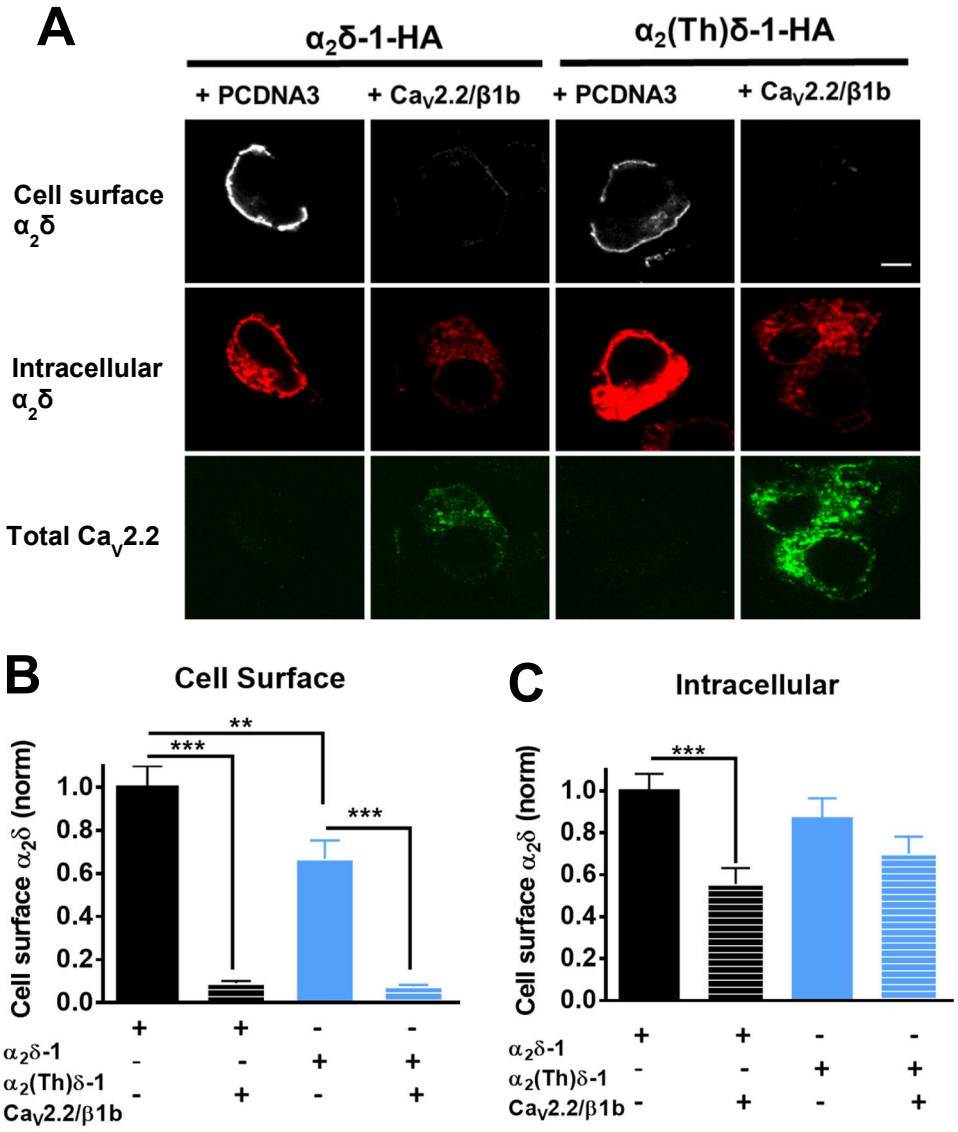

Figure 3.3 Cell surface and intracellular expression of WT and (Th) α$_2$δ-1 in the presence or absence of Ca$_V$2.2 and β1b

(A) Example confocal images of cell-surface (top row) and intracellular (middle row) HA-tagged α$_2$δ-1 wild type or α$_2$(Th)δ-1 expressed in N2a cells with either Ca$_V$2.2/β1b or empty vector PCDNA3 (bottom row). (Scale bar 5μm). **(B)** Normalised mean cell surface fluorescence (bar chart) of α$_2$δ-1 (black, n = 78), α$_2$δ-1 + Ca$_V$2.2/β1b (black striped, n = 61), α$_2$(Th)δ-1 (blue, n = 59), α$_2$ (Th)δ-1 + Ca$_V$2.2/β1b (blue striped, n = 51). **(C)** Normalised mean intracellular fluorescence (bar chart) of α$_2$δ-1 (black), α$_2$δ-1 + Ca$_V$2.2/β1b (black striped), α$_2$(Th)δ-1 (blue), α$_2$ (Th)δ-1 + Ca$_V$2.2/β1b (blue striped). Data were collected across 2 separate transfections. Data analysis was blinded. Data are plotted ± SEM values. Statistical significance was determined using Bonferroni and post hoc tests ****p<0.001*, ***p<0.01*.

3.2.3 α_2(3C)δ-1 shows partial reduction in cell-surface and intracellular expression relative to WT α_2δ-1

Human Rhinovirus (HRV) is a small single stranded virus belonging to the *picorinviridae* family (Palmenberg *et al*., 2011). HRV encodes three proteases (2A, 3CD and 3C) which are responsible for processing of viral proteins and have also been linked to cleavage of host cell transcription machinery for the purpose of shutting down replication of host proteins and leading to upregulation of viral transcription and translation (Svitkin *et al.*, 1999). Unlike thrombin, 3C-protease is exogenous to mammalian cells and is not predicted to cleave endogenous sequences in α_2δ. α_2(3C)δ-1 and α_2(3C)δ-3 express as single unprocessed proteins with α_2 and δ cleavage inducible by coexpression of 3C-protease (Kadurin *et al*., 2016).

Using the same confocal microscopy approach described for α_2(V6)δ and α_2(Th)δ (Section 2.4.1), I compared the expression and localisation of WT and (3C) α_2δ-1 in N2a cells in the presence or absence of $Ca_V2.2$ and β1b subunits (Fig 3.4A). I found that mean cell-surface signal intensity for α_2(3C)δ-1 is 28% lower than WT α_2δ-1 when expressed in the absence of additional channel subunits (Fig 3.4B). While statistically significant, this disparity in cell-surface staining between WT and (3C) α_2δ-1 (28% reduction) is smaller than that observed for α_2(V6)δ-1 (62% reduction). Intracellular signal intensity for α_2(3C)δ-1 was found to be 52% lower than for WT α_2δ-1 (Fig 3.4C), making it difficult to conclude whether α_2(3C)δ-1 has proportionally reduced membrane expression or whether the difference observed in cell-surface signal is due to lower total expression of α_2(3C)δ-1 relative to WT α_2δ-1. Indeed, as the difference in intracellular signal for WT and (3C) α_2δ-1 appears larger than the difference in cell-surface signal, it may be the case that α_2(3C)δ-1 has a similar or greater plasma membrane expression compared to WT α_2δ-1 as a proportion of its total expression in a cell.

When expressed with $Ca_V2.2$ and β1b subunits, I observe the characteristic loss of cell-surface staining for α_2(3C)δ-1, which is 78% lower than that for α_2(3C)δ-1 expressed with empty vector (Fig 3.4B); once again the loss of cell-surface signal intensity can be attributed to occlusion of the HA-eptiope of α_2(3C)δ-1 through its interaction with $Ca_V2.2$. However, I do not observe a change in intracellular signal intensity for α_2(3C)δ-1 when expressed with or without Ca_V subunits (Fig 3.4C), despite a 26% reduction in the intracellular signal of WT α_2δ-1 when expressed with Ca_V subunits. This result mirrors my observations for α_2(Th)δ-1 (Fig 3.3C) and may be indicative of an altered intracellular interaction between unprocessed α_2δ-1 mutants and $Ca_V2.2$. Furthermore, the lack of change in intracellular signal intensity when α_2(3C)δ-1 is expressed with $Ca_V2.2$ provides good evidence that the observed loss of cell-surface α_2(3C)δ-1 signal is not due to a decrease in total α_2(3C)δ-1 expression under these conditions.

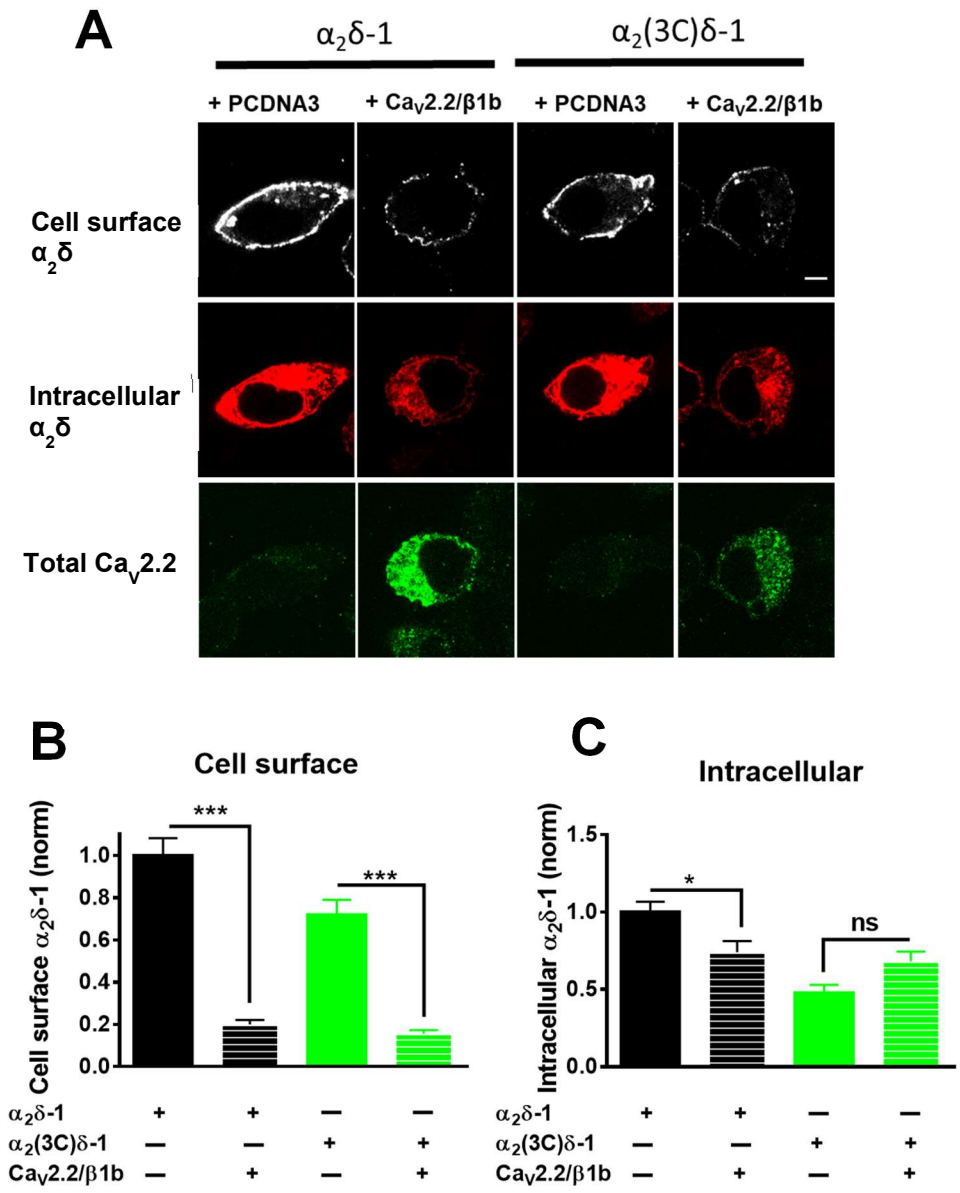

Figure 3.4 Cell-surface and intracellular expression of WT and (3C) $\alpha_2\delta$-1 in the presence or absence of $Ca_V2.2$ and β1b

(A) Example confocal images of cell-surface (top row) and intracellular (middle row) HA-tagged WT $\alpha_2\delta$-1 or α_2(3C)δ-1 expressed in N2a cells with either $Ca_V2.2$/β1b or empty vector PCDNA3 (bottom row). (Scale bar 5μm). **(B)** Normalised mean cell surface fluorescence (bar chart) of $\alpha_2\delta$-1 (black, n = 197), $\alpha_2\delta$-1 + $Ca_V2.2$/β1b (black striped, n = 175), α_2(3C)δ-1 (green, n = 204), α_2 (3C)δ-1 + $Ca_V2.2$/β1b (green striped, n = 193). **(C)** Normalised mean intracellular fluorescence (bar chart) of $\alpha_2\delta$-1 (black), $\alpha_2\delta$-1 + $Ca_V2.2$/β1b (black striped), α_2(3C)δ-1 (green), α_2 (3C)δ-1 + $Ca_V2.2$/β1b (green striped). Data collected from 3 separate transfections. Data analysis were blinded. Data are plotted ± SEM values. Statistical significance was determined using 1-way ANOVA and Bonferroni and post hoc test ****p<0.001.*

3.2.4 Induced cleavage of α_2(3C)δ-3 does not affect cell-surface or intracellular expression

As demonstrated by Kadurin et al (2016), cleavage of α_2(3C)δ-1 and α_2(3C)δ-3 can be induced by coexpression of 3C-protease, allowing a more direct comparison of the role of proteolytic processing on the expression and trafficking of α_2δ. The effect of induced cleavage on α_2(3C)δ-1 was previously examined by Ivan Kadurin of the Dolphin lab, and found not to influence total or cell-surface α_2(3C)δ-1 expression (Kadurin *et al.*, 2016). However, I considered the possibility that induced cleavage may differentially influence α_2δ subtypes. Here, I investigate whether induced cleavage of α_2(3C)δ-3 affects cell-surface or total α_2(3C)δ-3 levels in cell lines. I expressed α_2(3C)δ-3 in N2a cells along with empty vector or 3C-protease, then used confocal microscopy to compare cell-surface and intracellular expression of α_2(3C)δ-3 under these conditions (Fig 3.5A). When comparing these conditions, I did not find any statistically significant change in either cell-surface signal (Fig 3.5B) or intracellular signal (Fig 3.5C). The inability of induced cleavage to rescue or enhance α_2(3C)δ-3 signal intensity suggests that proteolytic processing of α_2δ-3 is not a determinant of trafficking or membrane occupation, at least when α_2δ is expressed without Ca_V channel subunits. However, it remains a possibility that induced cleavage of α_2(3C)δ-3 does not precisely replicate endogenous processing of WT α_2δ-3. With this caveat in mind, it should be noted that induced cleavage of α_2(3C)δ-3 has been shown to rescue whole-cell currents through $Ca_V2.2$, as shown with α_2(Th)δ-3 (Kadurin et al, 2016). Together, these results imply a trafficking-independent role for α_2δ when expressed in non-neuronal cell lines.

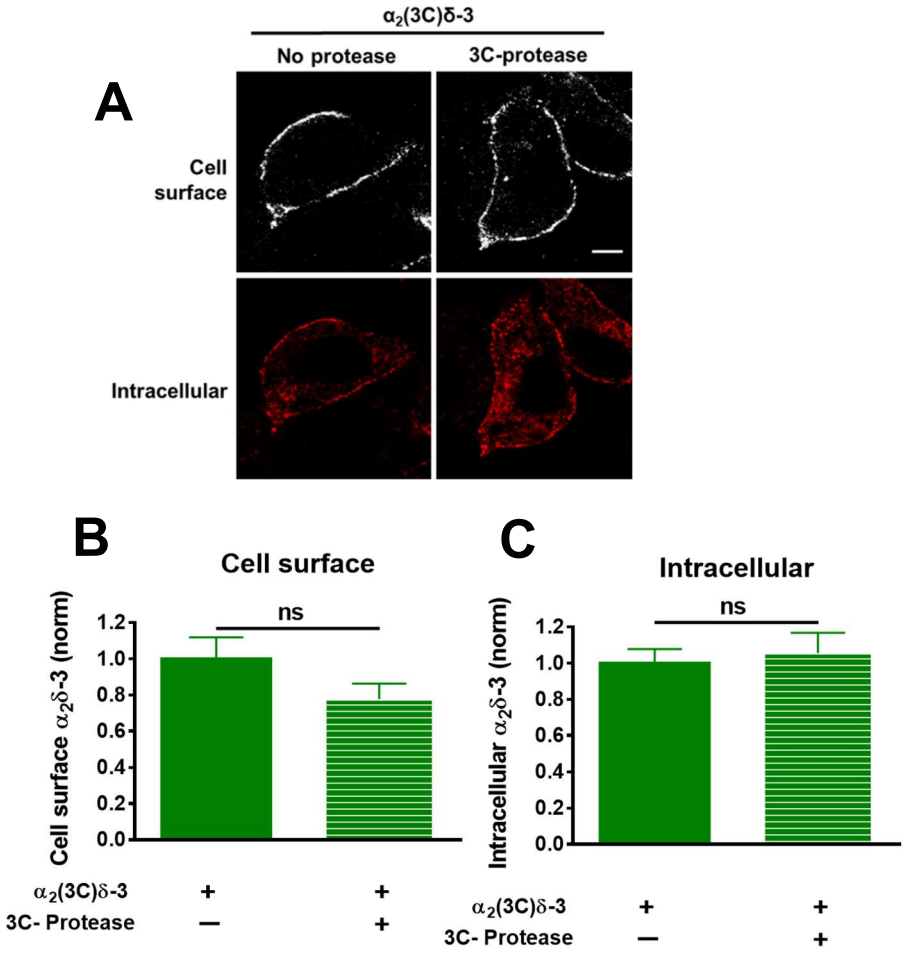

Figure 3.5 Cell-surface and intracellular expression of α_2(3C)δ-3 with and without induced α_2δ cleavage.

(A) Confocal Images showing cell-surface (upper row) and intracellular (lower row) α_2(3C)δ-3-HA in N2a cells, with empty vector (panel 1) or 3C-protease (panel 2). Scale bar 5µm. **(B)** Lack of effect of 3C-protease (bar chart) on cell-surface expression of α_2(3C)δ-3 (green bar, n = 164) or α_2(3C)δ-3 with 3C-protease (green, striped bar, n = 187). **(C)** Lack of effect of 3C-protease (Bar chart) on intracellular expression of α_2(3C)δ-3 (green bar) or α_2(3C)δ-3 with 3C-protease (green, striped bar). Data were collected across 3 separate transfections. Data analysis was blinded. Data are plotted ± SEM values. Statistical difference determined by Student's t test, ns = P>0.05.

3.3 The influence of $\alpha_2\delta$ cleavage on $Ca_V2.2$ expression and localisation

3.3.1 Proteolytic processing of $\alpha_2\delta$-1 is not required for trafficking of the $Ca_V2.2$ complex in cell lines.

To investigate whether $\alpha_2\delta$ processing was required for enhancing the trafficking of the $Ca_V2.2$ complex, I transiently expressed exofacially-tagged $Ca_V2.2$-bbs and β1b in undifferentiated N2a cells and compared cell-surface and total $Ca_V2.2$-bbs expression when coexpressed with either WT or (3C) $\alpha_2\delta$ using confocal microscopy and image analysis. After 48 h expression, N2a cells were live-labelled with α-BTX AF488 to identify the plasma membrane-inserted $Ca_V2.2$ population. Cells were then fixed, permeabilised and immunostained for the II-III loop epitope of $Ca_V2.2$, used to measure total $Ca_V2.2$ expression (Fig 3.6A). This revealed that both WT and (3C) $\alpha_2\delta$-1 are able to enhance cell-surface $Ca_V2.2$ expression by ~130% when compared to their expression in the absence of $\alpha_2\delta$ (Fig 3.6B). In addition, expression of $Ca_V2.2$, as assessed by II-III loop antibody staining, showed an increase of (70%) and (48%) with coexpression of WT or (3C) $\alpha_2\delta$-1 respectively (Fig 3.6C). Furthermore, no difference was observed in either cell-surface or total $Ca_V2.2$ expression when coexpressed with HRV3C protease (Fig 3.6D, E, F). These data strongly suggest that the function of $\alpha_2\delta$-1 as an enhancer of $Ca_V2.2$ expression in cell lines does not require proteolytic processing.

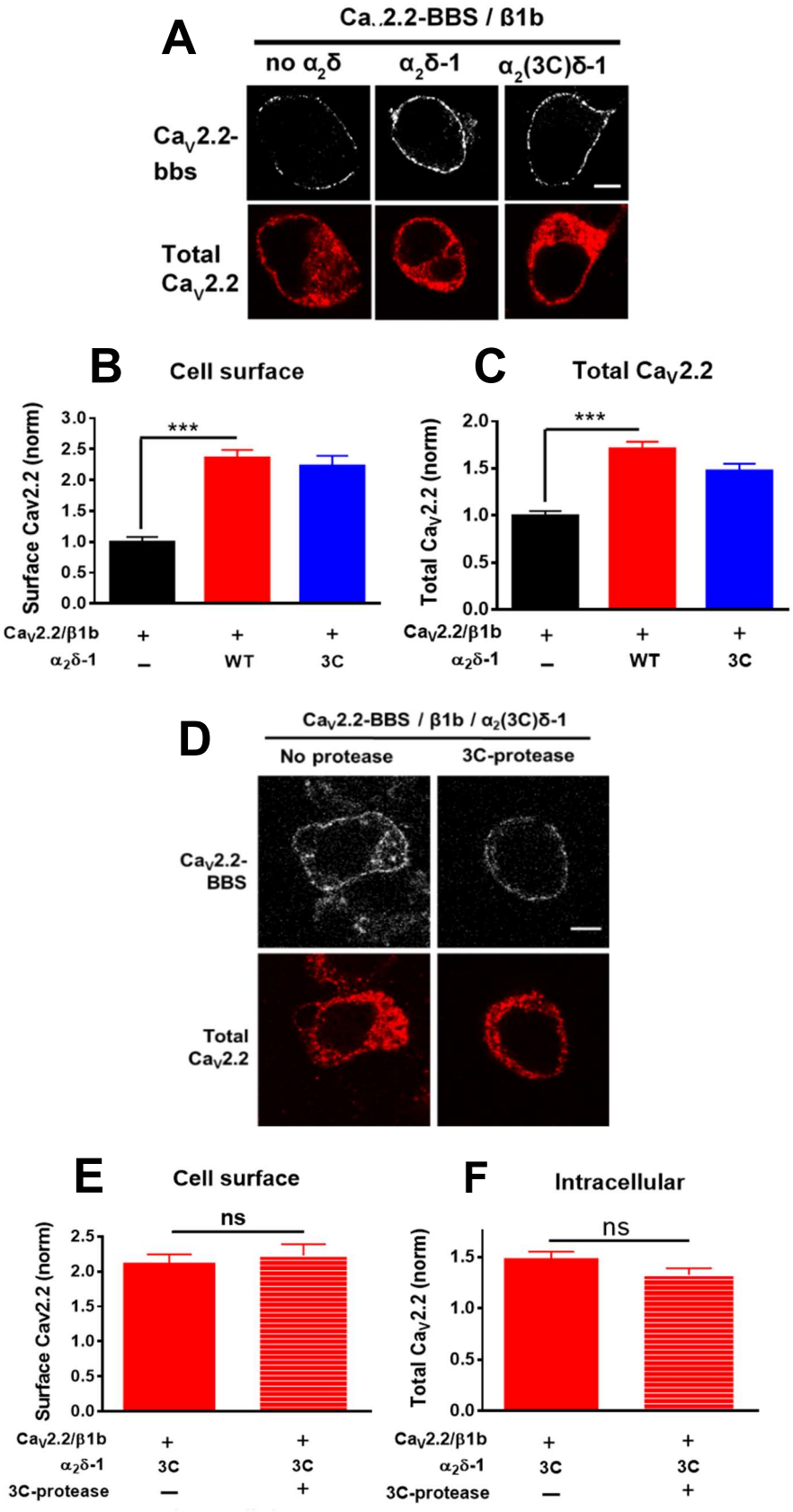

Figure 3.6 Cell-surface and total expression of $Ca_V2.2$-bbs coexpressed with β1b and either WT, (3C) or no $\alpha_2\delta$-1

Figure 3.6 Cell-surface and total expression of $Ca_V2.2$-bbs coexpressed with β1b and either WT, (3C) or no $\alpha_2\delta$-1

(A) Confocal images of cell-surface $Ca_V2.2$-bbs expression with β1b, and empty vector (left), WT $\alpha_2\delta$-1 (middle) or α_2(3C)δ-1 (right) in N2a cells. Top row: cell-surface $Ca_V2.2$-bbs (grey-scale; bottom row: total $Ca_V2.2$ (red). Scale bar 5 μm. **(B)** Normalised mean cell-surface $Ca_V2.2$-bbs expression (bar chart) with β1b and: empty vector (black bar, n = 206), WT $\alpha_2\delta$-1 (red bar, n = 191) or α_2(3C)δ-1 (blue bar, n = 181). **(C)** Normalised mean total $Ca_V2.2$-bbs expression (bar chart) with β1b and: empty vector (black bar), WT $\alpha_2\delta$-1 (red bar) or α_2(3C)δ-1 (blue bar). **(D)** Confocal images of cell-surface $Ca_V2.2$-bbs with β1b, α_2(3C)δ-1 and: empty vector (left panel) or 3C-protease (right panel). Top row: cell-surface $Ca_V2.2$-bbs (grey-scale), bottom row: total $Ca_V2.2$ (red). Scale bar 5μm. **(E)** Lack of effect of 3C-protease (bar chart) on cell-surface expression of $Ca_V2.2$-bbs with β1b, α_2(3C)δ-1, and: empty vector (red bar, n = 181) or 3C-protease (red striped bar, n = 200). **(F)** Total $Ca_V2.2$-bbs expression with β1b, α_2(3C)δ-1 and: empty vector (red bar) or 3C-protease (red, striped bar). Data were collected across 3 separate transfections. Data analysis was blinded. Data are plotted ± SEM values. Statistical differences were determined using one-way ANOVA and Bonferroni post-hoc test; ***p<0.001.

3.3.2 Proteolytic processing of $\alpha_2\delta$-3 is not required for trafficking of the $Ca_V2.2$ complex in N2a cell lines.

$\alpha_2\delta$-3 is topologically similar to $\alpha_2\delta$-1, undergoes proteolytic processing, and enhances currents through Ca_V channels in a similar fashion. In this study, I used confocal microscopy to examine whether proteolytic $\alpha_2\delta$-3 processing influences the expression and localisation of $Ca_V2.2$-bbs in N2a cell lines using the same approach described in (section 3.5). $Ca_V2.2$-bbs and β1b subunits were transiently expressed in N2a cells along with either $\alpha_2\delta$-3 WT, α_2(3C)δ-3 or empty vector and probed for cell-surface and total $Ca_V2.2$ expression (Fig. 3.7A). I find that cell-surface expression of $Ca_V2.2$-bbs is 31% higher when coexpressed with $\alpha_2\delta$-3 than empty vector (Fig 3.7B). When $Ca_V2.2$-bbs was coexpressed with α_2(3C)δ-3, I observed a small 8% increase in cell-surface $Ca_V2.2$ relative to empty vector which was not statistically significant (Fig 3.7B). Surprisingly, cell-surface $Ca_V2.2$ expression with α_2(3C)δ-3 was not found to be significantly different from $Ca_V2.2$

expressed with WT $\alpha_2\delta$-3. When comparing total $Ca_V2.2$ levels, I found that WT and (3C) $\alpha_2\delta$-3 coexpression increases II-III loop signal intensity by 47% and 31% respectively (Fig 3.7C) with no statistically significant difference between these values suggesting that proteolytic $\alpha_2\delta$-3 processing does not influence total $Ca_V2.2$ expression in cell lines. Using the same approach, I compared cell-surface and total $Ca_V2.2$-bbs when expressed with β1b and α_2(3C)δ-3 in the presence or absence of 3C-protease (Fig 3.7D). However, I found no difference in either cell-surface (Fig 3.7E) or total (Fig 3.7F) $Ca_V2.2$-bbs between these conditions, providing further evidence that proteolytic $\alpha_2\delta$ processing does not play a prominent role in the expression or localisation of $Ca_V2.2$ in non-neuronal cell lines. Interestingly, α_2(3C)δ-3 has reduced influence on cell-surface $Ca_V2.2$-bbs expression relative to WT, but this is not rescued by coexpression of 3C-protease. This could mean that the conformation of cleaved α_2(3C)δ-3 does not recapitulate the WT form, preventing complete rescue of function. From these data alone, it is difficult to determine if proteolytic processing is necessary for $\alpha_2\delta$-3-mediated enhancement of cell-surface $Ca_V2.2$ expression.

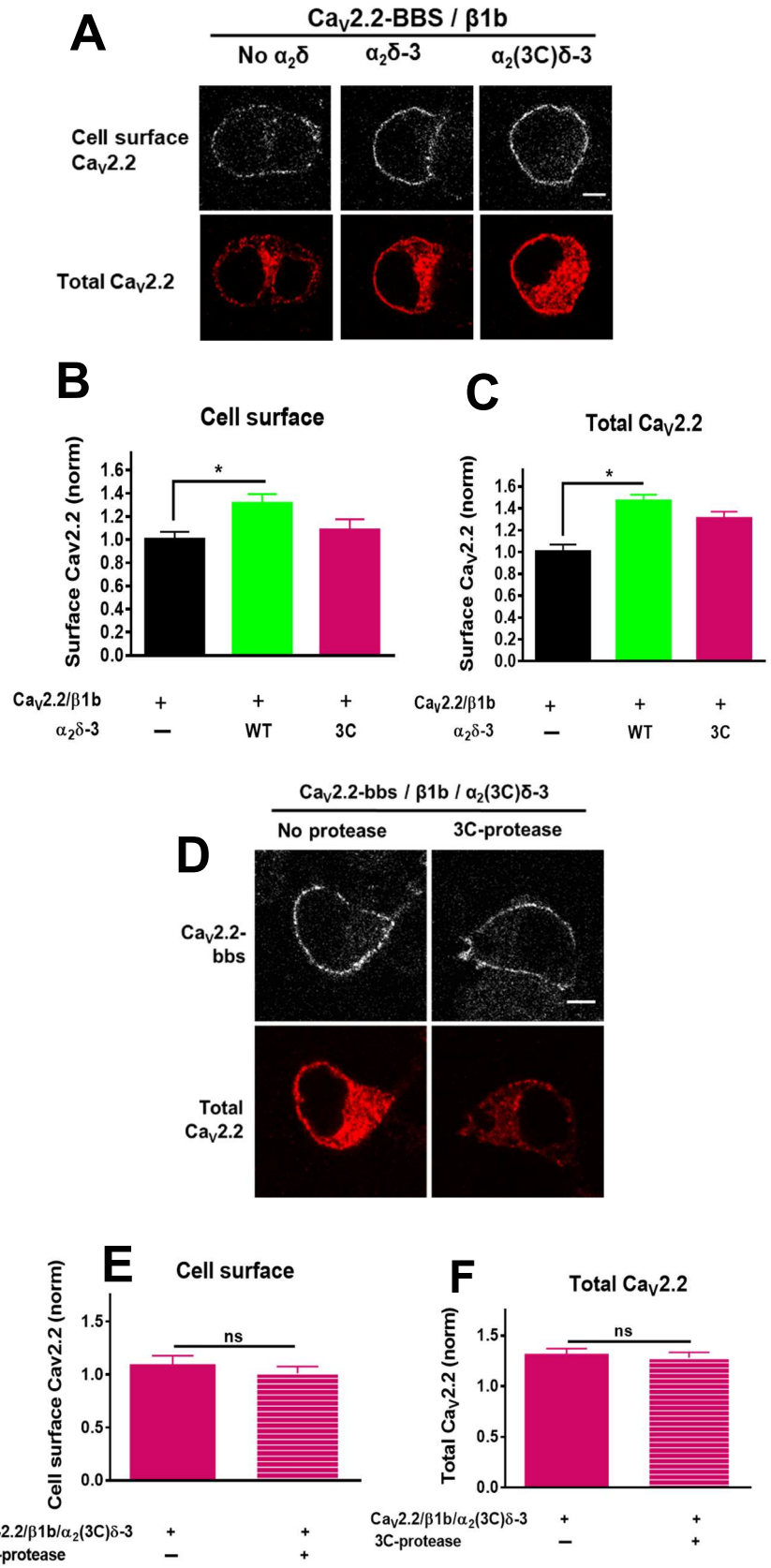

Fig 3.7 Cell surface and total expression of $Ca_V2.2$-bbs coexpressed with β1b and either WT, (3C) or no $\alpha_2\delta$-3

Figure 3.7 Cell surface and total expression of $Ca_V2.2$-bbs coexpressed with β1b and either WT, (3C) or no $\alpha_2\delta$-3

(A) Confocal images of cell-surface $Ca_V2.2$-bbs expression with β1b, and: empty vector (left), WT $\alpha_2\delta$-3-HA (middle) or α_2(3C)δ-3-HA (right) in N2a cells. Top row: cell-surface $Ca_V2.2$-bbs (grey-scale); bottom row: total $Ca_V2.2$ (red). Scale bar 5 μm. **(B)** Normalised mean cell-surface $Ca_V2.2$-bbs (bar chart) with: empty vector (black bar, n = 188), WT $\alpha_2\delta$-3 (green bar, n = 164) or α_2(3C)δ-3 (magenta bar, n = 181). **(C)** Normalised mean total $Ca_V2.2$-bbs (bar chart) with: empty vector (black bar), WT $\alpha_2\delta$-3 (green bar) or α_2(3C)δ-3 (magenta bar). **(D)** Confocal images of cell-surface $Ca_V2.2$-bbs with β1b, α_2(3C)δ-3 and: empty vector (left panel) or 3C-protease (right panel). Top row: cell-surface $Ca_V2.2$-bbs (grey-scale), bottom row: total $Ca_V2.2$ (red). Scale bar 5μm. **(E)** Lack of effect of 3C-protease (bar chart) on cell-surface expression of $Ca_V2.2$-bbs with β1b, α_2(3C)δ-1, and: empty vector (magenta bar, n = 164) or 3C-protease (magenta striped bar, n = 187). **(F)** Total $Ca_V2.2$-bbs expression with β1b, α_2(3C)δ-3 and: empty vector (magenta bar bar) or 3C-protease (magenta striped bar). Data were collected across 3 separate transfections. Data analysis was blinded. Data are plotted ± SEM values. Statistical differences were determined using one-way ANOVA and Bonferroni post-hoc test; *p<0.05

3.4. α_2(3C)δ-1 retains $Ca_V2.2$ trafficking enhancement in tsA-201 cells under basal and hyperpolarised conditions

Whole-cell patch clamp recordings in tsA-201 cells have shown that uncleaved α_2(3C)δ-1 does not enhance currents through $Ca_V2.2$ channels, however this is partially rescued by coexpression of 3C-protease (Kadurin *et al.*, 2016). In N2a cell lines, α_2(3C)δ-1 is able to promote $Ca_V2.2$ trafficking, however α_2(3C)δ-1 is unable to facilitate $Ca_V2.2$ traffic when expressed in primary hippocampal neurons (Kadurin *et al.*, 2016). Here, I sought to determine whether the inability of α_2(3C)δ-1 to enhance $Ca_V2.2$ currents in tsA-201 cells might be due to a loss of $Ca_V2.2$ trafficking – as seen in hippocampal neurons – or a loss of function distinct from the role of $\alpha_2\delta$ in Ca_V trafficking. To do this, I transiently expressed bbs-tagged $Ca_V2.2$ and β1b in tsA-201 cells with either $\alpha_2\delta$-1, α_2(3C)δ-1 or empty vector. Thereafter, cells were probed for cell-surface and total $Ca_V2.2$-bbs (Fig 3.8A) as

described (section 3.5). I found that cell-surface $Ca_V2.2$-bbs signal intensity is higher when coexpressed with either WT $\alpha_2\delta$-1 (123%) or α_2(3C)δ-1 (62%) relative to no $\alpha_2\delta$ (Fig 3.8B). In addition total $Ca_V2.2$ expression was increased by 46% with $\alpha_2\delta$-1 and 36% with α_2(3C)δ-1 compared with no $\alpha_2\delta$ (Fig 3.8C). These results are largely consistent with my observations in N2a cells showing that uncleaved α_2(3C)δ-1 increases both the total and plasma membrane-inserted population of $Ca_V2.2$. It should be noted that α_2(3C)δ-1 produced a smaller increase in plasma membrane $Ca_V2.2$ than WT under these conditions, However, as cell-surface $Ca_V2.2$ expression was 62% higher with α_2(3C)δ-1 than no $\alpha_2\delta$ (Fig 3.8B), the complete inability of α_2(3C)δ-1 to enhance $Ca_V2.2$ currents in tsA-201 cells is unlikely to be the result of diminished cell-surface channel expression.

The resting membrane potential of excitable cells such as pyramidal neurons is approximately -70mV, while tsA-201 cells have a typical membrane potential of around -20mV (Kadurin *et al.*, 2016). This study considered the possibility that membrane hyperpolarisation in neurons might account for the difference in $\alpha_2\delta$-enhanced $Ca_V2.2$ plasma membrane expression observed between these cell types. To test this, I expressed the two-pore K^+ channel, TASK-3, in tsA-201 cells along with $Ca_V2.2$-bbs, β1b and either $\alpha_2\delta$-1, α_2(3C)δ-1 or empty vector. TASK-3 is a constitutively active K^+ channel and hyperpolarised the plasma membrane when expressed in tsA-201 cells to about -70mV (Kadurin et al, 2016). After 48 h expression I again used α-BTX AF488 live-labelling and post-fixation immunocytochemistry to identify membrane-inserted and total $Ca_V2.2$ in these cells which was assessed using confocal microscopy and image analysis (Fig 3.8D). I found that $Ca_V2.2$-bbs plasma membrane expression is increased by 164% when coexpressed with WT $\alpha_2\delta$-1 and 150% when expressed with α_2(3C)δ-1 relative to no $\alpha_2\delta$ (Fig 3.8E). Total $Ca_V2.2$ was also increased when expressed with $\alpha_2\delta$-1 (31%) or α_2(3C)δ-1 (30%) relative to no $\alpha_2\delta$ (Fig 3.8F). These data are in line

with previous observations in both N2a and non-hyperpolarised tsA-201 cell lines, it therefore seems highly unlikely that membrane polarity is a key determinant of $\alpha_2\delta$-1-mediated Ca_V trafficking and membrane expression.

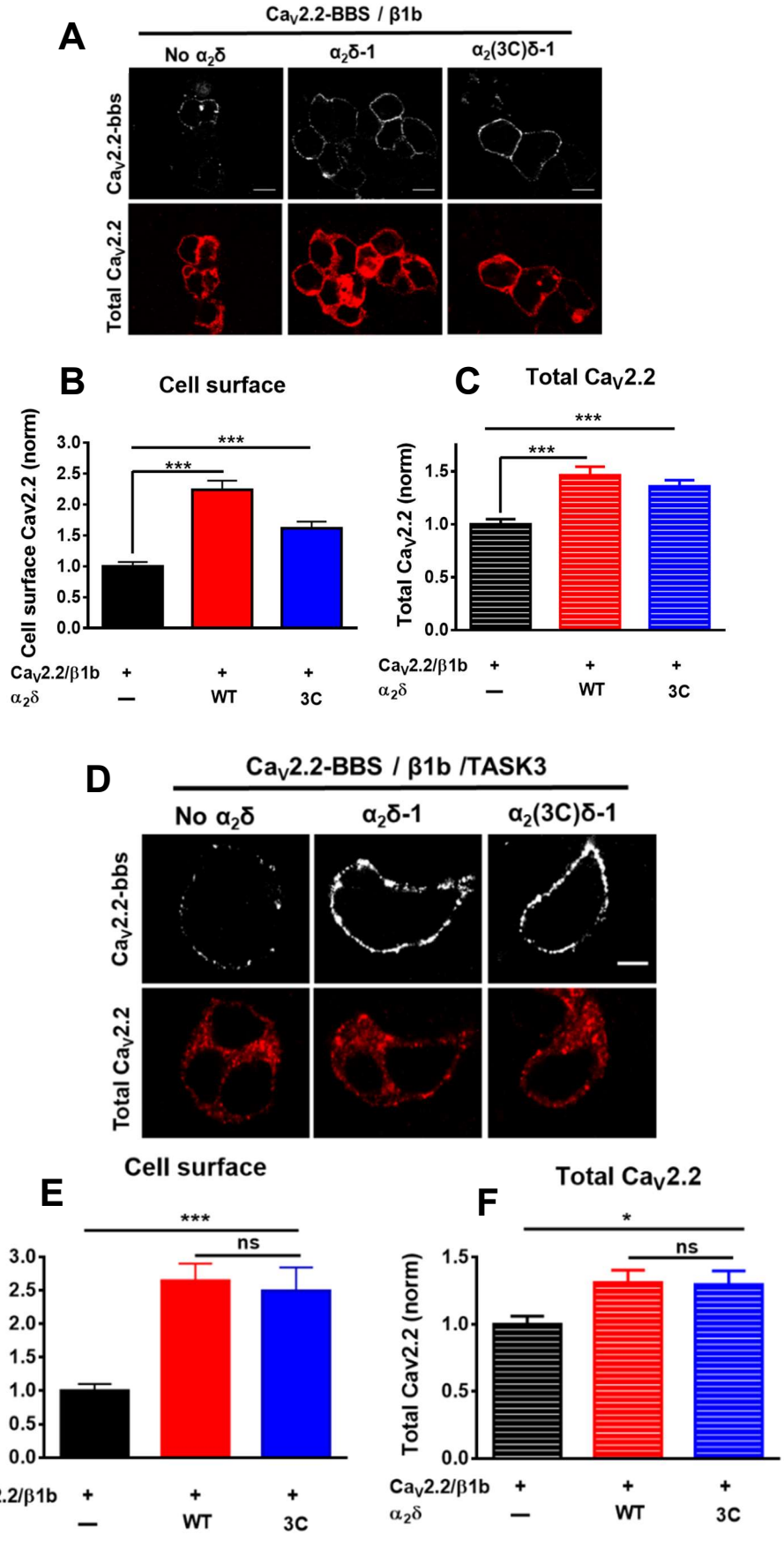

Fig 3.8. Legend continued on page 94.

Figure 3.8 Cell-surface and total expression of $Ca_V2.2$-bbs coexpressed with β1b and either WT, (3C) or no $\alpha_2\delta$-1 in tsA-201s under basal and hyperpolarised conditions

(A) Confocal images of cell-surface $Ca_V2.2$-bbs expression with β1b, and: empty vector (left), WT $\alpha_2\delta$-1-HA (middle) or α_2(3C)δ-1-HA (right) in tsA-201 cells. Top row: cell-surface $Ca_V2.2$-bbs (grey-scale); bottom row: total $Ca_V2.2$ (red). Scale bar 10 μm**. (B)** Normalised mean cell-surface $Ca_V2.2$-bbs expression (bar chart) in tsA-201 cells with β1b empty vector (black bar, n = 128), WT $\alpha_2\delta$-1 (red bar, n = 120) or α_2(3C)δ-1 (blue bar, n = 121). **(C)** Normalised mean total $Ca_V2.2$-bbs expression in tsA-201 cells with β1b empty vector (black bar), WT $\alpha_2\delta$-1 (red bar) or α_2(3C)δ-1 (blue bar). **(D)** Example confocal images of cell-surface $Ca_V2.2$-bbs expression with β1b, TASK3, and empty vector (left), WT $\alpha_2\delta$-1-HA (middle) or α_2(3C)δ-1-HA (right) in tsA-201 cells. Top row: $Ca_V2.2$-bbs cell-surface staining (grey-scale); bottom row: total $Ca_V2.2$ (red). Scale bar 5μm **(E)** Normalised mean cell-surface $Ca_V2.2$-bbs expression (bar chart) in tsA-201 cells co-expressing TASK3, with empty vector (black bar, n = 70), WT $\alpha_2\delta$-1 (red bar, n = 73) or α_2(3C)δ-1 (blue bar, n = 81). **(F)** Normalised mean total $Ca_V2.2$-bbs expression (bar chart) in tsA-201 cells with β1b empty vector (black, striped bar), WT $\alpha_2\delta$-1 (red, striped bar) or α_2(3C)δ-1 (blue, striped bar). Data are plotted ± SEM values. Statistical significance was determined using one-way ANOVA and Bonferroni post-hoc test ***p<0.001, *p<0.05.

3.5 Summary

The aim of this study was to establish the functional consequences of proteolytic processing of $\alpha_2\delta$ on the subcellular localisation of $\alpha_2\delta$ and the α_1 subunit $Ca_V2.2$ in non-neuronal cell lines. This study complemented parallel work carried out in primary neuronal cultures to help develop a more complete understanding of the role of proteolytic $\alpha_2\delta$ processing (Kadurin *et al.*, 2016). To achieve this, I first characterised the cell-surface and intracellular expression of three $\alpha_2\delta$ cleavage mutants: α_2(V6)δ-1-HA, α_2(Th)δ-1-HA and α_2(3C)δ-1-HA in which the endogenous "LEAVEME" cleavage site between α_2 and δ was substituted for a non-cleavable sequence. Western blot analysis has shown that each of these $\alpha_2\delta$ cleavage mutants express as a single unprocessed band. However, cleavage of α_2(Th)δ-3 and α_2(3C)δ-1 can be induced by coexpression of Thrombin or 3C protease

respectively (Kadurin *et al.*, 2016). I used confocal microscopy to compare the level of cell-surface and intracellular α_2(V6)δ-1-HA, α_2(Th)δ-1-HA and α_2(3C)δ-1-HA relative to WT α_2δ-1-HA expressed in N2a cell lines; each α_2δ-1 variant was expressed in the presence or absence of Ca_V2.2 and β1b subunits (Fig 3.2-3.4). I found that cell-surface expression relative to WT α_2δ-1 is reduced for α_2(V6)δ-1 (62%), α_2(Th)δ-1 (33%) and α_2(3C)δ-1 (24%) in the absence of additional subunits (Fig 3.2B, 3.3B, 3.4B). Coexpression of Ca_V2.2 and β1b produced a proportional reduction in cell-surface signal intensity for both WT and uncleaved α_2δ-1 mutants typically between 70-90% relative to their signal when expressed independently of Ca_V2.2 (Fig 3.2B, 3.3B, 3.4B). Previous studies have shown the loss of α_2δ-HA signal with Ca_V2.2 coexpression to be a consequence of HA epitope occlusion resulting from interactions between the α_2 domain of α_2δ-1 and Ca_V2.2 (Cassidy *et al.*, 2014), my results suggest that such an interaction is conserved in the uncleaved α_2δ mutants.

Notably, α_2(V6)δ-1 showed a 65% higher intracellular signal intensity than WT when expressed without Ca_V subunits (Fig 3.2C) which, when coupled with diminished cell-surface expression, could indicate intracellular α_2(V6)δ-1 aggregation, possibly as a consequence of the large hydrophobic valine sequence present. No such effect was observed for α_2 (Th)δ-1 or α_2(3C)δ-1, with the former displaying no difference in intracellular signal from WT (Fig 3.3B) and the latter showing a 40% reduction in relative intracellular signal (Fig 3.4B). The effect of induced proteolysis on α_2δ localisation was assessed by expressing α_2(3C)δ-3-HA in N2a cells with and without 3C-protease coexpression (Fig 3.5A). However, I found no change in either cell-surface or intracellular α_2(3C)δ-3 expression when coexpressed with 3C-protease (Fig 3.5B, C). Next, I compared the cell-surface and total expression of exofacially bbs-tagged Ca_V2.2 when coexpressed with β1b and either WT or (3C) α_2δ-1 in N2a cells (Fig 3.6A). WT α_2δ-1 increased cell-surface

$Ca_V2.2$-bbs expression by 136%, while α_2(3C)δ-1 coexpression resulted in a 124% increase in cell-surface $Ca_V2.2$-bbs relative to no $\alpha_2\delta$ (Fig 3.6B). Total $Ca_V2.2$ levels, measured by expression of the intracellular II-III loop epitope, was increased by with both WT $\alpha_2\delta$-1 (70%) and α_2(3C)δ-1 (47%) (Fig 3.6C) relative to no $\alpha_2\delta$. In addition, I found no difference in total or cell-surface $Ca_V2.2$-bbs when expressed with α_2(3C)δ-1 and either 3C-protease or empty vector (Fig 3.6E, F). I then used the same approach to compare the effect of WT $\alpha_2\delta$-3 or α_2(3C)δ-3 on $Ca_V2.2$-bbs (Fig 3.8A). I find that WT $\alpha_2\delta$-3 produced a relatively small but consistent 31% increase in cell-surface $Ca_V2.2$-bbs, while α_2 (3C)δ-3 showed only a 9% increase that was not statistically different from no $\alpha_2\delta$ (Fig 3.7B). An increase in $Ca_V2.2$ II-III loop expression was observed with coexpression of either WT $\alpha_2\delta$-3 (47% increase) or α_2(3C)δ-3 (31% increase) (Fig 3.7C). As with α_2(3C)δ-1, I saw no change in either cell-surface or intracellular $Ca_V2.2$-bbs when expressed with α_2(3C)δ-3 and either 3C-protease or empty vector (Fig 3.7E, F). I next examined the effect of α_2(3C)δ-1 on $Ca_V2.2$-bbs trafficking in tsA-201 to establish whether my results in undifferentiated N2a cells were consistent in another non-neuronal cell line. Using the same approach as previously described (section 3.2.1), I compared cell-surface and total $Ca_V2.2$-bbs expression in tsA-201 cells when coexpressed with β1b and either WT $\alpha_2\delta$-1, α_2 (3C)δ-1 or no $\alpha_2\delta$ (Fig 3.8A). Under these conditions, I found that α_2(3C)δ-1 enhanced cell-surface $Ca_V2.2$-bbs by (60%) with WT $\alpha_2\delta$-1 producing a (140%) increase relative to no $\alpha_2\delta$ (Fig 3.8B). Total $Ca_V2.2$ was increased by both WT and (3C) $\alpha_2\delta$-1 by ~30% (Fig 3.8C). tsA-201 cells have a membrane potential of between -10mV and -30mV while hippocampal neurons are typically around -70mV; I tested whether the difference in membrane potential could explain discrepancies observed in the trafficking of unprocessed $\alpha_2\delta$ and $Ca_V2.2$ between neurons and non-neuronal cell lines (Kadurin *et al.*, 2016). To do this, I expressed the constitutively active K^+ channel TASK3 in tsA-201 cells to hyperpolarise the plasma membrane together with

$Ca_V2.2$-bbs, β1b and either WT $\alpha_2\delta$-1, α_2(3C)δ-1 or no $\alpha_2\delta$ and measured cell-surface and total $Ca_V2.2$ as described previously (section 3.5). Under hyperpolarised conditions, I found that both WT and (3C) $\alpha_2\delta$-1 produced a ~2.5-fold increase in cell-surface $Ca_V2.2$ and a 30% increase in total $Ca_V2.2$ level relative to no $\alpha_2\delta$ (Fig 3.8D, E). I found no difference in the effect of $\alpha_2\delta$-1 WT or α_2(3C)δ-1 on $Ca_V2.2$ under hyperpolarised conditions, suggesting that membrane polarity is not a determinant of $\alpha_2\delta$-mediated $Ca_V2.2$ trafficking.

3.6 Discussion

Proteolytic cleavage between the α_2 and δ moieties of $\alpha_2\delta$ is reported for all known subtypes (Annette C. Dolphin, 2012). This form of post-translational processing is well established for each $\alpha_2\delta$ subtype. However, the functional significance of proteolytic processing has been difficult to determine, in part due to a failure to identify the relevant protease(s) responsible, as well as the subcellular location of proteolysis. Previous studies have shown that $\alpha_2\delta$-1 in brain and muscle tissue is almost entirely in its processed form (Jay *et al.*, 1991; Patel *et al*., 2003), this is also true of cerebellar $\alpha_2\delta$-2 (Davies *et al.*, 2006). Incomplete $\alpha_2\delta$ proteolysis is found in heterologous expression systems, although this is primarily for intracellular $\alpha_2\delta$ with very little pro-$\alpha_2\delta$ at the plasma membrane (Davies *et al.*, 2010; Kadurin *et al.*, 2012). Native pro-$\alpha_2\delta$ has also been reported at the cell bodies of DRG neurons although these populations are fully processed at the axons (Bauer *et al.*, 2009); of particular note is that this axonal $\alpha_2\delta$ is fully processed in intracellular vesicles suggesting that proteolytic processing occurs during or prior to trafficking from the cell soma. However, cleavage of the α_2(Th)δ-3 mutant can be induced by application of external Thrombin with a commensurate increase in Ca_V2 currents demonstrating restoration of function (Kadurin *et al.*, 2016).

Mutations to positions around the cleavage site of $\alpha_2\delta$-1 were previously shown to reduce but not abolish Ca_V current enhancement (Andrade *et al.*, 2007) suggesting a role for $\alpha_2\delta$-1 processing therein. It has since been conclusively established that $\alpha_2\delta$ processing is required for $Ca_V2.2$ current enhancement from studies using non-cleavable $\alpha_2\delta$ mutants (Kadurin *et al.*, 2016). Experiments in heterologous systems have variously shown that $\alpha_2\delta$s increase maximal Ca_V conductance by 3-10 fold (Cantí *et al.*, 2005; Hendrich *et al.*, 2008). This does not appear to be result of changes to single channel properties with only a minimal change reported in Ca_V open probability and no change in single channel conductance (Wakamori *et al.*, 1999). A hyperpolarising shift in voltage-dependent activation of $Ca_V1.2$ by $\alpha_2\delta$-1 is reported, this would increase the probability of channel activation in neurons, although this shift is far smaller in $Ca_V2.2$ and is unlikely to account for the observed $\alpha_2\delta$-mediated current enhancement (Savalli *et al.*, 2016; Cantí *et al.*, 2005; Kadurin *et al.*, 2012). The minimal effect of $\alpha_2\delta$ on Ca_V single-channel properties, could lead one to conclude that $\alpha_2\delta$-mediated current enhancement is a product of increased plasma membrane Ca_V expression, documented in previous reports (Cassidy *et al.*, 2014) as well as the present study (Fig 3.4). However, recent studies with non-cleavable $\alpha_2\delta$ mutants reveal that they do not amplify Ca_V currents in cell lines (Kadurin *et al.*, 2016) which, coupled to fact that they still amplify Ca_V surface expression (at least for $\alpha_2\delta$-1), demonstrates a partitioning of $\alpha_2\delta$ function between enhancement of Ca_V trafficking and enhancement of Ca_V currents. To further complicate matters, uncleaved α_2(3C)δ is unable to facilitate trafficking of $Ca_V2.2$ from the cell body to neuronal processes when expressed in primary neuronal cultures, however this can be rescued by induced cleavage with 3C-protease (Kadurin *et al.*, 2016). This strongly suggests that additional features - present in neurons but absent in non-neuronal cell lines – provide a layer of regulation to the Ca_V trafficking which prevents or severely limits exit of the immature complex from the cell body. Surprisingly, $Ca_V2.2$ expressed with α_2(3C)δ-1 and α_2(3C)δ-3 was

not found to accumulate in neuronal cell bodies, despite inhibited trafficking to the neurites (Kadurin *et al.*, 2016); this could indicate that immature $Ca_V/\alpha_2\delta$ complexes are routinely degraded in neurons. Interestingly, α_2(3C)δ-1 and α_2(3C)δ-3 were able themselves to traffic to hippocampal neurites when expressed independently of additional Ca_V subunits (Kadurin *et al.*, 2016) which may suggest that the conformation of α_2(3C)δ in complex with $Ca_V2.2$ precludes an interaction(s) with relevant trafficking proteins.

It is tempting to consider that $\alpha_2\delta$ offers a degree of temporal regulation to Ca_V activity as a means of controlling Ca^{2+} flux. Ca^{2+} acts as a second messenger in a multitude of cellular processes such as activating transcription factors and Ca^{2+} dependent kinases. The potency of Ca^{2+} as a second messenger requires that intracellular Ca^{2+} be tightly controlled, with basal cytosolic free Ca^{2+} generally in the nM range in most cells. Higher intracellular Ca^{2+} concentrations are found in the mitochondria and ER which act as Ca^{2+} buffers in conjunction with a preponderance of Ca^{2+}-binding proteins (Solovyova & Verkhratsky, 2002). The ER is a principal Ca^{2+} store, with luminal free [Ca^{2+}] typically between 500μM – 1mM under basal conditions (Solovyova & Verkhratsky, 2002). The ER membrane potential is mainly determined by a large K^+-selective conductance mediated by Trimeric Intracellular Cation (TRIC) channels (Garcia & Miller, 1984; Yazawa *et al.*, 2007). As such, the ER membrane potential is shunted towards the Nernst potential of K^+ (0mV) since cytosolic and ER luminal [K^+] are similar (Somlyo *et al.*, 1981). As the ER membrane potential is close to 0mV, one might expect nascent Ca_V channels in the ER to be in an open or inactivated conformation which, due to the sizeable [Ca^{2+}] gradient between ER and cytosol, should precipitate depletion of ER Ca^{2+} through these open channels, something that has not been reported. An interesting possibility, is that pro-$\alpha_2\delta$ serves to inhibit immature Ca_V channels during these early stages of synthesis with subsequent $\alpha_2\delta$ processing occurring

only once the Ca_V complex has exited the ER. Consistent with this notion, unprocessed α_2(3C)δ-1 enhances cell-surface Ca_V2.2 in heterologous systems (Fig 3.6B) but does not enhance Ca_V2.2 currents over those without α_2δ (Kadurin *et al.*, 2016). This would strongly suggest that the additional plasma membrane Ca_V population is inactive and indicate an inhibitory role for unprocessed α_2δ.

Chapter 4. Mutations to Ca^{2+} binding glutamate residues in $Ca_V2.2$ pore disrupt channel trafficking

4.1 Introduction

Voltage-gated calcium channels are highly Ca^{2+} selective, allowing exclusive Ca^{2+} permeation despite far higher extracellular concentrations of monovalent cations, particularly Na^+, under physiological conditions. The high fidelity of VGCC permeation is largely determined by a conserved glutamate residue in the pore-forming loop between S5 and S6 in each domain of $Ca_V\alpha_1$ (illustrated below, Fig.4.1). Seminal work on the L-type channel (α1C), in which these glutamates were systematically substituted, revealed that these residues form a high affinity Ca^{2+} binding site and substitution of all four glutamates to glutamine or alanine was sufficient to abolish Ca^{2+} or Cd^{2+} block of monovalent cation currents (Yang *et al*., 1993; Ellinor *et al*., 1995). More recently, a study using the bacterial voltage-gated Na^+ channel, (Na_VAb) has developed our understanding of the Ca_V selectivity filter (Tang *et al*., 2014). Na_VAb is a homotetrameric channel closely related to vertebrate Ca_Vs and possessing similar structural features. The Na_VAb selectivity filter is comprised of four identical pore motifs **"^{175}TLESWSM^{181}"** and substitution of the underlined residues to aspartate is sufficient to impart Ca^{2+} selectivity on the mutant channel, termed Ca_VAb (Tang *et al*., 2014); notably, E177 is positionally equivalent to the glutamate residues of mammalian Ca_V selectivity filters. While Na_VAb carries an outward Na^+ current and is Ca^{2+}-impermeant, Ca_VAb allows a voltage-dependent inward Ca^{2+} current (Tang *et al*., 2014). Crystallographic and physiological analysis of Ca_VAb revealed the presence of three sequential Ca^{2+} binding sites, site 1, 2 and 3 from an extracellular to intracellular view. Site 1 and 2 coordinate high affinity Ca^{2+} binding, site 1 is thought to confer Ca^{2+} selectivity while site 2 – the highest Ca^{2+} binding affinity site – appears to be required for

divalent cation block. Site 3 is found to have a lower Ca^{2+} affinity consistent with a role facilitating Ca^{2+} exit from the selectivity filter into the central cavity (Tang *et al.*, 2014). The four conserved glutamate residues in the Ca_V selectivity filter are predicted to coordinate site 2 through their side chain carbonyl groups (Tang *et al*., 2014; Wu *et al*., 2016). In the model proposed by Tang et al (2014), the proximity of each Ca^{2+} binding site to one another precludes concurrent Ca^{2+} occupation of all three sites. Instead, only sites 1 and 3 or site 2 may be Ca^{2+}-bound, prompting a sequential movement of Ca^{2+} through the selectivity filter as extracellular Ca^{2+} approaches site 1 (Tang *et al*., 2014).

Pore mutants of Ca_V channels have been used in a number of studies to elucidate the effect of non-conducting Ca_Vs on pre and postsynaptic function and have been suggested to function as dominant negative mutants (Cao *et al*., 2004; Cao & Tsien., 2010; Krey *et al*., 2013). However, there has been relatively little direct investigation into whether these pore mutants are normally expressed and trafficked either in cell lines or a neuronal context. Initial studies of pore mutant L-types noted the presence of a large outward current in cells expressing these constructs, taking this as evidence that the channels are well expressed at the plasma membrane (Yang *et al*., 1993; Ellinor *et al*., 1995). In addition, some studies have used intracellularly-tagged Ca_V pore mutants in fluorescence imaging experiments, defining them as membrane-inserted based on overlapping signal peaks with known plasma membrane markers (Cao *et al*., 2004). This method can give false positives as proteins may be in membranes very close to the plasma membrane without being inserted, particularly in an overexpression system. In the past, our group has argued that labelling of the exofacial surface of Ca_Vs is required to reliably quantitate cell surface Ca_V expression, at least with regards to imaging experiments (Cassidy *et al.*, 2014). The ability to distinguish between cell surface and intracellular populations is of particular importance when interpreting data from

ostensibly non-conducting channels, as diminished currents could be attributed to reduced channel conductance, reduced cell surface expression, or a combination of these factors. A previous study by Cao et al (2004) explored the idea that cell-surface expression of Ca_V channels at the presynaptic membrane is limited to a finite number of channel-preferring slots (Cao *et al.*, 2004). The study found that expression of pore-mutated $Ca_V2.1$ reduced EPSC generation in primary hippocampal neurons, attributing this to competition between non-conducting $Ca_V2.1$ mutants and endogenous WT $Ca_V2.1$ for available presynaptic slots (Cao *et al.*, 2004); Cell surface expression of pore-mutated $Ca_V2.1$ was assessed by measuring the overlap of fluorescence intensity between N-terminally GFP-tagged $Ca_V2.1$ constructs with the membrane-targeted Lyn tyrosine kinase, concluding that cell-surface expression of pore-mutants was not significantly different from WT (Cao *et al.*, 2004). As mentioned earlier, this method of assessing cell-surface channel expression can be susceptible to inaccuracy as it does not distinguish between plasma-membrane inserted channels and intracellular channels in close proximity to the plasma membrane. This can be especially problematic when using overexpression systems due to the elevated intracellular expression of the given protein.

The Dolphin lab developed a number of exofacially-tagged $Ca_V2.2$ and $Ca_V2.1$ pore mutants, wherein the conserved P-loop glutamate residues were substituted for lysine or alanine. The Ca_V2 pore mutants were developed in order to directly address whether such mutants retain the trafficking and localisation characteristics of their WT counterparts. The aim of the present study was to identify whether the conserved P-loop glutamate residues of $Ca_V2.2$ were determinants of trafficking and cell surface expression in neurons and non-neuronal cell lines.

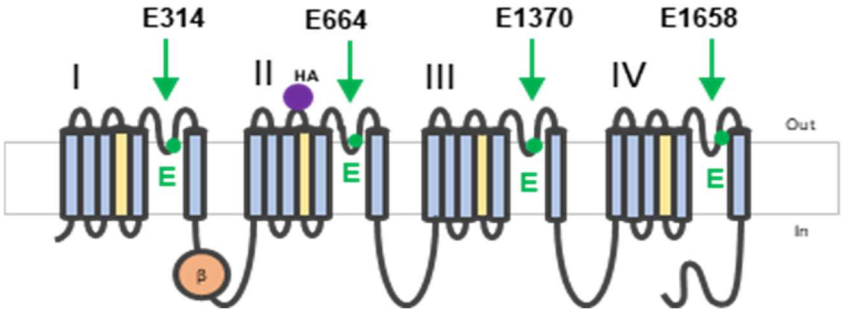

Figure 4.1 Diagram of $Ca_V2.2$-HA in complex with β.

The position of the exofacial HA tag in Domain II is shown in purple. Conserved P-loop glutamate residues of each domain are indicated by green arrows.

4.2. Mutation of domain IV P-loop glutamate to lysine ablates cell-surface expression of $Ca_V2.2$

In this study, I used an immunocytochemical approach to compare the cell-surface expression of an exofacially-HA tagged $Ca_V2.2$ pore mutant to WT channels in N2A cells (Fig 4.2). N2a cells were transiently transfected with either WT or $E_{IV}K$ $Ca_V2.2$ along with auxiliary $\alpha_2\delta$-1 and β1b subunits 48 hours prior to fixation. Fixed cells were then probed for cell-surface HA-tag expression under non-permeabilised conditions to identify the population of plasma membrane-inserted channels, followed by permeabilisation and immunostaining for the intracellular II-III loop epitope of $Ca_V2.2$; II-III loop staining was used to quantify total $Ca_V2.2$ expression in cells. Visualisation of the II-III loop suggested that both WT and $E_{IV}K$ $Ca_V2.2$ were well expressed in N2A cells (Fig 4.2A). However, detection of the exofacial HA-tag on the cell surface was severely diminished for $E_{IV}K$ relative to WT channels (Fig 4.2.A).

Cell-surface and total $Ca_V2.2$ expression was quantified using the ImageJ freehand tool (as described, Methods 2.4.4) to manually draw and measure fluorescence

along the perimeter and total area (excluding the nucleus) of cells positive for II-III loop expression. Mean cell surface $E_{IV}K$ $Ca_V2.2$ expression was reduced by 88% relative to WT $Ca_V2.2$ (Fig 4.2.B). In contrast, II-III loop staining was more than 2-fold higher for $E_{IV}K$ relative to the control (Fig 4.2.C) strongly suggesting that reduced $E_{IV}K$ membrane expression did not occur through an inability of the pore mutant to express in this cell line. From these data it would be difficult to attribute reduced whole-cell currents through $Ca_V2.2$ $E_{IV}K$ to an inability of the channel to permit current rather than a reduction in plasma-membrane expression. Previous studies have interpreted P-loop mutant Ca_V channels as being well expressed at the plasma membrane, even suggesting a dominant negative effect due to competing with WT channels for position in the presynaptic membrane (Cao *et al.*, 2004), if other pore-mutants have similarly impaired membrane expression such results may require reinterpretation.

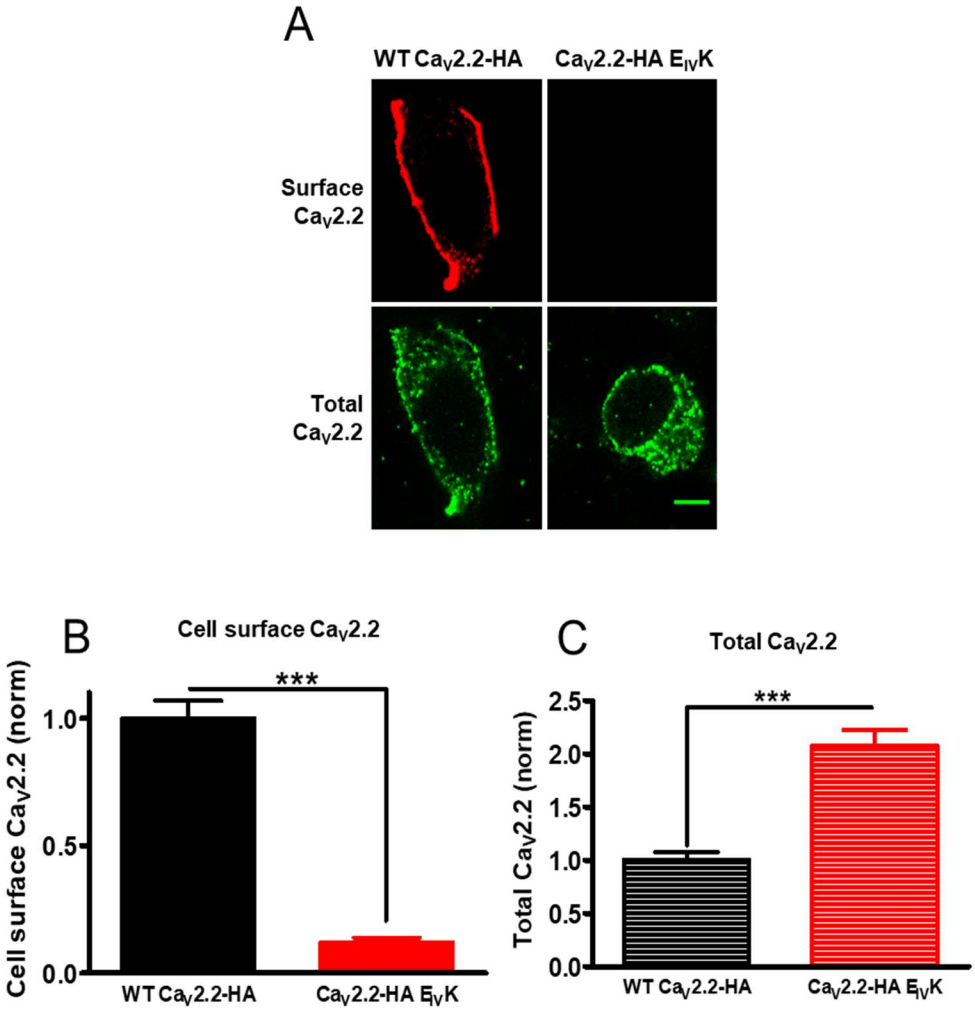

Figure 4.2 Expression of WT and $E_{IV}K$ pore mutant $Ca_V2.2$-HA in N2a cells.

(A) Confocal images of wild-type (left) and $E_{IV}K$ (right) $Ca_V2.2$-HA expressed in N2a cells. Cell surface expression using HA Ab in non-permeabilised cells (top row) total expression with II-III loop Ab in permeabilised cells (bottom row) (scale bar = 5µm). **(B)** Normalised mean cell-surface $Ca_V2.2$ expression of WT $Ca_V2.2$-HA with $\beta1b/\alpha_2\delta$-1 (black; n = 66 cells), $Ca_V2.2$-HA $E_{IV}K$ with $\beta1b/\alpha_2\delta$-1 (red; n = 70 cells) **(C)** Normalised mean total expression of $Ca_V2.2$ for conditions in panel B. Data were collected from 2 separate transfections. Data analysis was blinded. Data are plotted ± SEM values. Statistical significance was determined using Student's unpaired t test (***$p<0.001$).

4.3. E to A P-loop $Ca_V2.2$ mutants show reduced plasma membrane expression but retain dependence on $\alpha_2\delta$ and β subunits for cell-surface expression.

The limited membrane expression of $Ca_V2.2$ $E_{IV}K$ (Fig 4.2B) suggests that a relatively small mutation in the pore-forming region of the channel can be sufficient to disrupt normal trafficking and/or folding. However, the severity of this effect makes it difficult to determine whether $E_{IV}K$ retains normal Ca^{2+} permeation. Previous mutational studies of the Ca_V P-loop glutamates have suggested an unequal contribution of these residues to the permeation pathway despite their seemingly equivalent positions (Tang et al, 2014). In our lab, a range of $Ca_V2.2$ pore mutants were generated featuring E to A substitutions to different domains. Whole-cell current recordings of these mutants revealed that inward Ba^{2+} currents are abolished by simultaneous mutation of all four P-loop glutamates to alanine, with partial inward current observed in single and double domain mutants.

In this study, I assessed the membrane insertion of two exofacially HA-tagged P-loop $Ca_V2.2$ mutants: Domain I E to A (E_IA) which has reduced inward current and Domain I, II, III, IV E-A ($E_{I,II,III,IV}A$) which has no inward current. The aim was to establish whether these partial or non-conducting $Ca_V2.2$ mutants retained normal trafficking functionality and to further examine whether they retained β and $\alpha_2\delta$ dependence for expression and localisation as seen for WT $Ca_V2.2$.

I first expressed HA-tagged WT, E_IA or $E_{I,II,III,III}A$ $Ca_V2.2$ with β1b in N2A cells in the presence or absence of $\alpha_2\delta$-1 and immunostained them under non-permeabilised conditions for exofacial HA expression (Fig 4.3A). Following this, cells were permeabilised and probed for II-III loop expression as a transfection marker and to identify the border of cells with little or no cell-surface staining. When coexpressed with $\alpha_2\delta$-1, cell surface E_IA and $E_{I,II,III,IIII}A$ was reduced by 54% and 68%

respectively relative to WT (Fig 4.3B) although membrane expression was clearly visible for both mutants unlike earlier findings for $E_{IV}K$ $Ca_V2.2$ (Fig 4.2B). In the absence of $\alpha_2\delta$, membrane-inserted $Ca_V2.2$ was similarly reduced in all conditions (Fig 4.3B) suggesting that both E_IA and $E_{I,II,III,IIII}A$ $Ca_V2.2$ retain an interaction with $\alpha_2\delta$-1 which enhances their cell surface expression consistent with previous reports for WT $Ca_V2.2$ (Cassidy et al, 2014).

Using the same approach, I then compared cell surface expression of WT, E_IA or $E_{I,II,III,IIII}A$ $Ca_V2.2$ expressed with $\alpha_2\delta$-1 in the presence or absence of β1b (Fig 4.3C). Once again, cell surface expression of both pore mutants was reduced relative to WT when expressed with $\alpha_2\delta$-1 and β1b: E_IA (51%) and $E_{I,II,III,IIII}A$ (39%) (Fig 4.3D). I found that cell surface $Ca_V2.2$ expression without β1b is reduced across all conditions; however, WT $Ca_V2.2$ appears to be more strongly affected than either pore mutant, in particular $E_{I,II,III,IIII}A$: WT (80% reduction), E_IA (75% reduction) and $E_{I,II,III,IIII}A$ (57% reduction) (Fig 4.3D).

These data strongly suggest that E-A mutations to P-loop glutamates in $Ca_V2.2$ disrupt membrane insertion but do not abolish it. There is little difference in cell surface expression between partially conducting E_IA and non-conducting $E_{I,II,III,IIII}A$ across the conditions tested (Fig 4.3B, Fig 4.3D). As such, it is unlikely that diminished cell surface expression is solely a function of lost channel permeation. It is interesting to note that $E_{I,II,III,IIII}A$ appeared to be less susceptible to the loss of β1b than WT which could indicate that mutations to the P-loop binding pockets affect the interaction of the α_1 subunit and β.

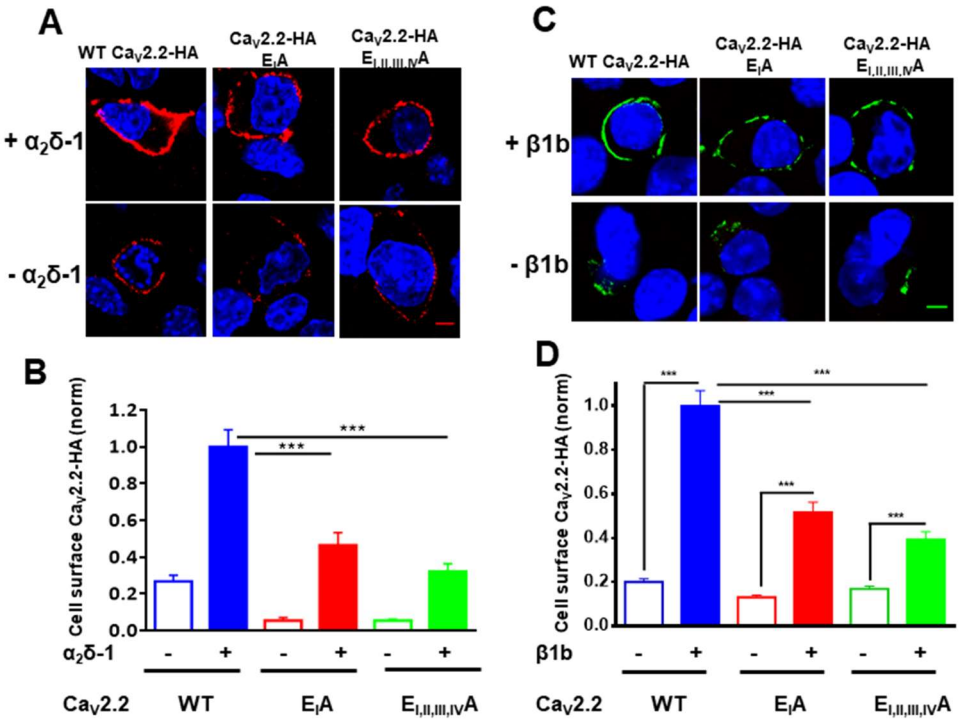

Figure 4.3 Cell-surface expression of WT, E_IA and $E_{I,II,III,IIII}A$ $Ca_V2.2$-HA in N2a cells in the presence or absence of $\alpha_2\delta$ and β subunits.

(A) Confocal images of WT $Ca_V2.2$-HA (left), $Ca_V2.2$-HA E_IA (middle) and $Ca_V2.2$-HA $E_{I,II,III,IV}A$ (right) in N2a cells when coexpressed with β1b and $\alpha_2\delta$-1 (top row) or in the absence of $\alpha_2\delta$-1 (bottom row) (scale bar = 5μm). **(B)** Normalised mean cell-surface expression (bar chart) of WT $Ca_V2.2$-HA with β1b (blue open; n = 150 cells), WT $Ca_V2.2$-HA with β1b/$\alpha_2\delta$-1 (blue solid; n = 126 cells) , $Ca_V2.2$-HA E_IA with β1b (red open; n = 69 cells), $Ca_V2.2$-HA E_IA with β1b/$\alpha_2\delta$-1 (red solid; n = 86 cells), $Ca_V2.2$-HA $E_{I,II,III,IV}A$ with β1b (green open; n = 134 cells), $Ca_V2.2$-HA $E_{I,II,III,IV}A$ with β1b/$\alpha_2\delta$-1 (green solid; n = 130 cells) in N2a cells. **(C)** Confocal images of WT $Ca_V2.2$-HA (left), $Ca_V2.2$-HA E_IA (middle) and $Ca_V2.2$-HA $E_{I,II,III,IV}A$ (right) in N2a cells when coexpressed with $\alpha_2\delta$-1 and β1b (top row) or in the absence of β1b (bottom row) (scale bar = 5μm). **(D)** Normalised mean cell-surface expression (Bar chart) WT $Ca_V2.2$-HA with $\alpha_2\delta$-1 (blue open; n = 116 cells), WT $Ca_V2.2$-HA with β1b/$\alpha_2\delta$-1 (blue solid; n = 95 cells) , $Ca_V2.2$-HA E_IA with $\alpha_2\delta$-1 (red open; n = 96 cells), $Ca_V2.2$-HA E_IA with β1b/$\alpha_2\delta$-1 (red solid; n = 97 cells), $Ca_V2.2$-HA $E_{I,II,III,IV}A$ with $\alpha_2\delta$-1 (green open; n = 81 cells), $Ca_V2.2$-HA $E_{I,II,III,IV}A$ with β1b/$\alpha_2\delta$-1 (green solid; n = 86 cells) in N2a cells. Data were collected across 3 separate transfections. Data analysis was blinded. Data are plotted ± SEM values. Statistical significance was determined using one-way ANOVA and Bonferroni post hoc tests (***$p<0.001$).

4.4. In the absence of β coexpression, cell-surface and intracellular $Ca_V2.2$ $E_{I,II,III,IIII}A$ is higher than WT $Ca_V2.2$ in N2a cells.

The interaction between $Ca_V\beta$ and the AID sequence of the $Ca_V\alpha_{1b}$ I-II loop facilitates correct folding of the α_1 subunit and masks a site targeting α_1 for proteasomal degradation (Waithe *et al.*, 2011). In the absence of β1b, cell surface expression of $E_{I,II,III,IIII}A$ $Ca_V2.2$ was reduced by a lower proportion than observed for WT (Fig 4.3D) raising the possibility that these P-loop $Ca_V2.2$ mutants are less β-dependent than WT $Ca_V2.2$. To further investigate this possibility, I expressed HA-tagged WT or $E_{I,II,III,IIII}A$ $Ca_V2.2$ in N2a cells with $\alpha_2\delta$-1 in the presence or absence of β1b, then used a double HA-immunostaining protocol (as described in methods 2.4.1) to identify distinct cell surface and intracellular $Ca_V2.2$ populations (Fig 4.4A). Many of the experiments in this study used an in-house anti-II-III loop antibody to quantify total $Ca_V2.2$ expression. However, during this time a lack of available, functional II-III loop antibody necessitated an alternative method to quantify intracellular $Ca_V2.2$. The approach used was to label cell-surface $Ca_V2.2$-HA from non-permeabilised N2a cells using an anti-HA rat antibody, followed by anti-rat biotin in order to mask cell-surface HA epitopes. Following this, N2a cells were permeabilised and probed for intracellular HA expression. Consistent with earlier observations, cell surface $E_{I,II,III,IIII}A$ is 50% lower than WT when expressed with β1b and, once again, the reduction in cell surface expression in the absence of β1b is more drastic for the WT (96.7%) than $E_{I,II,III,IIII}A$ (75.5%) (Fig 4.4B). When expressed with β1b, there is little difference in relative intracellular expression of WT and $E_{I,II,III,IIII}A$ (112% of WT) $Ca_V2.2$ (Fig 4.4C). However in the absence of β1b, I observe a statistically significant 38.6% decrease in intracellular expression of WT $Ca_V2.2$ and a more modest 20.4% decrease for $E_{I,II,III,IIII}A$ (Fig 4.4C). Together

these data suggest that both cell surface and intracellular expression of $E_{I,II,III,IIII}A$ are higher than WT $Ca_V2.2$ in the absence of β1b and support the notion that $E_{I,II,III,IIII}A$ is less β-dependent than WT.

The conserved P-loop glutamate residues of Ca_V channels are strongly suggested to form a high affinity Ca^{2+} binding site that facilitates the highly selective entry of Ca^{2+} into the central vestibule (Tang et al, 2014). An interesting but unexplored possibility is that binding of Ca^{2+} to these sites is also important for the interaction of α_1 and auxiliary β subunits during early stages of channel maturation. It is possible that the loss of Ca^{2+} binding within the selectivity filter disrupts α_1-β binding. Alternatively, the β-AID interaction could promote Ca^{2+} binding in the channel pore, with the coordinated Ca^{2+} ion facilitating further structural maturation. In either instance, one would expect normal folding and trafficking of the mutant channels to be disrupted, consistent with the observations in this study.

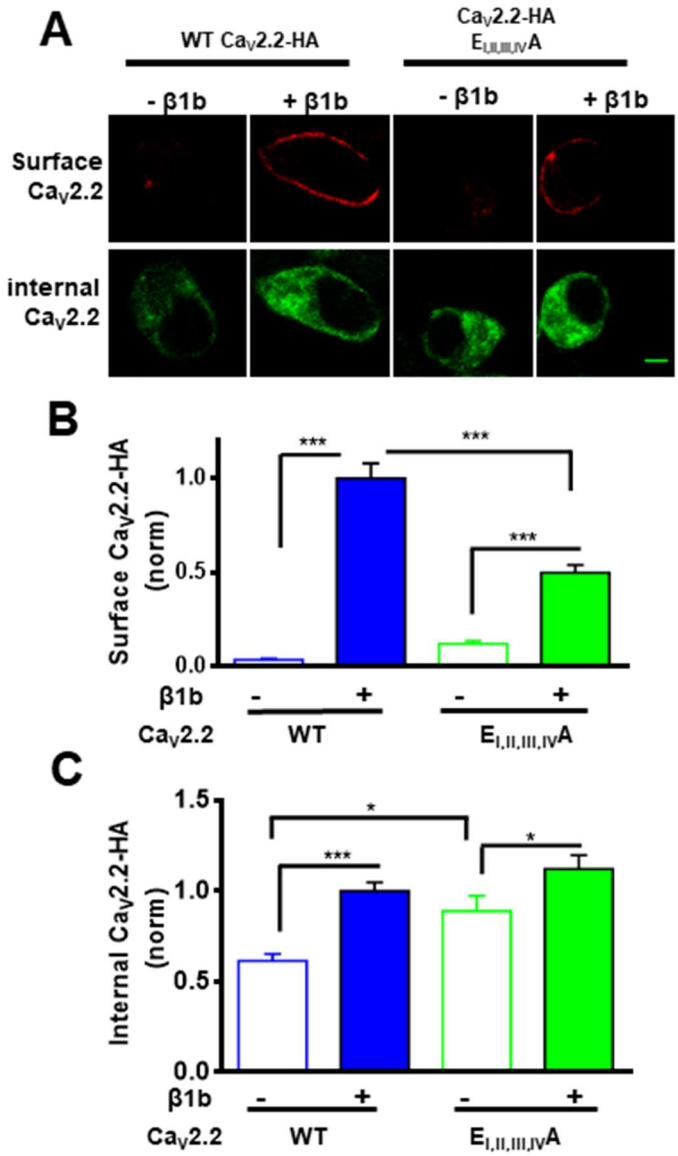

Figure 4.4 Cell-surface and intracellular expression of WT and $E_{I,II,III,IIII}A$ $Ca_V2.2$ in the presence or absence of β1b.

(A) Confocal images of cell-surface $Ca_V2.2$ (top panel) and intracellular $Ca_V2.2$ (bottom panel) in N2a cells expressing: WT $Ca_V2.2$ with $\alpha_2\delta$-1 or $Ca_V2.2$-HA $E_{I,II,III,IV}A$ with $\alpha_2\delta$-1 in the presence or absence of β1b (scale bar = 5 μm) **(B)** Normalised mean cell-surface expression (bar chart) of $Ca_V2.2$-HA with β1b (blue open; n = 116 cells) , $Ca_V2.2$-HA with β1b/$\alpha_2\delta$-1 (blue solid; n = 95 cells) , $Ca_V2.2$-HA E_IA with β1b (red open; n = 96 cells), $Ca_V2.2$-HA E_IA with β1b/$\alpha_2\delta$-1 (red solid; n = 97 cells), $Ca_V2.2$-HA $E_{I,II,III,IV}A$ with β1b (green open; n = 81 cells), $Ca_V2.2$-HA $E_{I,II,III,IV}A$ with β1b/$\alpha_2\delta$-1 (green solid; n = 86 cells) in N2a cells. **(C)** Normalised mean intracellular $Ca_V2.2$-HA expression for conditions in panel G. Data were collected across 3 separate transfections. Data analysis was blinded. Data are plotted ± SEM values. Statistical significance was determined using one-way ANOVA and Bonferroni post hoc tests (*$p<0.05$, ***$p<0.001$).

4.5 E-A $Ca_V2.2$ pore mutants have reduced neurite expression in primary hippocampal cultures but retain $\alpha_2\delta$ dependence

In hippocampal neurons, trafficking of $Ca_V2.2$ to the neurites and plasma membrane insertion therein is largely dependent on proteolytically processed $\alpha_2\delta$; however, processed $\alpha_2\delta$ is not required for plasma membrane $Ca_V2.2$ expression in non-neuronal cell lines such as tsA-201 cells and undifferentiated N2a cells (Cassidy *et al.*, 2014; Kadurin *et al.*, 2016). When expressed in tsA-201 cells, non-cleaved $\alpha_2\delta$-1 was shown to increase cell-surface $Ca_V2.2$ expression but was unable to enhance whole-cell Ca_V currents (Kadurin *et al.*, 2016). These observations led to the idea of a neuron-specific mechanism that prevents immature $Ca_V2.2$ complexes from trafficking to the neurites (Kadurin *et al.*, 2016). In this study, I sought to determine whether non-functional or partially-functional $Ca_V2.2$ mutants expressed in hippocampal neurons are able to efficiently traffic to the neurites when compared to WT $Ca_V2.2$. To do this, I expressed WT $Ca_V2.2$-HA, $Ca_V2.2$-HA E_IA or $Ca_V2.2$-HA $E_{I,II,III,IIII}A$ in primary rat hippocampal neurons with β1b, free mCherry as a transfection marker, and either $\alpha_2\delta$-1 or empty vector. After 7 d expression, neurons were fixed and immunostained for cell-surface HA under non-permeabilised conditions and imaged using confocal microscopy (Fig 4.4.1A). I then compared the level of plasma membrane-inserted $Ca_V2.2$-HA between these conditions in hippocampal neurites at least 100µm from the cell soma (Fig 4.4.1.B). When expressed with β1b and $\alpha_2\delta$-1, I find that cell-surface neurite $Ca_V2.2$-HA is reduced by 55% and 76% for $Ca_V2.2$-HA E_IA and $Ca_V2.2$-HA $E_{I,II,III,IIII}A$ respectively, relative to WT $Ca_V2.2$-HA (Fig 4.4.1B). When $\alpha_2\delta$-1 is absent, relative cell-surface expression is reduced by 67% for WT $Ca_V2.2$-HA, 61% for $Ca_V2.2$-HA E_IA and 59% for $Ca_V2.2$-HA $E_{I,II,III,IIII}A$ (Fig 4.4.1B). These data suggest that $Ca_V2.2$-HA E_IA and

$Ca_V2.2$-HA $E_{I,II,III,IIII}A$ have a reduced ability to express at the neurite cell surface, however they appear to retain a similar dependence on $\alpha_2\delta$ to that shown by WT $Ca_V2.2$, as there was a proportional loss of cell-surface expression for each $Ca_V2.2$ variant in the absence of $\alpha_2\delta$ (Fig 4.4.1B). These data do not quantify total $Ca_V2.2$-HA expression within the neurites, so it is unclear whether $Ca_V2.2$-HA E_IA and $Ca_V2.2$-HA $E_{I,II,III,IIII}A$ have impaired trafficking to the neurites themselves or whether they reach the neurites but are unable to insert into the plasma membrane as efficiently as WT $Ca_V2.2$.

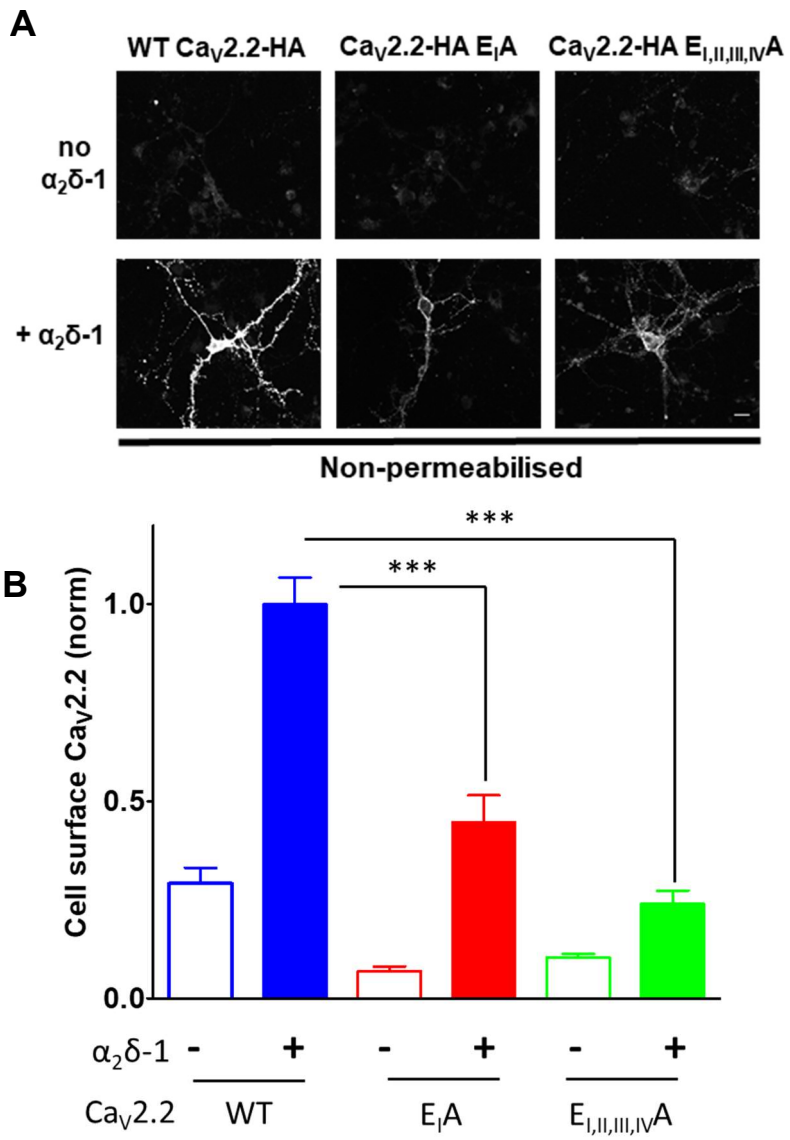

Figure 4.4.1 Plasma membrane-inserted $Ca_V2.2$ is reduced at hippocampal neurites for E-A $Ca_V2.2$ pore mutants.

(A) Confocal Images of WT $Ca_V2.2$-HA (left), $Ca_V2.2$-HA E_IA (middle) or $Ca_V2.2$-HA $E_{I,II,III,IV}A$ (right) expressed in non-permeabilised hippocampal neurons when coexpressed with β1b in the absence of $\alpha_2\delta$-1 (top panel) or with $\alpha_2\delta$-1 coexpression (bottom panel) (scale bar = 20μm). (B) Normalised mean cell-surface HA expression (bar chart) for HA in neuronal processes of non-permeabilised hippocampal neurons transfected with: WT $Ca_V2.2$-HA/β1b (blue open; n = 33 cells), $Ca_V2.2$-HA/β1b/$\alpha_2\delta$-1 (blue solid; n = 41 cells), $Ca_V2.2$-HA E_IA/β1b (red open; n = 20 cells), $Ca_V2.2$-HA E_IA/β1b/$\alpha_2\delta$-1 (red solid; n = 21 cells) or $Ca_V2.2$-HA $E_{I,II,III,IV}A$/β1b (green open; n = 36 cells processes), $Ca_V2.2$-HA $E_{I,II,III,IV}A$/β1b/$\alpha_2\delta$-1 (green solid; n = 26 cells). Data were collected across 3 separate transfections. Data analysis was blinded. Data are plotted ± SEM values. Statistical significance was determined using one-way ANOVA and Bonferroni post hoc tests (***p<0.001).

4.5.1 Total expression of E-A $Ca_V2.2$ pore mutants at hippocampal neurites is reduced relative to WT $Ca_V2.2$.

$Ca_V2.2$-HA E_IA and $Ca_V2.2$-HA $E_{I,II,III,IIII}A$ were shown to have diminished cell-surface expression in hippocampal neurites, relative to WT $Ca_V2.2$ (Fig 4.4.1B). Reduced neurite cell-surface expression of these P-loop $Ca_V2.2$ mutants could reflect a defect in trafficking to the neurites as well as – or instead of – an inability to insert into the plasma membrane of the neurites. To test this, I expressed WT $Ca_V2.2$, $Ca_V2.2$-HA E_IA or $Ca_V2.2$-HA $E_{I,II,III,IIII}A$ in primary rat hippocampal neurons with β1b and $\alpha_2\delta$-1 and free mCherry as a transfection marker. After 7 d expression, neurons were fixed, permeabilised and probed for total HA in neurites beginning 100µm from the soma (Fig 4.4.2A). I found that total $Ca_V2.2$-HA expression is reduced by 52% for $Ca_V2.2$-HA E_IA and 51% for $Ca_V2.2$-HA $E_{I,II,III,IIII}A$ relative to WT $Ca_V2.2$ (Fig 4.4.2B). The reduction of total neurite expression of $Ca_V2.2$ E_IA and $E_{I,II,III,IV}A$ could suggest that these mutants are poorly trafficked to the neurites relative to WT $Ca_V2.2$. It is possible that reduced cell-surface $Ca_V2.2$-HA E_IA and $Ca_V2.2$-HA $E_{I,II,III,IIII}A$ at hippocampal neurites is primarily a consequence of defective trafficking from the neuronal soma, rather than an inability of the mutant channels to localise to the neurite plasma membrane.

While $Ca_V2.2$-HA E_IA and $Ca_V2.2$-HA $E_{I,II,III,IIII}A$ have reduced neurite expression relative to WT $Ca_V2.2$, the difference is similar to my earlier observations for plasma membrane expression of $Ca_V2.2$-HA E_IA and $Ca_V2.2$-HA $E_{I,II,III,IIII}A$ in undifferentiated N2a cells (Fig 4.3B). It therefore seems unlikely that reduced neurite expression of $Ca_V2.2$-HA E_IA and $Ca_V2.2$-HA $E_{I,II,III,IIII}A$ is a consequence of a neuron-specific regulatory mechanism.

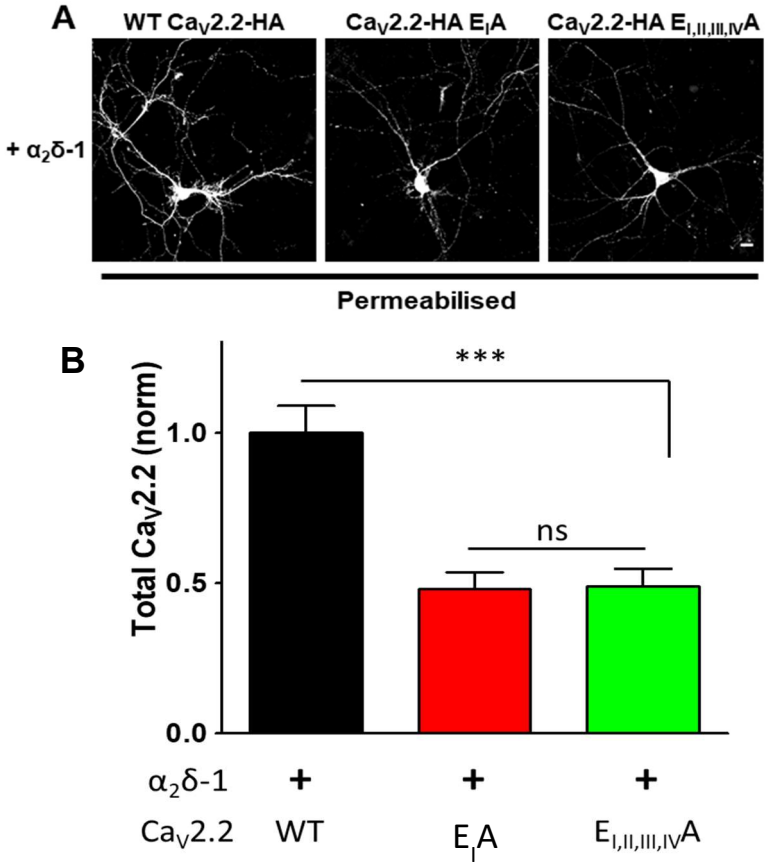

Figure 4.4.2. Total expression of E-A $Ca_V2.2$ pore mutants is reduced at hippocampal neurites relative to WT $Ca_V2.2$

(A) Confocal images of WT $Ca_V2.2$-HA (left), $Ca_V2.2$-HA E_IA (middle) or $Ca_V2.2$-HA $E_{I,II,III,IV}A$ (right) in permeabilised rat hippocampal neurons coexpressed with β1b and $\alpha_2\delta$-1 (scale bar = 20μm). (B) Normalised mean total expression (bar chart) for WT $Ca_V2.2$-HA (blue, n = 97 cells), $Ca_V2.2$-HA E_IA (red, n = 71 cells) or $Ca_V2.2$-HA $E_{I,II,III,IV}A$ (green, n = 55 cells processes) in permeabilised hippocampal processes coexpressed with β1b and $\alpha_2\delta$-1. Data were collected across 3 separate transfections. Data analysis was blinded. Data are plotted ± SEM values. Statistical significance was determined using one-way ANOVA and Bonferroni post hoc tests (***$p<0.001$; ns: $p>0.05$).

4.6 Summary

In this study I sought to establish whether trafficking and plasma membrane expression of $Ca_V2.2$ is influenced by mutations to conserved P-loop glutamate residues which coordinate a Ca^{2+}-binding site thought to be responsible for the high Ca^{2+} fidelity of permeation of these channels (Tang *et al.*, 2014). To achieve this I compared the cell-surface and total expression of exofacially HA tagged WT, $E_{IV}K$, E_IA and $E_{I,II,III,IIII}A$ $Ca_V2.2$ in undifferentiated N2a cells. Thereafter I compared the neurite expression of WT, E_IA and $E_{I,II,III,IIII}A$ $Ca_V2.2$ to determine whether my observations in cell lines were conserved in neurons. I find that $E_{IV}K$ $Ca_V2.2$ has extremely limited plasma membrane expression in N2a cells despite showing extremely high total expression relative to WT $Ca_V2.2$ (Fig.4.2). Following this, I compared cell-surface expression of WT, E_IA and $E_{I,II,III,IIII}A$ $Ca_V2.2$ in N2a cells when expressed in the presence or absence of $\alpha_2\delta$ and β subunits. I found that $Ca_V2.2$ $E_{IV}A$ (which has partial inward current) and $Ca_V2.2$ $E_{I,II,III,IIII}A$ (no inward current) have reduced cell-surface expression relative to WT by 49% and 61% respectively when expressed with $\alpha_2\delta$-1 and β1b (Fig 4.3B). In the absence of $\alpha_2\delta$-1, cell-surface expression of WT, E_IA and $E_{I,II,III,IIII}A$ $Ca_V2.2$ is similarly reduced (Fig 4.3B). In the absence of β1b, I observe a reduction in cell-surface expression of 80% for WT, 75% for E_IA and 57% for $E_{I,II,III,IIII}A$ $Ca_V2.2$ (Fig 4.3D). Further investigation showed that intracellular expression of WT $Ca_V2.2$ is reduced by 38% in the absence of β whereas intracellular $E_{I,II,III,IIII}A$ $Ca_V2.2$ expression had a smaller 20% reduction under these conditions (Fig 4.4B) which could suggest that $E_{I,II,III,IIII}A$ $Ca_V2.2$ expression is less dependent on β than WT channels. I next compared WT, E_IA and $E_{I,II,III,IIII}A$ $Ca_V2.2$ expression at the neurites of primary hippocampal neurons and found that both cell-surface and total neurite expression was reduced for E_IA and $E_{I,II,III,IIII}A$ $Ca_V2.2$ relative to WT (Fig 4.4.1, Fig 4.4.2). Cell-surface neurite expression was lower for both E_IA (55% reduction) and $E_{I,II,III,IIII}A$ $Ca_V2.2$

(76% reduction) relative to WT $Ca_V2.2$ (Fig 4.4.1B) when expressed with β1b and $\alpha_2\delta$-1. Cell-surface expression was proportionally reduced for WT, E_IA and $E_{I,II,III,IIII}A$ $Ca_V2.2$ in the absence of $\alpha_2\delta$-1 (Fig 4.4.1B). When comparing total neurite expression, I found that E_IA and $E_{I,II,III,IIII}A$ $Ca_V2.2$ are 52% and 51% lower than WT respectively (Fig 4.4.2B) suggesting that these mutants have impaired trafficking to the neurites resulting in a commensurate loss of cell-surface neurite expression.

4.7 Discussion

All members of the Ca_V channel family permit highly selective Ca^{2+} current due to the presence of a conserved glutamate residue in the pore-forming loop of each domain. These conserved glutamates have been shown to form the second of three consecutive Ca^{2+} binding site responsible for the high Ca^{2+} fidelity of these channels. A number of early studies introduced mutations to these P-loop residues for the purpose of investigating permeation mechanisms in these channels (Yang *et al.*, 1993; Sather *et al.*, 1994) , while later physiological experiments have used P-loop Ca_V mutants as non-conducting channels, with some suggesting that they function as dominant negatives, under the belief that they are well expressed at the plasma membrane due to the presence of a large outward current (Cao *et al.*, 2004). In this study, the P-loop $Ca_V2.2$ mutants E_IA and $E_{I,II,III,IIII}A$ were shown to have diminished neurite expression relative to WT $Ca_V2.2$ (Fig 4.4.2B), as such the findings of a number of previous studies involving P-loop mutants may require reinterpretation. In particular, the slots hypothesis proposed by Cao et al (2004) suggests that plasma membrane insertion of Ca_V channels at presynaptic terminal active zones is restricted by a finite number of available slots for these channels to occupy (Cao *et al.*, 2004). Among the pieces of evidence given for this hypothesis, was the finding that expression of the non-functional $Ca_V2.1$(E4A) mutant –

featuring E-A substitutions of all 4 conserved P-loop glutamates – reduced synaptic transmission, which was interpreted as a consequence of competition with WT $Ca_V2.1$ for presynaptic slots (Cao *et al.*, 2004). $Ca_V2.1$ (E4A) was characterised as having normal cell surface expression in HEK293 cells, although this assessment relied on fluorescence overlap between a known plasma membrane marker and intracellularly GFP-tagged $Ca_V2.1$(E4A) (Cao *et al.*, 2004) which does not definitively identify $Ca_V2.1$(E4A) as plasma membrane-inserted.

Previous work by Kadurin et al (2016), suggested the presence of an intracellular trafficking checkpoint in neurons that prevents immature or incorrectly folded $Ca_V2.2$ channels from reaching the cell surface. This hypothesis was based on the observation that $Ca_V2.2$ channels are unable to traffic to the cell surface in hippocampal neurons when in the absence of $\alpha_2\delta$ or when expressed with non-proteolytically processed $\alpha_2\delta$ (Kadurin *et al.*, 2016). Unprocessed $\alpha_2\delta$ does not permit voltage-dependent activation of Ca_V2 channels leading to the hypothesis that $\alpha_2\delta$ might act as a sensor for channel functionality as part of this trafficking checkpoint (Kadurin *et al.*, 2016). The long term aim of the present study, was to determine whether non-conducting $Ca_V2.2$ pore mutants are able to express and traffic efficiently to the cell surface in neurons, or whether mutations to these residues – which disrupt Ca^{2+}binding in the pore – preclude trafficking due to the presence of a neuronal checkpoint mechanism. However, when examining the expression and trafficking of a number of P-loop $Ca_V2.2$ mutants in non-neuronal cell lines, I found that these channels already have severely diminished cell-surface expression, despite coexpression with $\alpha_2\delta$ and β subunits. One interpretation for this result is that either binding of Ca^{2+} in the pore, or Ca^{2+} conduction through the pore, is necessary for normal channel trafficking. Previous studies have shown that Ca^{2+} remains bound to the pore of Ca_V1 channels even at μM Ca^{2+} levels (Yang *et al.*, 1993). An interesting possibility is that Ca^{2+} binding to

the pore is involved in optimising the structure of the channel for trafficking potentially through interactions with auxiliary subunits. One way this might occur would be by allowing the β subunit to promote α-helix formation in the I-II linker which is required for correct folding and trafficking of the channel (Findeisen & Minor, 2009). Consistent with this idea, I found that cell-surface $Ca_V2.2$ $E_{I,II,III,IIII}A$ expressed in N2a cells is higher than WT $Ca_V2.2$ when expressed in the absence of the β subunit, while the reverse is true with β coexpression (Fig 4.4B,C). This could suggests that β is less effective at promoting $Ca_V2.2$ $E_{I,II,III,IIII}A$ trafficking than WT $Ca_V2.2$, potentially indicating an impaired interaction between these subunits or an impaired effect of β on the mutant channels. It seems unlikely that $Ca_V2.2$ pore mutants have an altered interaction with $\alpha_2\delta$ subunits as I observe a proportional decrease in plasma membrane expression for both WT and E-A pore mutants when expressed in the absence of $\alpha_2\delta$ in N2a cells (Fig 4.3B) and hippocampal neurons (Fig 4.4.1B). These data also strongly suggest that neither Ca^{2+} binding to the pore or Ca^{2+} conductance through the pore are criteria of the neuron-specific intracellular trafficking checkpoint proposed by Kadurin et al (2016).

Chapter 5 Trafficking of $\alpha_2\delta$ and $Ca_V2.2$

5.1. Introduction

$\alpha_2\delta$s have long been known to enhance whole-cell currents through Ca_V channels (Gurnett *et al*., 1996; Felix *et al.*, 1997; Wakamori *et al*., 1999). However, there is limited evidence that $\alpha_2\delta$s influence the single-channel properties of Ca_Vs. As such $\alpha_2\delta$-enhanced Ca_V currents have often been attributed to increased channel trafficking and plasma membrane-insertion (Wakamori *et al*., 1999; Davies *et al.*, 2006; Hendrich *et al.*, 2008; Cassidy *et al.*, 2014). The recent development of functional exofacially-tagged Ca_V2 constructs has allowed us to define populations of plasma membrane-inserted Ca_V2 channels. This was previously used to demonstrate that $\alpha_2\delta$-1 does indeed increase cell-surface $Ca_V2.2$ expression (Cassidy *et al*., 2014). However, more recent studies on the proteolytic processing of $\alpha_2\delta$ found that unprocessed $\alpha_2\delta$-1 is unable to enhance macroscopic Ca_V currents despite increasing cell-surface $Ca_V2.2$ in cell lines (Kadurin *et al*., 2016). This provides convincing evidence that $\alpha_2\delta$-mediated increases in $Ca_V2.2$ currents can only partially relate to changes in cell-surface $Ca_V2.2$ expression. Presently it is unclear if $\alpha_2\delta$s differ significantly in their ability to enhance Ca_V currents and it remains to be seen if $\alpha_2\delta$ subtypes have uniform trafficking mechanisms particularly with regard to their effect on Ca_V localisation.

In a previous study by Tran Van Minh & Dolphin (2010), it was found that cell-surface $\alpha_2\delta$-2, heterologously expressed in tsA-201 cells, was increased through recycling from Rab11a-dependent endosomes back to the plasma membrane. Rab11a belongs to the 66 strong Rab family of small GTPases which regulate a multitude of intracellular trafficking pathways, facilitating membrane targeting, cargo sorting and vesicle fusion events through recruitment of effectors and direct interactions with cargo proteins (see Li & Marlin, 2015 review for details). Inhibition

of Rab11a-dependent recycling can be achieved through expression of the dominant negative mutant Rab11aS25N, which is locked in an inactive GDP-bound conformation. Cell-surface expression of $\alpha_2\delta$-2 is reduced in the presence of Rab11aS25N with subsequent application of Gabapentin providing no further decrease (Tran-Van-Minh & Dolphin, 2010). These data provide a mechanistic explanation of Gabapentin action whereby $\alpha_2\delta$-2 bound to Gabapentin is prevented from recycling to the plasma membrane via Rab11-positive endosomes, resulting in a loss of cell-surface expression. Mutational studies have suggested that Gabapentin binds to an RRR motif in the α_2 domain present only in $\alpha_2\delta$-1 and $\alpha_2\delta$-2. Gabapentin is thought to displace an endogenous $\alpha_2\delta$ ligand, potentially inducing a conformational change that prevents trafficking through the Rab11a-recycling pathway. While the putative endogenous ligand has yet to be identified, the amino acids leucine and isoleucine have been found to bind $\alpha_2\delta$, albeit with a lower affinity than Gabapentin (Brown *et al.*, 1998). Leucine and isoleucine are present at micromolar concentrations in human cerebrospinal fluid making them interesting candidates as endogenous small molecule modulators of $\alpha_2\delta$ (Perry *et al.*, 1975). It is interesting to consider the possibility that $\alpha_2\delta$ subtypes might be differentially regulated through small molecule binding. Modulation of $\alpha_2\delta$ by small molecules might allow for subcellular partitioning among $\alpha_2\delta$ subtypes. Indeed, divergence in $\alpha_2\delta$ localisation would presumably influence the trafficking and localisation of associated Ca_V channels.

The initial aim of this chapter was to determine whether enhancement of plasma membrane $Ca_V2.2$ expression – a feature of $\alpha_2\delta$-1 function – is conserved among other $\alpha_2\delta$ subtypes. Thereafter, I sought to elucidate the mechanisms through which $\alpha_2\delta$s increase cell-surface $Ca_V2.2$, and to understand how this process influences the localisation and function of $Ca_V2.2$ in cell lines and hippocampal neurons. To achieve this, I used immunocytochemical, live-labelling and

electrophysiological approaches to compare the effect of different $\alpha_2\delta$ subtypes on the trafficking and function of exofacially-tagged $Ca_V2.2$. I find that $\alpha_2\delta$s have a differential effect on $Ca_V2.2$ trafficking, with $\alpha_2\delta$-1 and $\alpha_2\delta$-2 increasing the net forward trafficking of $Ca_V2.2$; by contrast $\alpha_2\delta$-3 was not found to influence $Ca_V2.2$ forward trafficking, over the period examined. Further examination suggests enhanced forward trafficking is a rab11a-dependent effect and that $\alpha_2\delta$-1 and $\alpha_2\delta$-2 participate in rab11a-positive recycling, whereas $\alpha_2\delta$-3 does not. A number of studies have linked both Rab11a and $\alpha_2\delta$-1 to neurite outgrowth and growth cone development (Eroglu *et al.*, 2009; van Bergeijk *et al.*, 2015; Nguyen *et al.*, 2016). As I have demonstrated distinct trafficking pathways for $\alpha_2\delta$-1 and $\alpha_2\delta$-3, it is tempting to consider that $\alpha_2\delta$s have subtype specific functions related to their distinct subcellular localisation.

5.2. $\alpha_2\delta$ subunits differentially affect $Ca_V2.2$ expression

In undifferentiated N2a cells, overexpression of $\alpha_2\delta$-1 was reported to increase cell-surface $Ca_V2.2$ by approximately 2-fold (Cassidy *et al.*, 2014). Here I compare steady-state plasma membrane and total $Ca_V2.2$-bbs expression in N2a cells when coexpressed with auxiliary β1b and either $\alpha_2\delta$-1, $\alpha_2\delta$-2 or $\alpha_2\delta$-3 compared to a control lacking $\alpha_2\delta$ (Fig 5.1A-C). I find that all three $\alpha_2\delta$ subtypes produce an increase in total and plasma membrane $Ca_V2.2$ expression when compared to control conditions. $\alpha_2\delta$-1 coexpression was shown to produce a 140% increase in relative plasma membrane $Ca_V2.2$ (Fig 5.1D) consistent with previous reports (Cassidy *et al.*, 2014; Kadurin *et al.*, 2016). However, $\alpha_2\delta$-2 and $\alpha_2\delta$-3 expression produced notably smaller increases to plasma membrane $Ca_V2.2$ of 42% and 31% respectively (Fig 5.1E, F).

Expression of the intracellular II-III loop epitope of $Ca_V2.2$ was used as a measure of total $Ca_V2.2$. I observe an increase in II-III loop expression in the presence of $\alpha_2\delta$-1 (74%), $\alpha_2\delta$-2 (23%) and $\alpha_2\delta$-3 (47%) relative to conditions lacking $\alpha_2\delta$ (Fig 5.1D-F). $\alpha_2\delta$-2 appears to produce the smallest increase in II-III loop expression among the subtypes tested. Interestingly, $\alpha_2\delta$-3 expression correlated with a greater increase in total $Ca_V2.2$ than with $\alpha_2\delta$-2 (47% and 23% respectively) but a smaller increase in cell-surface $Ca_V2.2$ expression (31% and 42% respectively) (Fig 5.1E, F). Increased presynaptic $Ca_V2.1$ expression has previously been reported with $\alpha_2\delta$-1 (Hoppa *et al.*, 2012) consistent with my observations for $Ca_V2.2$ in N2a cells. My data suggest that $\alpha_2\delta$-1 and $\alpha_2\delta$-2 produce a greater increase in cell-surface $Ca_V2.2$ than total $Ca_V2.2$. This may indicate that these $\alpha_2\delta$ subtypes actively promote $Ca_V2.2$ trafficking to, or stability at, the plasma membrane. It is possible that increases to cell-surface $Ca_V2.2$ are secondary to an increase in total $Ca_V2.2$ when $\alpha_2\delta$ is expressed. However, in this scenario one might expect a commensurate increase in cell-surface and total $Ca_V2.2$ expression with $\alpha_2\delta$, which is not observed in the presence of $\alpha_2\delta$-3.

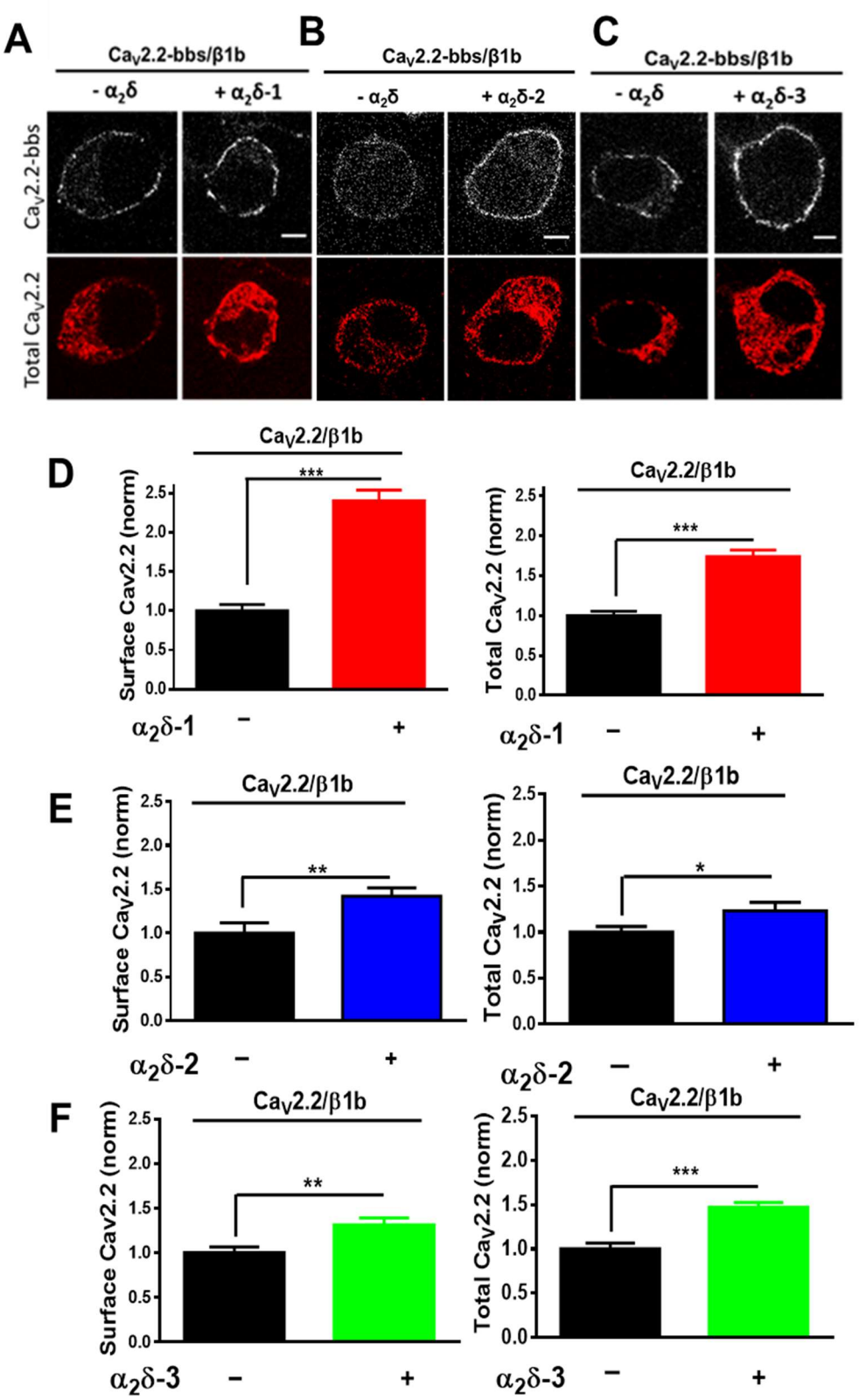

Figure 5.1 Steady-state expression of CaV2.2-bbs/β1b with $\alpha_2\delta$-1, -2 or -3 in N2a cells.

Figure 5.1. Steady-state expression of $Ca_V2.2$-bbs/β1b with $\alpha_2\delta$-1, $\alpha_2\delta$-2 or $\alpha_2\delta$-3 in N2a cells.

(A) Confocal images of N2a cells expressing $Ca_V2.2$-bbs with β1b and either no $\alpha_2\delta$ (left column) or $\alpha_2\delta$-1 (right column). Top row, BTX-488 live-labelling. Bottom row, permeabilised II-III loop immunostaining. Scale bar = 5μm. **(B)** Confocal images of N2a cells expressing $Ca_V2.2$-bbs with β1b and either: no $\alpha_2\delta$ (left column) or $\alpha_2\delta$-2 (right column). Top row, BTX-488 live-labelling. Bottom row, permeabilised II-III loop immunostaining. Scale bar = 5μm. **(C)** Confocal images of N2a cells expressing $Ca_V2.2$-bbs with β1b and either: no $\alpha_2\delta$ (left column) or $\alpha_2\delta$-3 (right column). Top row, BTX-488 live-labelling. Bottom row, permeabilised II-III loop immunostaining. Scale bar = 5μm. **(D)** Normalised mean cell-surface (left) or total (right) $Ca_V2.2$-bbs (bar chart) with β1b and either: no $\alpha_2\delta$ (black, n = 191) or $\alpha_2\delta$-1 (red, n = 205). **(E)** Normalised mean cell-surface (left) or total (right) $Ca_V2.2$-bbs (bar chart) with β1b and no $\alpha_2\delta$ (black, n = 99) or $\alpha_2\delta$-2 (blue, n = 88). **(F)** Normalised mean cell-surface (left) or total (right) $Ca_V2.2$-bbs (bar chart) with β1b and no $\alpha_2\delta$ (black, n = 188) or $\alpha_2\delta$-3 (green, n = 188). Mean fluorescence intensities were normalised to $Ca_V2.2$-bbs/β1b condition for each experiment then pooled from 3 separate transfections. Data analysis was blinded. Data are plotted ± SEM values. Statistical significance was determined using Student's unpaired t test, $^{**}P < 0.01$, $^{***}P < 0.001$.

5.3. $\alpha_2\delta$-1 and $\alpha_2\delta$-2 enhance net forward $Ca_V2.2$ trafficking

The above study provided evidence that steady-state plasma membrane $Ca_V2.2$ expression is enhanced by $\alpha_2\delta$-1 and $\alpha_2\delta$-3, albeit to differing degrees (Fig.5.1). I considered two possible explanations for $\alpha_2\delta$s-enhanced cell-surface $Ca_V2.2$: (1) $\alpha_2\delta$s increase forward trafficking of $Ca_V2.2$ to the cell surface (2) $\alpha_2\delta$s reduce the rate of $Ca_V2.2$ endocytosis from the cell surface. Previously, Cassidy et al (2014) compared rates of $Ca_V2.2$ endocytosis when expressed in N2a cells in the presence or absence of $\alpha_2\delta$-1. This study reported that, while $\alpha_2\delta$-1 enhanced plasma membrane $Ca_V2.2$ expression, the rate of $Ca_V2.2$ endocytosis was not altered by expression of $\alpha_2\delta$-1 (Cassidy *et al.*, 2014). In the present study, I used an α-BTX live-labelling approach to compare the rates of net forward $Ca_V2.2$ trafficking in N2a cells expressing $Ca_V2.2$-bbs and β1b with either: $\alpha_2\delta$-1, $\alpha_2\delta$-2, $\alpha_2\delta$-3 or empty vector pcDNA3 (control) (Fig 5.2A). When compared to control

conditions, I find that coexpression of $\alpha_2\delta$-1 and $\alpha_2\delta$-2 produced significantly higher cell surface $Ca_V2.2$ at each time point tested (Fig 5. 2B). Cell-surface $Ca_V2.2$ levels between control and $\alpha_2\delta$-3 conditions did not differ significantly up to the 45 min time point, becoming statistically significant at 60 min; this increase of 23% at 60 min is consistent with earlier steady-state observations (Fig 5.2B). Estimates for initial rates of net forward $Ca_V2.2$ trafficking were made using the slope value of a straight line between the first two time points (0-15 minutes) for each condition. I found no significant difference in initial $Ca_V2.2$ trafficking rates between control and $\alpha_2\delta$-3 conditions, 0.029 and 0.034 a.u. min respectively (Fig 5.2D). However, I report a significant increase in initial rate of $Ca_V2.2$ traffic with $\alpha_2\delta$-1 coexpression, 0.079 a.u.min (Fig 5.2E) suggesting that $\alpha_2\delta$-1 actively accelerates this process. Together these data support a role for $\alpha_2\delta$-1 and $\alpha_2\delta$-2 in enhancing plasma membrane-insertion of $Ca_V2.2$ by increasing the rate of forward trafficking. $\alpha_2\delta$-3 had no clear effect on the initial forward $Ca_V2.2$ trafficking rate despite a slight increase in maximal cell surface $Ca_V2.2$ (23%) relative to control at 60 mins (Fig 5.2B) consistent with my observations of steady-state $Ca_V2.2$ expression. It should be noted that this assay only estimates “net” forward movement and I cannot discount changes in rate of endocytosis that may be present, this will be addressed in future work. However, current literature has found no direct effect of $\alpha_2\delta$-1 on $Ca_V2.2$ endocytosis (Cassidy *et al.*, 2014; Dahimene *et al.*, 2018)

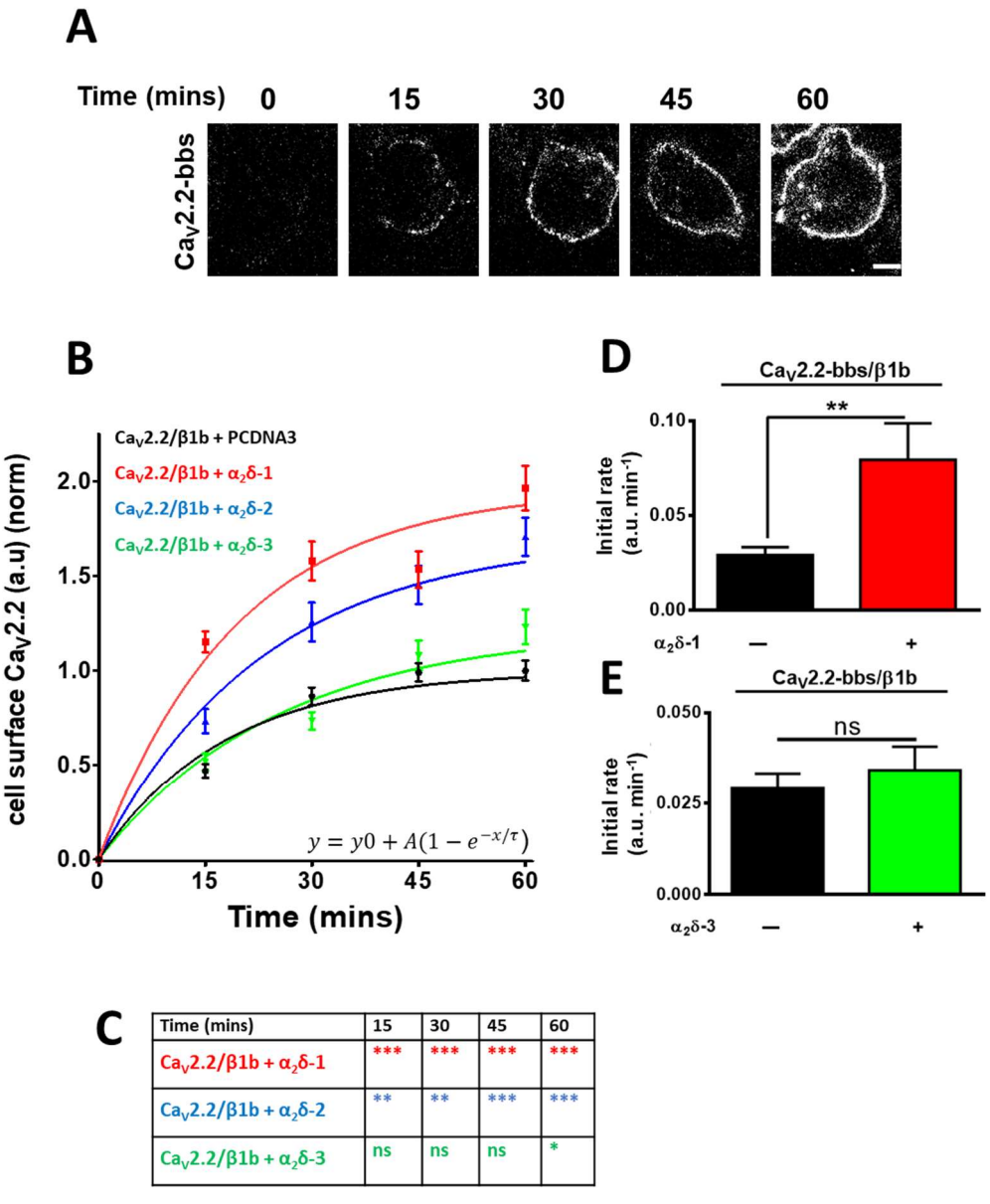

C

Time (mins)	15	30	45	60
$Ca_V2.2/\beta1b + \alpha_2\delta$-1	***	***	***	***
$Ca_V2.2/\beta1b + \alpha_2\delta$-2	**	**	***	***
$Ca_V2.2/\beta1b + \alpha_2\delta$-3	ns	ns	ns	*

Figure 5.2. Net forward trafficking of $Ca_V2.2$-bbs expressed with β1b and either either $\alpha_2\delta$-1, $\alpha_2\delta$-2, $\alpha_2\delta$-3 or empty vector PCDNA3

Figure 5.2. Net forward trafficking of $Ca_V2.2$-bbs expressed with β1b and either $\alpha_2\delta$-1, $\alpha_2\delta$-2, $\alpha_2\delta$-3 or empty vector PCDNA3

(A) Example images from forward trafficking assay for $Ca_V2.2$-bbs expressed in N2a cells with β1b and $\alpha_2\delta$-1. Cells were live-labelled with α-BTX-AF488 for 0, 15, 30, 45 and 60 minutes. Scale bar = 5μm. **(B)** Normalised mean cell-surface $Ca_V2.2$-bbs fluorescence over time in N2a cells expressing $Ca_V2.2$-bbs and β1b with either $\alpha_2\delta$-1, $\alpha_2\delta$-2, $\alpha_2\delta$-3, or PCDNA3. Cells were live-labelled with α-BTX-AF488 for 0, 15, 30, 45 and 60 minutes at 37ºC following pre-incubation with unlabelled α-BTX at 17ºC for 30 minutes. An average of 30-60 cells were analysed per time point, for each condition in an individual experiment. The data were collected as paired experiments between $Ca_V2.2$/β1b + PCDNA3 (control) and $Ca_V2.2$/β1b + $\alpha_2\delta$. 3 transfections were carried out per $Ca_V2.2$/β1b + $\alpha_2\delta$ condition, with a total of 9 for $Ca_V2.2$/β1b + PCDNA3. Individual experiments were normalised to mean 60 min fluorescence of the paired $Ca_V2.2$/β1b + PCDNA3 condition, before being pooled together. Data were plotted using Graphpad 5 software and fitted with a one-phase exponential association equation shown on graph. **(C)** Statistical comparison of mean fluorescence values again control condition at each time point was determined using one-way ANOVA and Bonferroni post-hoc tests. **(D, E)** Initial rate of net forward $Ca_V2.2$-bbs trafficking. The gradient of straight line between 0-15 min was obtained as an average for each individual experiment and summarised (in a.u. min). Panel D compares $Ca_V2.2$/β1b + PCDNA3 (black, n=3) and $Ca_V2.2$/β1b + $\alpha_2\delta$-1 (red, n=3). Panel E compares $Ca_V2.2$/β1b + PCDNA3 (black, n=3) and $Ca_V2.2$/β1b + $\alpha_2\delta$-3 (green, n=3). **P<0.01 (Student's unpaired t-test). Data are plotted ± SEM values.

5.4. $\alpha_2\delta$-3 expression and localisation is unaffected by Rab11a-recyling

Trafficking through Rab11a-positive recycling endosomes enhances $\alpha_2\delta$-2 membrane expression with Gabapentinoids shown to interrupt $\alpha_2\delta$-2 recycling through this pathway (Tran-Van-Minh & Dolphin, 2010). The α_2 domain of $\alpha_2\delta$-1 and $\alpha_2\delta$-2 possess a triple RRR motif – identified through alanine scanning mutagenesis - required for GBP binding and lacking in $\alpha_2\delta$-3 and $\alpha_2\delta$-4 (Wang *et al.*, 1999). This study considered the possibility that $\alpha_2\delta$-1 and $\alpha_2\delta$-2 enhance cell-surface $Ca_V2.2$ expression by facilitating the recycling of $Ca_V2.2$ through Rab11a-

positive endosomes. Further to this, I speculated that $\alpha_2\delta$-3 traffics independently of the Rab11a-positive recycling endosomes and consequently is unable to enhance $Ca_V2.2$ forward trafficking through this pathway. To test my hypothesis, I used the dominant negative Rab11aS25N mutant in which a key serine to asparagine substitution locks Rab11a in an inactive GDP-bound state. Previously, Rab11aS25N has been confirmed to inhibit $\alpha_2\delta$-2 forward trafficking, and a similar result is expected for $\alpha_2\delta$-1 (Tran-Van-Minh & Dolphin, 2012). Here I use immunocytochemistry to compare cell-surface and intracellular expression of HA-tagged $\alpha_2\delta$-1 and $\alpha_2\delta$-3 in N2a cells when paired with Rab11aS25N (Fig 5.3A). Cell-surface $\alpha_2\delta$-3 immunostaining is typically weaker than $\alpha_2\delta$-1, so antigen retrieval was applied to all samples prior to immunostaining in order to maximise available HA signal. I find a reduction in relative cell-surface and intracellular $\alpha_2\delta$-1-HA staining of 47% and 26% respectively, when expressed with Rab11aS25N (Fig 5.3B, C). $\alpha_2\delta$-3 showed no significant difference in either cell surface or intracellular expression whether expressed with Rab11aS25N or empty vector (Fig 5.3B, C). These data provide evidence that $\alpha_2\delta$-1 - like $\alpha_2\delta$-2 - is regulated by Rab11a-dependent recycling and suggest that $\alpha_2\delta$-3 does not traffic through this endosomal pathway.

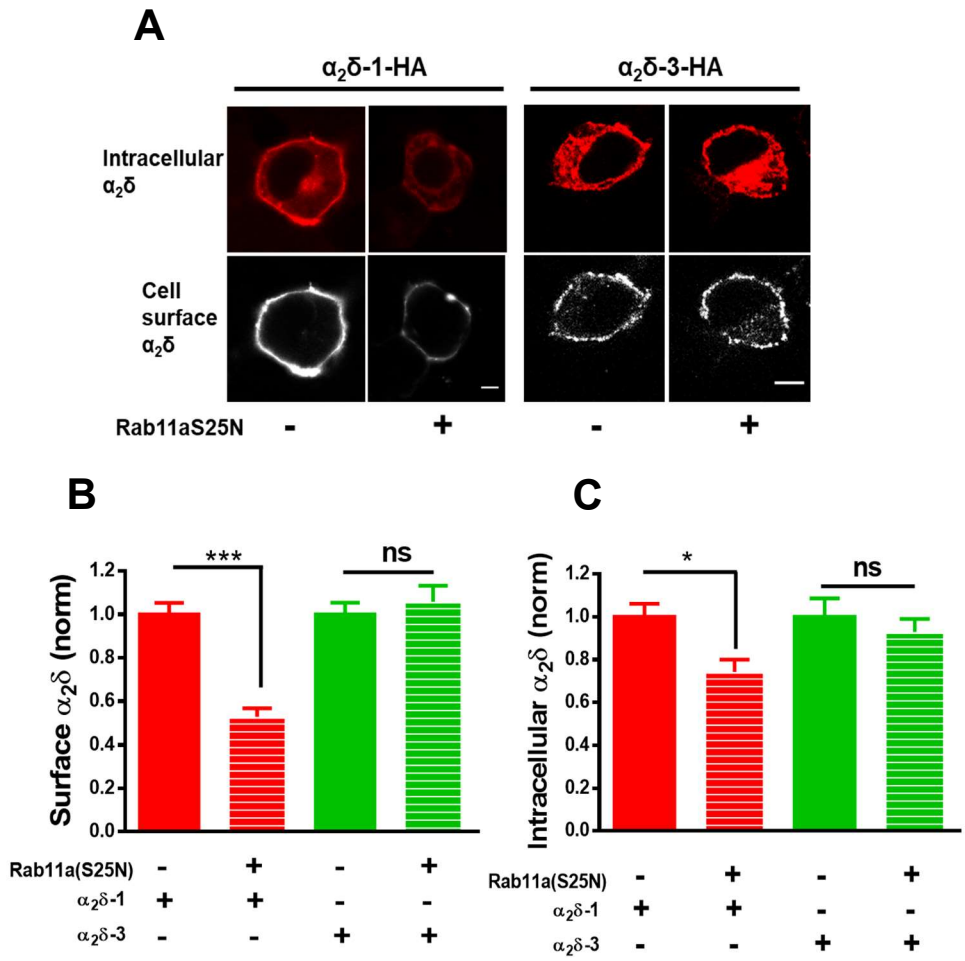

Figure 5.3. Steady-state cell-surface expression of HA-tagged α₂δ-1 and α₂δ-3 in the presence or absence of Rab11aS25N.

(A) Confocal images of cell-surface (bottom row) and intracellular (top row) HA staining in N2a cells expressing α₂δ-1-HA (left) or α₂δ-3-HA (right) in the presence or absence of Rab11aS25N. Scale bar = 5µm. **(B)** Normalised mean cell-surface α₂δ expression: α₂δ-1 control (red), α₂δ-1 + Rab11aS25N (red, striped), α₂δ-3 control (green), α₂δ-3 + Rab11aS25N (green, striped). **(C)** Normalised mean total α₂δ expression: α₂δ-1 control (red), α₂δ-1 + Rab11aS25N (red, striped), α₂δ-3 control (green), α₂δ-3 + Rab11aS25N (green, striped). Mean fluorescence intensities were normalised to α₂δ control conditions for each experiment and then pooled from 3 separate transfections. Each cell was measured for cell surface and total HA expression: α₂δ-1 control (n = 159), α₂δ-1 + Rab11aS25N (n = 161), α₂δ-3 control (n = 134), α₂δ-3 + Rab11aS25N (n = 135). Data analysis was blinded. Data are plotted ± SEM values. Statistical significance was determined using Student's unpaired t test, **P* <0.05, ****P* <0.001.

5.5. Cell-surface $Ca_V2.2$ expression is reduced by Rab11aS25N when $\alpha_2\delta$-1 or $\alpha_2\delta$-2 are present.

Rab11a-recycling enhances the plasma membrane expression of both $\alpha_2\delta$-1 and $\alpha_2\delta$-2. Inhibition of $\alpha_2\delta$-2 recycling through Rab11a-positive endosomes has been shown to reduce whole-cell $Ca_V2.2$ currents (Tran-Van-Minh & Dolphin, 2010). However, a direct effect on plasma membrane insertion of associated Ca_V channels has yet to be demonstrated. Here I compare the plasma membrane expression of exofacially-tagged $Ca_V2.2$-bbs with β1b in N2a cells when coexpressed with $\alpha_2\delta$-1, $\alpha_2\delta$-3 or no $\alpha_2\delta$ (empty vector PCDNA3) in the presence or absence of Rab11aS25N (Fig 5.4A). bbs-tagged $Ca_V2.2$ was used to maintain consistency with my previous experiments. Consistent with my earlier reports, I find that plasma membrane–inserted $Ca_V2.2$ increased by 92% and 38% when coexpressed with $\alpha_2\delta$-1 and $\alpha_2\delta$-3 respectively (Fig 5.4B). However, I find that Rab11aS25N coexpression reduced the plasma membrane expression of $Ca_V2.2$ by 53% when $\alpha_2\delta$-1 was present but had no effect with $\alpha_2\delta$-3 or no $\alpha_2\delta$ (Fig 5.4B). Following this, I compared the effect of Rab11aS25N on plasma membrane $Ca_V2.2$-bbs in the presence or absence of $\alpha_2\delta$-2 (Fig 5.4C). As with $\alpha_2\delta$-1, cell-surface $\alpha_2\delta$-2 expression is reduced by Rab11aS25N (Tran-Van-Minh & Dolphin, 2010). As such, Rab11aS25N was expected reduce cell-surface $Ca_V2.2$-bbs levels when coexpressed with $\alpha_2\delta$-2. I find that cell-surface $Ca_V2.2$ expressed with $\alpha_2\delta$-2 and β1b is reduced by 35% in the presence of Rab11aS25N (Fig 5.4D). I find no change in cell-surface $Ca_V2.2$ when Rab11aS25N was expressed with $\alpha_2\delta$-3 or with no $\alpha_2\delta$ (Fig 5.4B). Interestingly, $\alpha_2\delta$-3 coexpression produced a 38% increase in $Ca_V2.2$ expression independent of Rab11aS25N coexpression. Together, these data suggest that $\alpha_2\delta$-1 and $\alpha_2\delta$-2 enhance cell-surface $Ca_V2.2$ expression through Rab11a-dependent recycling which $Ca_V2.2$ is unable to access independently. $\alpha_2\delta$-3 appears to traffic independently of Rab11a, and inhibition of Rab11-recycling

does not affect cell-surface expression of $\alpha_2\delta$-3 or coexpressed $Ca_V2.2$. Despite this, the $\alpha_2\delta$-3-mediated increase in cell-surface $Ca_V2.2$ is present, regardless of Rab11a-recycling, suggesting that $\alpha_2\delta$-3 promotes cell-surface $Ca_V2.2$ through a manner distinct from $\alpha_2\delta$-1 and $\alpha_2\delta$-2.

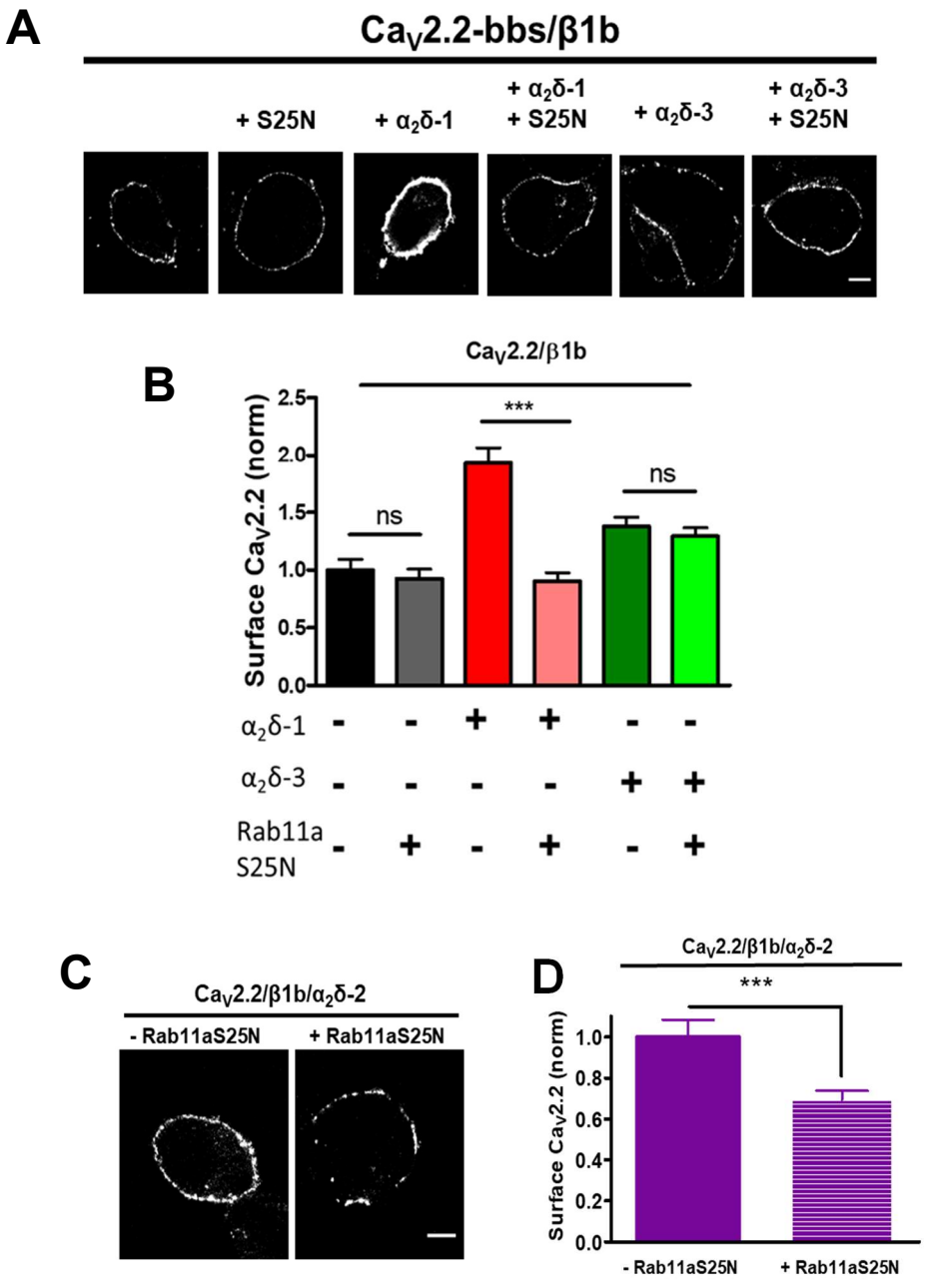

Figure 5.4. Steady-state cell-surface $Ca_V2.2$ is reduced by Rab11aS25N only when expressed with $\alpha_2\delta$-1 $\alpha_2\delta$-2.

Figure 5.4. Steady-state cell-surface $Ca_V2.2$ is reduced by Rab11aS25N only when expressed with $\alpha_2\delta$-1 and $\alpha_2\delta$-2.

(A) Confocal images of cell-surface $Ca_V2.2$-bbs expressed in N2a cells with β1b and either: $\alpha_2\delta$-1, $\alpha_2\delta$-3 or no $\alpha_2\delta$ (empty vector) in the presence or absence of Rab11aS25N. Scale bar = 5µm. **(B)** Normalised mean cell-surface $Ca_V2.2$-bbs with β1b expressed in N2a cells with: no $\alpha_2\delta$ (black, n = 142), no $\alpha_2\delta$ + Rab11aS25N (grey, n = 145), $\alpha_2\delta$-1 (red, n = 148), $\alpha_2\delta$-1 + Rab11aS25N (pink, n = 140), $\alpha_2\delta$-3 (dark green, n = 132), $\alpha_2\delta$-3 + Rab11aS25N (light green, n = 144). Statistical significance was determined using one-way ANOVA and bonferroni post hoc tests, ns>0.05, ***P <0.001. **(C)** Confocal images of cell-surface $Ca_V2.2$-bbs/β1b expressed in N2a cells with $\alpha_2\delta$-2 in the presence or absence of Rab11aS25N. Scale bar = 5µm. **(D)** Normalised mean cell-surface $Ca_V2.2$-bbs expressed in N2a with β1b and either: $\alpha_2\delta$-2 + empty vector (black, n = 97), $\alpha_2\delta$-2 + Rab11aS25N (purple, striped, n = 114). Data are collected from 3 separate transfections. Data analysis was blinded. Data are plotted ± SEM values. Student's unpaired t test, ***P <0.001.

5.6. Rab11aS25N reduces neurite $Ca_V2.2$ expression in primary hippocampal cultures when coexpressed with $\alpha_2\delta$-1

Previously, I have demonstrated that $Ca_V2.2$ can be well expressed and inserted into the plasma membrane of non-neuronal cells in the absence of $\alpha_2\delta$ (Cassidy *et al.*, 2014; Kadurin *et al.*, 2016). However, in primary hippocampal neurons $\alpha_2\delta$ expression - and proteolytic processing of $\alpha_2\delta$ - was found to be essential for efficient expression and localisation of $Ca_V2.2$ to the neurites (Kadurin *et al.*, 2016). Here, I examine whether $Ca_V2.2$ expression is influenced by Rab11a at both hippocampal neurites and soma in an $\alpha_2\delta$-dependent manner. To do this, I expressed and immunostained GFP-$Ca_V2.2$-HA in primary rat hippocampal neurons with β1b, free mCherry and either: empty vector (PCAGGS), $\alpha_2\delta$-1 or $\alpha_2\delta$-3. Each condition was paired with an empty vector (control) or Rab11aS25N (Fig 5.5A). For these experiments, I use an exofacially HA-tagged and N-terminally GFP-tagged $Ca_V2.2$ construct allowing me to quantify cell-surface and total $Ca_V2.2$ expression in non-permeabilised neurons. In accordance with previous reports,

neurite and soma expression of $Ca_V2.2$ was extremely low in the absence of $\alpha_2\delta$. I report a 233% increase in neurite $Ca_V2.2$-HA expression with $\alpha_2\delta$-1 and 177% with $\alpha_2\delta$-3 relative to empty vector controls (Fig 5.5B). Neurite GFP expression was also elevated with both $\alpha_2\delta$-1 and $\alpha_2\delta$-3 coexpression by ~122% in each case (Fig 5.5C). Consistent with my findings in N2a cells, neurite $Ca_V2.2$-HA was reduced by coexpression of Rab11aS25N only when expressed with $\alpha_2\delta$-1 and not $\alpha_2\delta$-3. I observed a 44% reduction in neurite $Ca_V2.2$-HA signal when expressed with $\alpha_2\delta$-1 + Rab11aS25N relative to the + $\alpha_2\delta$-1 control (Fig 5.5B). However, I saw no change in neurite GFP expression between conditions expressing $\alpha_2\delta$-1 with either Rab11aS25N or empty vector (Fig 5.5C). This result suggests that Rab11aS25N reduces plasma membrane-inserted $Ca_V2.2$ at the neuronal processes when expressed with $\alpha_2\delta$-1, rather than by depleting the $Ca_V2.2$ population. I report no change in neurite HA or GFP signal intensity between conditions expressing Rab11aS25N or empty vector when $Ca_V2.2$ is paired with $\alpha_2\delta$-3 or no $\alpha_2\delta$ in agreement with my observations in N2a cells (Fig 5.5B, C). I next examined cell-surface GFP-$Ca_V2.2$-HA expression at the neuronal cell body of these primary hippocampal neurons (Fig 5.5D). Contrary to my findings at the hippocampal neurites, I found no difference in plasma membrane $Ca_V2.2$ expression between conditions with or without Rab11aS25N regardless of whether $\alpha_2\delta$ was coexpressed (Fig 5.5E). This could indicate that the role of Rab11a-recycling is absent or limited at the cell soma relative to the neurites. Although the possibility should be considered that $Ca_V2.2$ overexpression at the soma might obscure small changes in channel trafficking therein. Interestingly, I find that plasma membrane $Ca_V2.2$ at the soma was 66% higher with $\alpha_2\delta$-3 than $\alpha_2\delta$-1 (Fig. 5.5E), contrasting with my observations in both hippocampal neurites and in cell lines. A simple explanation for this discrepancy would be that $\alpha_2\delta$-3 is less efficient at promoting the trafficking of $Ca_V2.2$ to the neurites, resulting in a bottleneck effect at the soma. However, it is possible that $\alpha_2\delta$-3 preferentially targets $Ca_V2.2$ to the soma,

reflecting different roles between $\alpha_2\delta$s in subcellular Ca_V localisation. Together my data suggest that Rab11a-recyling enhances neurite $Ca_V2.2$ expression in an $\alpha_2\delta$-dependent manner and suggest that Rab11a-recycling is less influential – if at all – at the neuronal cell body.

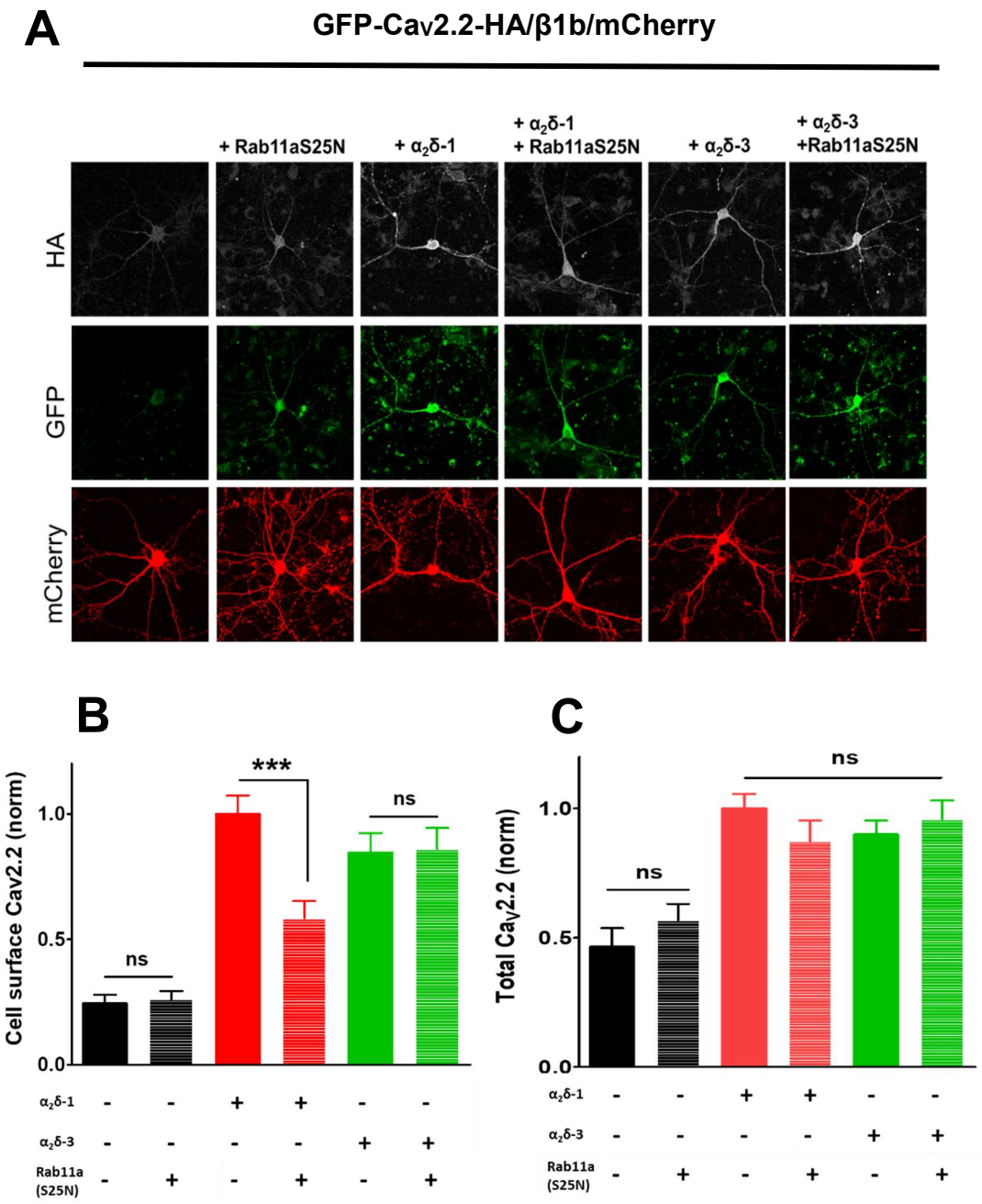

Fig 5.5 Rab11aS25N reduces plasma membrane-inserted $Ca_V2.2$ at hippocampal neurite when expressed with $\alpha_2\delta$-1 but not $\alpha_2\delta$-3

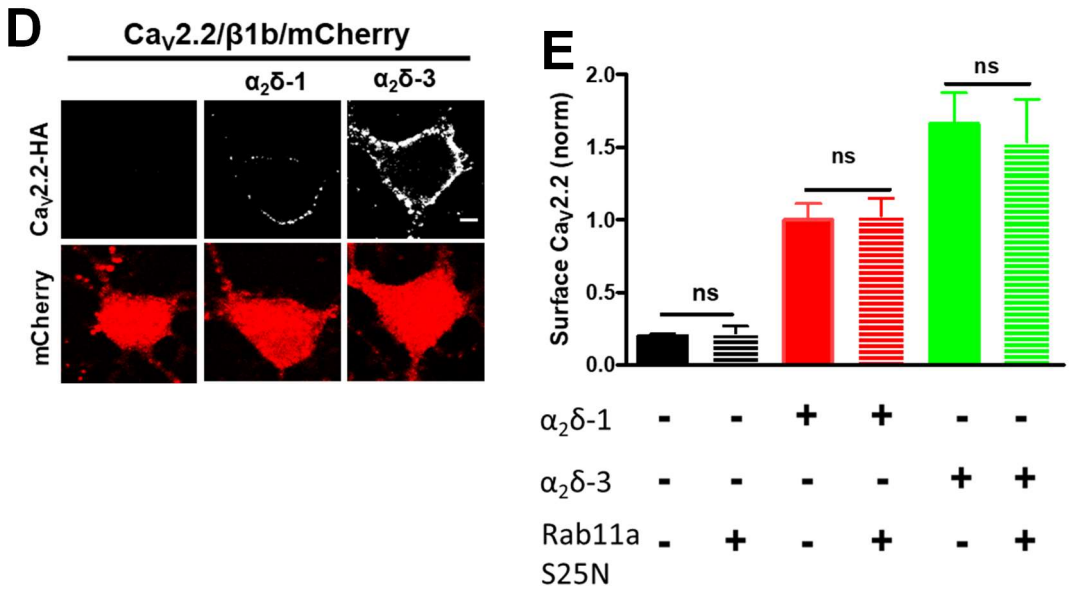

Figure 5.5. Rab11aS25N reduces plasma membrane-inserted $Ca_V2.2$ at hippocampal neurite when expressed with $\alpha_2\delta$-1 but not $\alpha_2\delta$-3

(A) Confocal images of rat hippo pyramidal neurons expressing GFP-Ca_V2.2-HA/β1b/mCherry with: empty vector, empty vector + Rab11aS25N, $\alpha_2\delta$-1, $\alpha_2\delta$-1 + Rab11aS25N, $\alpha_2\delta$-3 or $\alpha_2\delta$-3 + Rab11a(S25N). Scale bar = 20 µm. **(B)** Normalised mean cell-surface GFP-Ca_V2.2-HA in the processes of pyramidal rat neurons expressed with β1b/mCherry and either: empty vector (black, n = 30 cells), Rab11aS25N (black, striped, n = 19 cells), $\alpha_2\delta$-1 (red, n = 51 cells), $\alpha_2\delta$-1 + Rab11aS25N (red, striped, n = 42 cells), $\alpha_2\delta$-3 (blue, n = 46 cells) or $\alpha_2\delta$-3 + Rab11aS25N (blue, striped, n = 40 cells). **(C)** Normalised mean total GFP-Ca_V2.2-HA in the processes of pyramidal rat neurons expressed with β1b/mCherry and either: empty vector (black), Rab11aS25N (black, striped), $\alpha_2\delta$-1 (red), $\alpha_2\delta$-1 + Rab11aS25N (red, striped), $\alpha_2\delta$-3 (blue) or $\alpha_2\delta$-3 + Rab11aS25N (blue, striped). Total of 3 transfections. **(D)** Confocal images of pyramidal rat neurons expressing GFP-Ca_V2.2-HA/β1b/mCherry at the cell soma with: empty vector, empty vector, $\alpha_2\delta$-1 or $\alpha_2\delta$-3 or $\alpha_2\delta$-3. Scale bar = 10 µm **(E)** Normalised mean cell-surface GFP-Ca_V2.2-HA expressed at the soma of pyramidal rat neurons with β1b/mCherry and either: empty vector (black, n = 30), Rab11aS25N (black, striped, n = 20), $\alpha_2\delta$-1 (red, n = 35), $\alpha_2\delta$-1 + Rab11aS25N (red, striped, n = 33), $\alpha_2\delta$-3 (blue, n = 44) or $\alpha_2\delta$-3 + Rab11aS25N (blue, striped n = 31). Data analysis was blinded. Data are plotted ± SEM values. Statistical significance was determined using one-way ANOVA and Bonferroni post hoc tests, ns>0.05, ***P <0.001.

5.7 Rab11aS25N reduces whole-cell $Ca_V2.2$ currents when coexpressed with Rab11a-sensitive $\alpha_2\delta$-1

Previously, we have demonstrated that $\alpha_2\delta$s have distinct roles in Ca_V trafficking regulation and enhancement of whole-cell currents (Kadurin *et al.*, 2016). While there is variance in the literature, studies using heterologous expression systems such as xenopus oocytes and HEK293 cells, have reported increases in Ca_V currents by as much as 9-fold (Gao *et al.*, 2000). Despite a sizeable increase in $Ca_V2.2$ currents (approximately 5-fold), only a 2-fold increase plasma membrane $Ca_V2.2$ with $\alpha_2\delta$-1 was reported using tsA201 cells (Cassidy *et al.*, 2014). This apparent discrepancy may reflect the limited availability of sites at the plasma membrane whereby nascent $Ca_V2.2$ may be localised to the cell surface but be inactive; if so, reductions in $Ca_V2.2$ membrane expression by Rab11aS25N may not correlate to significant changes in whole-cell $Ca_V2.2$ currents. Here, I investigate whether the reduction in cell-surface $Ca_V2.2$ expression by Rab11aS25N correlates to a change in whole-cell Ca_V currents and whether any change I observe is $\alpha_2\delta$-dependent. I used voltage-clamp recording to measure whole-cell Ba^{2+} currents in tsA201 cells expressing $Ca_V2.2/\beta1b/\alpha_2\delta$-1 with either Rab11aS25N or empty vector (Fig 5.6A). I find that mean Ba^{2+} current density (pA/pF) is reduced by 58% when $\alpha_2\delta$-1 and Rab11aS25N are coexpressed compared to $\alpha_2\delta$-1 expressed alone (Fig 5.6A, B). Mean maximum conductance (G_{max}) values were 1.4±0.2 pS/pF and 0.7±0.1 pS/pF for $\alpha_2\delta$-1 control and $\alpha_2\delta$-1 + Rab11aS25N conditions respectively (Fig 5.6C). I saw no significant changes to steady-state inactivation or $V_{50\ act}$ between $\alpha_2\delta$-1 control and $\alpha_2\delta$-1 + Rab11aS25N conditions (Fig 5.6D, E) agreeing with a conclusion that current density changes occurred as a result of reduced membrane $Ca_V2.2$ expression rather than changes to biophysical properties. This data does not discount the possibility of changes to the single channel conductance of $Ca_V2,2$, although Rab11a has not been reported

to influence single channel conductance properties and there is limited evidence to suggest that $\alpha_2\delta$s strongly influence these properties either.

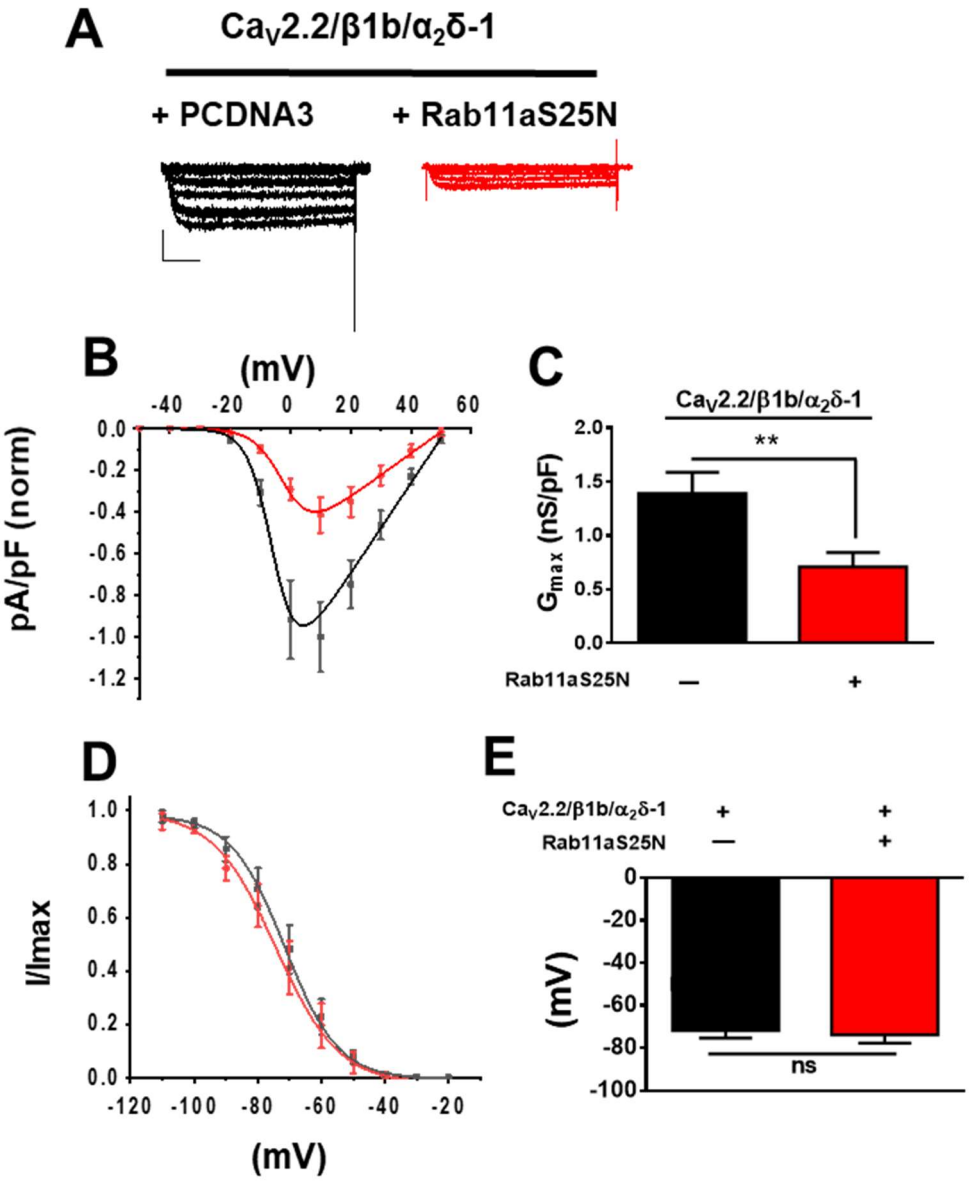

Figure 5.6 Rab11aS25N reduces whole-cell Ca$_V$2.2 currents when expressed with $\alpha_2\delta$-1

Figure 5.6. Rab11aS25N reduces whole-cell $Ca_V2.2$ currents when expressed with $\alpha_2\delta$-1

(A) Example whole-cell current traces of $Ca_V2.2$ with: β1b/$\alpha_2\delta$-1 (black) and β1b/$\alpha_2\delta$-1 + Rab11aS25N (red). **(B)** Mean IV plots for $Ca_V2.2$ with: β1b/$\alpha_2\delta$-1 (black squares, *n* = 15) and β1b/$\alpha_2\delta$-1 + Rab11aS25N (red circles, *n* = 14) fitted by a modified Boltzmann function (see methods). **(C)** Mean G_{max} values obtained by fitting each individual trace in panel B to a modified Boltzmann function $Ca_V2.2$/β1b/$\alpha_2\delta$-1 (black) 1.389 ± 0.1979 nS/pF, $Ca_V2.2$/β1b/$\alpha_2\delta$-1 + Rab11aS25N (red) 0.7085 ± 0.1352 nS/pF. **(D)** Mean steady-state inactivation for $Ca_V2.2$ with: β1b/$\alpha_2\delta$-1 (black squares; *n* = 7), β1b/$\alpha_2\delta$-1 + Rab11aS25N (red circles; *n* = 7). **(E)** Mean $V_{50,\ inact}$ obtained by fitting each individual trace in panel D to Boltzmann function, $Ca_V2.2$/β1b/$\alpha_2\delta$-1 (black) -71.81 ± 3.577 mV and $Ca_V2.2$/β1b/$\alpha_2\delta$-1 + Rab11aS25N (red) -73.78 ± 3.943 mV. Data are plotted ± SEM values. Student's unpaired t-test ns>0.05, **p<0.01.

5.8 Rab11aS25N has no effect on $\alpha_2\delta$-3-mediated $Ca_V2.2$ current enhancement

Having established that Rab11aS25N reduces both $\alpha_2\delta$-1 cell-surface expression and $\alpha_2\delta$-1-mediated $Ca_V2.2$ current enhancement it was necessary to confirm whether a similar reduction occurred in $\alpha_2\delta$-3-mediated current enhancement. In agreement with my immunocytochemistry data, I found no difference in mean current density (Fig 5.7A. B), G_{max} (Fig 5.7C), $V_{50\ act}$ of $Ca_V2.2$ (Fig 5.7D) or steady-state inactivation (Fig 5.7E) when Rab11aS25N was coexpressed with either $\alpha_2\delta$-3 + Rab11aS25N or $\alpha_2\delta$-3 alone. This result is consistent with my earlier observations that cell-surface expression of $Ca_V2.2$ is unaffected by Rab11a-recycling when expressed with $\alpha_2\delta$-3 or in the absence of $\alpha_2\delta$.

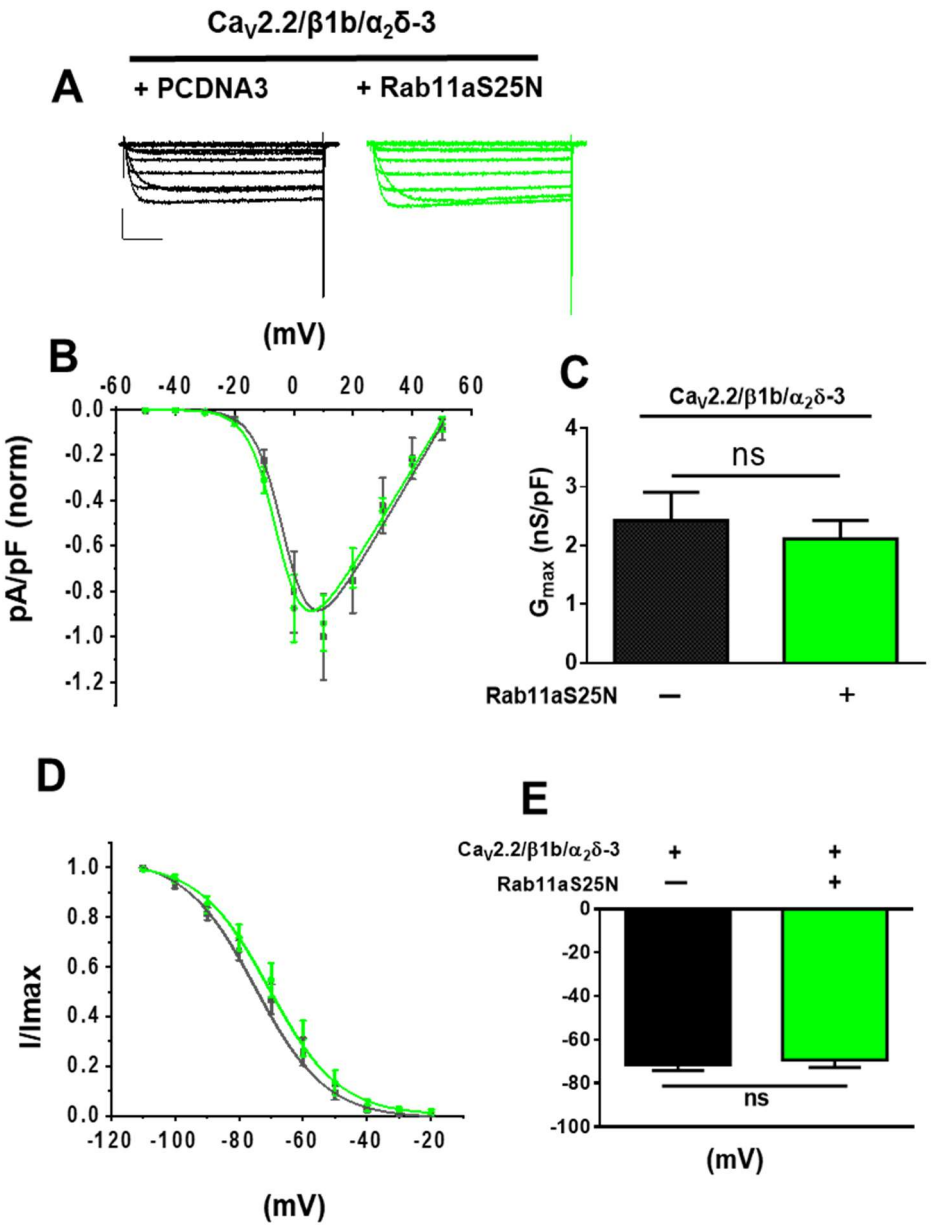

Figure 5.7 Rab11aS25N has no effect on whole-cell α$_2$δ-3-mediated Ca$_V$2.2 current enhancement

(A) Example whole-cell current traces of Ca$_V$2.2 with: β1b/α$_2$δ-3 (black) and β1b/α$_2$δ-3 + Rab11aS25N (green). **(B)** Mean IV plots for Ca$_V$2.2 with: β1b/α$_2$δ-3 (black squares; *n* = 15) and β1b/α$_2$δ-3 + Rab11aS25N (red circles; *n* = 14 fitted by a modified Boltzmann function (see methods). **(C)** Mean G_{max} values obtained by fitting each individual trace in panel B to a modified Boltzmann function, Ca$_V$2.2/β1b/α$_2$δ-3 (black) 2.424 ± 0.484 nS/pF, Ca$_V$2.2/β1b/α$_2$δ-3 + Rab11aS25N (green) 2.111 ± 0.318 nS/pF. **(D)** Mean steady-state inactivation for Ca$_V$2.2 with: β1b/α$_2$δ-1 (black squares; *n* = 7), Ca$_V$2.2/β1b/α$_2$δ-1 + Rab11aS25N (red circles; *n* = 7). **(E)** Mean $V_{50,\ inact}$ obtained by fitting each individual trace in panel D to Boltzmann function Ca$_V$2.2/β1b/α$_2$δ-1 (black) -71.48 ± 2.52 mV and Ca$_V$2.2/β1b/α$_2$δ-1 + Rab11aS25N (green) -69.32 ± 3.38 mV. Data are plotted ± SEM values. Student's unpaired t-test, ns >0.05.

5.9 Rab11aS25N reduces net forward trafficking of $\alpha_2\delta$-1

Here, I use a forward trafficking assay to compare net forward trafficking rates of $\alpha_2\delta$-1-bbs in the presence or absence of Rab11aS25N (Fig 5.8A). I find that net-forward trafficking of $\alpha_2\delta$-1-bbs is reduced by coexpression of Rab11aS25N with a 41% reduction in cell-surface $\alpha_2\delta$-1-bbs with Rab11aS25N after 30 minutes (Fig 5.8B), consistent with my measurements cell-surface $\alpha_2\delta$-1-HA + Rab11aS25N under steady-state conditions. I then compared net forward trafficking rates for $Ca_V2.2$-bbs/β1b when expressed with: empty vector, empty vector + Rab11aS25N, $\alpha_2\delta$-1 + empty vector or $\alpha_2\delta$-1 + Rab11aS25N (Fig 5.8C). I find that coexpression of $\alpha_2\delta$-1 enhances net-forward trafficking of $Ca_V2.2$ and that the presence of Rab11aS25N is sufficient to abolish this increase (Fig 5.8 D). In addition, I saw no difference in net forward $Ca_V2.2$ trafficking rates between conditions lacking $\alpha_2\delta$-1 and $\alpha_2\delta$-1 + Rab11aS25N (Fig 5.8D). These data support the conclusion that $\alpha_2\delta$-1 membrane expression is enhanced by forward-trafficking from Rab11a-positive recycling endosomes, and that $Ca_V2.2$ can traffic through this pathway only when coexpressed with Rab11a-sensitive $\alpha_2\delta$s.

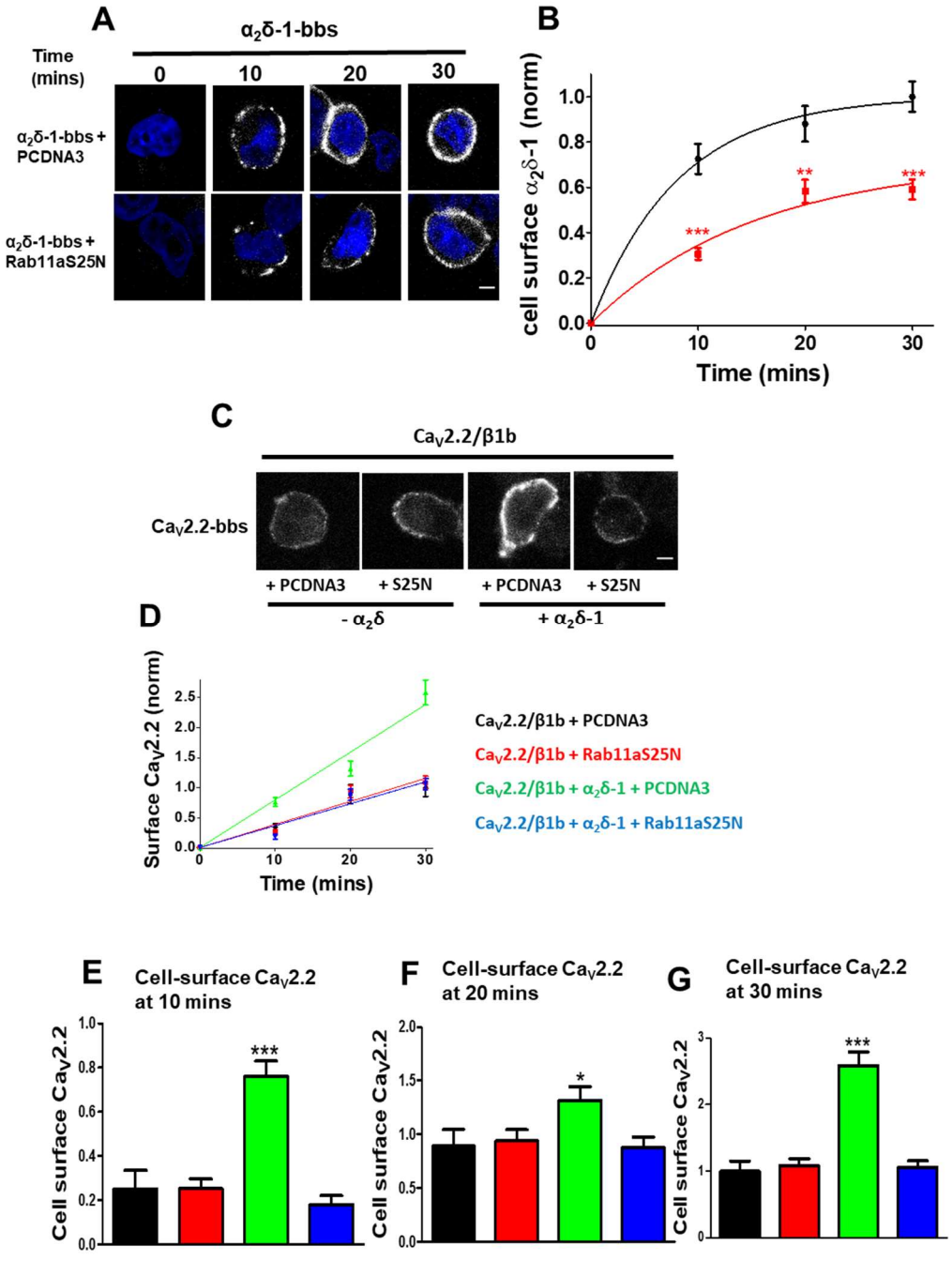

Figure 5.8 Rab11aS25N reduces net forward trafficking of $\alpha_2\delta$-1 and $Ca_V2.2/\alpha_2\delta$-1

Figure 5.8 Rab11aS25N reduces net forward trafficking of $\alpha_2\delta$-1 and $Ca_V2.2/\alpha_2\delta$-1

(A) Confocal images of $\alpha_2\delta$-1-bbs expressed in tsA-201 cells with either empty vector PCDNA3 (top row) or Rab11aS25N (bottom row) at each time point of net forward trafficking assay. Nuclei staining with DAPI. Scale bar = 5µm. **(B)** Net forward $\alpha_2\delta$-1-bbs trafficking. Normalised mean cell-surface $\alpha_2\delta$-1-bbs expressed with either Rab11aS25N or empty vector. Cells were live-labelled with α-BTX-AF488 for 0, 10, 20, and 30 minutes at 37ºC following pre-incubation with unlabelled α-BTX at 17ºC for 30 minutes. Data were collected across 3 transfections with approximately 30 to 50 cells analysed per time point in each experiment. Individual experiments were normalised to mean 30 min fluorescence of $\alpha_2\delta$-1-bbs condition, before being pooled together. Data were plotted using Graphpad 5 software and curve fitted using a one-phase exponential association equation (shown on graph). Statistical significance was determined using Student's t test to compare mean fluorescence values between conditions at each time point, $^{**}P<0.01$, $^{***}P<0.001$. **(C)** Confocal images of cell-surface $Ca_V2.2$-bbs expressed in N2a cells with β1b and either PCDNA3 or $\alpha_2\delta$-1 in the presence or absence of Rab11aS25N after 30 min of net forward trafficking assay. Scale bar = 5µm. **(D)** Net forward $Ca_V2.2$-bbs trafficking assay. Normalised mean cell-surface $Ca_V2.2$-bbs expressed in N2a cells with β1b and: PCDNA3 (black), PCDNA3 + Rab11aS25N (red), $\alpha_2\delta$-1 + PCDNA3 (blue) and $\alpha_2\delta$-1 + Rab11aS25N (green). Cells were live-labelled with α-BTX-AF488 for 0, 10, 20 and 30 minutes at 37ºC following pre-incubation with unlabelled α-BTX at 17ºC for 30 minutes. An average of 30-50 cells were analysed per time point, for each condition. Data represents all cells from 3 transfections. **(E, F, G)** mean fluorescence values at 10, 20, and 30 min time points from panel B. Data analysis was blinded. Data are plotted ± SEM values. Statistical significance was determined using one-way ANOVA and Bonferroni post hoc tests ($^{*}P<0.05$, $^{***}P<0.001$)

5.10. Summary

In this study I have shown that $\alpha_2\delta$s differentially enhance plasma membrane expression of exofacially-tagged $Ca_V2.2$ in both cell lines and primary neuronal cultures (Fig.5.2, Fig.5.5). When expressed in N2a cells, I find that $\alpha_2\delta$-1, $\alpha_2\delta$-2 and $\alpha_2\delta$-3 enhance cell-surface and total $Ca_V2.2$ levels, albeit to varying degrees (Fig 5.1). Upon further investigation, I find that $\alpha_2\delta$-1 and $\alpha_2\delta$-2 actively promote net forward $Ca_V2.2$ traffic through Rab11a-dependent recycling endosomes (Fig 5.2). However, $\alpha_2\delta$-3 does not appear to participate in Rab11a-dependent

recycling (Fig. 5.3) and did not increase net forward $Ca_V2.2$ trafficking (Fig.5.2). Despite this, I do report a consistent increase in both total (47%) and plasma membrane-inserted (30%) $Ca_V2.2$ with $\alpha_2\delta$-3 under steady-state conditions (Fig.5.1). Further investigation using the dominant negative Rab11aS25N mutant, showed that Rab11a-depedent recycling enhances cell-surface $Ca_V2.2$ expression only in the presence of Rab11a-sensitive $\alpha_2\delta$-1 or $\alpha_2\delta$-2 (Fig 5.4). Inhibition of Rab11a-recycling had no effect on $Ca_V2.2$ localisation when expressed with $\alpha_2\delta$-3 or no $\alpha_2\delta$; these results were consistent in both N2a cell lines and at primary hippocampal neurites, although I saw no effect at hippocampal cell bodies (Fig.5.5). Inhibition of Rab11a-dependent recycling reduced whole-cell $Ca_V2.2$ currents in tsA201 cells when expressed with $\alpha_2\delta$-1 (Fig 5.6) but had no effect with $\alpha_2\delta$-3 (Fig.5.7). Using our forward trafficking assay, I demonstrated that net forward $\alpha_2\delta$-1-bbs trafficking is reduced by Rab11aS25N consistent with reports by Tran-Van-Minh & Dolphin (2010) for $\alpha_2\delta$-2-bbs trafficking. Furthermore, Rab11aS25N reduced $Ca_V2.2$ forward traffic when $\alpha_2\delta$-1 was coexpressed (Fig.5.8). I find no difference in net $Ca_V2.2$ trafficking rates between conditions expressing "$\alpha_2\delta$-1 + Rab11aS25N" and "no $\alpha_2\delta$" suggesting that – in non-neuronal cell lines - $\alpha_2\delta$-1-enhanced $Ca_V2.2$ plasma membrane-insertion is principally driven by Rab11a-depdendent recycling. In primary hippocampal neurons, I find that $Ca_V2.2$ membrane expression is largely dependent on $\alpha_2\delta$, both at the cell soma and neuronal processes (Fig.5.5). Under basal conditions, cell-surface $Ca_V2.2$ was most abundant at the hippocampal processes when paired with $\alpha_2\delta$-1, and cell soma when paired with $\alpha_2\delta$-3. Inhibition of Rab11a-recycling did diminish cell surface $Ca_V2.2$ at the neurites in the presence of $\alpha_2\delta$-1. However, $Ca_V2.2$ expression with $\alpha_2\delta$-1 + Rab11aS25N was still significantly higher than in the absence of $\alpha_2\delta$ entirely. As I do not see an effect of Rab11a-inhibition on $Ca_V2.2$ at neuronal cell bodies, it would suggest that $Ca_V2.2$ traffic from the soma to processes, requires $\alpha_2\delta$ but through a Rab11a-independent pathway.

5.11 Discussion

Earlier work has shown that $\alpha_2\delta$-2 participates in recycling through Rab11a-positive recycling endosomes and that this pathway appears to be interrupted by Gabapentin (Tran-Van-Minh & Dolphin, 2010). Gabapentinoid drugs - which bind to both $\alpha_2\delta$-1 and $\alpha_2\delta$-2 - inhibit recycling of $\alpha_2\delta$-2 through Rab11a-positive endosomes thereby reducing forward trafficking and cell-surface expression of $\alpha_2\delta$-2. $\alpha_2\delta$-3 and $\alpha_2\delta$-4 do not bind gabapentin and lack an RRR motif - the putative GBP binding site - present in the α_2 domain of $\alpha_2\delta$-1 and $\alpha_2\delta$-2. The RRR motif is positioned just upstream of the VWA domain in α_2. It has been hypothesised that gabapentinoids displace an endogenous ligand for the RRR site necessary for proper function in $\alpha_2\delta$-1 and $\alpha_2\delta$-2 (Davies *et al.*, 2006; Hendrich *et al.*, 2008). Previous mutational studies using the $\alpha_2\delta$-1(R217A) or $\alpha_2\delta$-2(R282A) mutants - which do not bind Gabapentin – found them to have reduced currents through Ca_Vs compared to WT counterparts, as well as reduced endosomal recycling (Davies *et al.*, 2006; Field *et al.*, 2006; Hendrich *et al.*, 2008; Tran-Van-Minh & Dolphin, 2010). These findings are consistent with the notion that binding of an endogenous ligand induces conformational changes to these $\alpha_2\delta$ – possibly at the VWA domain – important for association of $\alpha_2\delta$-1 and $\alpha_2\delta$-2 with endosomal sorting partners. As $\alpha_2\delta$-3 lacks a Gabapentin binding site and does not strongly influence $Ca_V2.2$ trafficking in cell lines, I speculated that it does not participate in Rab11a-dependent recycling and is thereby unable to promote forward trafficking of $Ca_V2.2$ through this pathway. In agreement with this, I find Rab11a-recyling did not influence $\alpha_2\delta$-3 trafficking and effects on $Ca_V2.2$ net forward trafficking was observed only in the presence of $\alpha_2\delta$-1 or $\alpha_2\delta$-2. Presently it is unclear why $\alpha_2\delta$-3 does not participate in Rab11a-dependent recycling. $\alpha_2\delta$-3 shares only 25.7% sequence homology with $\alpha_2\delta$-1 (ClustalO) which may result in conformational differences that preclude an interaction with Rab11a or a Rab11a effector. This

result could hint at diverging roles among $\alpha_2\delta$ subtypes in both subcellular Ca_V localisation as well as Ca_V-independent activity. A number of previous studies have provided evidence for $\alpha_2\delta$ functions independent of direct action of Ca_Vs. An example of Ca_V-independent $\alpha_2\delta$ function was previously described in Drosophila reporting that the $\alpha_2\delta$-3 homologue, *Straightjacket,* promotes the generation of synaptic boutons at motor neuron terminals however, depletion of α_1 subunits did not influence synaptic bouton generation (Kurshan *et al*., 2009). More recently, it was reported that UNC-36, a homologue of $\alpha_2\delta$ in *C. elegans*, binds to a synaptic adhesion molecule, Neurexin-1, decreasing UNC-36 availability at synaptic elements and resulting in a decrease in acetylcholine release at neuromuscular junctions (Tong *et al*., 2017). As part of this study, heterologously expressed mammalian Neurexin-1α was shown to selectively bind $\alpha_2\delta$-3 and reduce $Ca_V2.2$ currents while having no effect with $\alpha_2\delta$-1 or $\alpha_2\delta$-2 coexpression. $\alpha_2\delta$-1 and $\alpha_2\delta$-2 showed no affinity for Neurexin-1α, presumably due to conformational differences with $\alpha_2\delta$-3. It is tempting to consider that the VWA domain of $\alpha_2\delta$-1/2, augmented by the binding of an endogenous ligand at the RRR motif, precludes an interaction with Neurexin-1α, although this is yet to be investigated. Surprisingly, a 2018 study by Brockhaus et al (2018) found that Neurexin-1α enhanced $Ca_V2.1$ currents in heterologous systems when expressed with $\alpha_2\delta$-1 but had no effect in the presence of $\alpha_2\delta$-3 (Brockhaus *et al.*, 2018). Tong et al (2017) and Brockhaus et al (2018) reach opposing conclusions regarding the subtype specificity of interactions between $\alpha_2\delta$ and Neurexin-1α. However, both studies suggest subtype-dependent interplay between $\alpha_2\delta$ and Neurexin-1α, indicative of distinct functional roles among $\alpha_2\delta$ subtypes.

Interestingly $\alpha_2\delta$-1 has also been reported to enhance synaptogenesis, independently of Ca_V channels, through extracellular interactions between the VWA domain of $\alpha_2\delta$-1 and Thrombospondins (TSPs). TSPs are multi-domain

extracellular matrix proteins typically secreted by astrocytes that perform a range of functions including synaptogenesis, in particular promoting the formation of silent synapses (Christopherson *et al*., 2005). *In vitro* application of Gabapentin has been found to reduce TSP-mediated synaptogenesis in cultured retinal ganglion neurons while having no effect on established synapses (Eroglu *et al*., 2009). The authors propose that Gabapentin allosterically inhibits the interaction between neuron-expressed $\alpha_2\delta$-1's VWA domain and Epidermal growth factor (EGF)-like repeats of TSPs in co-cultured astrocytes and were able to inhibit TSP-induced synapse formation through application of antibodies directed against the VWA domain of $\alpha_2\delta$-1. More recently, a study by Lana et al. (2016) further investigated the relationship between $\alpha_2\delta$s and TSP4, finding an inverse correlation between the binding of $\alpha_2\delta$-1 to Gabapentin or to TSP4 (Lana *et al*., 2016). However, Lana et al (2016) were unable to demonstrate any interaction between cell-surface expressed $\alpha_2\delta$-1 and TSP4 nor were they able to demonstrate the importance of the EGF-like domains of TSP4 in this interaction, as has been previously reported, concluding that $\alpha_2\delta$-1 and TSP4 may only interact intracellularly at high concentrations; It should also be noted that this study was carried out using heterologous expression in tsA-201 cells which may lack as-yet-unknown mediators of the TSP4-$\alpha_2\delta$-1 interaction.

$\alpha_2\delta$s have been shown to promote exocytosis from presynaptic terminals through two distinct mechanisms: enhancing presynaptic Ca_V expression and increasing vesicle release probability (Hoppa *et al*., 2012). Increases or decreases to $\alpha_2\delta$-1 expression were shown to enhance or reduce presynaptic $Ca_V2.1$ respectively in primary hippocampal neurons, a result confirmed for $\alpha_2\delta$-2 and $\alpha_2\delta$-3 (Hoppa *et al*., 2012). The same study found that overexpression of eGFP-tagged $Ca_V2.1$ alone did not increase presynaptic $Ca_V2.1$ despite significant increases in somatic Ca_V expression. My data largely agree with Hoppa et al (2012), finding a significant

reduction in both total and plasma membrane-inserted $Ca_V2.2$ at hippocampal neurites in the absence of $\alpha_2\delta$ coexpression (Fig. 5.6). While I am able to visualise neurite $Ca_V2.2$ expression without overexpressing $\alpha_2\delta$ present I must consider that my data does not specifically assess presynaptic Ca_V expression or discount a compensatory role for endogenously expressed $\alpha_2\delta$. In future work, presynaptic markers such as vesicular glutamate transporter (vGlut), could be used to identify and quantify presynaptic $Ca_V2.2$ expression, while endogenous $\alpha_2\delta$ could potentially be knocked down using shRNAs or CRISPR approaches.

Chapter 6

General discussion and future perspectives

6.1 Proteolytic $\alpha_2\delta$ processing

Proteolytic processing is a well-established post-translational modification present in all $\alpha_2\delta$ subtypes (Dolphin, 2013). A previous study by Andrade et al (2007) alluded to the functional importance of $\alpha_2\delta$ processing for Ca_V current enhancement. This study mapped the $\alpha_2\delta$-1 cleavage site to a hexapeptide sequence from R941 and V946 (Andrade *et al.*, 2007). Point mutations at the cleavage site of $\alpha_2\delta$-1 were sufficient to reduce, but not abolish whole-cell $Ca_V2.2$ current enhancement (Andrade *et al.*, 2007). In addition, mutation of the entire hexapeptide sequence was required to abolish cleavage entirely (Andrade *et al.*, 2007). Subsequent studies by the Dolphin lab have partially agreed with Andrade et al (2007) requiring a 6-peptide mutation to entirely abolish cleavage of $\alpha_2\delta$-1 (Ferron *et al.,* 2018; Kadurin *et al.*, 2016). Interestingly, the cleavage-insensitive $\alpha_2\delta$ mutants generated by the Dolphin lab exhibit a complete loss of Ca_V current-enhancement not previously reported (Kadurin *et al.*, 2016). The discrepancy between older and more recent studies on $\alpha_2\delta$ processing may reflect subtle differences in the exact position of the hexapeptide mutation: K943 to M948 in Kadurin et al., R941 to V946 in Andrade et al (2007) but may also relate to the coexpression of auxiliary β_1b in contemporary studies rather than β_3 previously. The requirement of a 6-residue mutation to completely abolish $\alpha_2\delta$-1 cleavage suggests the cleavage site is rather robust, possibly due to redundancy among the protease(s) responsible. Furthermore, the difficultly of inhibiting $\alpha_2\delta$ cleavage presents a challenge for any future attempts to design small molecule modulators of this process either as a potential therapy or molecular tool.

In chapter 3, the behaviour of proteolytically-insensitive $\alpha_2\delta$ was examined in heterologous expression systems complementing parallel work in primary neuronal cultures (Kadurin *et al*., 2016). Comparing $\alpha_2\delta$ behaviour in neuronal or non-neuronal cells reveals a context-dependent effect of $\alpha_2\delta$ proteolysis. When expressed in non-neuronal cell lines, unprocessed α_2(3C)δ mutants display no defects in their ability to enhance cell-surface $Ca_V2.2$ expression, however, they are unable to enhance whole-cell Ca_V conductance despite increasing the total number of plasma membrane-inserted Ca_V channels (Kadurin *et al*., 2016). On this evidence, one might conclude that "pro-$\alpha_2\delta$" acts as an inhibitor of Ca_V conductance while retaining its role as a facilitator of Ca_V transport. However, examining the function of pro-$\alpha_2\delta$ mutants in primary hippocampal neurons reveals a clear proteolysis-dependent effect on Ca_V trafficking to the neurites (Kadurin *et al*., 2016). $Ca_V2.2$ appears to be largely unable to exit the neuronal soma in the absence of proteolytically processed $\alpha_2\delta$ and coexpression of α_2(3C)δ mutants does not significantly increase $Ca_V2.2$ neurite expression (Kadurin *et al*., 2016). However, coexpression of 3C-protease with α_2(3C)δ is sufficient to rescue neurite $Ca_V2.2$ expression (Kadurin *et al*., 2016). Interestingly, uncleaved α_2(3C)δ itself does not exhibit defects in neuronal trafficking when expressed alone, suggesting that the conformation of the immature $\alpha_2\delta$-$Ca_V2.2$ complex precludes efficient trafficking to the neurites (Kadurin *et al*., 2016). Importantly, in both neuronal and non-neuronal cells, induced cleavage of α_2(3C)δ constructs with 3C-protease rescues normal $\alpha_2\delta$ function. This is shown by enhanced whole-cell $Ca_V2.2$ currents (tsA-201 cells) and increased neurite $Ca_V2.2$ expression (primary hippocampal neurons) (Kadurin *et al*., 2016).

As discussed earlier, α_2(3C)δ retains the ability to promote cell-surface $Ca_V2.2$ expression in cell lines despite being unable to enhance whole-cell $Ca_V2.2$ currents. This may indicate that unprocessed $\alpha_2\delta$ suppresses channel activation.

Recently, Savalli et al (2016) utilised voltage-clamp fluorometry to track the activation of the four voltage-sensor domains of $Ca_V1.2$ expressed with β_3 in the presence or absence of $\alpha_2\delta$-1. This study found that the voltage-dependence of the channel had a rightward shift in the absence of $\alpha_2\delta$-1 such that currents would generally develop at non-physiological membrane potentials (Savalli *et al*., 2016). The authors attribute the positive shift in voltage-dependence to weak VSD-pore interactions in the absence of $\alpha_2\delta$. In the presence of $\alpha_2\delta$-1, the voltage-sensitivity of VSDI-III was increased thereby facilitating channel activation (Savalli *et al.*, 2016). As unprocessed α_2(3C)δ does not enhance channel activation, it is possible that pro-$\alpha_2\delta$ might stabilise the down-state of the VSDs, thereby reducing the voltage-sensitivity of the channel. In principle, this could be investigated using the techniques employed by Savalli et al (2016) on Ca_V channels coexpressed with the uncleaved α_2(3C)δ mutants developed by the Dolphin lab.

The importance of Ca^{2+} as a modulator of numerous physiological functions necessitates extremely tight regulation of intracellular [Ca^{2+}]. As such, it is tempting to consider that proteolytic maturation of $\alpha_2\delta$ subunits offers temporal VGCC regulation whereby "pro-$\alpha_2\delta$" inhibits channel activity prior to appropriate subcellular localisation. As discussed in Chapter 3, the ER is a principal Ca^{2+} store with a basal membrane potential close to 0 mV (Solovyova & Verkhratsky, 2002). At 0 mV, one might expect nascent VGCCs to adopt an open conformation, potentially facilitating the flow of Ca^{2+} from ER to cytosol. It is possible that pro-$\alpha_2\delta$ prevents this outcome by inhibiting the channel prior to exit from the ER.

6.2 Ca^{2+}-binding sites in the VGCC selectivity filter

The selectivity filter of VGCCs is thought to be comprised of three sequential Ca^{2+} binding sites (Tang *et al.*, 2014; Wu *et al.*, 2016). The second Ca^{2+} binding site (site 2) is formed by four P-loop glutamate residues, with each domain repeat contributing one glutamate residue (see Chapter 4, Fig 4.1). Previous studies have introduced point mutations to the P-loop Ca_V glutamates, with concurrent mutation of all four residues apparently sufficient to abolish Ca^{2+} permeability (Ellinor *et al.*, 1995; Yang *et al.*, 1993). Indeed, Cao et al (2004, 2010) utilised $Ca_V2.1$ and $Ca_V2.2$ mutants featuring four P-loop E to A substitutions as a dominant negative channel (Cao *et al.*, 2004; Cao & Tsien, 2010). Previously, P-loop Ca_V mutants were believed to be well expressed at the plasma membrane owing to the presence of a large outward current (Cao *et al.*, 2004). However, direct quantification of plasma membrane Ca_V populations has been lacking due to the difficulty of exofacially tagging these channels without disrupting channel function. In chapter 4, I present data quantifying the plasma membrane expression of exofacially HA-tagged $Ca_V2.2$ P-loop glutamate mutants in both neuronal and non-neuronal cell types. Relative to WT $Ca_V2.2$, plasma membrane expression was diminished for all P-loop mutants tested. Of particular note, the introduction of a single E to K substitution in the IV repeat domain of $Ca_V2.2$ produced an 88% reduction in cell-surface expression relative to WT, while total $Ca_V2.2$ expression (measured by II-III loop staining) was found to be 2-fold higher than WT. This result could suggest that $E_{IV}K$ $Ca_V2.2$ is unable to efficiently exit either the ER or Golgi network to reach the plasma membrane. Intracellular retention of $Ca_V2.2$ could be indicative of significant protein misfolding, however, in such an event, one might expect the construct to be targeted for ubiquitination and subsequent degradation. Given that D_{IV} E-K $Ca_V2.2$ exhibited far higher total expression that WT, it seems unlikely to be subject to extensive proteolytic degradation. It is clear however, that mutation

of a single P-loop glutamate residue can be sufficient to substantially alter the trafficking behaviour of the channel, something not considered in previous studies. I next compared the plasma membrane expression of two additional P-loop $Ca_V2.2$ mutants featuring E to A substitutions; D_I E-A and $D_{I,II,III,IV}$ E-A $Ca_V2.2$ which exhibited partial or complete loss of inward current respectively (data unpublished). Importantly, these constructs do exhibit a large outward current, consistent with previous studies (Cao and Tsien, 2010). When compared to WT $Ca_V2.2$, cell-surface expression was reduced for both E to A mutants (E_IA 49%, $E_{I,II,III,IV}A$ 61%) in N2a cells when expressed with auxiliary $\alpha_2\delta$-1 and β_{1b} subunits. Cell-surface expression of either E to A $Ca_V2.2$ pore mutants did not appear to be diminished to the extent seen for $E_{IV}K$ $Ca_V2.2$. In addition, the difference in cell-surface expression between E_IA and $E_{I,II,III,IV}A$ $Ca_V2.2$ was subtle, despite $E_{I,II,III,IV}A$ $Ca_V2.2$ possessing more mutations. With these data in mind, it seems unlikely that the reduced plasma membrane expression of P-loop $Ca_V2.2$ mutants is solely due to a loss of channel permeation. Previous reports, supported in the present study, suggest that $\alpha_2\delta$-1 coexpression with $Ca_V2.2$ increases plasma membrane $Ca_V2.2$ by approximately 2-fold (Cassidy *et al.*, 2014). I considered the possibility that E to A P-loop $Ca_V2.2$ mutants might be unable to interact normally with $\alpha_2\delta$-1, reducing the $\alpha_2\delta$-1-mediated increase cell-surface $Ca_V2.2$ expression. However, I find that both WT and E to A P-loop $Ca_V2.2$ mutants display comparable reductions in cell-surface expression in the absence of $\alpha_2\delta$-1. These data would seem to indicate that the relationship between $Ca_V2.2$ and $\alpha_2\delta$-1 is unaffected by mutations to P-loop glutamates insofar as this relates to channel trafficking. I next considered that P-loop $Ca_V2.2$ mutants may in fact be deficient in their interaction with auxiliary β subunits. I compared the cell-surface expression of WT, E_IA and $E_{I,II,III,IIII}A$ $Ca_V2.2$ in the presence or absence of β1b. I find that cell-surface expression of WT, E_IA and $E_{I,II,III,IIII}A$ $Ca_V2.2$ is reduced in the absence of β1b, however the relative decrease in cell-surface expression was greater for WT $Ca_V2.2$ than either P-loop

mutant. β subunits have a well-defined role in promoting correct folding of $Ca_V2.2$ as well preventing polyubiquitination and proteasomal degradation of $Ca_V2.2$ allowing exit from the ER (Waithe *et al*., 2011). I examined whether intracellular $Ca_V2.2$ expression of WT and $E_{I,II,III,IIII}A$ $Ca_V2.2$ was comparable in the absence of β1b by immunostaining the extracellular HA-tag present on my $Ca_V2.2$ constructs, prior to permeabilisation and immunostaining for intracellular HA-tag expression. This method allowed me to distinguish and quantify cell-surface and intracellular $Ca_V2.2$-HA populations. In the absence of β1b, I find relative cell-surface and intracellular expression of $E_{I,II,III,IV}A$ $Ca_V2.2$ to be higher relative than WT $Ca_V2.2$. It is not immediately apparent why mutations to P-loop glutamates would influence the relationship between $Ca_V2.2$ and β1b. A possible consideration is that Ca^{2+} binding to sites within the selectivity filter is important in facilitating structural rearrangements in the channel, potentially affecting the interaction with β1b. If so, one might expect reduced cell-surface expression of P-loop glutamate mutants and higher levels of intracellular retention, something observed for both $E_{I,II,III,IV}A$ and previously with E_IK $Ca_V2.2$.

Structural rearrangements of α_1 upon β subunit binding are thought to extend from I-II linker to S6 of domain I (IS6). 22 residues bridge the gap between the C-terminal cytoplasmic end of IS6 and the N-terminal end of the AID α-helix, referred to at the AID-IS6 linker (Opatowsky *et al*., 2004; Van Petegem *et al*., 2004). Findeisen & Minor (2009) have argued that the $Ca_V\beta$ and IS6-AID linker strongly influence CDI, VDI and CDF properties of the α_1 subunit. The residues of IS6-AID linker denote a high α-helix propensity; α-helix formation of the AID sequence (upon β binding) is likely to induce helix formation in the IS6-AID linker. Mutational studies of the IS6-AID linker, featuring a mid-sequence GGG insertion to prevent putative helix formation, suggest that α-helix rearrangement is required for IS6-AID linker-mediated effects on VDI (Findeisen & Minor, 2009). Given the proximity of

IS6 to the pore, and its involvement in VDI, it is possible that structural changes to the IS6-AID linker upon β subunit binding are involved in correct folding of the channel pore.

It has been demonstrated that trafficking regulation of $Ca_V2.2$ can vary considerably when expressed in a neuronal or non-neuronal context (Kadurin *et al.*, 2016). It was necessary to determine whether P-loop $Ca_V2.2$ mutants have reduced cell-surface expression in primary neurons, consistent with my observations in N2a cells (Fig 4.2B, Chapter 4). In non-permeabilised hippocampal neurons E_IA and $E_{I,II,III,IV}A$ $Ca_V2.2$ exhibit reduced cell-surface neurite expression relative to WT $Ca_V2.2$, when expressed with $\alpha_2\delta$-1 and β1b subunits (Fig 4.3.1B). In the absence of $\alpha_2\delta$, cell-surface neurite $Ca_V2.2$ expression was reduced by ~60% for WT and P-loop E-A $Ca_V2.2$ mutants (Fig 4.3.1B, Chapter 4). I then repeated this assay under permeabilised conditions to compare total neurite expression of WT, E_IA and $E_{I,II,III,IV}A$ $Ca_V2.2$. I find that total neurite expression of E_IA and $E_{I,II,III,IV}A$ $Ca_V2.2$ is ~50% lower than WT $Ca_V2.2$ (Fig 4.3.2, Chapter 4). These data suggest that both E-A $Ca_V2.2$ P-loop mutants have reduced trafficking to the neurites with a commensurate reduction in neurite cell-surface expression.

As mentioned earlier, the four P-loop glutamates are conserved in all members of the VGCC family, which along with other residues in the P1 and P2 helices, form three Ca^{2+} binding sites. Structure function studies by Tang et al (2014) using the mutant channel Ca_VAb suggest that the middle site has the highest Ca^{2+} affinity and provides the molecular basis for divalent cation block (Tang *et al.*, 2014). Site 2 is likely to be constitutively bound to Ca^{2+} and this may contribute to the stability of structural features within the channel that influence its interactions with other binding partners. However, as there is no current structural information for VGCCs lacking these high affinity Ca^{2+} binding sites, it is difficult to speculate further on this point. The present findings do suggest that extreme care should be taken when

using P-loop Ca_V mutants as a model for non-conducting or even dominant negative channels. In particular, previous interpretations of P-loop mutants as lacking Ca^{2+} conductance may be difficult to interpret due to the likelihood of diminished cell-surface expression (Cao *et al.*, 2004).

6.3 Distinct trafficking mechanisms among $\alpha_2\delta$ subtypes

All $\alpha_2\delta$ subtypes have been shown to enhance whole-cell Ca_V currents in a number of heterologous expression systems (Gurnett *et al.*, 1997; Liu *et al.*, 1996; Wakamori *et al.*, 1999). The ability of $\alpha_2\delta$s to enhance whole-cell Ca_V currents has often been attributed to an $\alpha_2\delta$-mediated increase in cell-surface Ca_V expression of the α_1 subunit. In chapter 5, I examined whether cell-surface $Ca_V2.2$ was similarly enhanced when expressed with different $\alpha_2\delta$ subtypes. I found that $\alpha_2\delta$-1 coexpression produced a 2-fold increase in cell-surface $Ca_V2.2$ consistent with previous reports, as well as a ~50% increase in total $Ca_V2.2$ expression (Cassidy *et al.*, 2014). Somewhat surprisingly, coexpression of $\alpha_2\delta$-3 produced only a ~30% increase in cell-surface $Ca_V2.2$ expression despite a ~50% increase in total $Ca_V2.2$ expression comparable to the effect of $\alpha_2\delta$-1. These data indicate that $\alpha_2\delta$s are unequal in their ability to enhance cell-surface $Ca_V2.2$ expression, but also suggests that increases in cell-surface $Ca_V2.2$ expression are not solely due to an increase in total $Ca_V2.2$ per cell, as this would have likely produced similar results for both $\alpha_2\delta$-1 and $\alpha_2\delta$-3, something I did not observe. Previously, $\alpha_2\delta$-1 has been reported to increase stability of the ternary $Ca_V1.2/\beta_3$ complex, demonstrated by a reduced rate of degradation upon arrest of protein synthesis (Bourdin *et al.*, 2015). This increased stability of the Ca_V complex may be a general feature of integrating $\alpha_2\delta$ subunits into the channel complex, independent of an additional role for $\alpha_2\delta$ in channel trafficking.

The development of exofacially-tagged $Ca_V2.2$ by Cassidy et al (2014) allowed for the first direct insight into how $\alpha_2\delta$-1 influences the trafficking of $Ca_V2.2$. Cassidy et al (2014) found that $\alpha_2\delta$-1 increased cell-surface $Ca_V2.2$ expression but found no difference in the rate of $Ca_V2.2$ endocytosis between conditions expressing or lacking $\alpha_2\delta$ (Cassidy *et al.*, 2014). With these data in mind, I used an α-BTX live-labelling assay to compare the net forward trafficking of $Ca_V2.2$ when expressed in N2a cells with β1b and either $\alpha_2\delta$-1, $\alpha_2\delta$-2, $\alpha_2\delta$-3 or no $\alpha_2\delta$. I found that coexpression of $\alpha_2\delta$-1 or $\alpha_2\delta$-2 considerably increased net forward $Ca_V2.2$ trafficking. However, the rate of $Ca_V2.2$ trafficking was not significantly different when expressed with either $\alpha_2\delta$-3 or without $\alpha_2\delta$.

Previously, Tran Van Minh & Dolphin (2010) provided compelling evidence that $\alpha_2\delta$-2 cell-surface expression is enhanced through recycling from Rab11a-positive recycling endosomes (Tran-Van-Minh & Dolphin, 2010). Indeed, the antiepileptic drug Gabapentin was shown to reduce cell-surface $\alpha_2\delta$-2 expression by inhibiting Rab11a-dependent recycling (Tran-Van-Minh & Dolphin, 2010). $\alpha_2\delta$-1 and $\alpha_2\delta$-2 possess a Gabapentin binding site in the α_2 domain, absent in $\alpha_2\delta$-3 and $\alpha_2\delta$-4. I considered the possibility that $\alpha_2\delta$-1 and $\alpha_2\delta$-2 facilitate Rab11a-dependent recycling of $Ca_V2.2$ whereas $\alpha_2\delta$-3 – and possibly $\alpha_2\delta$-4 – cannot. To confirm whether Rab11a-recycling is conserved among $\alpha_2\delta$ subtypes, I compared steady-state cell-surface expression of $\alpha_2\delta$-1 and $\alpha_2\delta$-3 in the presence or absence of Rab11aS25N, a dominant negative mutant. I found that $\alpha_2\delta$-1 cell-surface expression is reduced when expressed with Rab11aS25N, while $\alpha_2\delta$-3 appears to be unaffected. Following this I compared cell-surface $Ca_V2.2$ expression when paired with either $\alpha_2\delta$-1, $\alpha_2\delta$-2, $\alpha_2\delta$-3 or no $\alpha_2\delta$ in the presence or absence of Rab11aS25N. Consistent with my hypothesis, Rab11aS25N reduced cell-surface $Ca_V2.2$ expression only when paired with $\alpha_2\delta$-1 or $\alpha_2\delta$-2. Rab11aS25N had no effect on $Ca_V2.2$ levels in the absence of $\alpha_2\delta$ or with $\alpha_2\delta$-3 coexpression. These

data were consistent in undifferentiated N2a cells as well as at the processes of primary hippocampal neurons. Interestingly, I found no effect of Rab11aS25N at the hippocampal soma which could suggest a small or absent role for Rab11a-dependent recycling at the neuronal cell body. As proof of principle, I compared whole-cell Ba^{2+} currents in tsA-201 cells expressing $Ca_V2.2$, β1b and either $\alpha_2\delta$-1 or $\alpha_2\delta$-3 in the presence or absence of Rab11aS25N. Whole-cell currents were reduced by Rab11aS25N coexpression only when paired with $\alpha_2\delta$-1 suggesting a loss of functional cell-surface $Ca_V2.2$. To confirm that Rab11aS25N was inhibiting the recycling of $\alpha_2\delta$-1/$Ca_V2.2$, I used α-BTX live-labelling to compare the net forward trafficking of bbs-tagged $\alpha_2\delta$-1 with or without Rab11aS25N. I also compared net forward trafficking of bbs-tagged $Ca_V2.2$ when expressed with $\alpha_2\delta$-1 or no $\alpha_2\delta$ in the presence or absence of Rab11aS25N. I found that net forward trafficking of $\alpha_2\delta$-1-bbs is reduced by Rab11aS25N, while net forward $Ca_V2.2$ trafficking is reduced by Rab11aS25N only when $\alpha_2\delta$-1 is present. Together, these data suggest that $\alpha_2\delta$-1 and $\alpha_2\delta$-2 enhance forward trafficking of $Ca_V2.2$ by allowing the channel to participate in Rab11a-dependent recycling.

$\alpha_2\delta$-3 was not found to enhance net forward trafficking of $Ca_V2.2$, although it did produce a consistent increase in steady state cell-surface $Ca_V2.2$ (20-30%) and total $Ca_V2.2$ expression (~50%) when compared to “no $\alpha_2\delta$” in cell lines. It is possible that $\alpha_2\delta$-3 reduces the rate of $Ca_V2.2$ internalisation, which would increase the plasma membrane $Ca_V2.2$ population. However, the live-labelling assay used in this study assesses “net” forward traffic and should account for significant changes in rate of endocytosis.

In Chapter 5, I have provided evidence that $\alpha_2\delta$ subtypes have a differential influence on the trafficking of $Ca_V2.2$ resulting in $\alpha_2\delta$-subtype specific changes to plasma membrane $Ca_V2.2$ expression. Rab11a-dependent recycling of $Ca_V2.2$ appears to be dependent on coexpression of the appropriate $\alpha_2\delta$ subtype.

However, it is unclear what the major distinguishing biophysical characteristics between $\alpha_2\delta$ subtypes are. As mentioned previously, $\alpha_2\delta$-1 and $\alpha_2\delta$-2 possess a Gabapentin-binding site (RRR motif) in the α_2 domain, absent in $\alpha_2\delta$-3 and $\alpha_2\delta$-4. Occupation of the RRR motif by Gabapentin was shown to be sufficient to abolish Rab11a-dependent recycling of $\alpha_2\delta$-2 (Tran-Van-Minh & Dolphin, 2010). The RRR motif of $\alpha_2\delta$-1 and $\alpha_2\delta$-2 is positioned just upstream of the VWA domain and Gabapentin has been proposed to displace the binding of an endogenous ligand, leading to conformational changes in the $\alpha_2\delta$ structure (Brown *et al*.,1998; Gee *et al*., 1996), possibly in the VWA domain, that impede protein-protein interactions involved in intracellular trafficking. It would be interesting to examine whether the introduction of a complete RRR motif equivalently positioned in $\alpha_2\delta$-3 would impart Rab11a-dependent recycling on both itself and coexpressed $Ca_V2.2$. If so, one could reasonably expect Gabapentin to obstruct $\alpha_2\delta$-3 recycling. The size and extensive glycosylation of $\alpha_2\delta$ proteins is poorly suited to structural studies utilising crystallographic or NMR-based methods, however structural comparisons between WT and RRR mutated $\alpha_2\delta$-1 variants, using cryoEM might shed some light on the features involved with participation in Rab11a-dependent recycling in the future.

The Low-density Lipoprotein Receptor-related Protein 1 (LRP1) is a large multifunctional endocytic receptor belonging to the LRP receptor family. *In vitro* experiments in tsA-201 cells have shown that LRP1 binds to $\alpha_2\delta$-1 and, when coexpressed with the ER chaperone Receptor-Associated Protein (RAP), increases the cell-surface expression of $\alpha_2\delta$-1 (Kadurin *et al*., 2017). In addition, LRP1/RAP increases cell-surface expression of $Ca_V2.2$ in an $\alpha_2\delta$-1-dependent manner. Recently, LRP1 was identified as a direct binding partner of β1-integrin, promoting endocytosis but also directing the complex toward Rab11-positive recycling endosomes (Theret *et al.*, 2017). It is possible that conformational

differences between $\alpha_2\delta$-1 and $\alpha_2\delta$-3 allow for the selective binding and direction of $\alpha_2\delta$-1 by LRP1 towards the Rab11-dependent recycling pathway.

Comparing cell-surface and total levels of $Ca_V2.2$ expressed in cell lines with or without $\alpha_2\delta$, I found that total $Ca_V2.2$ – measured through II-III loop epitope expression - was 40-50% lower in the absence of $\alpha_2\delta$. Both $\alpha_2\delta$-1 and $\alpha_2\delta$-3 produce a similar increase in total $Ca_V2.2$ expression, despite significant differences observed at the cell surface. It is possible that the discrepancy in cell surface $Ca_V2.2$ expression reflects distinct endosomal sorting pathways between these conditions. Upon endocytosis of plasma membrane proteins to the early endosome, cargo is initially segregated between entry to the lysosomal pathway for degradation, recycling pathways or retrograde transport to the trans-Golgi network (TGN). Sorting Nexins (SNXs), which are typically localised to the early endosome are heavily involved in cargo sorting, with SNX17 and SNX27 reportedly involved in retrieving cargo destined for lysosomal degradation (Steinberg *et al*., 2012). It may be that Ca_V channels are normally targeted for lysosomal degradation upon arrival at the early endosome with $\alpha_2\delta$ subunits interacting directly or indirectly with SNX proteins to direct Ca_Vs away from the lysosomal pathway. If so, one would expect expression levels of $Ca_V2.2$ in the absence of $\alpha_2\delta$ subunits to be reduced, which was observed in the present study.

Net forward $Ca_V2.2$ trafficking rates were not significantly different in the presence or absence of $\alpha_2\delta$-3. This would seem to suggest that $\alpha_2\delta$-3 does not alter forward trafficking pathways to which $Ca_V2.2$ is targeted. The $Ca_V2.2/\alpha_2\delta$-3 complex does not appear to be targeted for Rab11-dependent recycling and total $Ca_V2.2$ expression was found to be similarly elevated by coexpression of either $\alpha_2\delta$-1 or $\alpha_2\delta$-3. This suggests that internalised $\alpha_2\delta$-3 or the $\alpha_2\delta$-3/$Ca_V2.2$ complex is not expressly targeted for either lysosomal degradation or towards rab11a-dependent recycling pathways. An interesting possibility is that internalised $\alpha_2\delta$-3 or $\alpha_2\delta$-3/Ca_V

complexes undergo retrograde transport to the TGN from which they might re-enter the secretory pathway. Sorting from the early endosome to the TGN is heavily mediated by the multi-protein Retromer complex (Seaman, 2012). Retromer itself is recruited to early endosomes by Rab7 and it would be interesting to see whether mutations to Rab7, such as the dominant negative T22N mutant would differentially affect $\alpha_2\delta$ trafficking (Wandinger-Ness & Zerial, 2014).

It has previously been shown that both $\alpha_2\delta$s expressed in cell lines and native $\alpha_2\delta$s, concentrate in cholesterol rich plasma membrane regions (DRMs/lipid rafts) (Kadurin *et al*., 2012). It is possible that $\alpha_2\delta$s might increase the capacity of the plasma membrane for Ca_V channels by increasing the number of membrane regions to which Ca_Vs can localise. This could explain how $\alpha_2\delta$-3 increases plasma-membrane $Ca_V2.2$ expression without influencing net-forward trafficking. This concept could potentially be investigated using cholesterol-depleting agents such as β-cyclodextrin on cell lines expressing exofacially-tagged $Ca_V2.2$ with and without $\alpha_2\delta$-3 (Mahammad & Parmryd, 2015). An alternative explanation for the elevation of total $Ca_V2.2$ with $\alpha_2\delta$ coexpression, is that inclusion of $\alpha_2\delta$ to the Ca_V complex increases stability of the structure making it less prone to misfolding and proteolytic degradation. It may be possible to investigate this by comparing the degree of colocalisation between Ca_V channels and lysosomal or proteasomal markers in the presence or absence of $\alpha_2\delta$ subunits.

6.4 Considerations and critique of experimental approach

6.4.1 Overexpression systems

The work presented here uses several overexpression systems to study the behaviour of $Ca_V2.2$ and the associated subunits. Overexpression is often necessary for fluorescence imaging due to the high expression requirement for

data acquisition. However, a number of caveats must be considered when interpreting data that relies on this approach. Principally, excessive protein expression in a given cell often results in aberrant protein localisation, likely due to overloading of endogenous trafficking mechanisms. Further to this, the trafficking of endogenous proteins might be hindered by competing overexpressed proteins. In addition, it may be difficult to interpret the secondary effects that a given overexpressed protein will exert on other cellular pathways, particularly when localised to unintended subcellular regions. A final consideration, particularly for fluorescence imaging, is signal saturation as a result of excessive protein expression. Measurements obtained from a saturated fluorescence signal will invariably underestimate the total fluorescence output. In turn, estimates of relative expression between proteins of interest will be skewed, with fluorescence from saturating proteins being underrepresented relative to non-saturating counterparts. To reduce the effect of signal saturation on confocal imaging experiments, laser power, pixel dwell times and gain settings were optimised to reduce saturation while maintaining an adequate signal-to-noise ratio during data acquisition. Thereafter individual cells that express saturating fluorescence signal, either at the cell surface or intracellularly, were excluded from analysis. While specific confocal settings may vary between experimental repeats, they are consistent for conditions in a single experiment and must be normalised to appropriate internal controls before data are pooled from experimental repeats.

6.4.2 Experimental diversity

In the present study, protein expression and localisation were principally determined using immunocytochemistry and confocal microscopy. While this method offers a significant body of information regarding these processes, this study acknowledges that additional methods of validation would improve

confidence in the data shown. In particular, western blotting and cell-surface biotinylation assays provide comparable insights into cell surface and intracellular protein expression using biochemical tools. These assays were used to independently validate the confocal data presented in Chapters 2 and 3 (Kadurin et al 2016; Meyer et al 2018 (submitted)). However, they have yet to be employed for the data presented in Chapter 5 and this will need to be addressed in future work.

6.4.3 Single section confocal imaging vs Z-stacks

A significant proportion of data presented in the present study uses an immunocytochemical approach to label cell surface and intracellular proteins of interest, subsequently quantified using confocal microscopy and image analysis. Confocal images contain y, x and z planes allowing for three-dimensional image construction by amalgamating sequential optical sections along the z axis, known as a z-stack. In principle, a z-stack will provide a more complete picture of fluorescence distribution across a cell than could be expected from a single optical section through a cell. However, to be effective z-stacks must be constituted from a large number of narrow optical sections, which is generally inappropriate for small and flat cell types such as N2a and tsA-201 cell lines used throughout this study. In addition, generating z-stacks, while useful for single cell analysis, is not practical when obtaining images from an extremely large cell population, as is the case when imaging from cell lines. Doing so would necessitate more specific cell selection during imaging acquisition which in turn introduces bias to the data acquisition process. The present study attempted to address the concerns of single optical section image acquisition by capturing tile scans rather than single field-of-view images. Through this method, it was possible to make high-throughput fluorescence measurements of a large number of cells, thus removing bias in cell

selection and reducing the influence of cell-to-cell variance in physical size and protein expression. In addition, optical section thickness was adjusted depending on the cell type being imaged. For cell line data acquisition, a 1 µm optical section was used with the focal plane of each tile being adjusted to bring the nuclear region of cells into focus, in order to improve consistency between imaged cells. With this section thickness, a small deviation in the z-plane would result in a significant loss of focus and fluorescence signal, suggesting that a large proportion of a cell's depth was acquired. Subsequent analysis excluded all out-of-focus cells acquired in each tile scan. Unlike the cell lines used in this study, primary neuronal cultures are relatively large with developed neuronal processes often occupying a sizeable three-dimensional space. In addition, the number of successfully transfected neurons per culture is far lower than can be achieved with cell line expression systems. As such, use of z-stacks is more appropriate to this system, and could have been employed when acquiring neuronal cell body images which were captured at a 63x magnification with 1 µm optical section. For acquisition of neuronal processes, the specifications used were a lower 20x magnification and 4.5 µm optical section. These settings reasonably accommodate the irregular structure of neurites. However, higher resolution image reconstitution could have been achieved through the use of narrow optical section z-stacks, if seeking more detailed intracellular data.

6.4.4 Stages of neuronal development

Neurons are polarised cells, with distinct somatodendritic and axonal components. Maintenance of neuronal polarity is largely dependent on the formation of the axonal initial segment (AIS). The AIS is a 10-60 µm region proximal to the axon and distal to the axonal hillock, which plays an important role in both action potential generation and maintenance of neuronal polarity (Jones and Svitkina,

2016; Nelson and Jenkins, 2017). Observations of hippocampal neurons *in vitro* suggest that AIS formation begins with the clustering of AnkyrinG (AnkG) following axon specification after 1.5 days *in vitro* (DIV) (Jones and Svitkina, 2016). After 7 DIV axons and dendrites progressively mature to form synapses although complete maturation of these processes and optimisation of the AIS may continue up to 21 DIV (Jones and Svitkina, 2016). In the present study, primary hippocampal neurons were cultured *in vitro* for 7 days prior to transfection and a further 7 days in culture thereafter, before fixation and immunostaining. At the point of transfection (DIV 7) the AIS is presumed to be established. As such, axonal accumulation of transfected $Ca_V2.2$ complexes should be beholden to sorting processes at the AIS.

Prior to AIS formation, it would be surprising if trafficking specificity differed significantly among the constructs used, due to the non-distinct nature of neurites prior to specification. However, all neuronal experiments were carried out in established *in vitro* cultures, in which cell polarity is achieved. It is difficult to speculate as to the specificity of trafficking among constructs used in this study. However, $Ca_V2.2/\alpha_2\delta$-3 coexpression did produce greater plasma membrane expression at the neuronal soma than $Ca_V2.2/\alpha_2\delta$-1 with an inverse observation at the neuronal processes. This may reflect differential cargo sorting at the AIS, however further investigation in developing neurons prior to AIS formation would be required to determine this.

6.5 Future perspectives

The present study has highlighted the complexity of the interplay between $Ca_V2.2$ and $\alpha_2\delta$ subunits. There is now considerable evidence that $\alpha_2\delta$ subunits generally play a key role in facilitating neuronal Ca_V transport. However, the nature of the Ca_V- $\alpha_2\delta$ relationship appears to be heavily dependent on both the subtype pairing

and cell type in which they are expressed. In neurons, $\alpha_2\delta$ subunits appear to be necessary for Ca_V cell-surface expression and trafficking to neurites. However, in non-neuronal cell lines, considerable levels of cell-surface Ca_V expression can be achieved in the absence of $\alpha_2\delta$. Comparative studies of $\alpha_2\delta$ behaviour between neuronal and non-neuronal expression systems suggest that $\alpha_2\delta$s have distinct mechanisms for regulating Ca_V trafficking and current enhancement (Kadurin *et al*., 2016). Proteolytic processing of $\alpha_2\delta$s has been identified as a crucial regulator of Ca_V activity, appearing to influence current enhancement in non-neuronal cell lines and channel trafficking in neurons. $\alpha_2\delta$-1 upregulation is closely associated with onset of neuropathic pain, presumably due to increased presynaptic Ca_V activity, or tighter coupling of Ca^{2+} entry- to neurotransmitter release. Recent studies strongly suggest that unprocessed $\alpha_2\delta$ is unable to facilitate transport of $Ca_V2.2$ from soma to neurite (Ferron *et al*., 2018; Kadurin *et al*., 2016). Identification of the protease(s) involved in $\alpha_2\delta$ processing could offer a novel target(s) for reducing the onset of neuropathic pain following nerve injury. However, it is currently unclear whether a single protease carries out this function, and whether inhibitors can be developed to target specific $\alpha_2\delta$ subtypes, to reduce the likelihood of off-target effects.

Investigation into the mechanism of Gabapentin action suggests that Rab11a-dependent recycling of $\alpha_2\delta$-1 and $\alpha_2\delta$-2 is interrupted, reducing forward trafficking of these $\alpha_2\delta$s with a commensurate decrease in Ca_V activity and trafficking. $\alpha_2\delta$-3 appears to traffic independently of Rab11a-recycling although an alternative endosomal pathway is yet to be determined. Rab7b has been identified as a mediator of endosome-to-TGN trafficking and this pathway can be disrupted by expression of the dominant-negative Rab7b T22N (Vonderheit & Helenius, 2005). In future studies, a potential role for retrograde trafficking in $\alpha_2\delta$-3 behaviour could be investigated using α-BTX live-labelling to track the endosomal movement of

bbs-tagged $\alpha_2\delta$s coexpressed with Rab7b T22N or the activating mutant Q67L (Bucci *et al*., 2000). While $\alpha_2\delta$-3 is not a target for any current therapies, the *CACNA2D3* gene has been implicated as a tumour-suppressor in several cancers (Wong *et al.*, 2013; Jin *et al.*, 2017). In particular, $\alpha_2\delta$-3 appears to be downregulated in unfavourable-prognosis neuroblastomas as well as some gastric carcinomas (Thorell *et al.*, 2009). Improving our understanding of $\alpha_2\delta$-3 behaviour may enable the design of specific $\alpha_2\delta$-3 modulators either in a therapeutic capacity or as molecular tools.

Current data regarding tissue or cell type specific expression of $\alpha_2\delta$ remains incomplete, largely due to the unavailability of reliable specific antibodies for specific subtypes. A notable exception is the extremely restricted expression of $\alpha_2\delta$-4, present mainly in the retina and endocrine tissues but largely absent in the brain (Wycisk *et al.*, 2006). $\alpha_2\delta$-1 appears to be the predominant subtype of the peripheral nervous system, with notably high expression in small nociceptive DRGs (Newton *et al.*, 2001). Available information from online expression databases, such as the human protein atlas, suggest that central protein expression of $\alpha_2\delta$-1 is highest in neuronal cells of the hippocampus, whereas $\alpha_2\delta$-2 is most prominent in the purkinje cells of the cerebellum as well as the caudate nucleus (Human Protein Atlas). $\alpha_2\delta$-1 and $\alpha_2\delta$-2 are reported to have lower expression in the cerebral cortex, with RNA expression of $\alpha_2\delta$-3 being notably high there.

Perhaps some insight can be gleaned from the therapeutic potential and side effects of gabapentin. While both $\alpha_2\delta$-1 and $\alpha_2\delta$-2 are binding targets of gabapentin, studies in $\alpha_2\delta$-2 -/- KO mice as well as the *ducky* mouse model suggest the therapeutic potential of gabapentin – at least in regards to neuropathic pain – are mediated by $\alpha_2\delta$-1, likely reflecting the dominance of $\alpha_2\delta$-1 at peripheral nerve terminals (Brodbeck *et al.*, 2002; Donato *et al.*, 2006). Anti-epileptic and anxiolytic

properties are also attributed to gabapentin, however the specific targets that facilitate these effects are difficult to determine. Indeed, there are recent reports that gabapentin directly activates KCNQ3 and KCNQ5 channels, as well as reducing currents through HCN4 channels(Tae *et al.*, 2017; Manville and Abbott, 2018). KCNQ channel activators such as retigabine are effective therapeutics in a number of epilepsy models, and it is possible that gabapentin acts similarly in this regard (Tatulian *et al.*, 2001). HCN4 channels, while predominantly expressed in pace maker regions of the heart, are also present at low levels in several hippocampal regions (Tae *et al.*, 2017). HCN4 knockdown in the dorsal hippocampus was recently reported to produce anxiety-like behaviour in mice further complicating attempts to identify the key facilitators of gabapentin activity (Günther *et al.*, 2019).

An aspect of $\alpha_2\delta$ behaviour that has been gaining attention, is the interplay between $\alpha_2\delta$ subtypes and interacting partners distinct from Ca_Vs, such as α-neurexins. The importance of these interactions is suggested by the distinct activity of $\alpha_2\delta$s between native tissue and heterologous expression systems. Modulation of $\alpha_2\delta$ activity through additional binding partners offers another layer to the regulation of Ca^{2+} entry and vesicle release at presynaptic terminals. A recent study examining the role of α-neurexins in primary hippocampal neurons, concluded that α-neurexins influence presynaptic Ca^{2+} entry through specific modulation of $\alpha_2\delta$-1 (Brockhaus *et al.*, 2018). Neurexins are large extracellular proteins, with 3 distinct genes (NRX1-3) each encoding a longer α form and shorter β form. Triple knockout (TKO) of α-Neurexin was found to reduce presynaptic Ca^{2+} entry and evoked-vesicle release in primary hippocampal cultures, which was partially rescued by overexpression of NRX1α (Brockhaus *et al.*, 2018). Coexpression of NRX1α and $\alpha_2\delta$-1 produced even greater Ca^{2+} entry/vesicle

release in TKO models as well as $Ca_V2.1$ current-enhancement in heterologous expression systems. Interestingly, coexpression of NRX1α with $\alpha_2\delta$-3 did not affect presynaptic Ca^{2+} entry or Ca_V currents in cell lines, indicative of distinct roles among $\alpha_2\delta$ subtypes. Quantum dot imaging of single $\alpha_2\delta$ proteins in both WT and α-Neurexin TKO hippocampal neurons, found that $\alpha_2\delta$-1 had increased plasma membrane motility in the absence of α-Neurexin while $\alpha_2\delta$-3 showed reduced motility under the same conditions. That α-Neurexins can exert seemingly opposed influence on different $\alpha_2\delta$ subtypes emphasises the complexity of $\alpha_2\delta$-regulation. Greater understanding of the interplay between Ca_Vs, auxiliary subunits and the increasing number of known regulators will be crucial to understanding normal and pathological neuronal function.

6.6 Conclusion

This study provides evidence that endosomal $Ca_V2.2$ trafficking is heavily influenced by the specific pairings with $\alpha_2\delta$ subtypes. Additionally, I find that post-translational proteolysis of $\alpha_2\delta$s is an essential regulatory step for normal $Ca_V2.2$ function affecting channel trafficking in neurons and current-enhancement in heterologous systems. Further determinants of Ca_V trafficking remain poorly understood, demonstrated by the surprising finding that point mutations to P-loop glutamate residues in $Ca_V2.2$ produce significant trafficking defects. My findings in this study highlight the importance of $\alpha_2\delta$ subtype distribution in understanding Ca_V behaviour in different cell-types.

Thank you for reading.

Bibliography

Altier, C. *et al.* (2006) 'ORL1 receptor-mediated internalization of N-type calcium channels.', *Nature neuroscience*, 9(1), pp. 31–40. doi: 10.1038/nn1605.

Altier, C. *et al.* (2011) 'The Cavβ subunit prevents RFP2-mediated ubiquitination and proteasomal degradation of L-type channels.', *Nature neuroscience*, 14(2), pp. 173–80. doi: 10.1038/nn.2712.

Anantharaman, V. and Aravind, L. (2000) 'Cache - a signaling domain common to animal Ca(2+)-channel subunits and a class of prokaryotic chemotaxis receptors.', *Trends in biochemical sciences*, 25(11), pp. 535–7. Available at: http://www.ncbi.nlm.nih.gov/pubmed/11084361 (Accessed: 29 October 2018).

Andrade, A. *et al.* (2007) 'Proteolytic cleavage of the voltage-gated Ca2+ channel α2δ subunit: Structural and functional features', *European Journal of Neuroscience*, 25(6), pp. 1705–1710. doi: 10.1111/j.1460-9568.2007.05454.x.

Arikkath, J. and Campbell, K. P. (2003) 'Auxiliary subunits: essential components of the voltage-gated calcium channel complex', *Current Opinion in Neurobiology*, 13(3), pp. 298–307. doi: 10.1016/S0959-4388(03)00066-7.

Arimura, N. and Kaibuchi, K. (2007) 'Neuronal polarity: From extracellular signals to intracellular mechanisms', *Nature Reviews Neuroscience*, 8(3), pp. 194–205. doi: 10.1038/nrn2056.

Arnot, M. I. *et al.* (2000) 'Differential modulation of N-type 1B and P/Q-type 1A calcium channels by different G protein subunit isoforms.', *The Journal of physiology*, 527 Pt 2, pp. 203–12. Available at: http://www.ncbi.nlm.nih.gov/pubmed/10970423 (Accessed: 28 October 2018).

Barclay, J. *et al.* (2001) 'Ducky mouse phenotype of epilepsy and ataxia is associated with mutations in the Cacna2d2 gene and decreased calcium channel current in cerebellar Purkinje cells.', *The Journal of neuroscience : the official journal of the Society for Neuroscience*, 21(16), pp. 6095–104. Available at: http://www.ncbi.nlm.nih.gov/pubmed/11487633 (Accessed: 29 October 2018).

Barr, F. and Lambright, D. G. (2010) 'Rab GEFs and GAPs', *Current Opinion in Cell Biology*, pp. 461–470. doi: 10.1016/j.ceb.2010.04.007.

Bauer, C. S. *et al.* (2009) 'The increased trafficking of the calcium channel subunit alpha2delta-1 to presynaptic terminals in neuropathic pain is inhibited by the alpha2delta ligand pregabalin.', *The Journal of neuroscience : the official journal of the Society for Neuroscience*, 29(13), pp. 4076–88. doi: 10.1523/JNEUROSCI.0356-09.2009.

Bauer, C. S., Tran-Van-Minh, A., *et al.* (2010) 'A new look at calcium channel α2δ subunits.', *Current opinion in neurobiology*. Elsevier Ltd, 20(5), pp. 563–71. doi: 10.1016/j.conb.2010.05.007.

Bauer, C. S., Rahman, W., *et al.* (2010) 'The anti-allodynic alpha(2)delta ligand pregabalin inhibits the trafficking of the calcium channel alpha(2)delta-1 subunit to presynaptic terminals in vivo.', *Biochemical Society transactions*, 38(2), pp. 525–8. doi: 10.1042/BST0380525.

Bean, B. P. (2007) 'The action potential in mammalian central neurons.', *Nature reviews. Neuroscience*, 8(6), pp. 451–65. doi: 10.1038/nrn2148.

Beedle, A. M. *et al.* (2004) 'Agonist-independent modulation of N-type calcium channels by ORL1 receptors.', *Nature neuroscience*, 7(2), pp. 118–25. doi: 10.1038/nn1180.

Bell, T. J. *et al.* (2004) 'Cell-specific alternative splicing increases calcium

channel current density in the pain pathway.', *Neuron*, 41(1), pp. 127–38. Available at: http://www.ncbi.nlm.nih.gov/pubmed/14715140.

Ben-Johny, M. and Yue, D. T. (2014) 'Calmodulin regulation (calmodulation) of voltage-gated calcium channels.', *The Journal of general physiology*. The Rockefeller University Press, 143(6), pp. 679–92. doi: 10.1085/jgp.201311153.

Benleulmi-Chaachoua, A. *et al.* (2016) 'Protein interactome mining defines melatonin MT $_1$ receptors as integral component of presynaptic protein complexes of neurons', *Journal of Pineal Research*, 60(1), pp. 95–108. doi: 10.1111/jpi.12294.

van Bergeijk, P. *et al.* (2015) 'Optogenetic control of organelle transport and positioning', *Nature*, 518(7537), pp. 111–114. doi: 10.1038/nature14128.

Bichet, D. *et al.* (2000) 'The I-II loop of the Ca2+ channel alpha1 subunit contains an endoplasmic reticulum retention signal antagonized by the beta subunit.', *Neuron*, 25(1), pp. 177–90. Available at: http://www.ncbi.nlm.nih.gov/pubmed/10707982.

Blesneac, I. *et al.* (2015) 'Phosphorylation of the Cav3.2 T-type calcium channel directly regulates its gating properties.', *Proceedings of the National Academy of Sciences of the United States of America*, 112(44), pp. 13705–10. doi: 10.1073/pnas.1511740112.

Blümer, J. *et al.* (2013) 'RabGEFs are a major determinant for specific Rab membrane targeting', *The Journal of Cell Biology*, 200(3), pp. 287–300. doi: 10.1083/jcb.201209113.

Boland, L. M. and Bean, B. P. (1993) 'Modulation of N-type calcium channels in bullfrog sympathetic neurons by luteinizing hormone-releasing hormone: kinetics and voltage dependence.', *The Journal of neuroscience : the official journal of the*

Society for Neuroscience, 13(2), pp. 516–33. Available at: http://www.ncbi.nlm.nih.gov/pubmed/7678856 (Accessed: 28 October 2018).

Bourdin, B. *et al.* (2010) 'Molecular determinants of the CaVbeta-induced plasma membrane targeting of the CaV1.2 channel.', *The Journal of biological chemistry*, 285(30), pp. 22853–63. doi: 10.1074/jbc.M110.111062.

Bourdin, B. *et al.* (2015) 'Functional characterization of CaV??2?? mutations associated with sudden cardiac death', *Journal of Biological Chemistry*, 290(5), pp. 2854–2869. doi: 10.1074/jbc.M114.597930.

Breitenkamp, A. F. S. *et al.* (2014) 'Rare Mutations of CACNB2 Found in Autism Spectrum Disease-Affected Families Alter Calcium Channel Function', *PLoS ONE*. Edited by M. E. Zwick, 9(4), p. e95579. doi: 10.1371/journal.pone.0095579.

Brockhaus, J. *et al.* (2018) 'Cellular/Molecular-Neurexins Together with 2-1 Auxiliary Subunits Regulate Ca 2 Influx through Ca v 2.1 Channels'. doi: 10.1523/JNEUROSCI.0511-18.2018.

Brodbeck, J. *et al.* (2002) 'The ducky mutation in Cacna2d2 results in altered Purkinje cell morphology and is associated with the expression of a truncated alpha 2 delta-2 protein with abnormal function.', *The Journal of biological chemistry*, 277(10), pp. 7684–93. doi: 10.1074/jbc.M109404200.

Brown, J. P. *et al.* (1998) 'Isolation of the [3H]gabapentin-binding protein/alpha 2 delta Ca2+ channel subunit from porcine brain: development of a radioligand binding assay for alpha 2 delta subunits using [3H]leucine.', *Analytical biochemistry*, 255(2), pp. 236–43. doi: 10.1006/abio.1997.2447.

Bucci, C. *et al.* (2000) 'Rab7: A Key to Lysosome Biogenesis', *Molecular Biology of the Cell*. Edited by S. R. Pfeffer, 11(2), pp. 467–480. doi: 10.1091/mbc.11.2.467.

Buonarati, O. R. *et al.* (2017) 'Proteolytic processing of the L-type Ca2+ channel alpha11.2 subunit in neurons', *F1000Research*, 6(0), p. 1166. doi: 10.12688/f1000research.11808.1.

Buraei, Z. and Yang, J. (2010) 'The β Subunit of Voltage-Gated Ca $^{2+}$ Channels', *Physiological Reviews*, 90(4), pp. 1461–1506. doi: 10.1152/physrev.00057.2009.

Burashnikov, E. *et al.* (2010) 'Mutations in the cardiac L-type calcium channel associated with inherited J-wave syndromes and sudden cardiac death', *Heart Rhythm*, 7(12), pp. 1872–1882. doi: 10.1016/j.hrthm.2010.08.026.

Campiglio, M. *et al.* (2013) 'Stable incorporation versus dynamic exchange of β subunits in a native Ca2+ channel complex.', *Journal of cell science*, 126(Pt 9), pp. 2092–101. doi: 10.1242/jcs.jcs124537.

Cantí, C. *et al.* (1999) 'Identification of residues in the N terminus of alpha1B critical for inhibition of the voltage-dependent calcium channel by Gbeta gamma.', *The Journal of neuroscience : the official journal of the Society for Neuroscience*. Society for Neuroscience, 19(16), pp. 6855–64. doi: 10.1523/JNEUROSCI.19-16-06855.1999.

Cantí, C. *et al.* (2005) 'The metal-ion-dependent adhesion site in the Von Willebrand factor-A domain of alpha2delta subunits is key to trafficking voltage-gated Ca2+ channels.', *Proceedings of the National Academy of Sciences of the United States of America*, 102(32), pp. 11230–5. doi: 10.1073/pnas.0504183102.

Cao, Y.-Q. *et al.* (2004) 'Presynaptic Ca2+ channels compete for channel type-preferring slots in altered neurotransmission arising from Ca2+ channelopathy.', *Neuron*, 43(3), pp. 387–400. doi: 10.1016/j.neuron.2004.07.014.

Cao, Y.-Q. and Tsien, R. W. (2010) 'Different relationship of N- and P/Q-type Ca2+ channels to channel-interacting slots in controlling neurotransmission at

cultured hippocampal synapses.', *The Journal of neuroscience : the official journal of the Society for Neuroscience*, 30(13), pp. 4536–46. doi: 10.1523/JNEUROSCI.5161-09.2010.

Carroll, K. S. *et al.* (2001) 'Role of Rab9 GTPase in facilitating receptor recruitment by TIP47.', *Science (New York, N.Y.)*, 292(5520), pp. 1373–6. doi: 10.1126/science.1056791.

Cassidy, J. S. *et al.* (2014) 'Functional exofacially tagged N-type calcium channels elucidate the interaction with auxiliary 2 -1 subunits', *Proceedings of the National Academy of Sciences*, 111(24), pp. 8979–8984. doi: 10.1073/pnas.1403731111.

Castiglioni, A. J., Raingo, J. and Lipscombe, D. (2006) 'Alternative splicing in the C-terminus of CaV2.2 controls expression and gating of N-type calcium channels.', *The Journal of physiology*, 576(Pt 1), pp. 119–34. doi: 10.1113/jphysiol.2006.115030.

Catterall, W. (2013) 'Calcium Channel Regulation in the Fight-Or-Flight Response', *Biophysical Journal*. Elsevier, 104(2), p. 7a. doi: 10.1016/j.bpj.2012.11.062.

Catterall, W. a (2011) 'Voltage-gated calcium channels.', *Cold Spring Harbor perspectives in biology*. Cold Spring Harbor Laboratory Press, 3(8), p. a003947. doi: 10.1101/cshperspect.a003947.

Chavrier, P. *et al.* (1990) 'Localization of low molecular weight GTP binding proteins to exocytic and endocytic compartments.', *Cell*, 62(2), pp. 317–29. Available at: http://www.ncbi.nlm.nih.gov/pubmed/2115402 (Accessed: 30 October 2018).

Chen, Y.-H. *et al.* (2004) 'Structural basis of the alpha1-beta subunit interaction

of voltage-gated Ca2+ channels.', *Nature*, 429(6992), pp. 675–80. doi: 10.1038/nature02641.

Cheung, J. and Hendrickson, W. A. (2010) 'Sensor domains of two-component regulatory systems.', *Current opinion in microbiology*, 13(2), pp. 116–23. doi: 10.1016/j.mib.2010.01.016.

Cole, R. L. *et al.* (2005) 'Differential distribution of voltage-gated calcium channel alpha-2 delta (alpha2delta) subunit mRNA-containing cells in the rat central nervous system and the dorsal root ganglia.', *The Journal of comparative neurology*, 491(3), pp. 246–69. doi: 10.1002/cne.20693.

Curtis, B. M. and Catterall, W. A. (1984) 'Purification of the calcium antagonist receptor of the voltage-sensitive calcium channel from skeletal muscle transverse tubules.', *Biochemistry*, 23(10), pp. 2113–8. Available at: http://www.ncbi.nlm.nih.gov/pubmed/6329263 (Accessed: 30 October 2018).

Dahimene, S. *et al.* (2018) 'The α2δ-like Protein Cachd1 Increases N-type Calcium Currents and Cell Surface Expression and Competes with α2δ-1', *CellReports*, 25, pp. 1610-1621.e5. doi: 10.1016/j.celrep.2018.10.033.

Davare, M. A. *et al.* (2001) 'A beta 2 Adrenergic Receptor Signaling Complex Assembled with the Ca2+ Channel Cav1.2', *Science*, 293(5527), pp. 98–101. doi: 10.1126/science.293.5527.98.

Davies, A. *et al.* (2006) 'The calcium channel alpha2delta-2 subunit partitions with CaV2.1 into lipid rafts in cerebellum: implications for localization and function.', *The Journal of neuroscience : the official journal of the Society for Neuroscience*, 26(34), pp. 8748–57. doi: 10.1523/JNEUROSCI.2764-06.2006.

Davies, A. *et al.* (2007) 'Functional biology of the alpha(2)delta subunits of voltage-gated calcium channels.', *Trends in pharmacological sciences*, 28(5), pp.

220–8. doi: 10.1016/j.tips.2007.03.005.

Davies, A. *et al.* (2010) 'The alpha2delta subunits of voltage-gated calcium channels form GPI-anchored proteins, a posttranslational modification essential for function.', *Proceedings of the National Academy of Sciences of the United States of America*, 107(4), pp. 1654–9. doi: 10.1073/pnas.0908735107.

Dolphin, Annette C (2012) 'Biochimica et Biophysica Acta The α 2 δ subunits of voltage-gated calcium channels ☆'.

Dolphin, Annette C. (2012) 'Calcium channel auxiliary α2δ and β subunits: trafficking and one step beyond.', *Nature reviews. Neuroscience*, 13(8), pp. 542–55. doi: 10.1038/nrn3311.

Dolphin, A. C. (2013) 'The α2δ subunits of voltage-gated calcium channels.', *Biochimica et biophysica acta*. Elsevier B.V., 1828(7), pp. 1541–9. doi: 10.1016/j.bbamem.2012.11.019.

Domene, C., Doyle, D. A. and Vénien-Bryan, C. (2005) 'Modeling of an ion channel in its open conformation.', *Biophysical journal*. The Biophysical Society, 89(1), pp. L01-3. doi: 10.1529/biophysj.105.060855.

Donato, R. *et al.* (2006) 'The ducky(2J) mutation in Cacna2d2 results in reduced spontaneous Purkinje cell activity and altered gene expression.', *The Journal of neuroscience : the official journal of the Society for Neuroscience*, 26(48), pp. 12576–86. doi: 10.1523/JNEUROSCI.3080-06.2006.

Dong, G. *et al.* (2007) 'NIH Public Access', 25(3), pp. 455–462. Available at: https://www.ncbi.nlm.nih.gov/pmc/articles/PMC1847580/pdf/nihms18029.pdf (Accessed: 29 November 2018).

Douglas, L. *et al.* (2006) 'Do voltage-gated calcium channel α 2 δ subunits require proteolytic processing into α 2 and δ to be functional ?', 34, pp. 894–898.

Dulubova, I. *et al.* (2005) ‘A Munc13/RIM/Rab3 tripartite complex: from priming to plasticity?’, *The EMBO journal*. European Molecular Biology Organization, 24(16), pp. 2839–50. doi: 10.1038/sj.emboj.7600753.

Dulubova, I. *et al.* (2007) ‘Munc18-1 binds directly to the neuronal SNARE complex.’, *Proceedings of the National Academy of Sciences of the United States of America*, 104(8), pp. 2697–702. doi: 10.1073/pnas.0611318104.

Edvardson, S., Oz, S. and Abulhijaa, F. A. (2013) ‘Early infantile epileptic encephalopathy associated with a high voltage gated calcium channelopathy’, *J Med Genet*, 50, pp. 118–123. doi: 10.1136/jmedgenet-2012-101223.

Elias, G. M. and Nicoll, R. A. (2007) ‘Synaptic trafficking of glutamate receptors by MAGUK scaffolding proteins.’, *Trends in cell biology*, 17(7), pp. 343–52. doi: 10.1016/j.tcb.2007.07.005.

Ellinor, P. T. *et al.* (1995) ‘Ca2+ channel selectivity at a single locus for high-affinity Ca2+ interactions’, *Neuron*, 15(5), pp. 1121–1132. doi: 10.1016/0896-6273(95)90100-0.

Eroglu, C. *et al.* (2009) ‘Gabapentin receptor alpha2delta-1 is a neuronal thrombospondin receptor responsible for excitatory CNS synaptogenesis.’, *Cell*, 139(2), pp. 380–92. doi: 10.1016/j.cell.2009.09.025.

Fankhauser, N. and Maser, P. (2005) ‘Identification of GPI anchor attachment signals by a Kohonen self-organizing map’, *Bioinformatics*, 21(9), pp. 1846–1852. doi: 10.1093/bioinformatics/bti299.

Felix, R. *et al.* (1997) ‘Dissection of functional domains of the voltage-dependent Ca2+ channel alpha2delta subunit.’, *The Journal of neuroscience : the official journal of the Society for Neuroscience*, 17(18), pp. 6884–91. Available at: http://www.ncbi.nlm.nih.gov/pubmed/9278523.

Ferron, L. *et al.* (2008) 'The stargazin-related protein gamma 7 interacts with the mRNA-binding protein heterogeneous nuclear ribonucleoprotein A2 and regulates the stability of specific mRNAs, including CaV2.2.', *The Journal of neuroscience : the official journal of the Society for Neuroscience*, 28(42), pp. 10604–17. doi: 10.1523/JNEUROSCI.2709-08.2008.

Ferron, L., Kadurin, I. and Dolphin, A. C. (2018) 'Proteolytic maturation of α2δ controls the probability of synaptic vesicular release', *eLife*, 7, pp. 1–12. doi: 10.7554/eLife.37507.

Field, M. J. *et al.* (2006) 'dependent calcium channels as a molecular target for pain mediating the analgesic actions of pregabalin', 103(46), pp. 17537–17542.

Findeisen, F. and Minor, D. L. (2009) 'Disruption of the IS6-AID Linker Affects Voltage-gated Calcium Channel Inactivation and Facilitation', *The Journal of General Physiology*, 133(3), pp. 327–343. doi: 10.1085/jgp.200810143.

Fu, Y. *et al.* (2011) 'Deletion of the distal C terminus of CaV1.2 channels leads to loss of beta-adrenergic regulation and heart failure in vivo.', *The Journal of biological chemistry*, 286(14), pp. 12617–26. doi: 10.1074/jbc.M110.175307.

Funke, L., Dakoji, S. and Bredt, D. S. (2005) 'Membrane-associated guanylate kinases regulate adhesion and plasticity at cell junctions.', *Annual review of biochemistry*, 74(1), pp. 219–45. doi: 10.1146/annurev.biochem.74.082803.133339.

Gao, B. *et al.* (2000) 'Functional properties of a new voltage-dependent calcium channel alpha(2)delta auxiliary subunit gene (CACNA2D2).', *The Journal of biological chemistry*, 275(16), pp. 12237–42. doi: 10.1074/jbc.275.16.12237.

Gao, T. *et al.* (1997) 'cAMP-dependent regulation of cardiac L-type Ca2+ channels requires membrane targeting of PKA and phosphorylation of channel

subunits.', *Neuron*, 19(1), pp. 185–96. Available at: http://www.ncbi.nlm.nih.gov/pubmed/9247274 (Accessed: 28 October 2018).

Garcia-Caballero, A. *et al.* (2016) 'A cell-permeant peptide corresponding to the cUBP domain of USP5 reverses inflammatory and neuropathic pain', *Molecular Pain*, 12, p. 174480691664244. doi: 10.1177/1744806916642444.

García-Caballero, A. *et al.* (2014) 'The Deubiquitinating Enzyme USP5 Modulates Neuropathic and Inflammatory Pain by Enhancing Cav3.2 Channel Activity', *Neuron*, 83(5), pp. 1144–1158. doi: 10.1016/j.neuron.2014.07.036.

Garcia, A. M. and Miller, C. (1984) 'Channel mediated monovalent cation-fluxes in isolated sarcoplasmic reticulum vesicles', *Journal of General Physiology*, 83(June), pp. 819–839.

Gee, Nicolas S *et al.* (1996) 'Membranes and Bioenergetics : The Novel Anticonvulsant Drug , Gabapentin (Neurontin), Binds to the Subunit of a Calcium Channel The Novel Anticonvulsant Drug , Gabapentin (Neurontin), Binds to the □ 2 □ Subunit of a Calcium Channel *', 271(10), pp. 5768–5776. doi: 10.1074/jbc.271.10.5768.

Gee, N S *et al.* (1996) 'The novel anticonvulsant drug, gabapentin (Neurontin), binds to the alpha2delta subunit of a calcium channel.', *The Journal of biological chemistry*, 271(10), pp. 5768–76. Available at: http://www.ncbi.nlm.nih.gov/pubmed/8621444.

Gong, H. C. C. *et al.* (2001) 'Tissue-specific Expression and Gabapentin-Binding Properties of Calcium Channel α2δ Subunit Subtypes', *Journal of Membrane Biology*, 184(1), pp. 35–43. doi: 10.1007/s00232-001-0072-7.

Günther, A. *et al.* (2019) 'HCN4 knockdown in dorsal hippocampus promotes anxiety-like behavior in mice', *Genes, Brain and Behavior*. John Wiley & Sons,

Ltd (10.1111), 18(2), p. e12550. doi: 10.1111/gbb.12550.

Gurnett, C. a, Felix, R. and Campbell, K. P. (1997) 'Extracellular interaction of the voltage-dependent Ca2+ channel alpha2delta and alpha1 subunits.', *The Journal of biological chemistry*, 272(29), pp. 18508–12. Available at: http://www.ncbi.nlm.nih.gov/pubmed/9218497.

Gurnett, C. a, De Waard, M. and Campbell, K. P. (1996) 'Dual function of the voltage-dependent Ca2+ channel alpha 2 delta subunit in current stimulation and subunit interaction.', *Neuron*, 16(2), pp. 431–40. Available at: http://www.ncbi.nlm.nih.gov/pubmed/8789958.

Hanson, P. I. *et al.* (1997) 'Structure and conformational changes in NSF and its membrane receptor complexes visualized by quick-freeze/deep-etch electron microscopy.', *Cell*, 90(3), pp. 523–35. Available at: http://www.ncbi.nlm.nih.gov/pubmed/9267032 (Accessed: 28 October 2018).

Hata, Y., Slaughter, C. A. and Südhof, T. C. (1993) 'Synaptic vesicle fusion complex contains unc-18 homologue bound to syntaxin.', *Nature*, 366(6453), pp. 347–51. doi: 10.1038/366347a0.

Hendrich, J. *et al.* (2008) 'Pharmacological disruption of calcium channel trafficking by the alpha2delta ligand gabapentin.', *Proceedings of the National Academy of Sciences of the United States of America*, 105(9), pp. 3628–33. doi: 10.1073/pnas.0708930105.

Herculano-Houzel, S. (2009) 'The human brain in numbers: a linearly scaled-up primate brain', *Frontiers in Human Neuroscience*, 3(November), pp. 1–11. doi: 10.3389/neuro.09.031.2009.

Hering, S. *et al.* (2018) 'Calcium channel gating.', *Pflugers Archiv : European journal of physiology*. Springer, 470(9), pp. 1291–1309. doi: 10.1007/s00424-

018-2163-7.

Herlitze, S. *et al.* (1996) ‘Modulation of Ca2+ channels βγ G-protein py subunits’, *Nature*, 380(6571), pp. 258–262. doi: 10.1038/380258a0.

Hobom, M. *et al.* (2000) ‘Neuronal distribution and functional characterization of the calcium channel alpha2delta-2 subunit.’, *The European journal of neuroscience*, 12(4), pp. 1217–26. Available at: http://www.ncbi.nlm.nih.gov/pubmed/10762351 (Accessed: 29 October 2018).

Hodgkin, A. L. and Huxley, A. F. (1952) ‘A quantitative description of membrane current and its application to conduction and excitation in nerve.’, *The Journal of physiology*. Wiley-Blackwell, 117(4), pp. 500–44. Available at: http://www.ncbi.nlm.nih.gov/pubmed/12991237 (Accessed: 28 October 2018).

Hoppa, M. B. *et al.* (2012) ‘A2Δ Expression Sets Presynaptic Calcium Channel Abundance and Release Probability.’, *Nature*. Nature Publishing Group, 486(7401), pp. 122–5. doi: 10.1038/nature11033.

Horgan, C. P. *et al.* (2010) ‘Rab11-FIP3 binds dynein light intermediate chain 2 and its overexpression fragments the Golgi complex.’, *Biochemical and biophysical research communications*, 394(2), pp. 387–92. doi: 10.1016/j.bbrc.2010.03.028.

Humphries, M. J. (2000) ‘Integrin structure.’, *Biochemical Society transactions*, 28(4), pp. 311–39. Available at: http://www.ncbi.nlm.nih.gov/pubmed/10961914 (Accessed: 29 October 2018).

Hutagalung, A. H. and Novick, P. J. (2011) ‘Role of Rab GTPases in Membrane Traffic and Cell Physiology’, *Physiological Reviews*, 91(1), pp. 119–149. doi: 10.1152/physrev.00059.2009.

Iwasaki, S. *et al.* (2000) ‘Developmental changes in calcium channel types

mediating central synaptic transmission.', *The Journal of neuroscience : the official journal of the Society for Neuroscience*, 20(1), pp. 59–65. Available at: http://www.ncbi.nlm.nih.gov/pubmed/10627581.

Jay, S. D. *et al.* (1990) 'Primary structure of the gamma subunit of the DHP-sensitive calcium channel from skeletal muscle.', *Science (New York, N.Y.)*, 248(4954), pp. 490–2. Available at: http://www.ncbi.nlm.nih.gov/pubmed/2158672 (Accessed: 30 October 2018).

Jay, S. D. *et al.* (1991) 'Structural characterization of the dihydropyridine-sensitive calcium channel alpha 2-subunit and the associated delta peptides.', *The Journal of biological chemistry*, 266(5), pp. 3287–93. Available at: http://www.ncbi.nlm.nih.gov/pubmed/1847144.

Jin, Y. *et al.* (2017) 'CACNA2D3 is downregulated in gliomas and functions as a tumor suppressor', *Molecular Carcinogenesis*, 56(3), pp. 945–959. doi: 10.1002/mc.22548.

Jones, S. L. and Svitkina, T. M. (2016) 'Axon Initial Segment Cytoskeleton: Architecture, Development, and Role in Neuron Polarity'. doi: 10.1155/2016/6808293.

De Jongh, K. S., Warner, C. and Catterall, W. A. (1990) 'Subunits of purified calcium channels. Alpha 2 and delta are encoded by the same gene.', *The Journal of biological chemistry*, 265(25), pp. 14738–41. Available at: http://www.ncbi.nlm.nih.gov/pubmed/2168391 (Accessed: 3 January 2019).

Kadurin, I. *et al.* (2012) 'Calcium currents are enhanced by α2δ-1 lacking its membrane anchor.', *The Journal of biological chemistry*, 287(40), pp. 33554–66. doi: 10.1074/jbc.M112.378554.

Kadurin, I. *et al.* (2016) 'Proteolytic maturation of α2δ represents a checkpoint for

activation and neuronal trafficking of latent calcium channels', *eLife*, 5(OCTOBER2016). doi: 10.7554/eLife.21143.

Kadurin, I. *et al.* (2017) 'LRP1 influences trafficking of N-type calcium channels via interaction with the auxiliary α2δ-1 subunit', *Scientific Reports*, 7. doi: 10.1038/srep43802.

Kaeser, P. S. *et al.* (2011) 'RIM proteins tether Ca2+ channels to presynaptic active zones via a direct PDZ-domain interaction.', *Cell*, 144(2), pp. 282–95. doi: 10.1016/j.cell.2010.12.029.

Karunasekara, Y., Dulhunty, A. F. and Casarotto, M. G. (2009) 'The voltage-gated calcium-channel beta subunit: more than just an accessory.', *European biophysics journal : EBJ*, 39(1), pp. 75–81. doi: 10.1007/s00249-009-0467-4.

Kato, A. S. *et al.* (2007) 'New Transmembrane AMPA Receptor Regulatory Protein Isoform, -7, Differentially Regulates AMPA Receptors', *Journal of Neuroscience*, 27(18), pp. 4969–4977. doi: 10.1523/JNEUROSCI.5561-06.2007.

Kerr, L. M. *et al.* (1988) 'Autoradiographic localization of calcium channels with [125I]omega-conotoxin in rat brain.', *European journal of pharmacology*, 146(1), pp. 181–3. Available at: http://www.ncbi.nlm.nih.gov/pubmed/2450766 (Accessed: 29 October 2018).

Kim, E. Y. *et al.* (2008) 'Structures of CaV2 Ca2+/CaM-IQ Domain Complexes Reveal Binding Modes that Underlie Calcium-Dependent Inactivation and Facilitation', *Structure*, 16(10), pp. 1455–1467. doi: 10.1016/j.str.2008.07.010.

Kisilevsky, A. E. *et al.* (2008) 'D1 receptors physically interact with N-type calcium channels to regulate channel distribution and dendritic calcium entry.', *Neuron*, 58(4), pp. 557–70. doi: 10.1016/j.neuron.2008.03.002.

Kitano, J. *et al.* (2003) 'Direct Interaction and Functional Coupling between

Metabotropic Glutamate Receptor Subtype 1 and Voltage-sensitive $Ca_v2.1$ Ca^{2+} Channel', *Journal of Biological Chemistry*, 278(27), pp. 25101–25108. doi: 10.1074/jbc.M303266200.

Klugbauer, N. *et al.* (2000) 'A family of γ-like calcium channel subunits', *FEBS Letters*, 470(2), pp. 189–197. doi: 10.1016/S0014-5793(00)01306-5.

Koishi, R. *et al.* (2004) 'A superfamily of voltage-gated sodium channels in bacteria.', *The Journal of biological chemistry*. American Society for Biochemistry and Molecular Biology, 279(10), pp. 9532–8. doi: 10.1074/jbc.M313100200.

Kurshan, P. T., Oztan, A. and Schwarz, T. L. (2009) 'Presynaptic alpha2delta-3 is required for synaptic morphogenesis independent of its Ca2+-channel functions.', *Nature neuroscience*, 12(11), pp. 1415–23. doi: 10.1038/nn.2417.

Laviv, T. *et al.* (2011) 'Compartmentalization of the GABAB receptor signaling complex is required for presynaptic inhibition at hippocampal synapses.', *The Journal of neuroscience : the official journal of the Society for Neuroscience*, 31(35), pp. 12523–32. doi: 10.1523/JNEUROSCI.1527-11.2011.

Lazniewska, J. and Weiss, N. (2017) 'Glycosylation of voltage-gated calcium channels in health and disease', *Biochimica et Biophysica Acta (BBA) - Biomembranes*, 1859(5), pp. 662–668. doi: 10.1016/j.bbamem.2017.01.018.

Li, C.-Y. *et al.* (2006) 'Calcium channel alpha2delta1 subunit mediates spinal hyperexcitability in pain modulation.', *Pain*, 125(1–2), pp. 20–34. doi: 10.1016/j.pain.2006.04.022.

Li, G. and Marlin, M. C. (2015) 'Rab GTPases', 1298, pp. 1–15. doi: 10.1007/978-1-4939-2569-8.

Lin, Z. *et al.* (1997) 'Identification of functionally distinct isoforms of the N-type Ca2+ channel in rat sympathetic ganglia and brain.', *Neuron*, 18(1), pp. 153–66.

Available at: http://www.ncbi.nlm.nih.gov/pubmed/9010213 (Accessed: 29 October 2018).

Lin, Z. *et al.* (1999) 'Alternative splicing of a short cassette exon in alpha1B generates functionally distinct N-type calcium channels in central and peripheral neurons.', *The Journal of neuroscience : the official journal of the Society for Neuroscience*, 19(13), pp. 5322–31. Available at: http://www.ncbi.nlm.nih.gov/pubmed/10377343 (Accessed: 29 October 2018).

Lindsay, A. J. *et al.* (2013) 'Identification and characterization of multiple novel Rab–myosin Va interactions', *Molecular Biology of the Cell*. Edited by P. J. Brennwald, 24(21), pp. 3420–3434. doi: 10.1091/mbc.e13-05-0236.

Liu, H. *et al.* (1996) 'Expression and subunit interaction of voltage-dependent Ca2+ channels in PC12 cells.', *The Journal of neuroscience : the official journal of the Society for Neuroscience*, 16(23), pp. 7557–65. Available at: http://www.ncbi.nlm.nih.gov/pubmed/8922412.

Liu, K. S. Y. *et al.* (2011) 'RIM-Binding Protein, a Central Part of the Active Zone, Is Essential for Neurotransmitter Release', *Science*, 334(6062), pp. 1565–1569. doi: 10.1126/science.1212991.

Lu, J. *et al.* (2006) 'Structural basis for a Munc13-1 homodimer to Munc13-1/RIM heterodimer switch.', *PLoS biology*. Public Library of Science, 4(7), p. e192. doi: 10.1371/journal.pbio.0040192.

Luo, Z. D. *et al.* (2001) 'Upregulation of dorsal root ganglion (alpha)2(delta) calcium channel subunit and its correlation with allodynia in spinal nerve-injured rats.', *The Journal of neuroscience : the official journal of the Society for Neuroscience*, 21(6), pp. 1868–75. Available at: http://www.ncbi.nlm.nih.gov/pubmed/11245671.

Macabuag, N. and Dolphin, A. C. (2015) ‘Alternative Splicing in CaV2.2 Regulates Neuronal Trafficking via Adaptor Protein Complex-1 Adaptor Protein Motifs’, *Journal of Neuroscience*, 35(43), pp. 14636–14652. doi: 10.1523/JNEUROSCI.3034-15.2015.

Mahammad, S. and Parmryd, I. (2015) ‘Cholesterol Depletion Using Methyl-β-cyclodextrin’, in *Methods in molecular biology (Clifton, N.J.)*, pp. 91–102. doi: 10.1007/978-1-4939-1752-5_8.

Manville, R. W. and Abbott, G. W. (2018) ‘Gabapentin Is a Potent Activator of KCNQ3 and KCNQ5 Potassium Channels.’, *Molecular pharmacology*. American Society for Pharmacology and Experimental Therapeutics, 94(4), pp. 1155–1163. doi: 10.1124/mol.118.112953.

Marais, E., Klugbauer, N. and Hofmann, F. (2001) ‘Calcium channel alpha(2)delta subunits-structure and Gabapentin binding.’, *Molecular pharmacology*, 59(5), pp. 1243–8. Available at: http://www.ncbi.nlm.nih.gov/pubmed/11306709 (Accessed: 29 October 2018).

McMahon, H. T. *et al.* (1995) ‘Complexins: cytosolic proteins that regulate SNAP receptor function.’, *Cell*, 83(1), pp. 111–9. Available at: http://www.ncbi.nlm.nih.gov/pubmed/7553862 (Accessed: 28 October 2018).

Mercer, A. J., Chen, M. and Thoreson, W. B. (2011) ‘Lateral Mobility of Presynaptic L-Type Calcium Channels at Photoreceptor Ribbon Synapses’, *Journal of Neuroscience*, 31(12), pp. 4397–4406. doi: 10.1523/JNEUROSCI.5921-10.2011.

Miaczynska, M. *et al.* (2004) ‘APPL proteins link Rab5 to nuclear signal transduction via an endosomal compartment.’, *Cell*, 116(3), pp. 445–56. Available at: http://www.ncbi.nlm.nih.gov/pubmed/15016378 (Accessed: 30 October 2018).

Michailidis, I. E. *et al.* (2014) ‘Age-Related Homeostatic Midchannel Proteolysis of Neuronal L-type Voltage-Gated Ca2+ Channels’, *Neuron*, 82(5), pp. 1045–1057. doi: 10.1016/j.neuron.2014.04.017.

Mori, M. X. *et al.* (2008) ‘Crystal Structure of the CaV2 IQ Domain in Complex with Ca2+/Calmodulin: High-Resolution Mechanistic Implications for Channel Regulation by Ca2+’, *Structure*, 16(4), pp. 607–620. doi: 10.1016/j.str.2008.01.011.

Narahashi, T. (1964) ‘TETRODOTOXIN BLOCKAGE OF SODIUM CONDUCTANCE INCREASE IN LOBSTER GIANT AXONS.’, *The Journal of general physiology*. The Rockefeller University Press, 47(5), pp. 965–74. Available at: http://www.ncbi.nlm.nih.gov/pubmed/14155438 (Accessed: 28 October 2018).

Neely, G. G. *et al.* (2010) ‘A genome-wide Drosophila screen for heat nociception identifies α2δ3 as an evolutionarily conserved pain gene.’, *Cell*, 143(4), pp. 628–38. doi: 10.1016/j.cell.2010.09.047.

Nelson, A. D. and Jenkins, P. M. (2017) ‘Axonal Membranes and Their Domains: Assembly and Function of the Axon Initial Segment and Node of Ranvier.’, *Frontiers in cellular neuroscience*. Frontiers Media SA, 11, p. 136. doi: 10.3389/fncel.2017.00136.

Newton, R. a *et al.* (2001) ‘Dorsal root ganglion neurons show increased expression of the calcium channel alpha2delta-1 subunit following partial sciatic nerve injury.’, *Brain research. Molecular brain research*, 95(1–2), pp. 1–8. Available at: http://www.ncbi.nlm.nih.gov/pubmed/11687271.

Nguyen, M. K. *et al.* (2016) ‘Optogenetic oligomerization of Rab GTPases regulates intracellular membrane trafficking’, *Nature Chemical Biology*, 12(6), pp. 431–436. doi: 10.1038/nchembio.2064.

Nowycky, M. C., Fox, A. P. and Tsien, R. W. (1985) 'Three types of neuronal calcium channel with different calcium agonist sensitivity', *Nature*, 316(6027), pp. 440–443. doi: 10.1038/316440a0.

Opatowsky, Y. *et al.* (2004) 'Structural analysis of the voltage-dependent calcium channel beta subunit functional core and its complex with the alpha 1 interaction domain.', *Neuron*, 42(3), pp. 387–99. Available at: http://www.ncbi.nlm.nih.gov/pubmed/15134636 (Accessed: 30 October 2018).

Orestes, P. *et al.* (2013) 'Reversal of neuropathic pain in diabetes by targeting glycosylation of Ca(V)3.2 T-type calcium channels.', *Diabetes*. American Diabetes Association, 62(11), pp. 3828–38. doi: 10.2337/db13-0813.

Palmenberg, A. C., Rathe, J. A. and Liggett, S. B. (2011) 'Analysis of complete genome sequences of Human Rhinovirus', *Journal of Allergy and Clinical Immunology*, 125(6), pp. 1190–1201. doi: 10.1016/j.jaci.2010.04.010.Analysis.

Park, H. J. *et al.* (2015) 'Asn-linked glycosylation contributes to surface expression and voltage-dependent gating of Cav1.2 Ca2+channel', *Journal of Microbiology and Biotechnology*, 25(8), pp. 1371–1379. doi: 10.4014/jmb.1501.01066.

Patel, R. *et al.* (2013) 'A2Δ-1 Gene Deletion Affects Somatosensory Neuron Function and Delays Mechanical Hypersensitivity in Response To Peripheral Nerve Damage.', *The Journal of neuroscience : the official journal of the Society for Neuroscience*, 33(42), pp. 16412–26. doi: 10.1523/JNEUROSCI.1026-13.2013.

Pellinen, T. *et al.* (2006) 'Small GTPase Rab21 regulates cell adhesion and controls endosomal traffic of β1-integrins', *The Journal of Cell Biology*, 173(5), pp. 767–780. doi: 10.1083/jcb.200509019.

Perry, T. L., Hansen, S. and Kennedy, J. (1975) 'CSF amino acids and plasma--CSF amino acid ratios in adults.', *Journal of neurochemistry*, 24(3), pp. 587–9. Available at: http://www.ncbi.nlm.nih.gov/pubmed/1113130 (Accessed: 4 January 2019).

Van Petegem, F. *et al.* (2004) 'Structure of a complex between a voltage-gated calcium channel β-subunit and an α-subunit domain', *Nature*, 429(6992), pp. 671–675. doi: 10.1038/nature02588.

Pfeffer, S. R. (2013) 'Rab GTPase regulation of membrane identity.', *Current opinion in cell biology*, 25(4), pp. 414–9. doi: 10.1016/j.ceb.2013.04.002.

Qin, N. *et al.* (1998) 'Modulation of human neuronal 1E -type calcium channel by a2d -subunit', pp. 1324–1331.

Ren, D. (2001) 'A Prokaryotic Voltage-Gated Sodium Channel', *Science*, 294(5550), pp. 2372–2375. doi: 10.1126/science.1065635.

Sandoval, A. *et al.* (2007) 'gamma1-dependent down-regulation of recombinant voltage-gated Ca2+ channels.', *Cellular and molecular neurobiology*, 27(7), pp. 901–8. doi: 10.1007/s10571-007-9210-9.

Sather, W. A., Yang, J. and Tsien, R. W. (1994) 'Structural basis of ion channel permeation and selectivity.', *Current opinion in neurobiology*, 4(3), pp. 313–23. Available at: http://www.ncbi.nlm.nih.gov/pubmed/7522675 (Accessed: 3 January 2019).

Sato, Y. *et al.* (2007) *Crystal structure of the Sec4pSec2p complex in the nucleotide exchanging intermediate state*. Available at: www.pnas.org/cgi/content/full/ (Accessed: 29 November 2018).

Savalli, N. *et al.* (2006) 'Voltage-dependent conformational changes in human Ca2+- and voltage-activated K+ channel, revealed by voltage-clamp fluorometry',

Proceedings of the National Academy of Sciences, 103(33), pp. 12619–12624. doi: 10.1073/pnas.0601176103.

Savalli, N. *et al.* (2016) 'The α 2 δ-1 subunit remodels Ca V 1.2 voltage sensors and allows Ca 2+ influx at physiological membrane potentials', *The Journal of General Physiology*, 148(2), pp. 147–159. doi: 10.1085/jgp.201611586.

Seaman, M. N. J. (2012) 'The retromer complex - endosomal protein recycling and beyond', *Journal of Cell Science*, 125(20), pp. 4693–4702. doi: 10.1242/jcs.103440.

Simons, K. and Ikonen, E. (1997) 'Functional rafts in cell membranes', *Nature*. Nature Publishing Group, 387(6633), pp. 569–572. doi: 10.1038/42408.

Soldati, T., Riederer, M. A. and Pfeffer, S. R. (1993) 'Rab GDI: a solubilizing and recycling factor for rab9 protein.', *Molecular biology of the cell*, 4(4), pp. 425–34. Available at: http://www.ncbi.nlm.nih.gov/pubmed/8389620 (Accessed: 30 October 2018).

Söllner, T. *et al.* (1993) 'A protein assembly-disassembly pathway in vitro that may correspond to sequential steps of synaptic vesicle docking, activation, and fusion.', *Cell*, 75(3), pp. 409–18. Available at: http://www.ncbi.nlm.nih.gov/pubmed/8221884 (Accessed: 28 October 2018).

Solovyova, N. and Verkhratsky, A. (2002) 'Monitoring of free calcium in the neuronal endoplasmic reticulum: An overview of modern approaches', *Journal of Neuroscience Methods*, 122(1), pp. 1–12. doi: 10.1016/S0165-0270(02)00300-X.

Somlyo, a V *et al.* (1981) 'Calcium Release and Ionic Changes in the Sarcoplasm ic Reticu l u m of Tetan ized Muscle : An Electron-Probe Study', *J Cell Biol.*, 90(3), pp. 577–594.

Spinosa, M. R. *et al.* (2008) 'Functional characterization of Rab7 mutant proteins

associated with Charcot-Marie-Tooth type 2B disease.', *The Journal of neuroscience : the official journal of the Society for Neuroscience*, 28(7), pp. 1640–8. doi: 10.1523/JNEUROSCI.3677-07.2008.

Steinberg, F. *et al.* (2012) 'SNX17 protects integrins from degradation by sorting between lysosomal and recycling pathways.', *The Journal of cell biology*. The Rockefeller University Press, 197(2), pp. 219–30. doi: 10.1083/jcb.201111121.

Südhof, T. C. (2012) 'Calcium control of neurotransmitter release.', *Cold Spring Harbor perspectives in biology*, 4(1), p. a011353. doi: 10.1101/cshperspect.a011353.

Svitkin, Y. V *et al.* (1999) 'Eukaryotic initiation factor 4GII (eIF4GII), but not eIF4GI, cleavage correlates with inhibition of host cell protein synthesis after human rhinovirus infection.', *Journal of virology*, 73(4), pp. 3467–72. Available at: http://www.pubmedcentral.nih.gov/articlerender.fcgi?artid=104114&tool=pmcentrez&rendertype=abstract.

Tadross, M. R., Dick, I. E. and Yue, D. T. (2008) 'Mechanism of Local and Global Ca2+ Sensing by Calmodulin in Complex with a Ca2+ Channel', *Cell*, 133(7), pp. 1228–1240. doi: 10.1016/j.cell.2008.05.025.

Tae, H. S. *et al.* (2017) 'Gabapentin modulates HCN4 channel voltage-dependence', *Frontiers in Pharmacology*, 8(AUG), pp. 1–13. doi: 10.3389/fphar.2017.00554.

Takahashi, M. *et al.* (1987) 'Subunit structure of dihydropyridine-sensitive calcium channels from skeletal muscle.', *Proceedings of the National Academy of Sciences of the United States of America*, 84(15), pp. 5478–5482. doi: 10.1073/pnas.84.15.5478.

Tang, L. *et al.* (2014) 'Structural basis for Ca2+ selectivity of a voltage-gated

calcium channel.', *Nature*. NIH Public Access, 505(7481), pp. 56–61. doi: 10.1038/nature12775.

Tatulian, L. *et al.* (2001) 'Activation of expressed KCNQ potassium currents and native neuronal M-type potassium currents by the anti-convulsant drug retigabine.', *The Journal of neuroscience : the official journal of the Society for Neuroscience*, 21(15), pp. 5535–45. Available at: http://www.ncbi.nlm.nih.gov/pubmed/11466425 (Accessed: 28 May 2019).

Theret, L. *et al.* (2017) 'Identification of LRP-1 as an endocytosis and recycling receptor for β1-integrin in thyroid cancer cells.', *Oncotarget*. Impact Journals, LLC, 8(45), pp. 78614–78632. doi: 10.18632/oncotarget.20201.

Thorell, K. *et al.* (2009) 'Verification of genes differentially expressed in neuroblastoma tumours: a study of potential tumour suppressor genes', *BMC Medical Genomics*. BioMed Central, 2(1), p. 53. doi: 10.1186/1755-8794-2-53.

Tran-Van-Minh, Alexandra and Dolphin, A. C. (2010) 'The alpha2delta ligand gabapentin inhibits the Rab11-dependent recycling of the calcium channel subunit alpha2delta-2.', *The Journal of neuroscience : the official journal of the Society for Neuroscience*, 30(38), pp. 12856–67. doi: 10.1523/JNEUROSCI.2700-10.2010.

Tran-Van-Minh, A and Dolphin, A. C. (2010) 'The alpha2delta ligand gabapentin inhibits the Rab11-dependent recycling of the calcium channel subunit alpha2delta-2', *J Neurosci*, 30(38), pp. 12856–12867. doi: 10.1523/JNEUROSCI.2700-10.2010.

Ullrich, O. *et al.* (1994) 'Membrane association of Rab5 mediated by GDP-dissociation inhibitor and accompanied by GDP/GTP exchange.', *Nature*, 368(6467), pp. 157–60. doi: 10.1038/368157a0.

Verhoeven, K. *et al.* (2003) 'Mutations in the Small GTP-ase Late Endosomal Protein RAB7 Cause Charcot-Marie-Tooth Type 2B Neuropathy', *The American Journal of Human Genetics*, 72(3), pp. 722–727. doi: 10.1086/367847.

Vonderheit, A. and Helenius, A. (2005) 'Rab7 Associates with Early Endosomes to Mediate Sorting and Transport of Semliki Forest Virus to Late Endosomes', *PLoS Biology*. Edited by K. L. Simons, 3(7), p. e233. doi: 10.1371/journal.pbio.0030233.

De Waard, M. *et al.* (1995) 'Properties of the alpha 1-beta anchoring site in voltage-dependent Ca2+ channels.', *The Journal of biological chemistry*, 270(20), pp. 12056–64. Available at: http://www.ncbi.nlm.nih.gov/pubmed/7744854 (Accessed: 30 October 2018).

Waithe, D., Ferron, L., Page, Karen M, *et al.* (2011) 'Beta-subunits promote the expression of Ca(V)2.2 channels by reducing their proteasomal degradation.', *The Journal of biological chemistry*, 286(11), pp. 9598–611. doi: 10.1074/jbc.M110.195909.

Waithe, D., Ferron, L., Page, Karen M., *et al.* (2011) 'β-Subunits Promote the Expression of Ca_V 2.2 Channels by Reducing Their Proteasomal Degradation', *Journal of Biological Chemistry*, 286(11), pp. 9598–9611. doi: 10.1074/jbc.M110.195909.

Wakamori, M., Mikala, G. and Mori, Y. (1999) 'Auxiliary subunits operate as a molecular switch in determining gating behaviour of the unitary N-type Ca2+ channel current in Xenopus oocytes.', *The Journal of physiology*, 517 (Pt 3(1999), pp. 659–72. Available at: http://www.pubmedcentral.nih.gov/articlerender.fcgi?artid=2269381&tool=pmcentrez&rendertype=abstract.

Wandinger-Ness, A. and Zerial, M. (2014) 'Rab Proteins and the

Compatmentalization of the Endosomal System', *Cold Spring Harbor Perspectives in Biology*, 6(11), p. a022616. doi: 10.1101/cshperspect.a022616.

Wang, H. *et al.* (2002) 'Chronic neuropathic pain is accompanied by global changes in gene expression and shares pathobiology with neurodegenerative diseases.', *Neuroscience*, 114(3), pp. 529–46. Available at: http://www.ncbi.nlm.nih.gov/pubmed/12220557.

Wang, M. *et al.* (1999) 'gabapentin binding', 320, pp. 313–320.

Wheeler, D. G. *et al.* (2012) 'Ca(V)1 and Ca(V)2 channels engage distinct modes of Ca(2+) signaling to control CREB-dependent gene expression.', *Cell*. NIH Public Access, 149(5), pp. 1112–24. doi: 10.1016/j.cell.2012.03.041.

Whittaker, C. A. and Hynes, R. O. (2004) 'Distribution and Evolution of von Willebrand / Integrin A Domains : Widely Dispersed Domains with Roles in Cell Adhesion and Elsewhere □', 13(October 2002), pp. 3369–3387. doi: 10.1091/mbc.E02.

Wong, Alissa Michelle Go *et al.* (2013) 'Characterization of *CACNA2D3* as a putative tumor suppressor gene in the development and progression of nasopharyngeal carcinoma', *International Journal of Cancer*, 133(10), pp. 2284–2295. doi: 10.1002/ijc.28252.

Wu, J. *et al.* (2016) 'Structure of the voltage-gated calcium channel Cav1.1 at 3.6 Å resolution', *Nature*. Nature Publishing Group, 537(7619), pp. 191–196. doi: 10.1038/nature19321.

Wycisk, K. A. *et al.* (2006) 'Structural and Functional Abnormalities of Retinal Ribbon Synapses due to *Cacna2d4* Mutation', *Investigative Opthalmology & Visual Science*, 47(8), p. 3523. doi: 10.1167/iovs.06-0271.

Yang, J. *et al.* (1993) 'Molecular determinants of Ca2+ selectivity and ion

permeation in L-type Ca2+ channels', *Nature*, 366(6451), pp. 158–161. doi: 10.1038/366158a0.

Yang, J. and Tsien, R. W. (1993) 'Enhancement of N- and L-type calcium channel currents by protein kinase C in frog sympathetic neurons.', *Neuron*, 10(2), pp. 127–36. Available at: http://www.ncbi.nlm.nih.gov/pubmed/8382496.

Yarotskyy, V. *et al.* (2012) 'Domain III regulates N-type (CaV2.2) calcium channel closing kinetics.', *Journal of neurophysiology*, 107(7), pp. 1942–51. doi: 10.1152/jn.00993.2011.

Yarotskyy, V. and Elmslie, K. S. (2010) 'Interference between two modulators of N-type (CaV2.2) calcium channel gating demonstrates that omega-conotoxin GVIA disrupts open state gating.', *Biochimica et biophysica acta*. Elsevier B.V., 1798(9), pp. 1821–8. doi: 10.1016/j.bbamem.2010.05.004.

Yazawa, M. *et al.* (2007) 'TRIC channels are essential for Ca2+ handling in intracellular stores', *Nature*, 448(7149), pp. 78–82. doi: 10.1038/nature05928.

Yue, D. T., Herzig, S. and Marban, E. (1990) 'Beta-adrenergic stimulation of calcium channels occurs by potentiation of high-activity gating modes.', *Proceedings of the National Academy of Sciences of the United States of America*. National Academy of Sciences, 87(2), pp. 753–7. Available at: http://www.ncbi.nlm.nih.gov/pubmed/1689051 (Accessed: 6 January 2019).

Zamponi, G. W. (2003) 'Calmodulin lobotomized: novel insights into calcium regulation of voltage-gated calcium channels.', *Neuron*, 39(6), pp. 879–81. Available at: http://www.ncbi.nlm.nih.gov/pubmed/12971887 (Accessed: 28 October 2018).